NUREG/CR-4115
EGG-2369

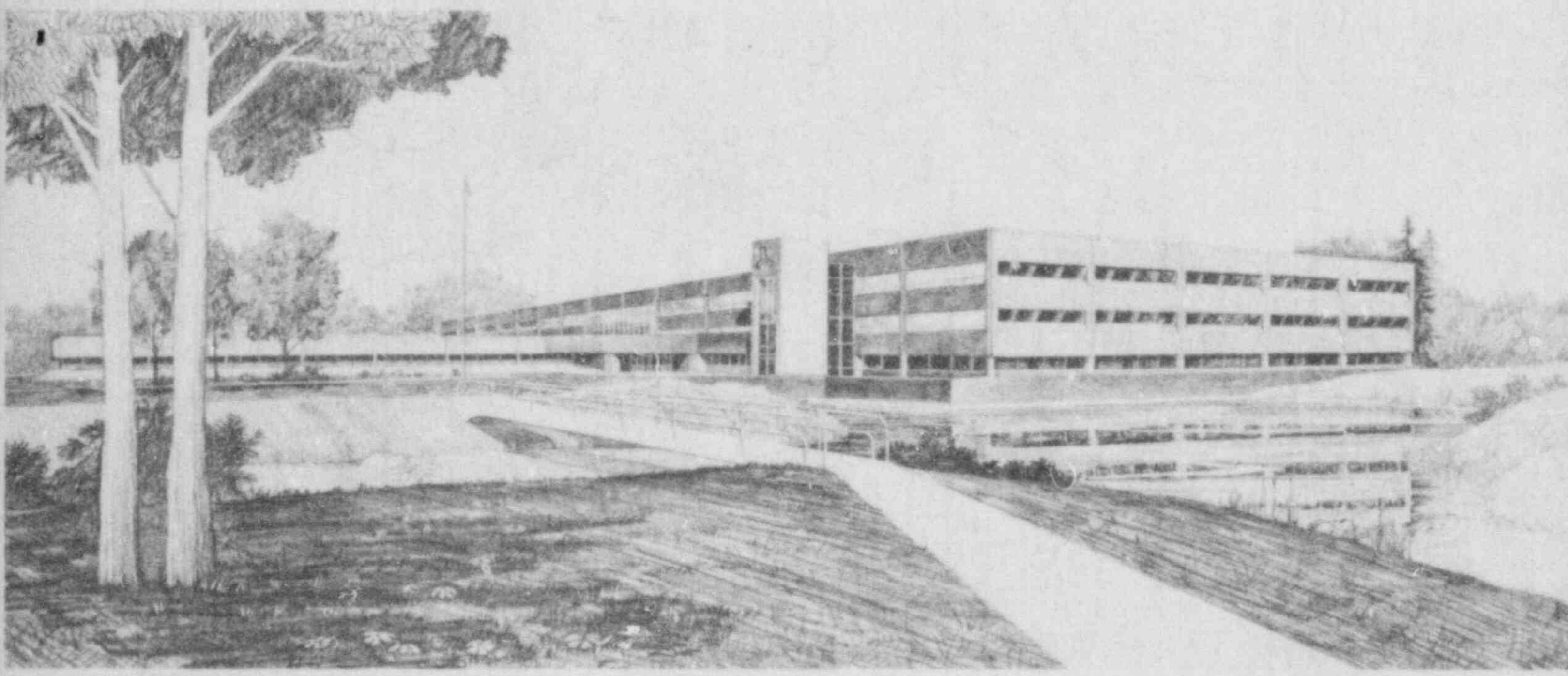

Idaho National Engineering Laboratory
Operated by the U.S. Department of Energy

International Standard Problem 13 (LOFT Experiment L2-5) Final Comparison Report

John D. Burtt

December 1984

Prepared for the
U.S. Nuclear Regulatory Commission
Under DOE Contract No. DE-AC07-76IDO1570

EG&G Idaho

Available from

GPO Sales Program
Division of Technical Information and Document Control
U.S. Nuclear Regulatory Commission
Washington, D.C. 20555

and

National Technical Information Service
Springfield, Virginia 22161

NUREG/CR-4115
EGG-2369
Distribution Category: R4

INTERNATIONAL STANDARD PROBLEM 13 (LOFT EXPERIMENT L2-5) FINAL COMPARISON REPORT

John D. Burtt

Published December 1984

EG&G Idaho, Inc.
Idaho Falls, Idaho 83415

Prepared for the
U.S. Nuclear Regulatory Commission
Washington, D.C. 20555
Under DOE Contract No. DE-AC07-76IDO1570
FIN No. A6047

ABSTRACT

LOFT Experiment L2-5 was designated International Standard Problem 13 by the Organization for Economic Cooperation and Development. Comparisons between measurements from Experiment L2-5 were made with calculations from 11 international participants using five different computer codes. LOFT Experiment L2-5 simulated a double ended guillotine cold leg rupture of a primary coolant loop of a large pressurized water reactor, coupled with a loss of offsite power.

FIN No. A6047--Code Assessment and Applications (Transient Analysis)

SUMMARY

The Organization for Economic Cooperation and Development designated Loss-of-Fluid Test (LOFT) Experiment L2-5 as International Standard Problem 13. Calculations were submitted by 11 participants using five computer codes. Eight calculations were preceded by model submittals and qualified as blind calculations. The four remaining calculations were classified as open submittals. Comparisons were made between participant calculations and measurements from Experiment L2-5.

Experiment L2-5 simulated a double ended offset shear guillotine cold leg rupture in a large pressurized water reactor. A loss of offsite power was also simulated with a reactor coolant pump trip and an emergency core coolant system injection delay.

The participants calculated the hydraulic response of L2-5 adequately, except where there were obvious modeling problems. Densities were calculated adequately in the sections where condensation did not occur. Break flows were generally over predicted. Clad temperature heatups were calculated adequately but quench times for cladding was predicted less well.

CONTENTS

FIGURES

TABLES

1. INTRODUCTION

Experiment L2-5, conducted in the Loss-of-Fluid Test (LOFT) was identified by the Organization for Economic Cooperation and Development (OECD) as International Standard Problem 13 (ISP-13). This report documents the comparisons between participant computer code calculations and measured results from LOFT Experiment L2-5. The results from Experiment L2-5 are documented in Reference 1.

LOFT Experiment L2-5 simulated a double ended, offset shear, guillotine cold leg rupture. The reactor coolant pumps were tripped and decoupled from their flywheels within 1 s after break initiation, simulating a loss of offsite power. Consistent with this loss of power, the high and low pressure emergency core coolant injection systems were delayed. The system description and initial conditions are presented in Section 2.

The purpose of this report is to present direct comparisons between the calculated parameters and LOFT L2-5 data. It is beyond the scope of this report to assess and analyze the reasons for discrepancies that occurred. The models used by the participants are summarized in Section 3. The eight blind calculations are compared with measurements and discussed in Section 4. Section 5 presents the comparison between measurements and results from the four open calculations. Section 6 contains the conclusions and recommendations drawn from the comparisons. Appendices A through L present details about each submittal as provided by the participants.

2. LOFT EXPERIMENT L2-5 DESCRIPTION

Experiment L2-5 was conducted on June 16, 1982 in the LOFT facility. The LOFT facility is located at the Idaho National Engineering Laboratory (INEL) and was operated for the United States Nuclear Regulatory Commission by the Department of Energy at the time of the experiment. This section describes the LOFT facility and presents the initial test conditions.

2.1 System Description

The LOFT system configuration for Experiment L2-5 is shown in Figure 1. The major components of the LOFT system are: a reactor vessel including a core with 1300 unpressurized nuclear fuel rods with an active length of 1.67 m; an intact loop with a pressurizer, steam generator, two pumps arranged in parallel, and piping connected to the break plane orifice; a broken loop with a simulated pump, simulated steam generator, two break plane orifices, two quick opening blowdown valves (QOBVs), and two isolation valves; an emergency core coolant system consisting of two accumulators, a high pressure injection system and a low pressure injection system; and a blowdown suppression system consisting of a header and suppression tank. The details of the LOFT system and instrumentation are presented in Reference 2.

2.2 Test Conditions

After operating the reactor at 36.0 MW for 40 effective full power hours to build up a fission decay product inventory, Experiment L2-5 was initiated by opening the two QOBVs, in the broken loop hot and cold legs. The primary coolant pumps were tripped by the operators at 0.94 ± 0.01 s. The pumps were not connected to their flywheels during the coastdown. High pressure injection and low pressure injection were delayed to 24 s and 37 s, respectively, to simulate the delay expected for a PWR emergency diesel to begin delivering power (in response to a loss of site power).

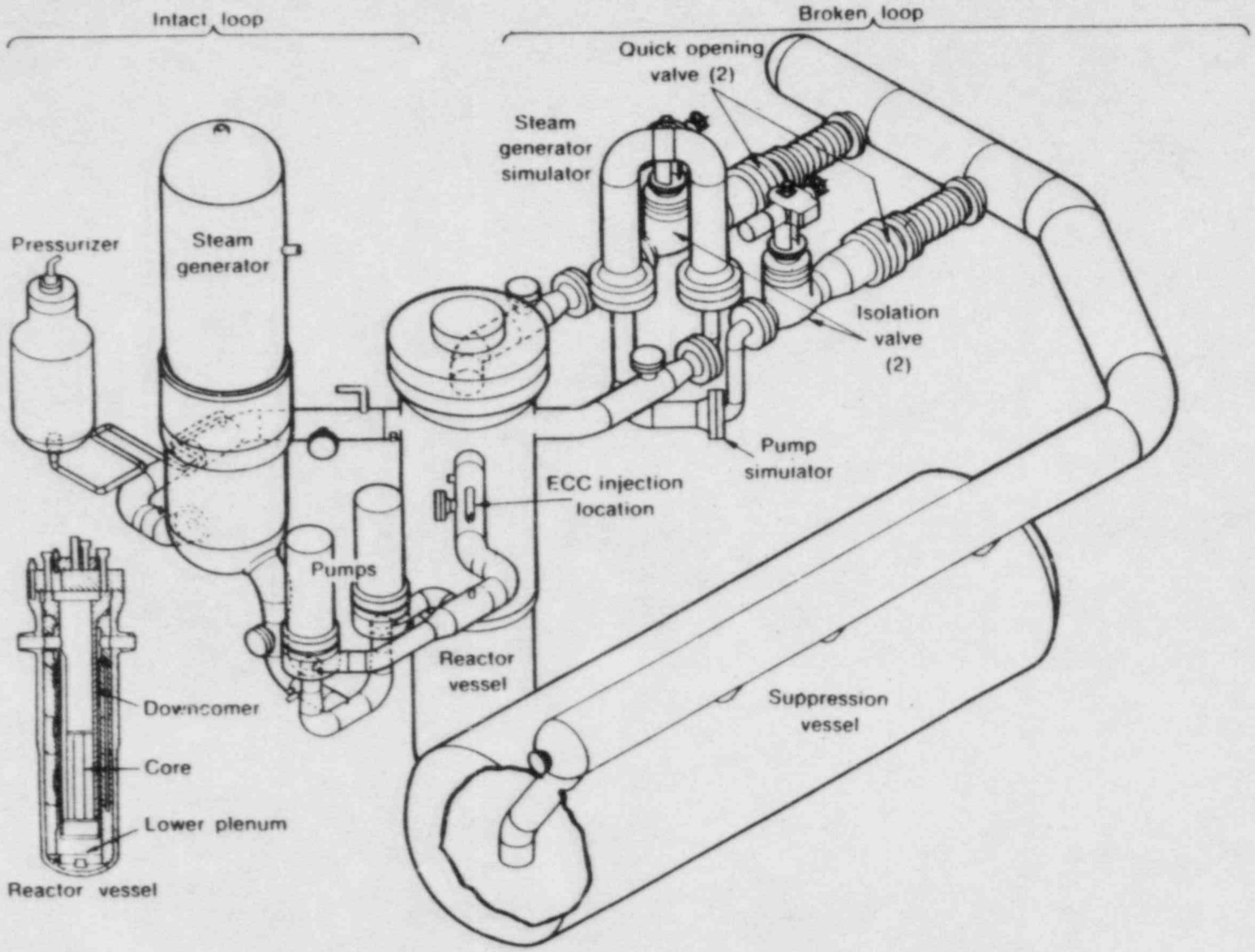

Figure 1. LOFT major components

2.3 Initial Conditions

A summary of the measured system conditions immediately prior to Experiment L2-5 initiation is shown in Table 1. The mass flow rate in the intact loop was 192.4 ± 7.8 kg/s. The intact loop hot leg pressure was 14.94 ± .06 MPa. The intact loop hot leg temperature was 589.7 ± 1.6 K. The initial core power was 36. ± 1.2 MW with a maximum l,near heat generation rate of 40.1 ± 3.0 kW/m.

TABLE 1. INITIAL CONDITIONS FOR LOFT EXPERIMENT L2-5

Parameter	Measured Value
Primary Coolant System	
Mass flow (kg/s)	192.4 ± 7.8
Hot leg pressure (MPa)	14.94 ± 0.06
Cold leg temperature (K)	556.6 ± 4.0
Hot leg temperature (K)	589.7 ± 1.6
Boron concentration (ppm)	668.0 ± 15
Reactor Vessel	
Power level (MW)	36.0 ± 1.2
Maximum linear heat generation rate (kW/m)	40.1 ± 3.0
Control rod position (above full-in position (m)	1.376 ± 0.01
Pressurizer	
Steam volume (m^3)	0.32 ± 0.02
Liquid volume (m^3)	0.61 ± 0.02
Liquid temperature (K)	615.0 ± 3
Liquid level (m)	1.14 ± 0.03
Broken Loop	
Cold leg temperature near reactor vessel (K)	554.3 ± 4.2
Hot leg temperature near reactor vessel (K)	561.9 ± 4.3
Steam Generator Secondary Side	
Liquid temperature (K)	547.1 ± 0.8
Pressure (MPa)	5.85 ± 0.06
Mass flow (kg/s)	19.1 ± 0.4

3. SUMMARY OF PARTICIPANT MODELS

Calculations were received from 11 participants of which eight were preceded by model submittals to qualify as blind calculations. Table 2 lists the participants and the identifier used for each participant in this report. Five different computer codes were used in the calculations. RELAP4/MOD6 was used in seven of the calculations and RELAP5 used in two analyses. Codes other than RELAP4 are identified as such on each comparison plot. The following discussion briefly summarizes the model of each participant.

3.1 Gesellschaft fur Reaktorsicherheit (GRS)

GRS used the DRUFAN 02 computer code to perform the blind calculation. The thermal hydraulic models in DRUFAN 02 are based on the solution for conservation of liquid mass, vapor mass, overall energy, and overall momentum. Determination of the critical flow at the break was made using a one dimensional nonequilibrium model which uses the geometry of the break path. The GRS calculation was terminated at 28.76 s after break initiation.

3.2 Japan Atomic Energy Research Institute (JAR)

The JAERI Division of Nuclear Safety Evaluation used an improved version of RELAP4/MOD6 for their blind calculation. Most of the major modifications to the code were developed for small break analyses, so the code used in the ISP-13 calculation was essentially equal to the original RELAP4/MOD6 code. Critical flow was calculated using Henry-Fauske/HEM with a discharge coefficient of 0.85 for both the subcooled and saturated region. The calculation was terminated 50 s after initiation of the break.

TABLE 2. SUMMARY OF ISP-13 PARTICIPANTS

Organization	Participant	Code	ID
Gcsellschaft fur Reaktorsicherheit mbh Forschungsgeland (West Germany)	W. Pointner	DRUFAN 02	GRS
Japan Atomic Energy Research Institute	F. Tanabe K. Yoshida	RELAP4/MOD6	JAR
Japan Atomic Energy Research Institute	M. Akimoto M. Hirano	THYDE-P1	JAT
Central Electricity Research Laboratories (United Kingdom)	A. H. Schriven	RELAP4/MOD6	CERL
Studsvik Energiteknik AB (Sweden)	O. Sandervag	RELAP5/MOD1	STUD
Eidgenossisches Institute fur Reaktorforschung (Switzerland)	S. Guntay S. N. Aksan	RELAP4/MOD6	EIR
Los Alamos National Laboratory (USA)	T. Knight	TRAC-PD2	LANL
ENEL-CRTN (Italy)	L. Bella F. Donatini	RELAP4/MOD6	ENEL
D'partimento di Construzioni Miccaniche e Nucleari (Italy)	M. Mazzini	RELAP4/MOD6	DCMN
Commissariat A l'Energie Atomique (France)	R. Pochard Y. Macheteau	RELAP4/MOD6	CEA
Technical Research Centre of Finland	H. Holmstrom V. Yrjola	RELAP5/MOD1, cycle 19	VTT

3.3 Japan Atomic Energy Research Institute (JAT)

The Nuclear Safety Code Development Laboratory at JAERI performed their blind calculation with THYDE-P1. The critical flow model used the modified Zaloudek and Moody correlations in the calculation with a Moody discharge coefficient of 0.6. Only the average core channel was modeled with THYDE-P1; no hot channel analysis was performed. The calculation was terminated 69.84 s after the initiation of the break.

3.4 Central Electricity Research Laboratories (CERL)

The CERL blind calculation was performed with RELAP4/MOD6. Critical flow was calculated using Henry-Fauske/HEM with a multiplier of 0.875 and a transition quality of 0.025. Separate hot pins and reflood models were used in conjunction with the average core blowdown model. The calculation was terminated 37 s after break initiation.

3.5 Studsvik Energiteknik AB (STUD)

Sweden's blind submittal of ISP-13 was performed using RELAP5/MOD1, Cycle 14. The RELAP5 critical flow model was used with a discharge coefficient of 0.87. The calculation was terminated 55 s after the break initiation.

3.6 Eidgenossisches Institut fur Reaktorforschung (EIR)

EIR performed both a blind and an open calculation for ISP-13 using RELAP4/MOD6. For the blind calculation only a single core volume was used; in the open calculation, two parallel, multivolume core channels were modeled. Except for the core, the blind and open models were identical. Critical flow was calculated using Henry-Fauske/HEM, with multipliers of 0.8 and 0.848 respectively. The blowdown portions of the calculations were terminated at 44 s, while separate reflood calculations were run out to 100 s.

3.7 Los Alamos National Laboratory (LANL)

The open calculation of ISP-13 submitted by LANL was performed using the TRAC-PD2/MOD1 computer code. TRAC-PD2 features a three dimensional treatment of the reactor vessel, two phase nonequilibrium hydrodynamic models and flow regime-dependent constitutive equations. The code does not contain a critical flow model; break flow was calculated using break geometry and a normal field equations in the code. The LANL calculation was terminated 100 s after break initiation.

3.8 ENEL-CRTN

The ENEL blind calculation was performed with RELAP4/MOD6. The model used two parallel, multivolume core channels, representing the average and hot channels. Henry-Fauske/HEM was used to calculate critical flow, with multipliers of 0.865 and 0.7 for subcooled and saturated flow respectively. The long term calculation was terminated at 160 s after break initiation. Due to problems with the output tape, only the short term plots (0-30s) were available for the comparisons in this report.

3.9 Dipartimento di Construzioni Meccaniche e Nucleari (DCMN)

DCMN performed an open calculation of ISP-13 using RELAP4/MOD6. Critical flow was modeled with Henry-Fauske/HEM with discharge coefficients of 0.84. Transition quality was set at 0.003. The MOD6 heat transfer package (HTS2) was used in the calculation. The calculation was terminated 30 s after break initiation.

3.10 Commissariat A l'Energie Atomique (CEA)

The CEA blind submittal was performed using RELAP4/MOD6. Henry-Fauske/HEM was used to model critical flow, with discharge coefficients of 1.0 and a transition quality of .0025. The calculation was terminated 56 s after break initiation.

3.11 Technical Research Center of Finland (VTT)

The VTT open calculation was performed using RELAP5/MOD1, Cycle 19. Updates to the FIDRAG subroutine, which calculates the drag between fluid phases, were added. A discharge coefficient of 0.84 was applied to the RELAP5 critical flow model. The calculation was terminated 60 s after the break was initiated.

4. SUMMARY OF BLIND RESULTS

Eight ISP-13 submittals were designated blind calculations. This designation was given to those participants who submitted the models to be used in the calculation prior to the performance of experiment L2-5. The comparison of these calculations with measured data is presented in the following sections.

4.1 Sequence of Events

The measured and calculated sequence of events for L2-5 are summarized in Table 3. The experiment was initiated by opening the two QOBVs. The primary coolant pumps were turned off and the primary coolant system depressurized to saturation, both by 1 s. The cladding temperatures in the central fuel assembly departed from saturation within 2 s. Accumulator injection began at 16.8 s. The maximum cladding temperature of 1077 K (1479°F) was reached at 28.5 s, just prior to the completion of lower plenum refill. High pressure injection (HPI) was initiated at 23.9 s; low pressure injection began at 37.3 s.

Most of the blind calculated sequence of events were in accord with data. The calculated end of subcooled blowdown ranged from 0.05 s (STUD, CEA) to 0.09 s (JAR). Reactor scram ranged from 0.0 s (EIR) to 0.25 s (STUD). Cladding temperatures began to deviate from saturation between 0.51 s (STUD) and 1.42 s (EIR). Both Japanese submittals tripped the reactor coolant pumps early, at the time of the break. The participants calculated pressurizer voiding between 5.0 s (ENEL) and 17 s (CEA), compared to the 15.4 s seen in the data. Accumulator initiation ranged from 12.8 (STUD) to 19.3 s (ENEL). The time of maximum peak clad temperatures calculated by the participants deviated significantly from data, ranging between 10 s (GRS) and 50 s (ENEL). Only CERL's calculation reached a peak within 5 s of data at 24.0 s but their peak clad temperature of 1155 K (1600°F) was significantly higher.

TABLE 3. MEASURED AND CALCULATED SEQUENCE OF EVENTS FOR LOFT EXPERIMENT L2-5

Event	L2-5	JAR	CERL	EIR	ENEL	GRS	JAT	STUD	CEA	LANL	EIR	DCMN	VTT
L2-5 initiated	0.0	0.0	0.0	0.0	--a	0.0	0.	0.0	0.	0.0	0.0	0.0	0.0
Subcooled blowdown ended	0.043	0.09	0.056	0-.1		0.07	0.1	0.05	.05	--	0.-.1	--	.06
Reactor scrammed	0.24	0.11	0.24	0.0	.1	0.097	0.0	0.251	.24	.24	0.0	.241	.1
Clad temperatures deviate from saturation	0.91	1.15	0.8	1.42	--	0.67	0.6	0.51	--	1.0	1.42	.9	.5
RCP trip	0.94	0.0	0.94	1.0	.9	1.0	0.0	0.951	.94	.24	1.0	.941	.94
Subcooled break flow end	3.4	3.04	4.1	3-4	3.3	3.3	4.0	4.0	--	4.0		3.5	4.0
PZR emptied	15.4	14.4	10.2	10.	5.0	12.1	--	15.0	17. 28.0	16.5(95%) (99%)	8.0	15.3	15.0
Accumulator initiated	16.8	17.36	16.8	13.8	19.3	16.02	17.0	12.85	15.2	17.75	15-16	16.6	16.3
HPI initiated	23.9	24.8	24.0	22.0	23.9	24.05	22.25	23.91	24.4	23.9	22.0	23.91	24.0
Maximum PC temperature reached	28.47	48.8	24.0	10.	50.0	10.0	5.0	12.85	--	50.0	38.0	--	5.2
LPI initiated	37.32	35.0	37.0	35.	37.3	--	34.75	37.31	36.3	37.32	35.0	--	37.2

a. -- = not calculated.

4.2 Pressure

The comparison between calculated pressurizer pressure and data is presented in Figure 2. JAR and CEA calculated a pressurizer depressurization slower than that seen in the experiment, while all other participants calculated a faster depressurization with STUD's calculated rate being the most severe. ENEL's calculation apparently included the isolation of the pressurizer component at 5.0 s.

Comparisons of pressure for the intact loop cold leg, broken loop hot leg, broken loop cold leg, and upper plenum are shown in Figures 3 through 5, respectively. Generally all participants, except ENEL, calculated pressure histories below that actually observed in the data. ENEL's calculation was consistently high out to 30 s. STUD again had the lowest pressures over all. The CEA calculation displayed some interesting discrepancies. Their calculation of cold leg pressures, both broken loop and intact loop were extremely close to data. However, the broken loop hot leg pressure calculated by Mssrs. Pochard and Macheteau showed an initial 5 MPa (725 psi) pressure drop below that of all the other participants. In the upper plenum, the CEA pressure history was decidedly higher than the rest of the calculations. Analyzing the reasons for this pressure discrepancy is beyond the scope of this report.

Comparison of the steam generator secondary pressure (Figure 6) was complicated by the range of initial conditions used in the calculations. STUD, GRS, and CEA all underpredicted the equilibrium pressure in the generator. JAR's initial pressure was much higher than data, but stabilized out only slightly high. JAT's and CERL's equilibrium pressure exceeded data substantially. EIR's calculation predicted the secondary pressure response quite well.

4.3 Fluid Temperatures

Calculated upper plenum temperatures when compared to data in Figure 7 showed the saturation temperatures corresponding to the respective pressure

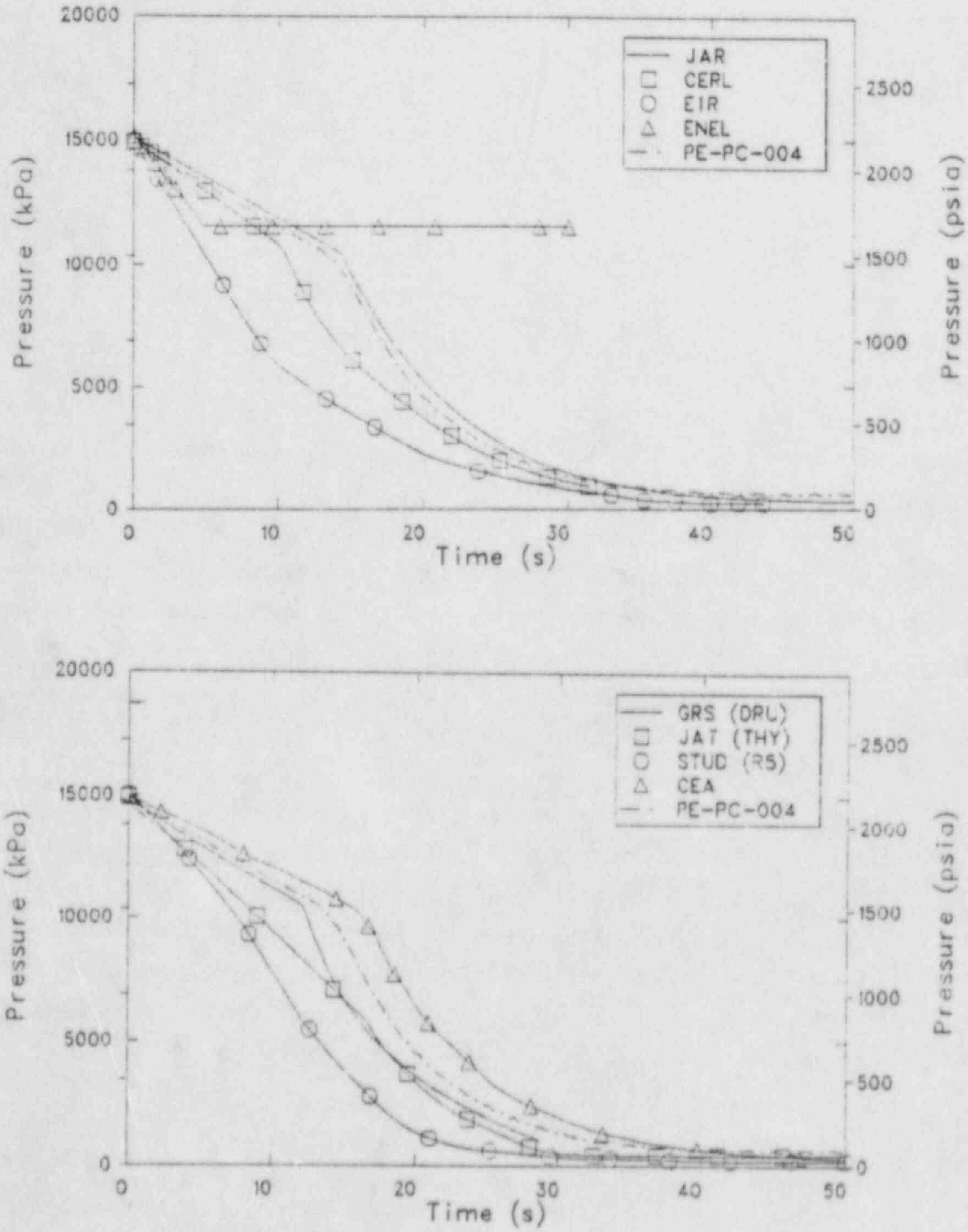

Figure 2. Comparison of measured and calculated pressurizer pressure for the blind calculations.

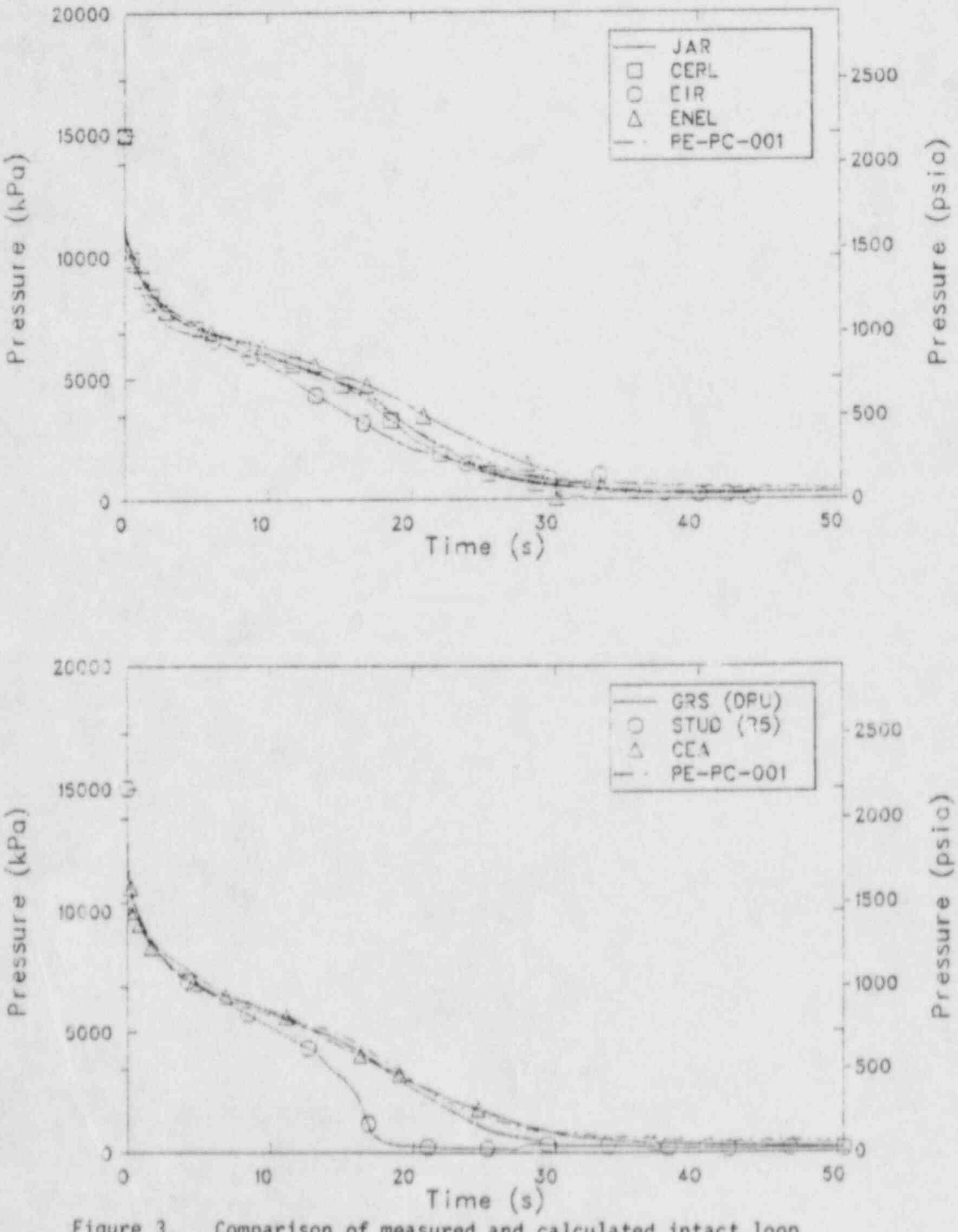

Figure 3. Comparison of measured and calculated intact loop cold leg pressure for the blind calculations.

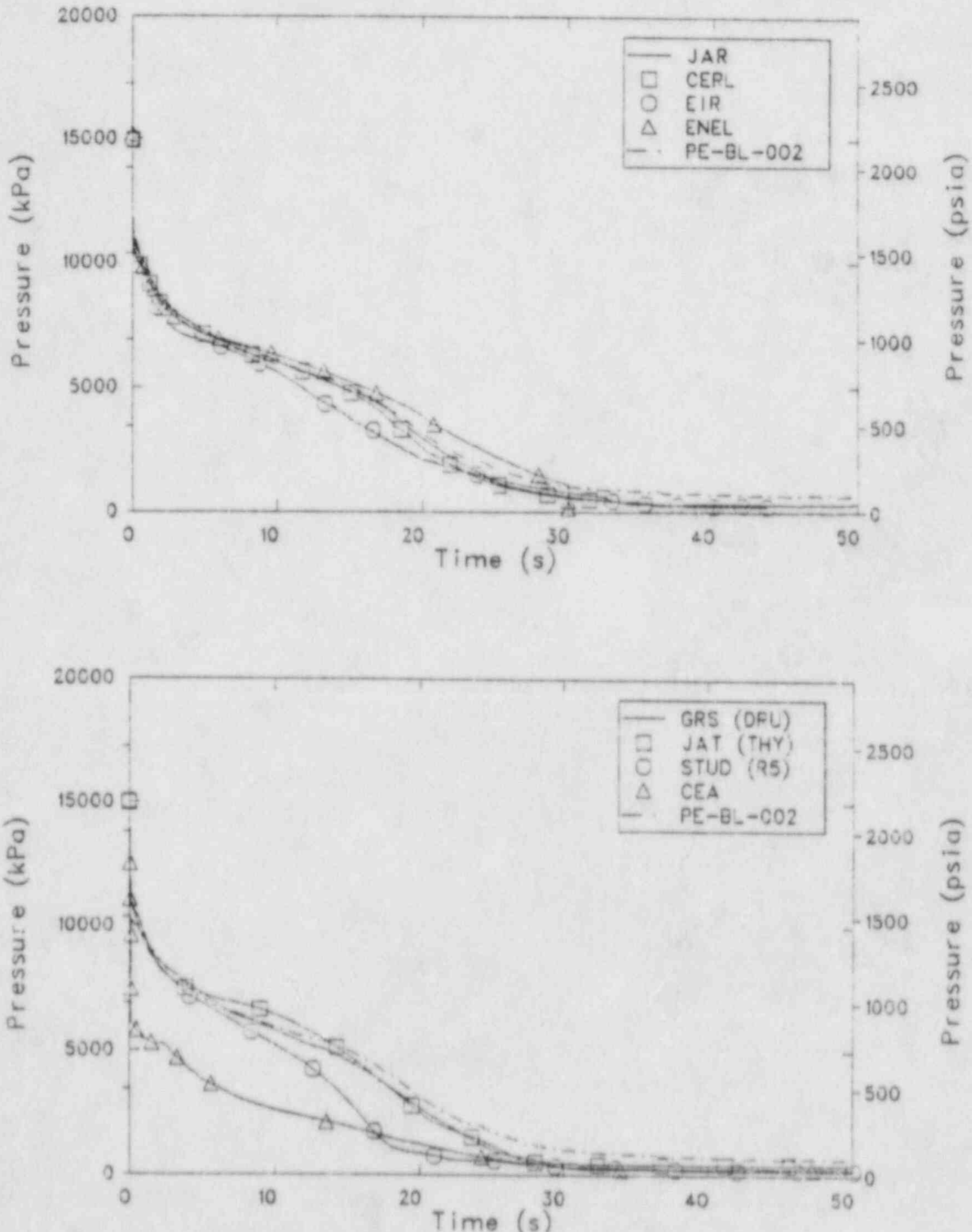

Figure 4a. Comparison of measured and calculated broken loop hot leg pressure for the blind calculations.

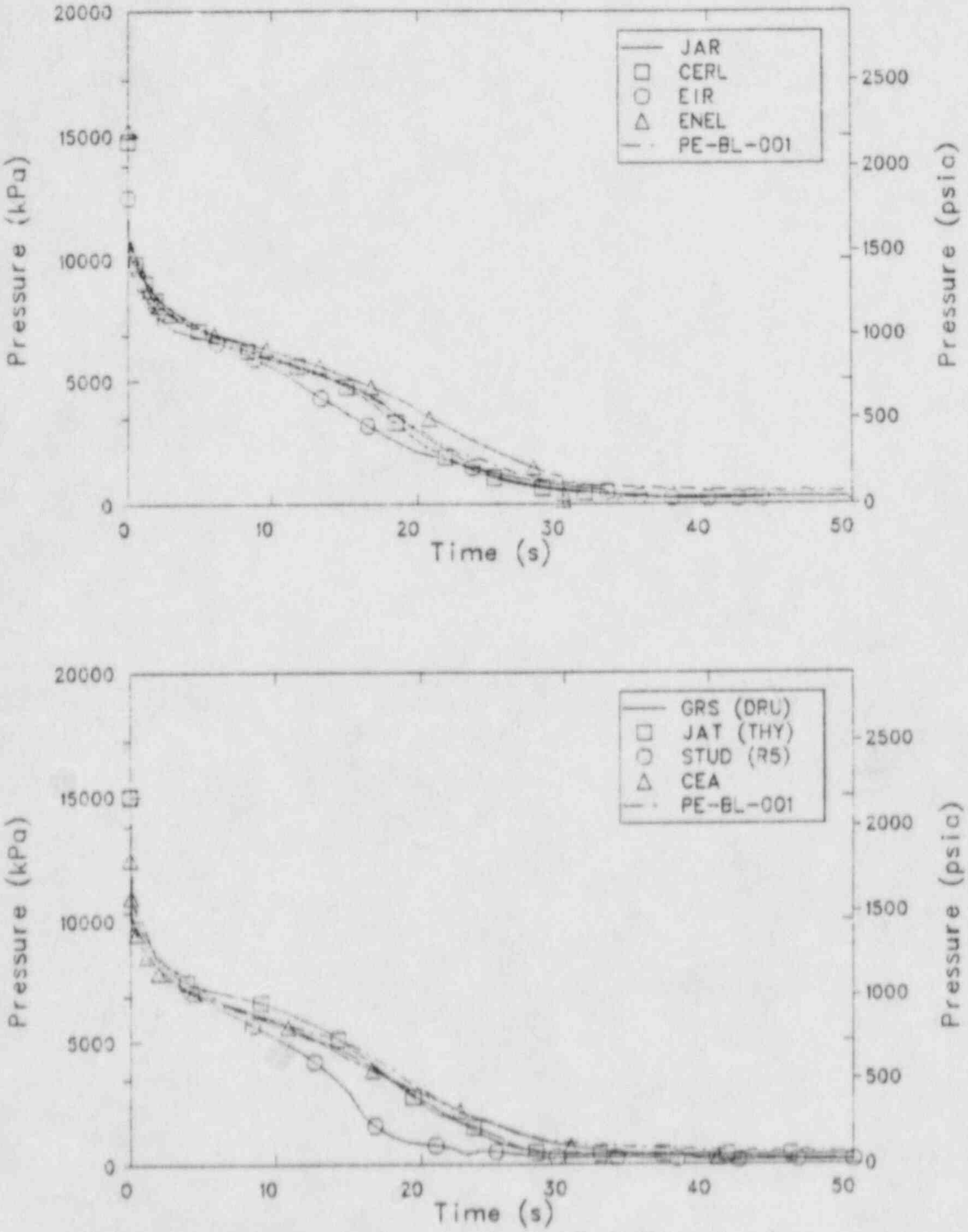

Figure 4b. Comparison of measured and calculated broken loop cold leg pressure for the blind calculations.

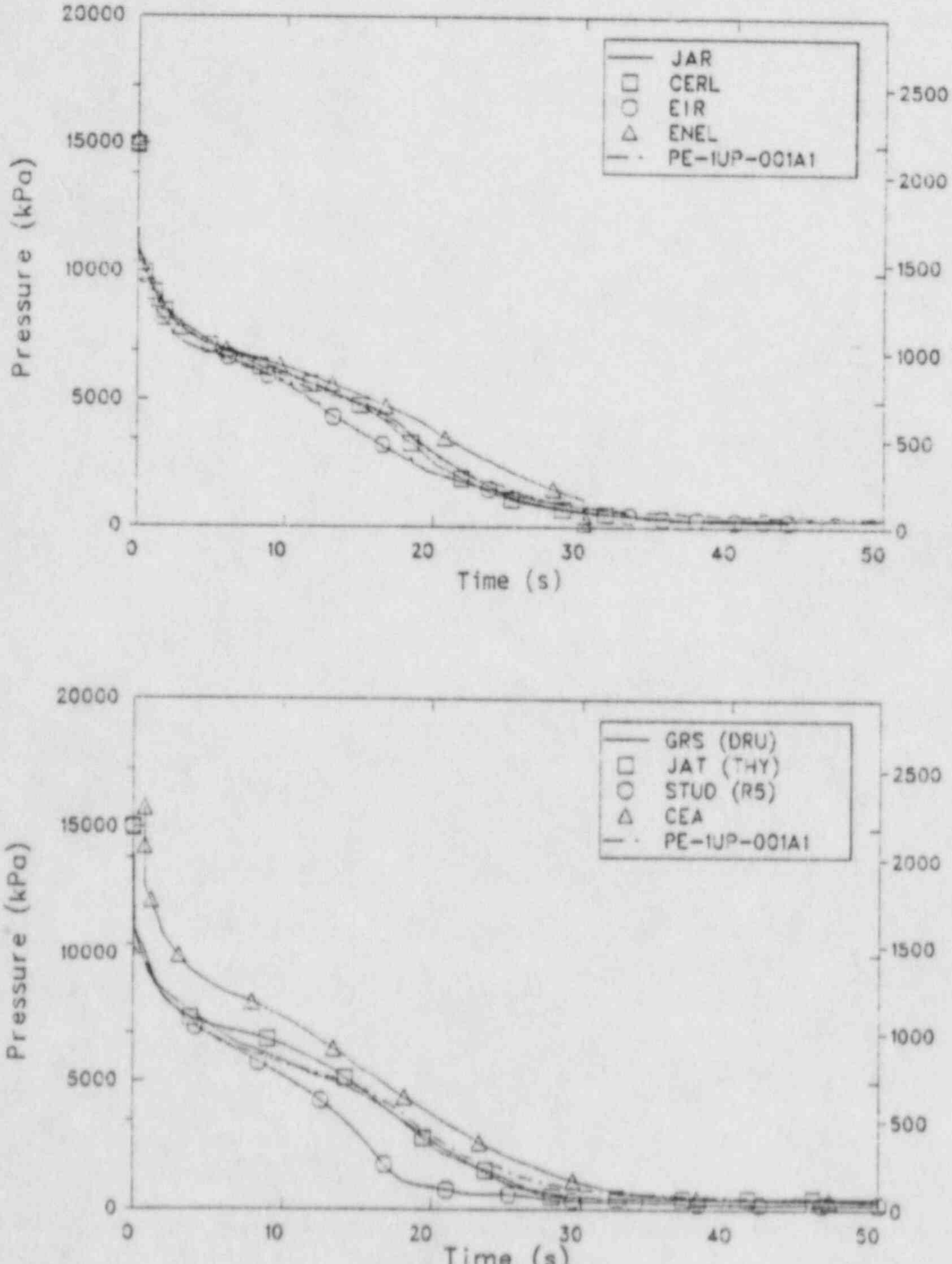

Figure 5. Comparison of measured and calculated upper plenum pressure for the blind calculations.

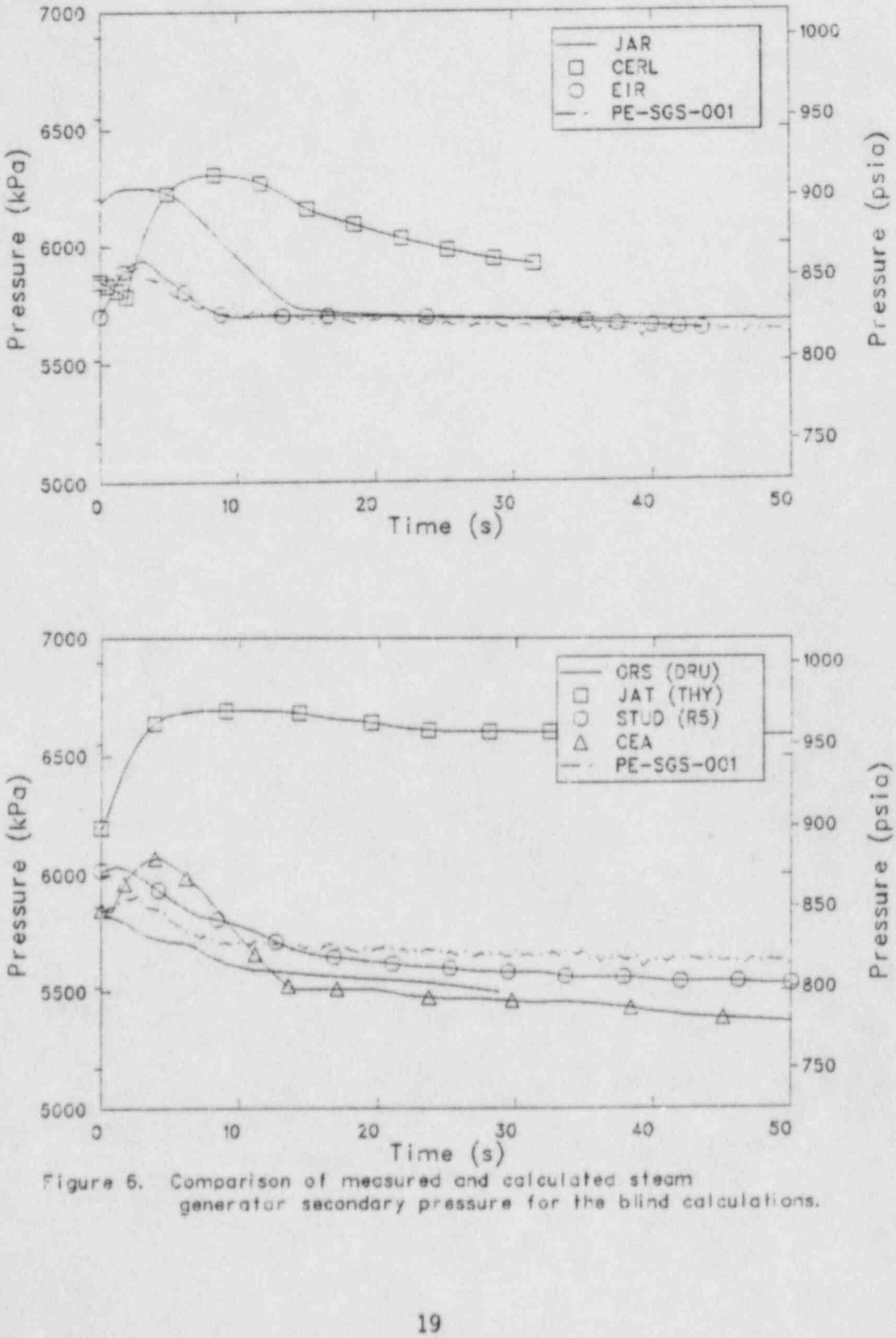

Figure 6. Comparison of measured and calculated steam generator secondary pressure for the blind calculations.

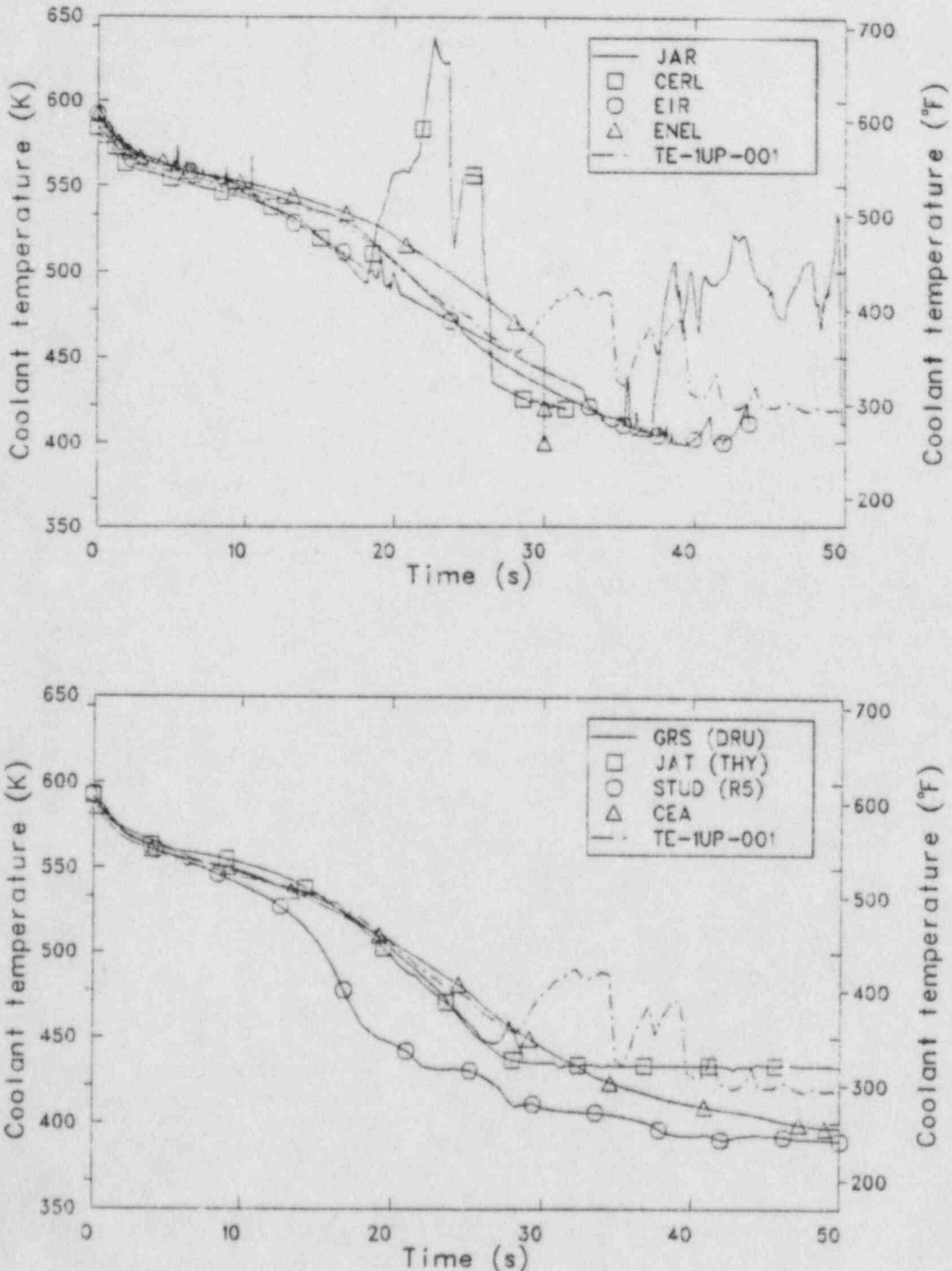

Figure 7. Comparison of measured and calculated upper plenum fluid temperature for the blind calculations.

histories. Ony ENEL and CEA fluid temperatures were consistently above data. Superheated fluid appeared in the data around 28 s. Several of the participants registered superheat at various times, ranging from 20 s (CERL) to 37 s (JAR). ENEL showed no superheat on the data plots, but their report plots show superheat beginning around 40 s. JAT, STUD and CEA showed no superheat at all in their upper plenum temperature histories.

Figure 8 compared calculated lower plenum temperatures with data, again showing the saturation temperature correspondence discussed above. JAR's RELAP4 calculation showed considerable superheat in the lower plenum starting at 27 s and quenches at 39 s. The JAT THYDE-P1 analysis registered an abrupt 68 K (124°F) drop in their temperature at 42 s, the only participant to calculate subcooling in the lower plenum.

In the intact loop cold leg temperature comparisons, seen in Figure 9, there was considerable variance in the fluid temperatures. None of the participants calculated the oscillatory behavior seen in the test. Most calculated some subcooling with GRS and JAT being the most pronounced, dropping to 310 K (100°F) at 20 s (GRS) and 31 s (JAT). The temperature drop in GRS, ENEL, and CERL appeared to correspond to the initiation of accumulator flow. There was no immediately available explanation for the drops seen by STUD and JAT.

Comparison of measured and calculated intact loop hot leg temperatures is presented in Figure 10. The LOFT experiment experienced some superheating in the hot leg around 28 s. Superheat was calculated by CERL (23 s), JAR (38 s) and JAT (34 s). None of the other participants calculated this superheating in the intact loop hot leg.

Pressurizer average temperature, shown in Figure 11 was underpredicted by all participants. This does not include the isolated pressurizer model used by ENEL.

The steam generator secondary temperatures, presented in Figure 12, reflect the various initial conditions used by the participants. In general the blind calculations, with the exception of JAT, remained above the equilibrium L2-5 temperature.

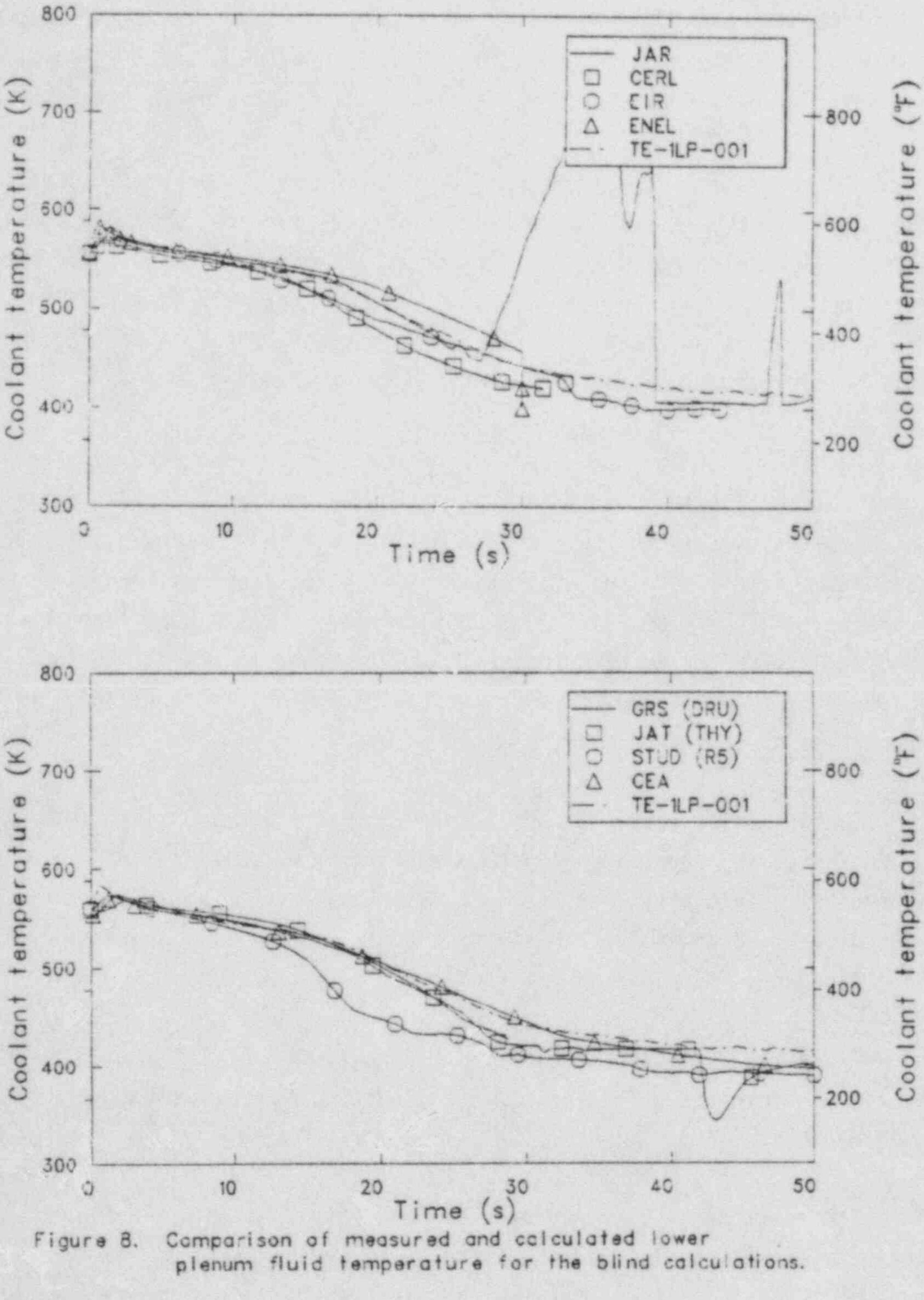

Figure 8. Comparison of measured and calculated lower plenum fluid temperature for the blind calculations.

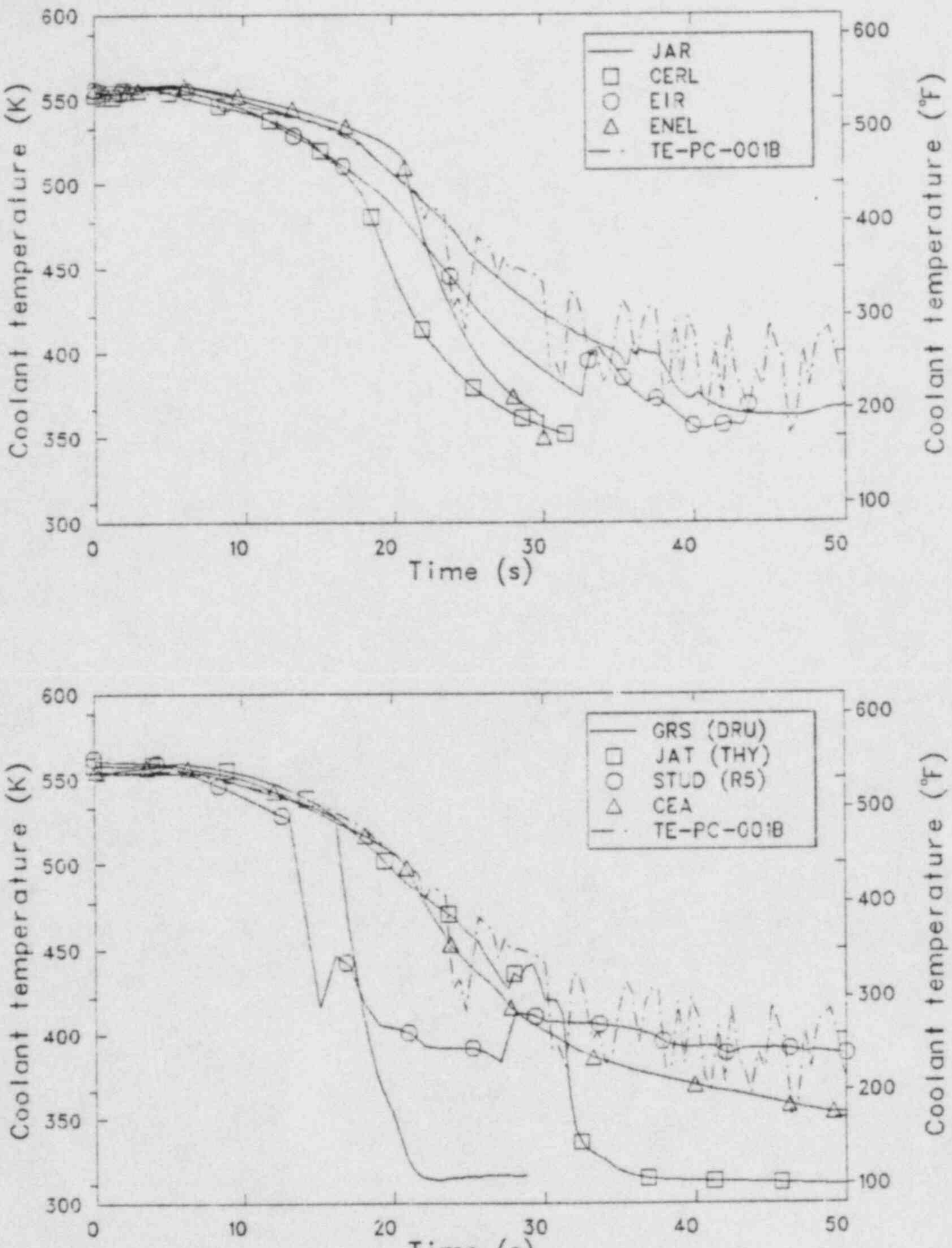

Figure 9. Comparison of measured and calculated intact loop cold leg temperature for the blind calculations.

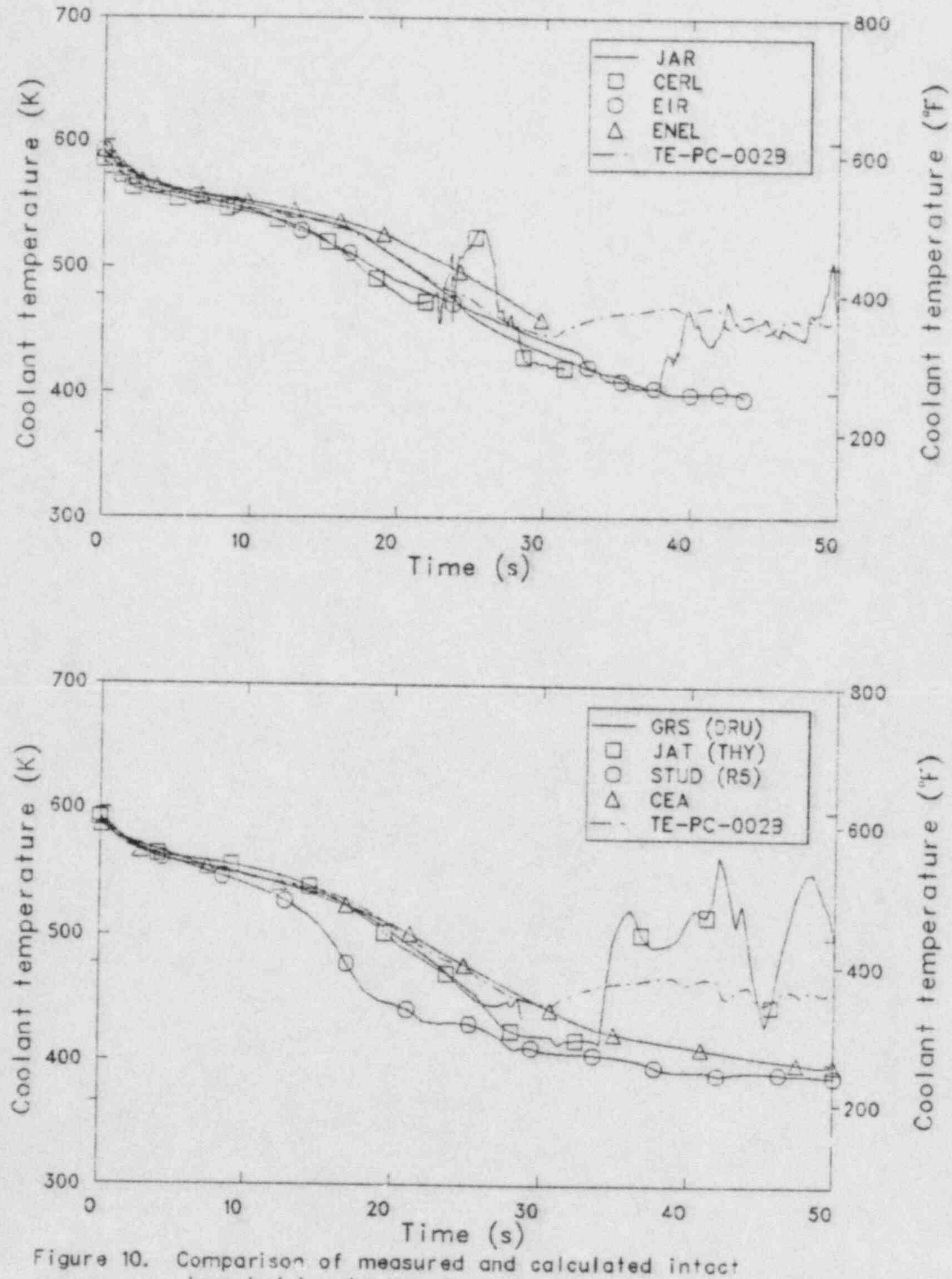

Figure 10. Comparison of measured and calculated intact loop hot leg temperature for the blind calculations.

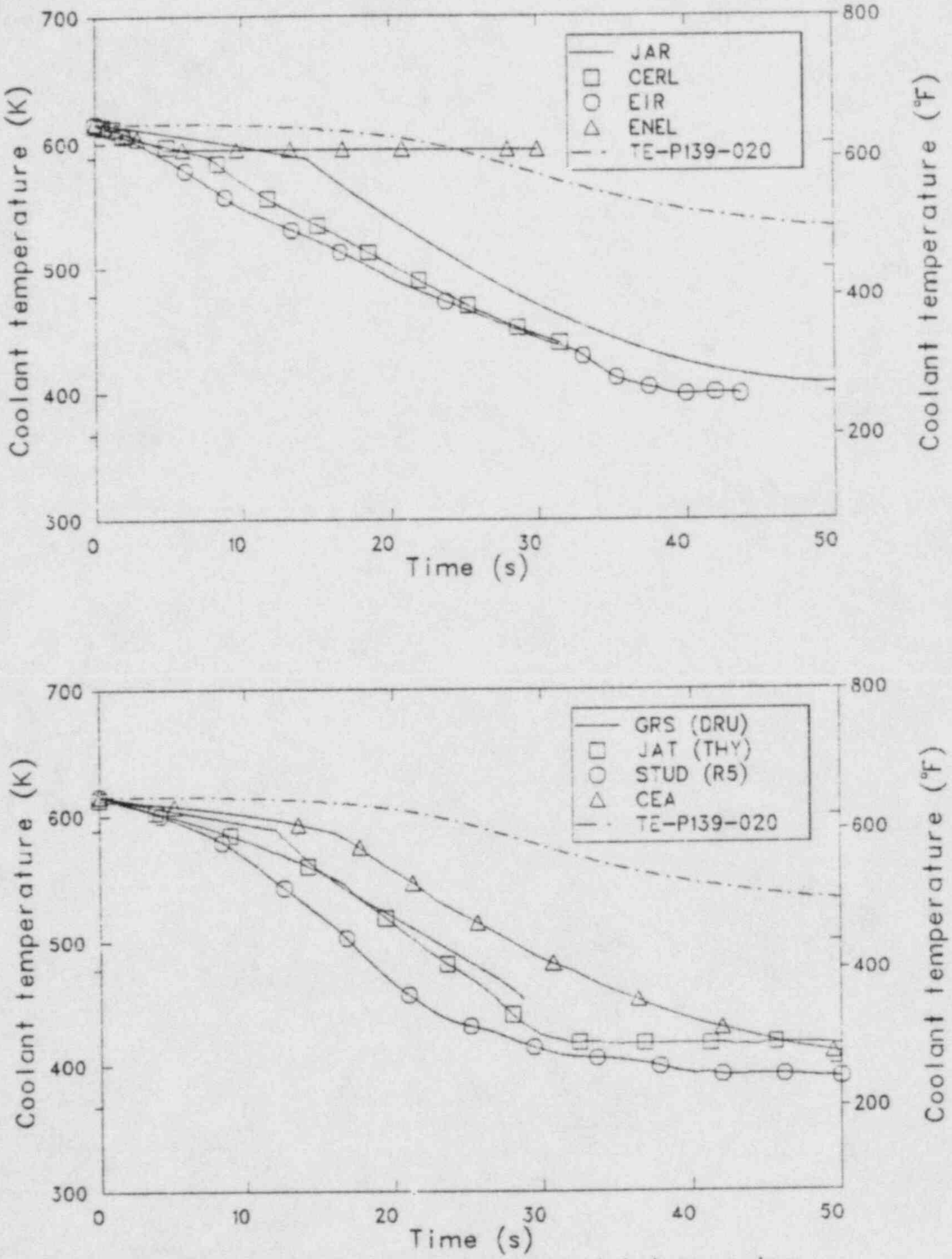

Figure 11. Comparison of measured and calculated pressurizer temperature for the blind calculations.

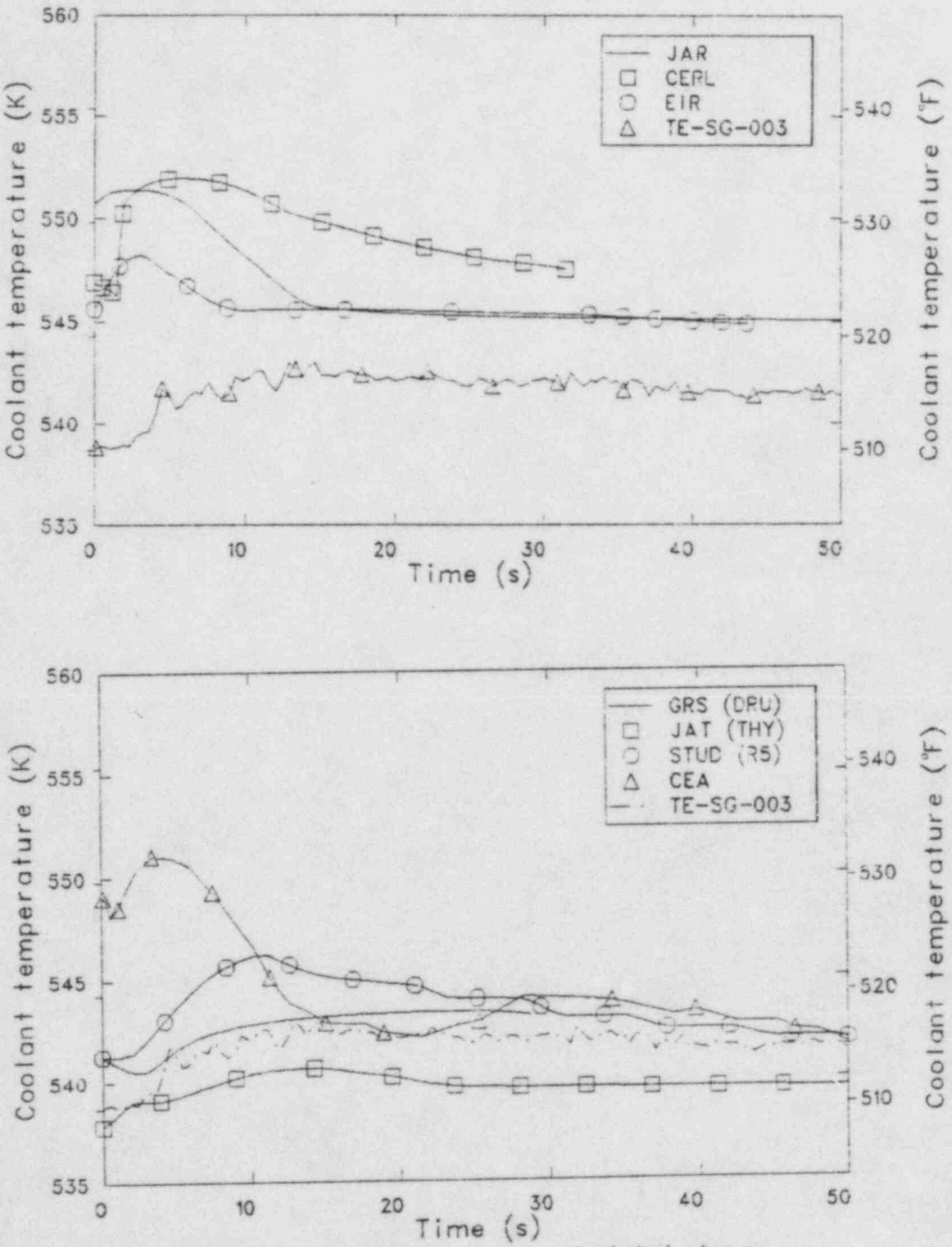

Figure 12. Comparison of measured and calculated steam generator secondary temperature for the blind calculations.

4.4 Fluid Density

The comparison between the calculated average volume density and the measured density in the intact loop cold leg showed significant differences as presented in Figure 13. Five calculations (CERL, EIR, ENEL, JAR, JAT) resulted in an initial voiding of the cold leg, followed by a complete refill. This refill time ranged from CERL's 16 s to JAT's 31 s. This refill was considerably different from the oscillations seen in the data. STUD calculated a single slug of liquid from 13 to 17 s, then calculated complete voiding. The remaining submittals simply voided the cold leg. The problem could be connected to the average density calculation and the difficulty the codes have calculating the effects of subcooled ECC injection.

There was better agreement between the average intact loop hot leg densities and the data taken in L2-5 as shown in Figure 14. By 30 s, all participants calculated a voided hot leg. JAT and ENEL calculated significantly higher density between 5 and 20 s than other submittals.

In the broken loop, both cold leg and hot leg shown in Figure 15 and 16 respectively, there was again considerable difference in the comparisons with the measured density and with the participants calculations themselves. All of blind calculations, with the exception of CERL, predicted a slower voiding in both legs during the first 10 s. In the hot leg, all participants' submittals showed a voided pipe after 20 s. In the cold leg, slug flow, seen in the data, was evident in the ENEL and CERL calculations. STUD, JAT, and EIR calculated major refills of the cold leg pipe starting at times ranging from 16 s (STUD) to 35 s (EIR). Both STUD's and JAT's analyses showed the cold leg pipe emptying again between 35 s and 42 s. EIR's calculation was terminated before the cold leg emptied.

4.5 Mass Flow

A comparison of the calculated core inlet flow, presented in Figure 17, shows the characteristic reversed core flow signature of a major cold leg break. All participants, except JAT, calculated approximately the

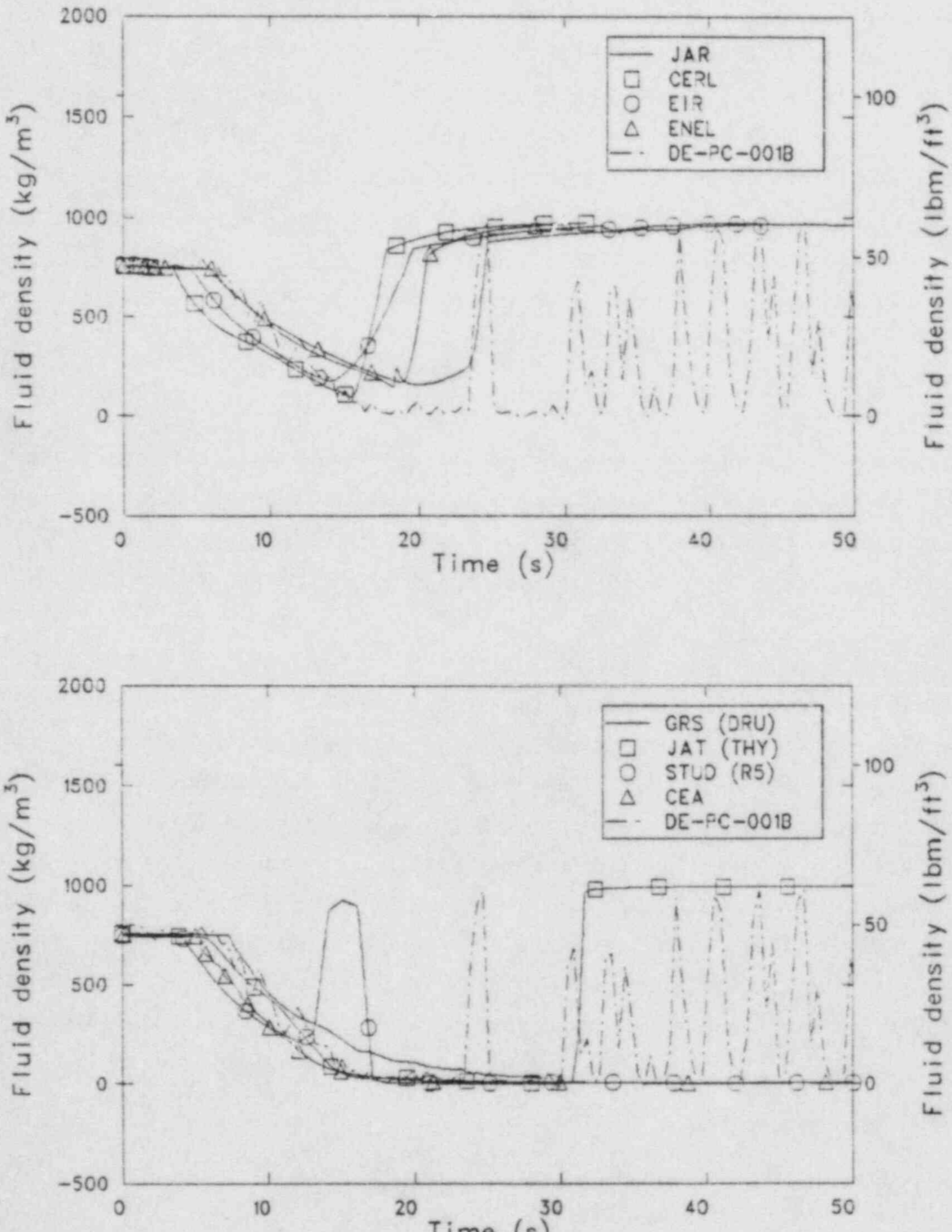

Figure 13. Comparison of measured and calculated intact loop cold leg density for the blind calculations.

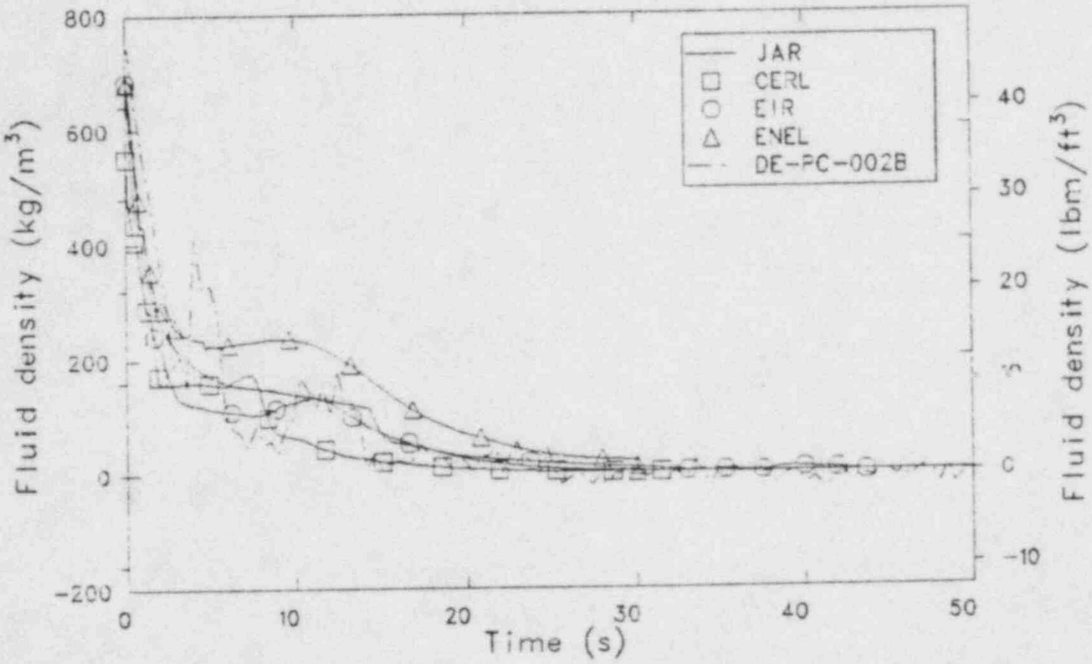

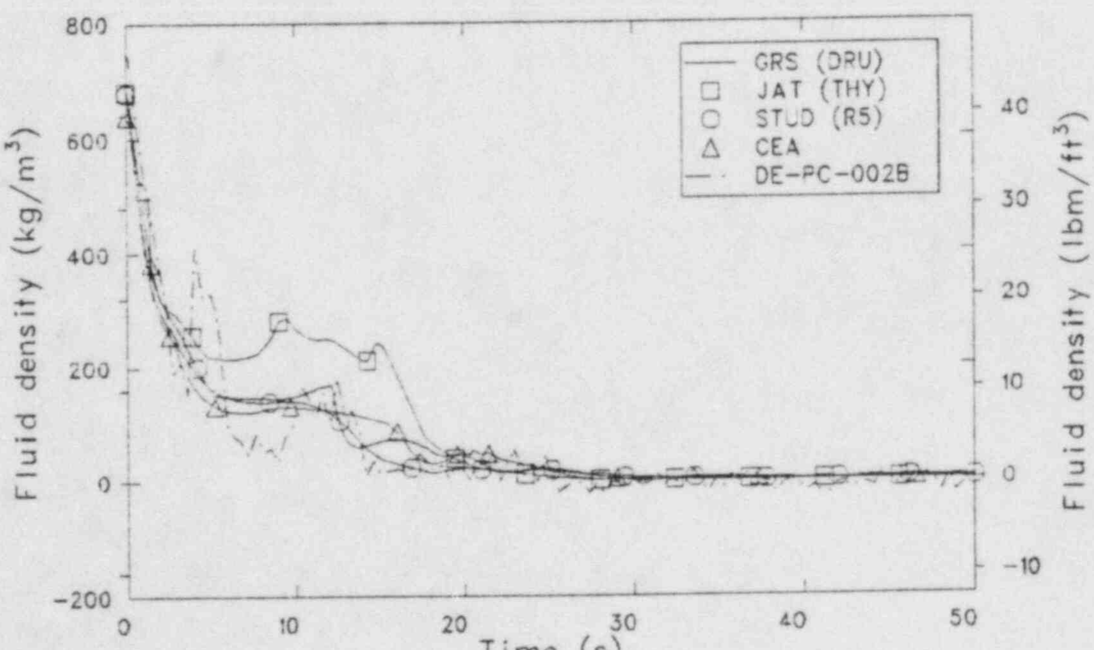

Figure 14. Comparison of measured and calculated intact loop hot leg density for the blind calculations.

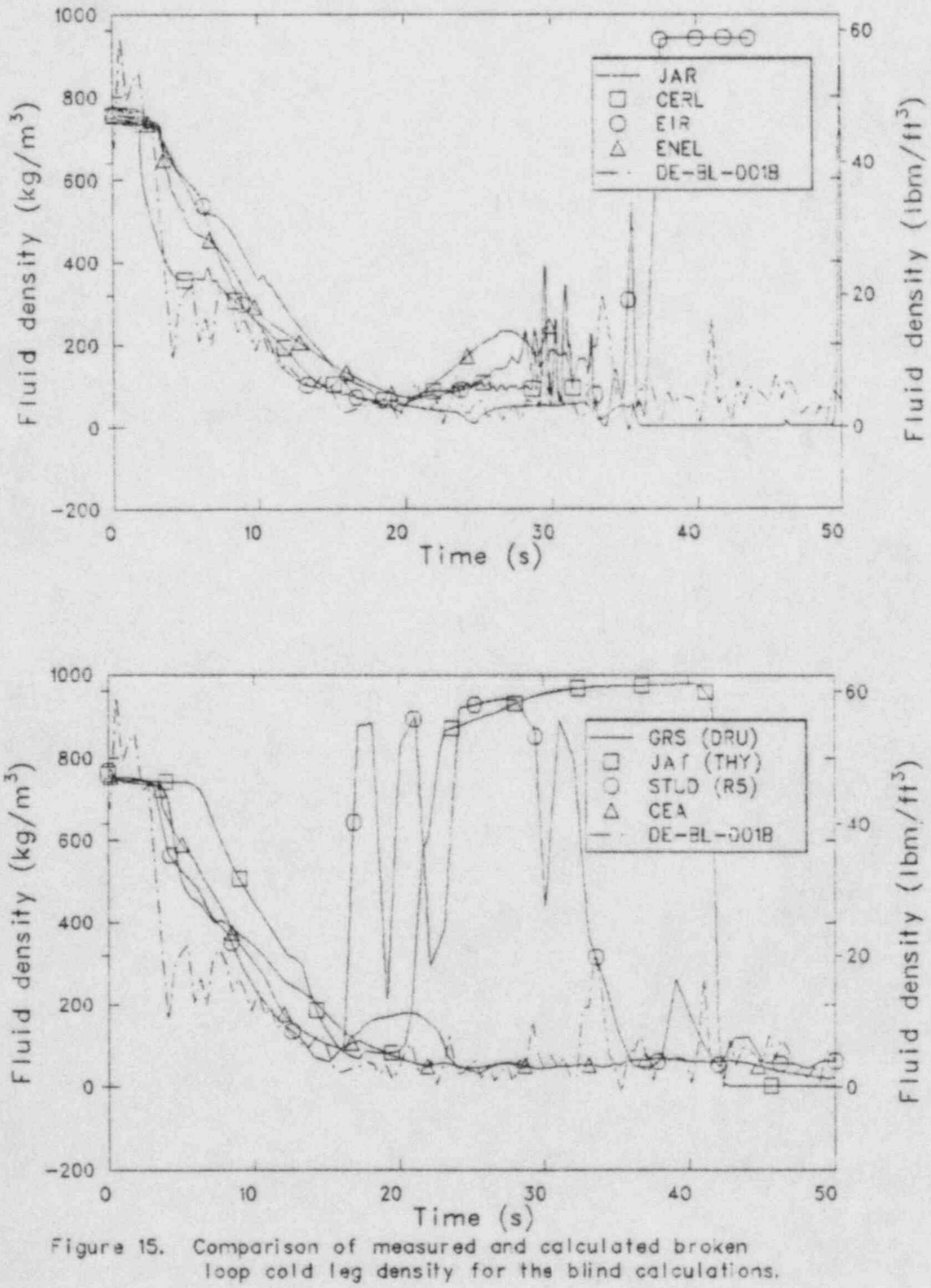

Figure 15. Comparison of measured and calculated broken loop cold leg density for the blind calculations.

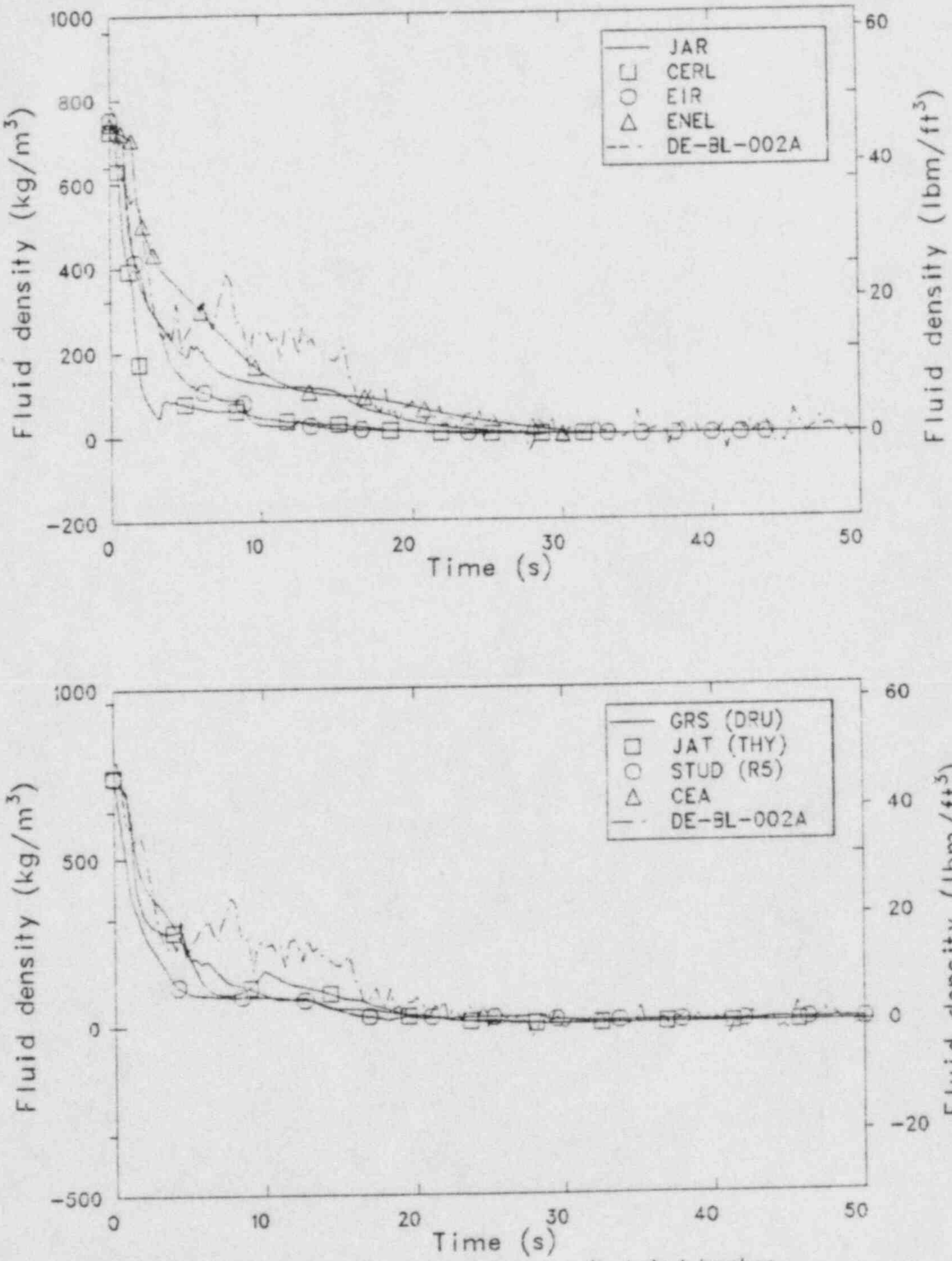

Figure 16. Comparison of measured and calculated broken loop hot leg density for the blind calculations.

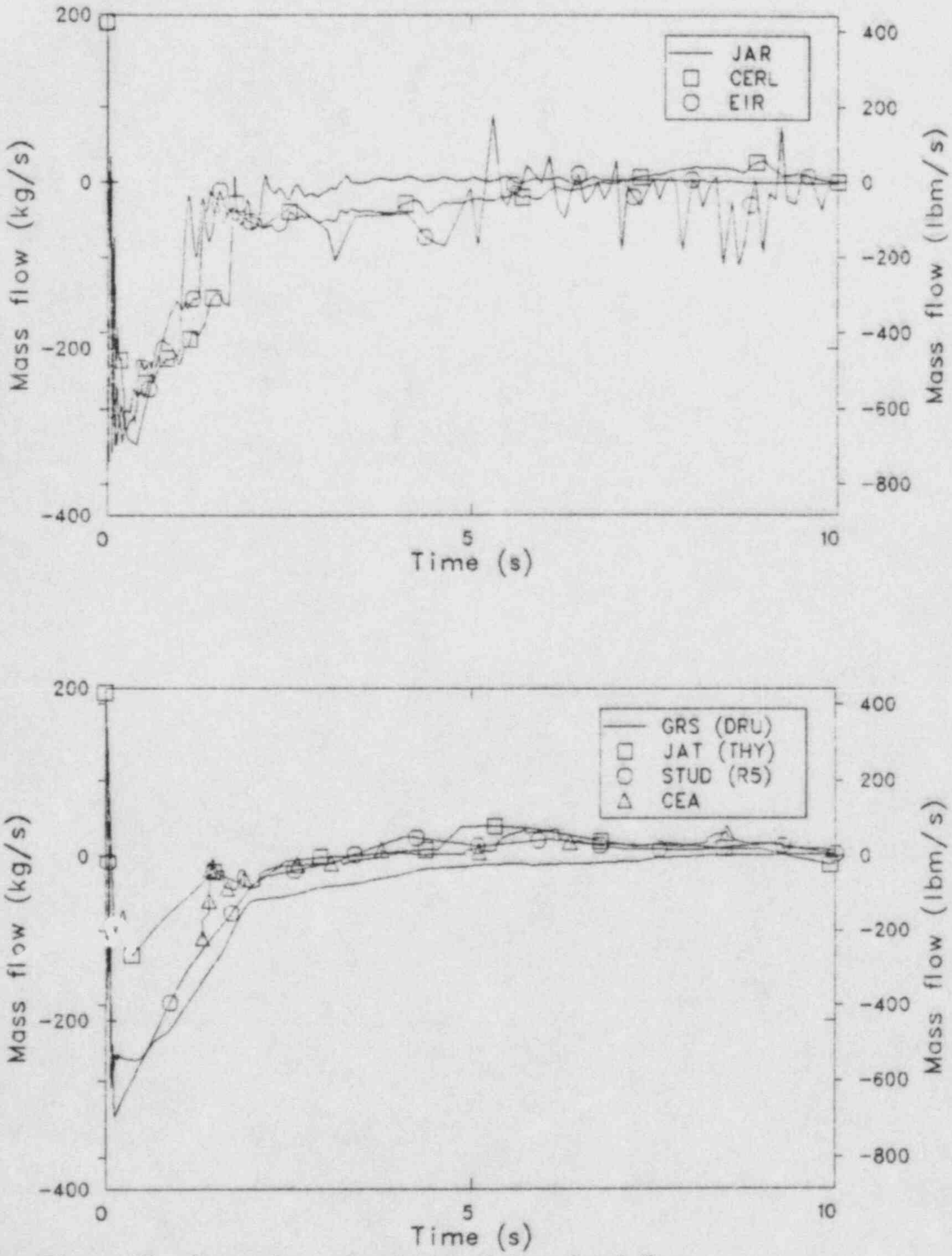

Figure 17. Comparison of calculated core inlet flows for the blind calculations.

same peak reverse flow rate. JAT's calculated peak flow was about 1/3 of that seen by the other calculations. By 10 s all calculated flows had essentially stopped.

For the calculation of a large pipe rupture, the break flow models were critical. As discussed in Section 3, virtually all participants used different models or multipliers for their break flow studies. Figure 18 and 19 present the results of these studies in comparison with data. In general the agreement between calculations and data is quite good. Peak cold leg flows calculated by CERL and CEA exceeded data significantly. In the hot leg only EIR underpredicted the break flow while most of the participants overpredicted the hot leg break flow. The discrepancies in break flow are better seen in Figure 20 which shows the integrated mass lost to the system through the breaks. EIR's calculated mass lost came the closest to matching data. JAT first underpredicted the mass lost during the first 9 s, then overpredicted. All other participants overpredicted the mass lost with STUD's mass lost being some 50% higher than data by 30 s.

Figure 21 shows the calculated mass inventory in the reactor vessel. While discrepancies in the initial mass make exact comparisons difficult, a qualitative review showed some explainable differences as well. EIR did not experience a refill in inventory, while STUD calculated an insurge between 15 s and 23 s, which emptied out by 30 s. GRS, JAT and JAR calculated refills starting between 25 s and 40 s.

Emergency core coolant injection is shown in Figures 22 and 23. All participants underpredicted the initial HPI peak flow. High pressure injection flow was overpredicted by STUD and JAT after the initial peak flow. Low pressure injection was calculated reasonably well by all participants, except JAR, which showed high flow as well as what appears to be some possible modeling problems.

4.6 Pump Speed

Pump coastdown, simulating the loss of offsite power in L2-5, is compared with data in Figure 24. Most participants followed the coastdown

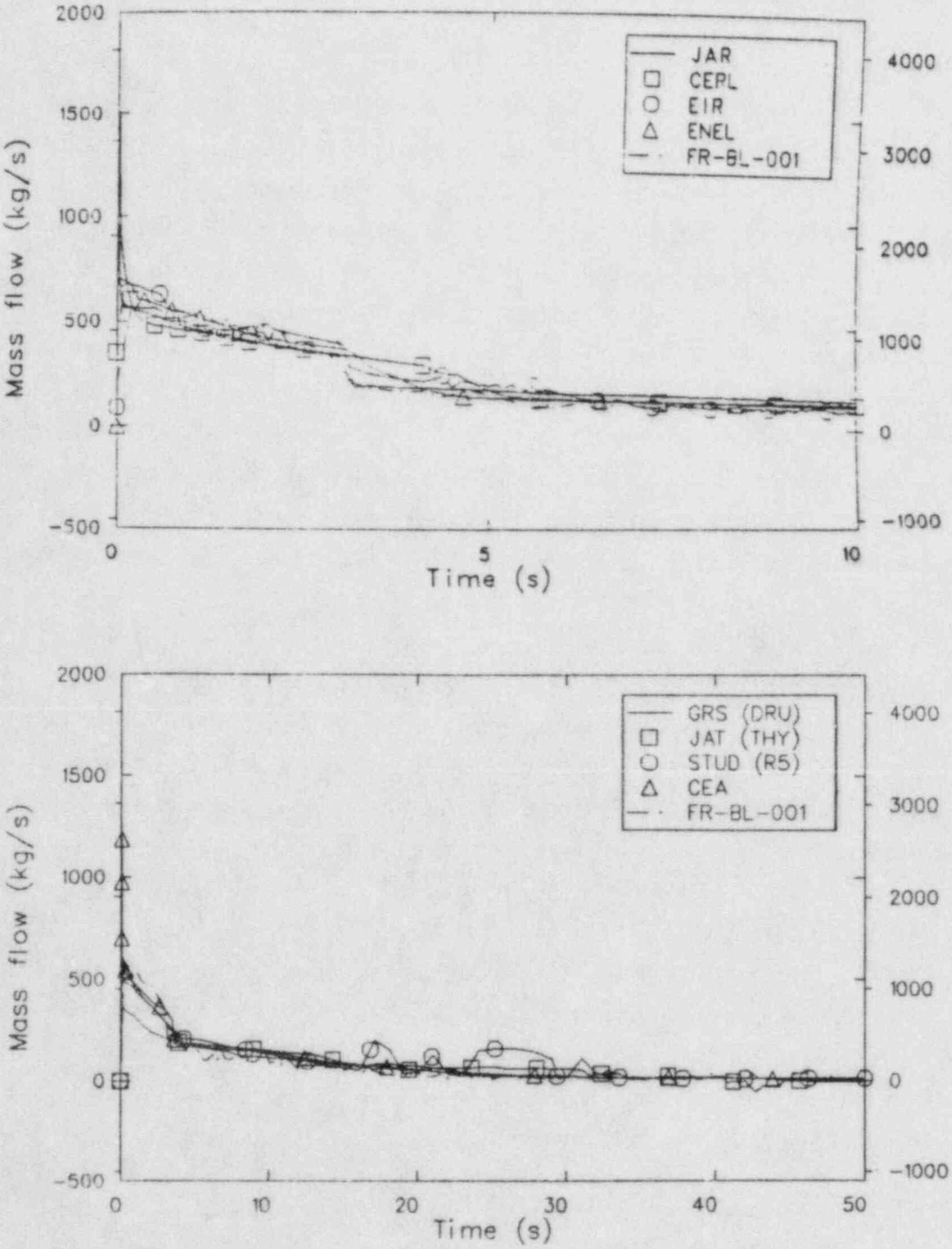

Figure 18. Comparison of measured and calculated broken loop cold leg break mass flow rate for the blind calculations.

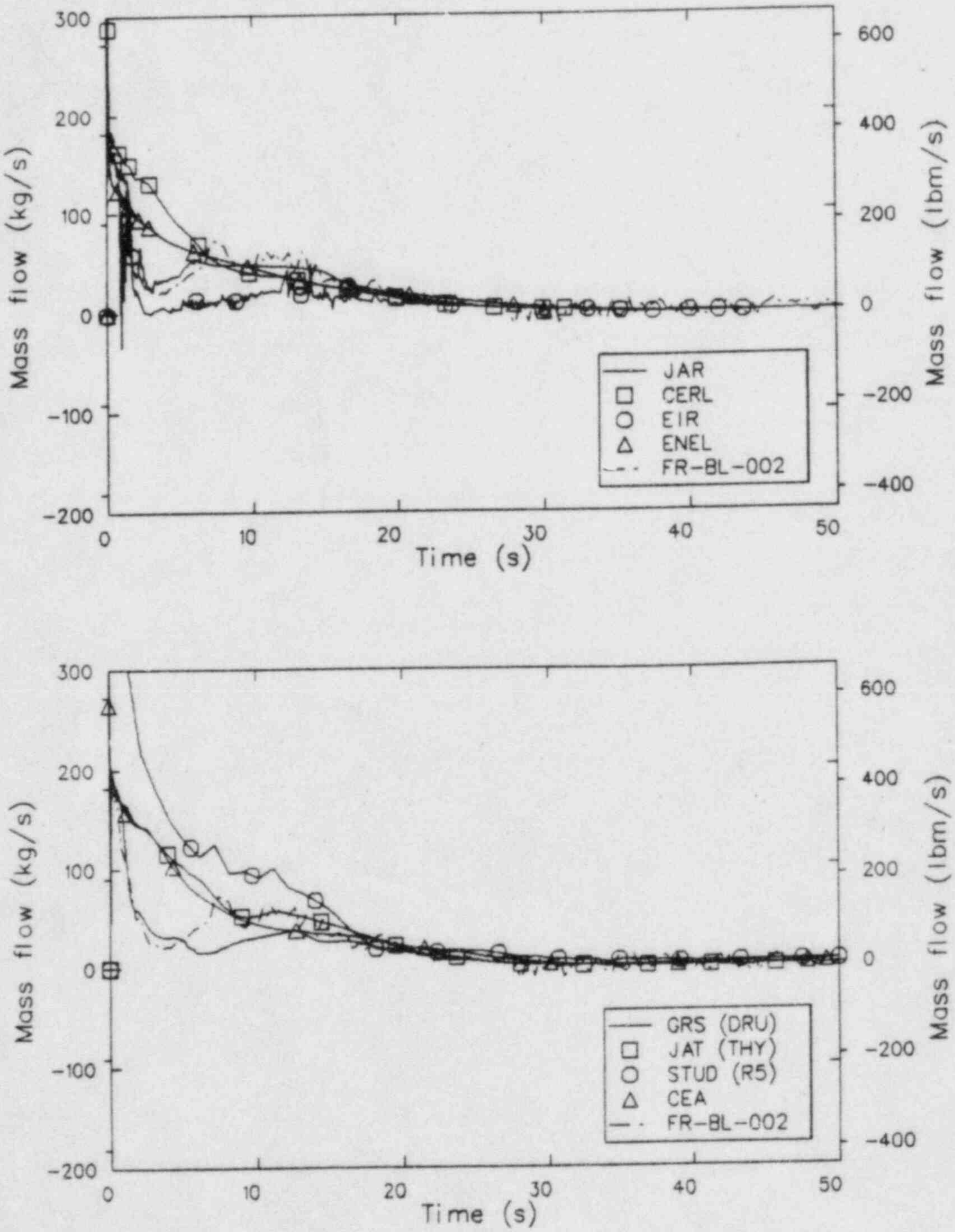

Figure 19. Comparison of measured and calculated broken loop hot leg break mass flow rate for the blind calculations.

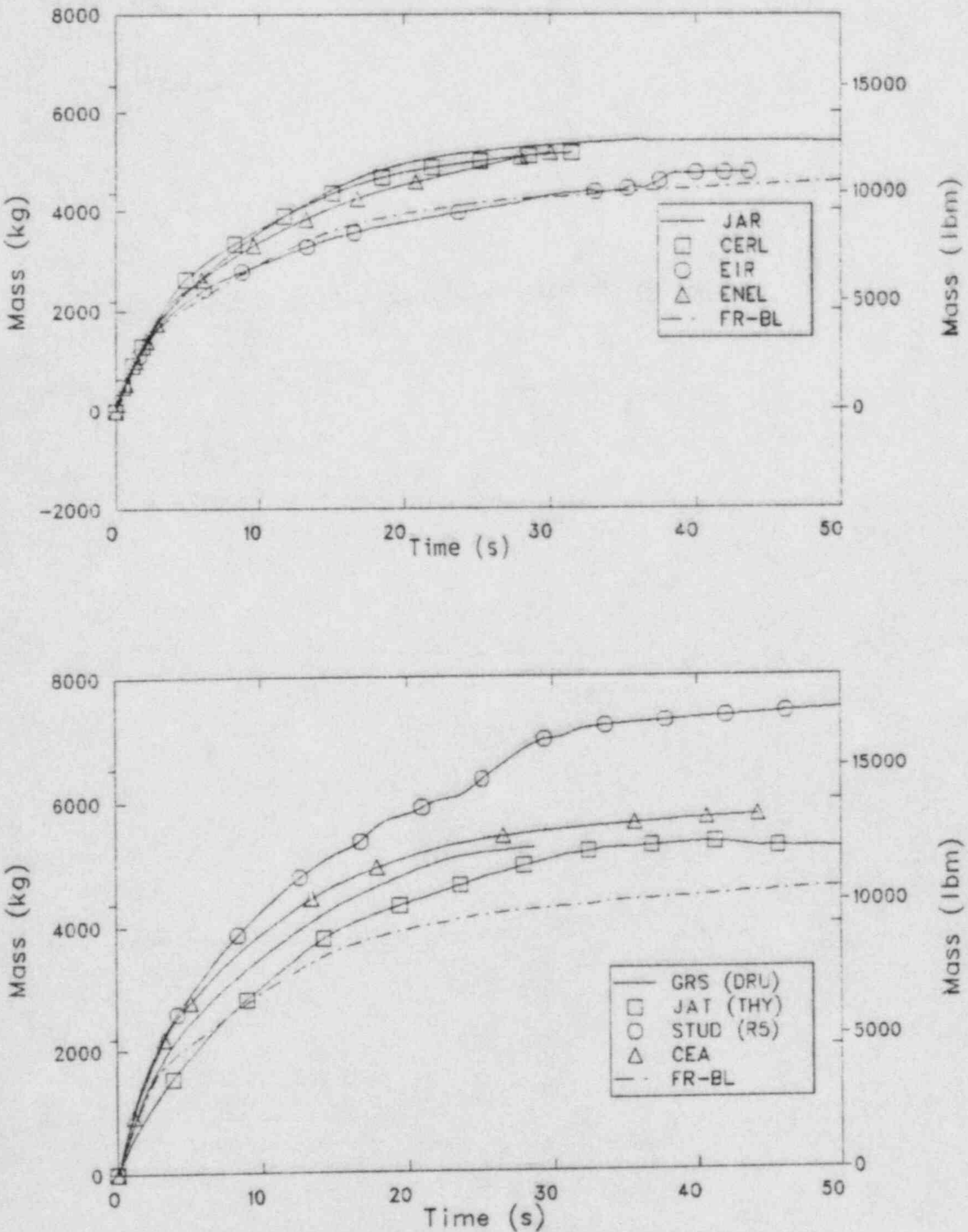

Figure 20. Comparison of measured and calculated integrated break flow for the blind calculations.

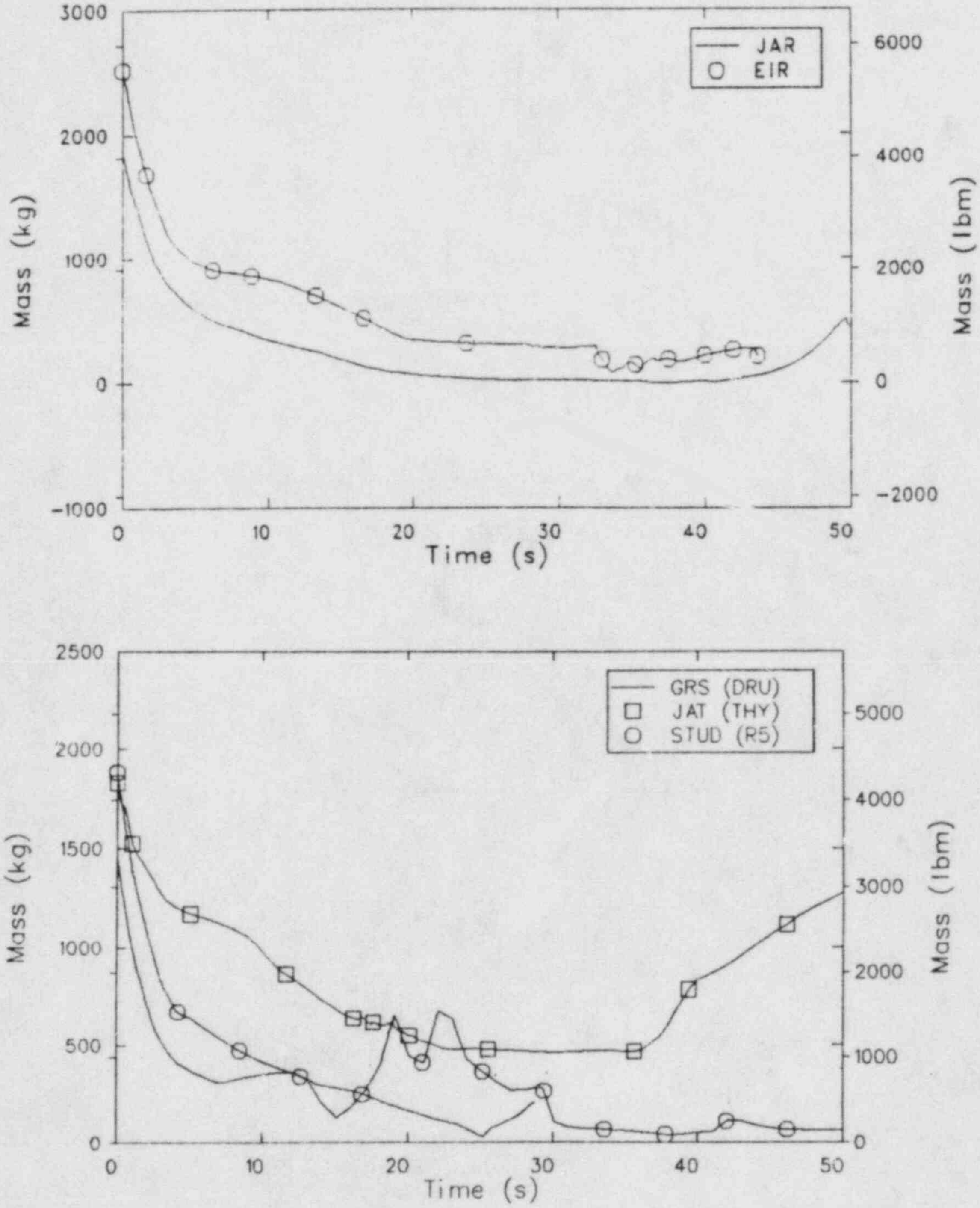

Figure 21. Comparison of calculated reactor vessel mass inventory for the blind calculations.

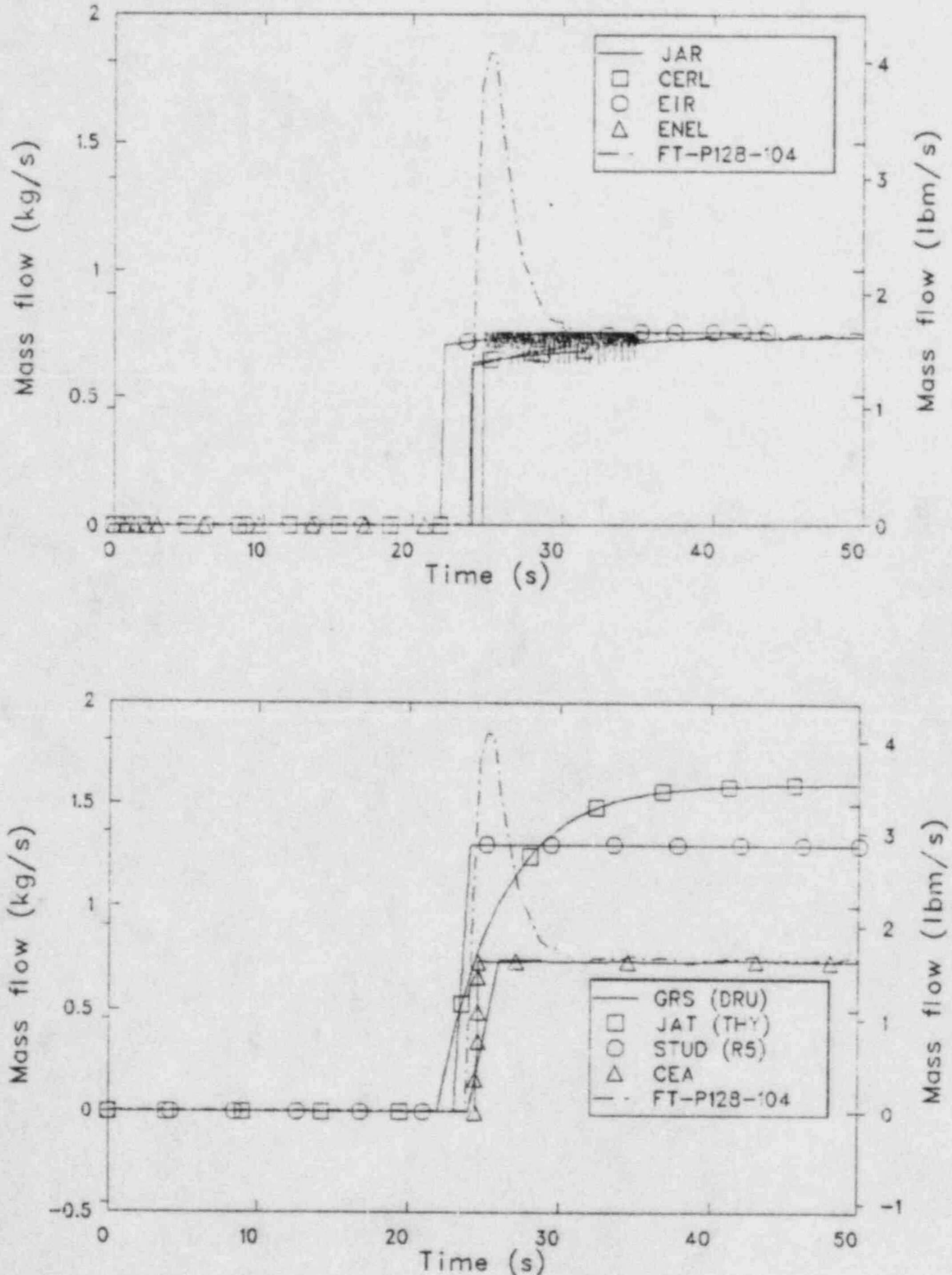

Figure 22. Comparison of measured and calculated HPIS flow for the blind calculations.

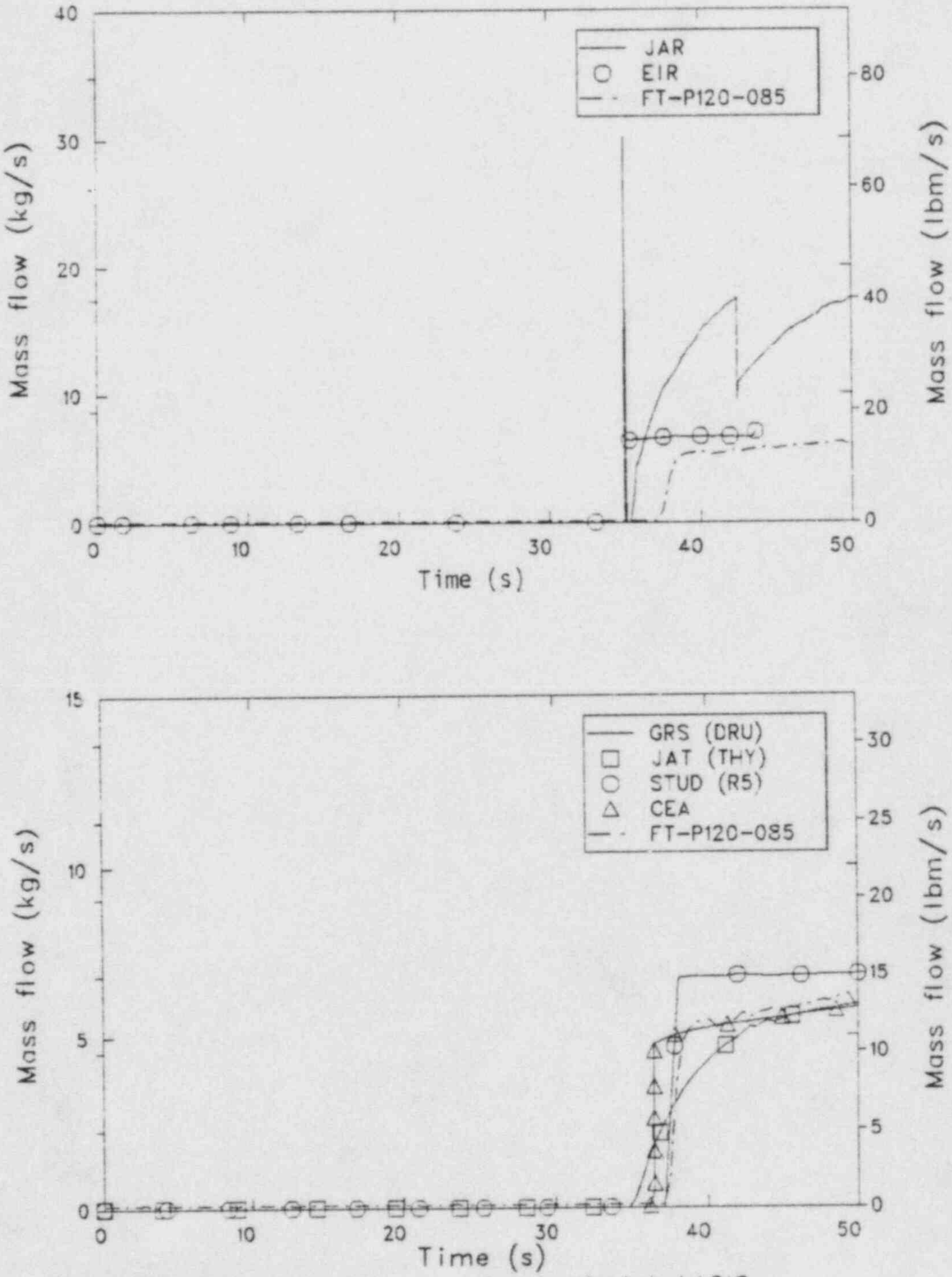

Figure 23. Comparison of measured and calculated LPIS flow for the blind calculations.

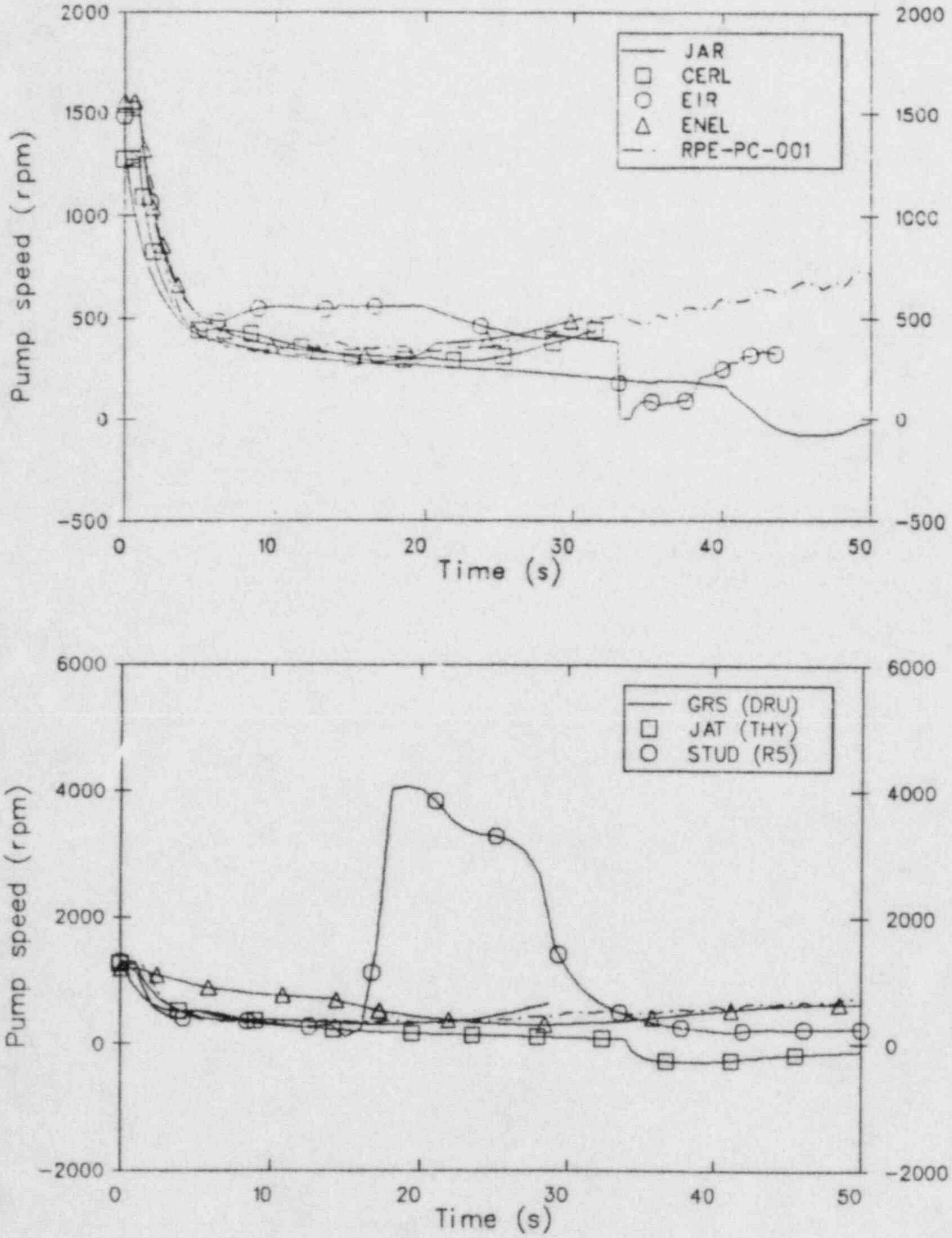

Figure 24. Comparison of measured and calculated reactor coolant pump speed for the blind calculations.

well, taking the various initial speeds into account. EIR calculated a much higher speed for the first 20 s, then degraded to an abrupt shut off at 34 s. Only the two Japanese submittals did not calculate a pump speed turnaround. STUD calculated a tremendous increase in pump speed, to nearly 400% of initial speed between 16 s and 31 s. This peak is similar to the pump speed increase experienced in L2-5 between 25 and 59 s, but the data never exceeded the pump's initial speed.

4.7 Rod Temperature

The comparison of cladding temperatures with data is difficult due to the variety of modeling techniques used by the participants to model the heat slabs in the core. With this in mind, Figures 25 and 26 present the comparisons with data for the 0.76 m (30 in.) elevation and 0.99 m (39 in.) elevation. For the first 30 s, GRS comes very close to matching the temperature profile at the 0.76 m level, with a peak slightly higher than data. JAR, ENEL, JAT and CEA all underpredict the temperatures but show the stable high temperature plateau seen in data. CERL overpredicts the temperature plateau, while STUD reaches the same peak as CERL but shows a definite quench. The quench seen in the STUD RELAP5 calculation starts at the same time as the increases in loop densities and the pump speed.

At the 0.99 m level, the data from L2-5 is characterized by two quenches at 15 s and 47 s. None of the participants, except EIR and JAT, calculated these quenches at the presented elevations. Initial increases in temperature were well predicted by all except EIR, which used an average core model for this elevation. Only JAR overpredicted the temperature prior to the 15 s data quench.

4.8 Summary

In summary, the eight blind calculations performed satisfactorily when calculating hydraulic behavior except when modeling problems, such as EIR's pressurizer, STUD's pump and JAR's LPIS, interfered. The predicted pressure-temperature histories were generally lower than data. Subcooling and superheat within the primary were not well predicted. Except in the intact loop cold leg, densities were adequately predicted. In the cold

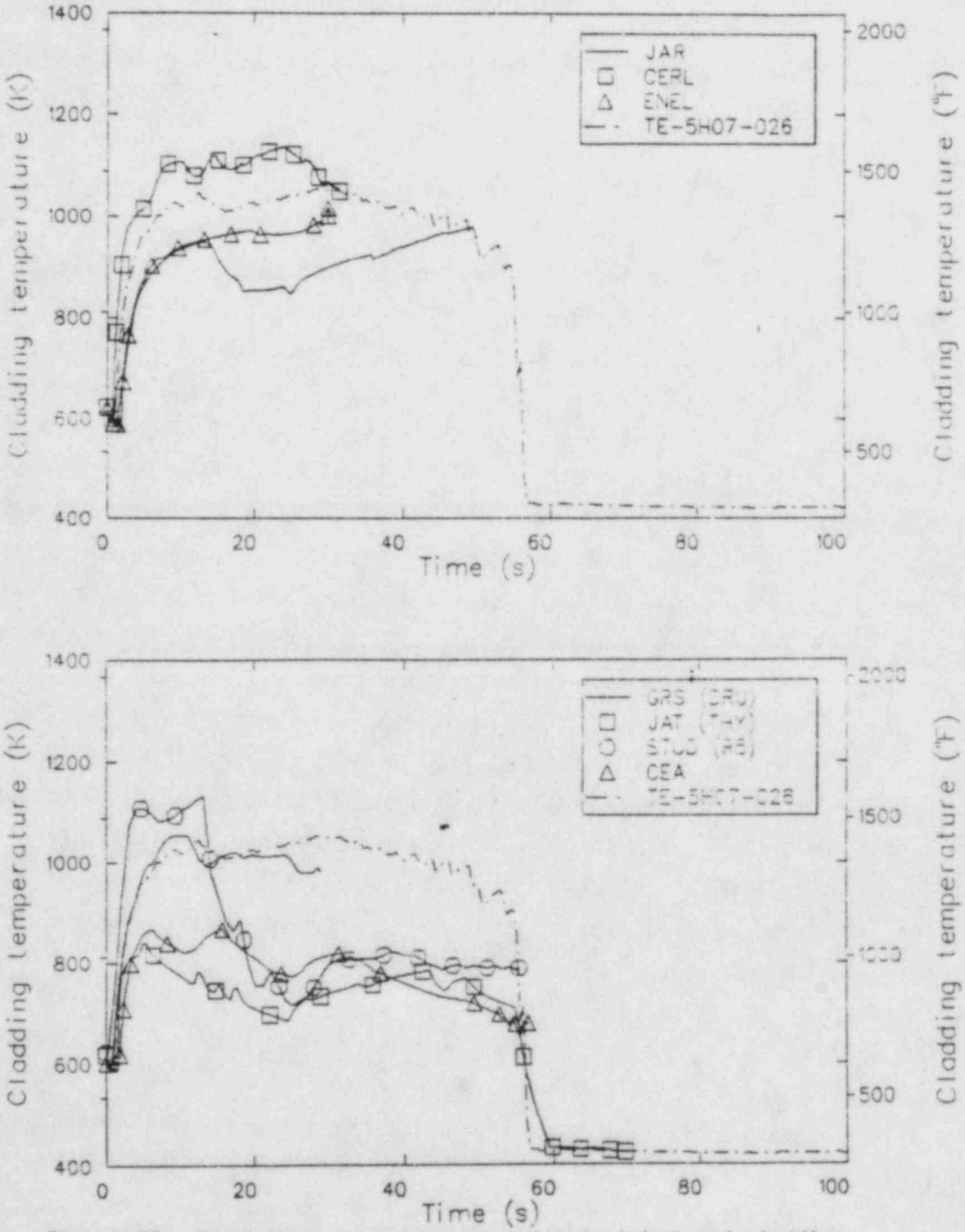

Figure 25. Comparison of measured and calculated rod cladding temperature at the 0.76m elevation for the blind calculations.

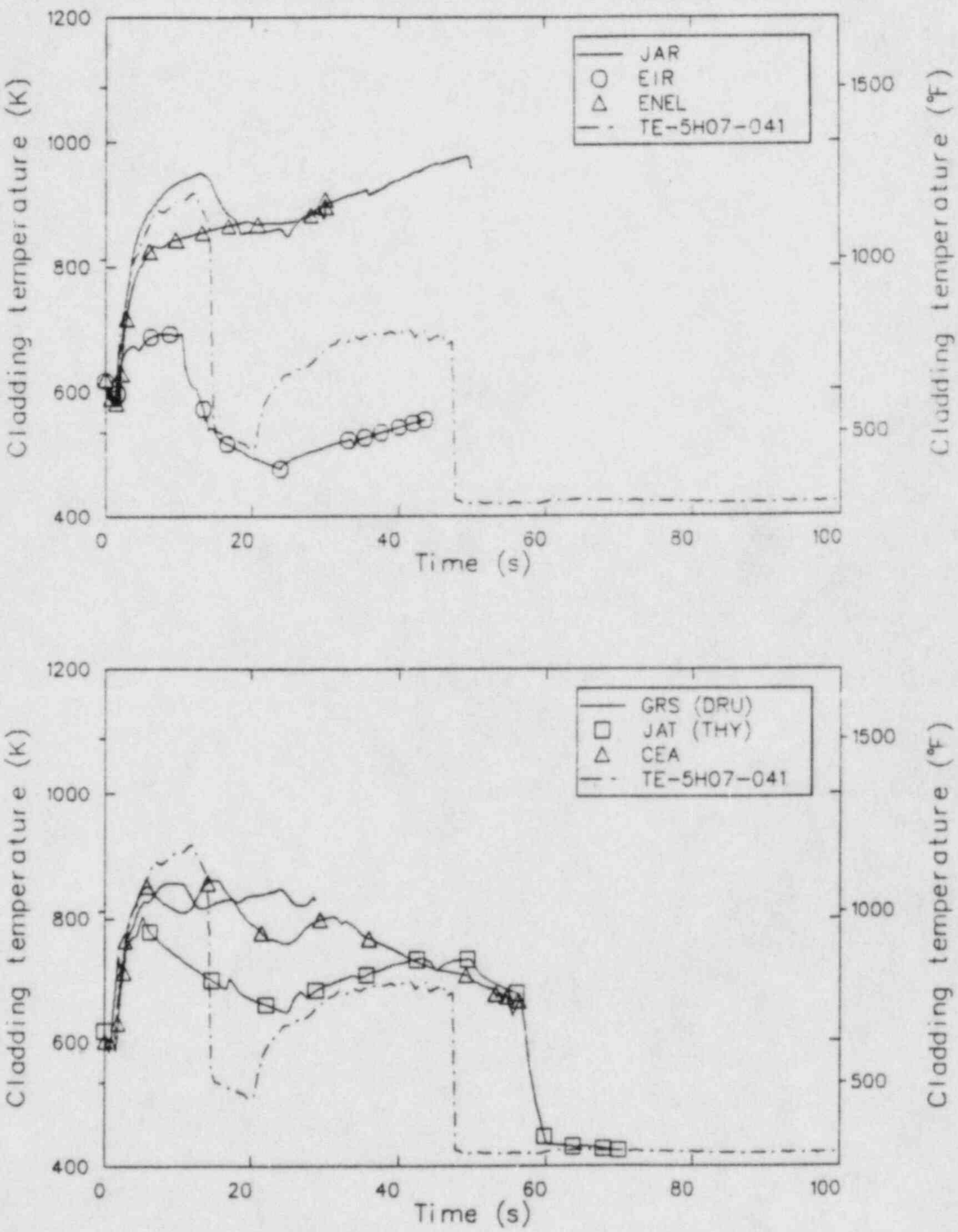

Figure 26. Comparison of measured and calculated rod cladding temperature at the .99m elevation for the blind calculations.

leg, however, the predictions ranged from liquid full to vapor full without the slug flow behavior seen in the data. Break flow and mass lost to the primary was overpredicted by all participants, except EIR. Calculations of ECC injection and pump speed were adequate except for the above mentioned modeling problems. Rod temperature profiles were very model dependant. Heatup rates were calculated well, while quenches of the clad were not predicted.

5. SUMMARY OF OPEN RESULTS

The calculations submitted by LANL, DCMN, VTT and the second EIR submittal were designated open calculations because the models used in these analyses were not submitted prior to the L2-5 experiment. These participants were allowed to make code or model changes to improve their predictions. Comparisons of experiment L2-5 data with the code predictions are provided in the following sections.

5.1 Sequence of Events

The measured and calculated sequence of events for the open calculation were included in Table 3. For the most part all open submittals calculated the experiment's sequence of events well. EIR and VTT scrammed the reactor earlier than the 0.24 s experiment scram. VTT predicted an early deviation from saturation temperatures while EIR predicted a later one. LANL tripped the pumps early at 0.24 s rather than 0.94 s. The participants calculated pressurizer voiding between 8 s (EIR) and 28 s (LANL). ECC initiation was well calculated. The time of peak clad temperatures, however, ranged from 5.2 s (VTT) to 50 s (LANL).

5.2 Pressure

The calculated pressure in the pressurizer, intact loop cold leg, broken loop hot leg, broken loop cold leg, and upper plenum are compared with data in Figures 27 to 31, respectively. EIR and VTT underpredicted the pressure in the pressurizer, while LANL and DCMN calculated the drop extremely well for the first 15 s, then overcalculated the pressure from 15 s to 40 s. In the loops and upper plenum, the same basic pattern was seen with EIR and VTT generally under the data and LANL and DCMN generally over. But all participants calculated the loop pressure history well.

Figure 32 shows the comparison between calculated secondary pressure and data. The EIR calculation showed the best comparison with data, following the pressure history quite well. The LANL calculation showed a slow oscillation in secondary pressure, while the VTT depressurized substantially.

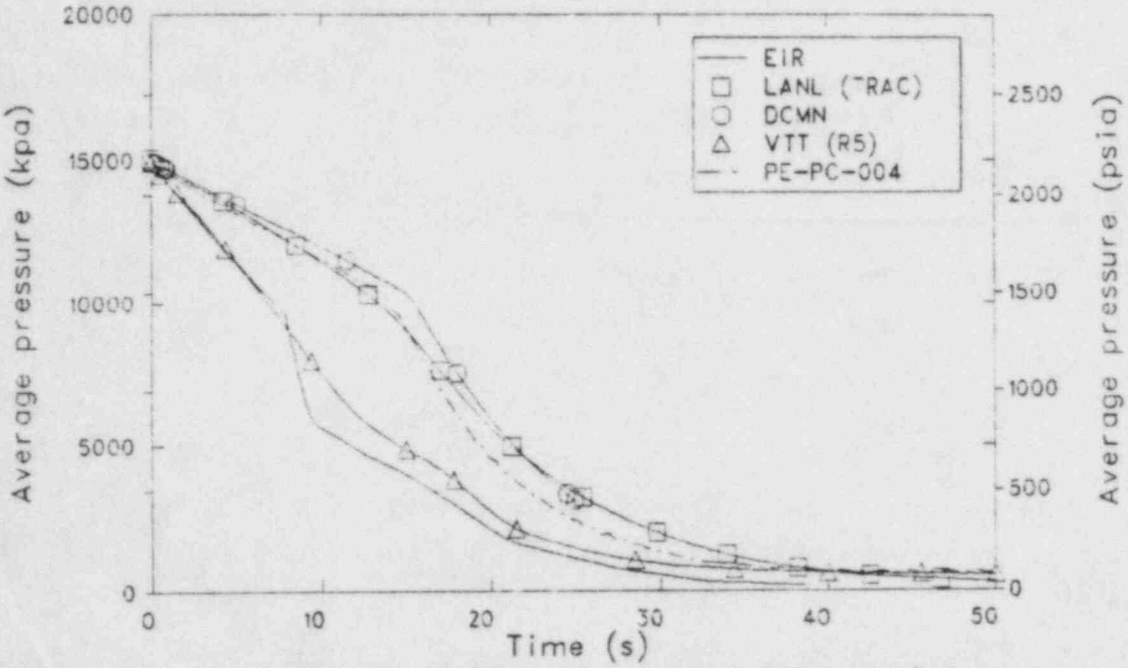

Figure 27. Comparison of measured and calculated pressurizer pressure for the open calculations.

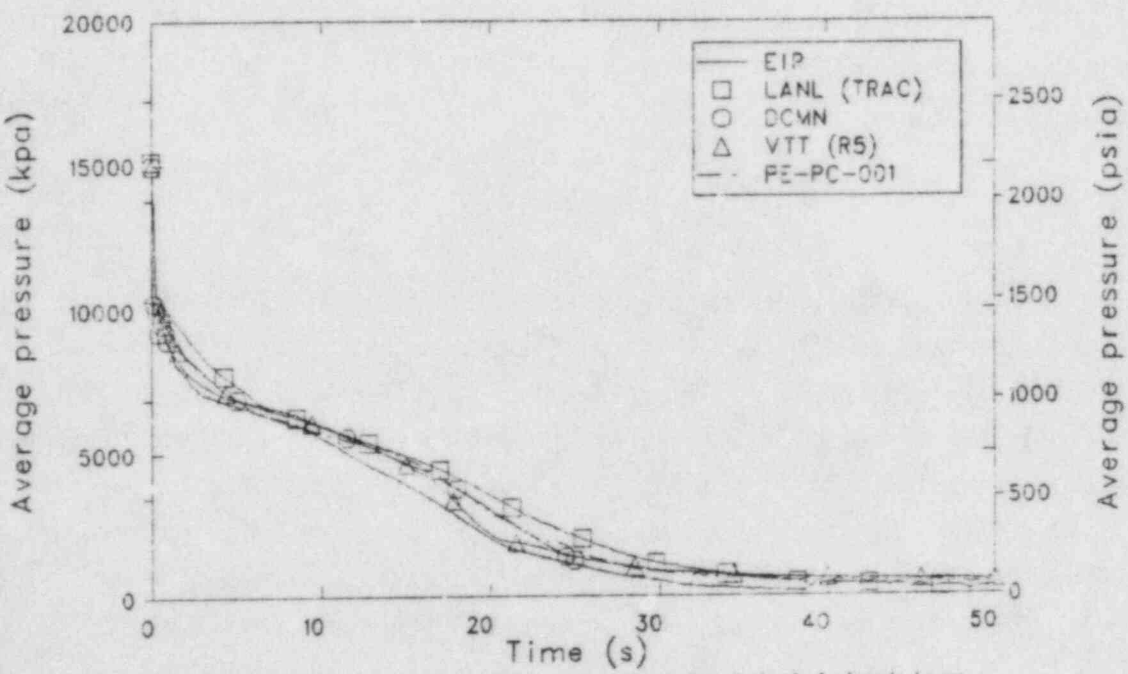

Figure 28. Comparison of measured and calculated intact loop cold leg pressure for the open calculations.

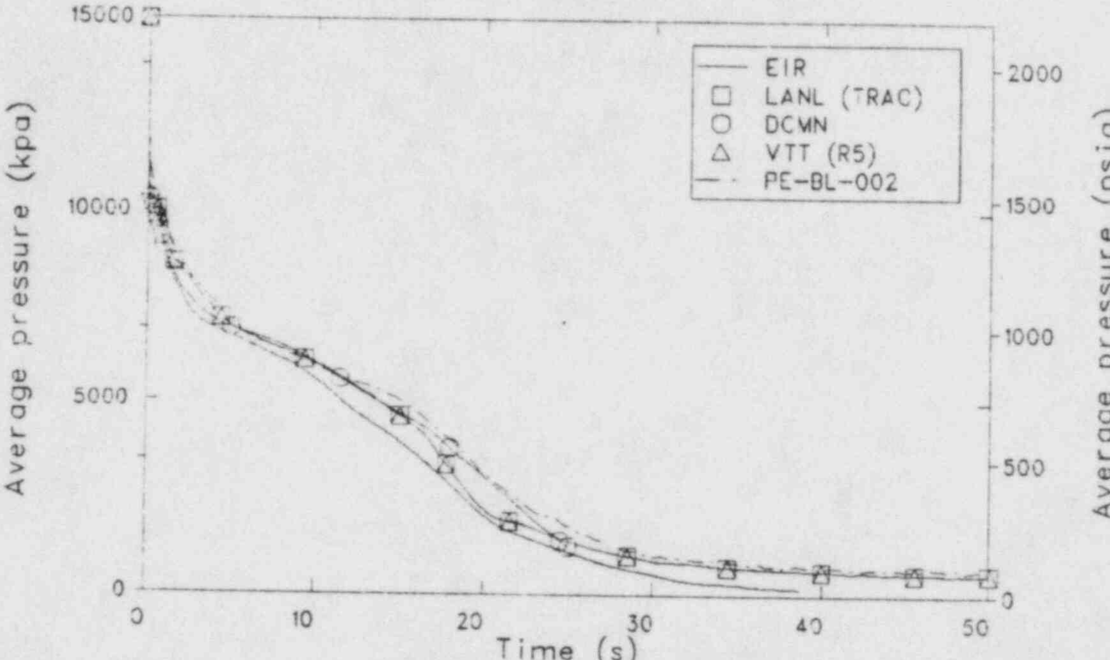

Figure 29. Comparison of measured and calculated broken loop hot leg pressure for the open calculations.

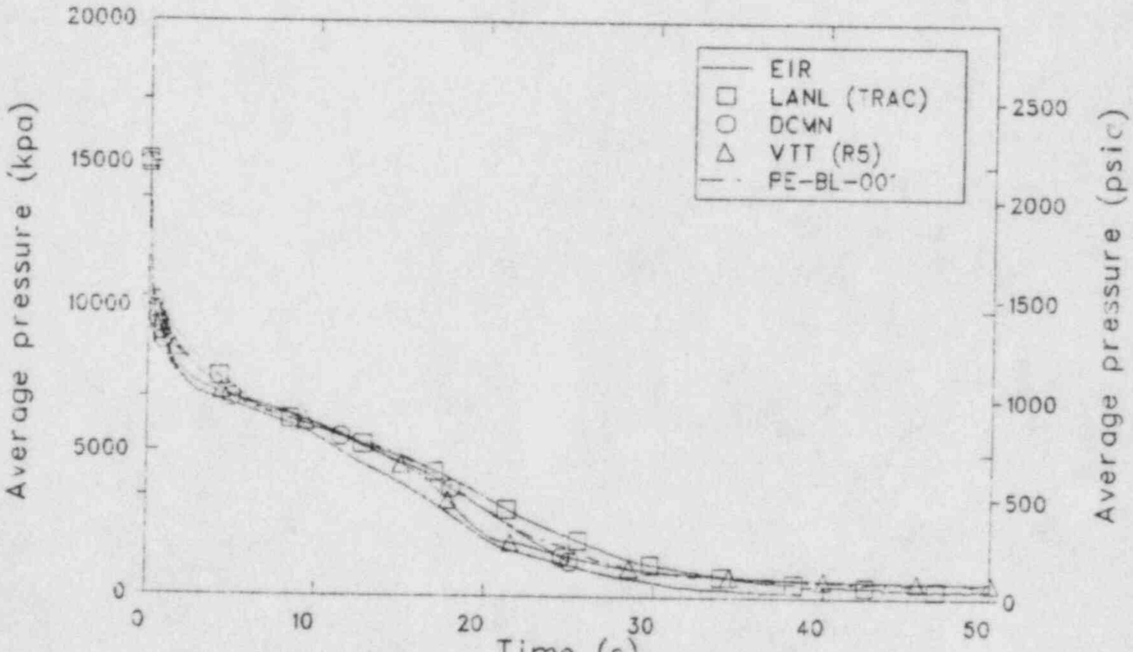

Figure 30. Comparison of measured and calculated broken loop cold leg pressure for the open calculations.

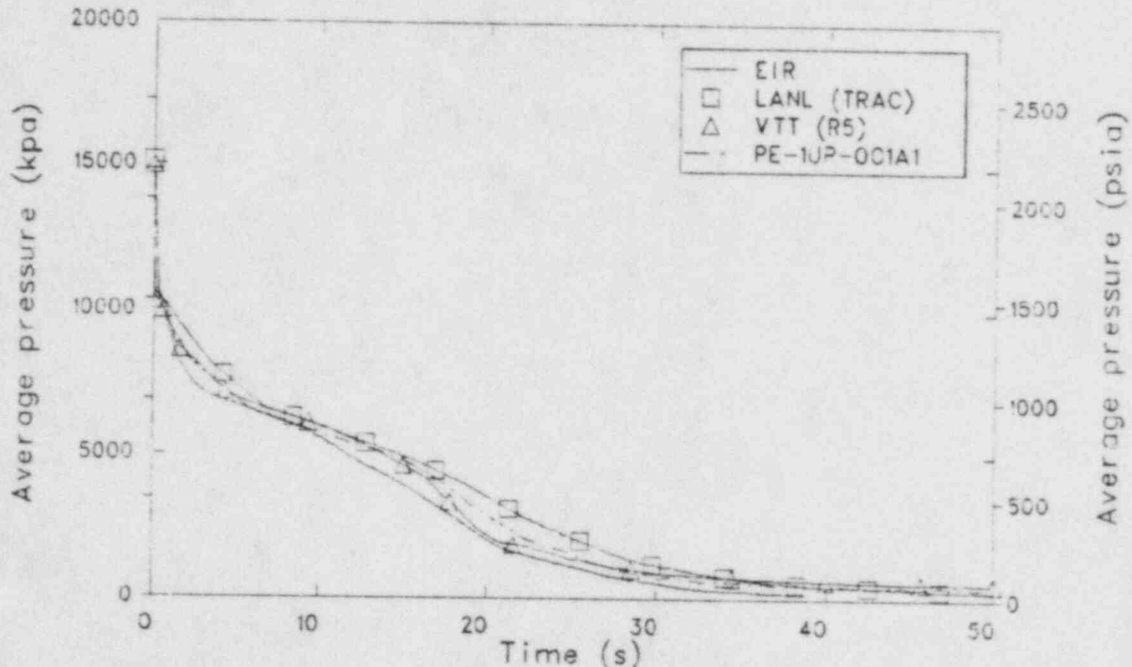

Figure 31. Comparison of measured and calculated upper plenum pressure for the open calculations.

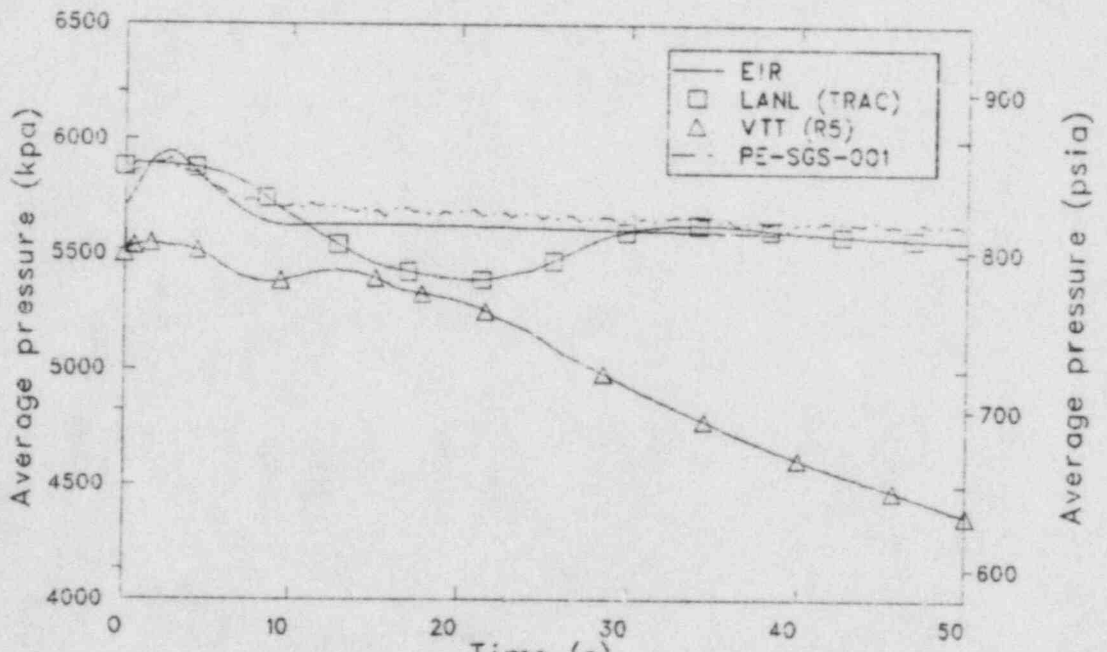

Figure 32. Comparison of measured and calculated steam generator secondary pressure for the open calculations.

5.3 Fluid Temperatures

Upper plenum temperatures are compared to data in Figure 33. For the first 28 s, the submittals showed the same relation to data as did the pressure histories, with EIR and VTT below data, and LANL and DCMN above. In this period, DCMN's RELAP4/MOD6 calculation followed data extremely well. At 28 s both the L2-5 data and EIR's calculation began to register some superheating. The magnitude of this superheat was higher in the calculation than in the data but the shape and trend of the curve was nearly identical.

Comparison of lower plenum and intact loop cold leg temperatures, shown in Figures 34 and 35, again show the same relationship as the pressure histories. EIR and TT were generally lower than data until 28 s when the cooldown calculated by VTT slowed enough to reverse the trend. LANL's temperatures were higher than data until the 35 to 40 s range when the comparison reversed. DCMN's lower plenum temperature comparison was excellent.

Hot leg temperatures (Figure 36) again showed some superheating in the data. As in the upper plenum, only EIR calculated the superheat but at much higher levels. Both LANL and VTT calculated a cooldown which followed their depressurization histories.

All the open calculations underpredicted the average coolant temperature in the pressurizer shown in Figure 37. Secondary temperatures compared in Figure 38 show better results. The VTT calculation's secondary cooldown followed the depressurization previously mentioned in Section 5.2. The remaining two calculations stabilized by 15 s and remained constant, with LANL calculating an average temperature nearly identical to data.

5.4 Fluid Densities

The measured density and the calculated average density in the intact loop cold leg is shown in Figure 39. The calculations all showed the cold leg voiding with subsequent slug behavior later in the transient. The time

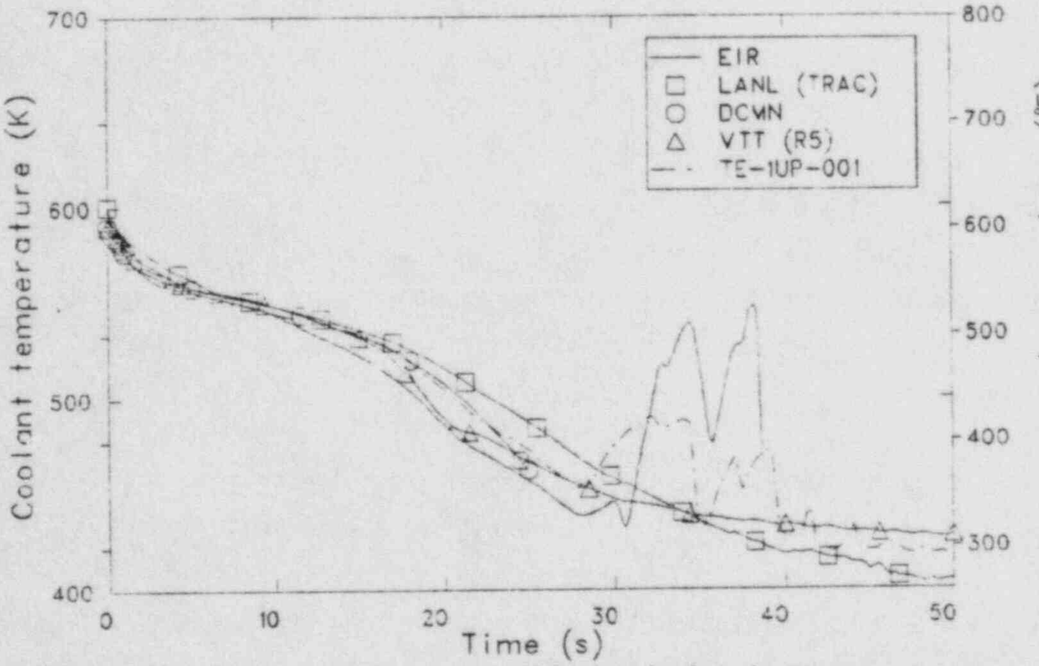

Figure 33. Comparison of measured and calculated upper plenum fluid temperature for the open calculations.

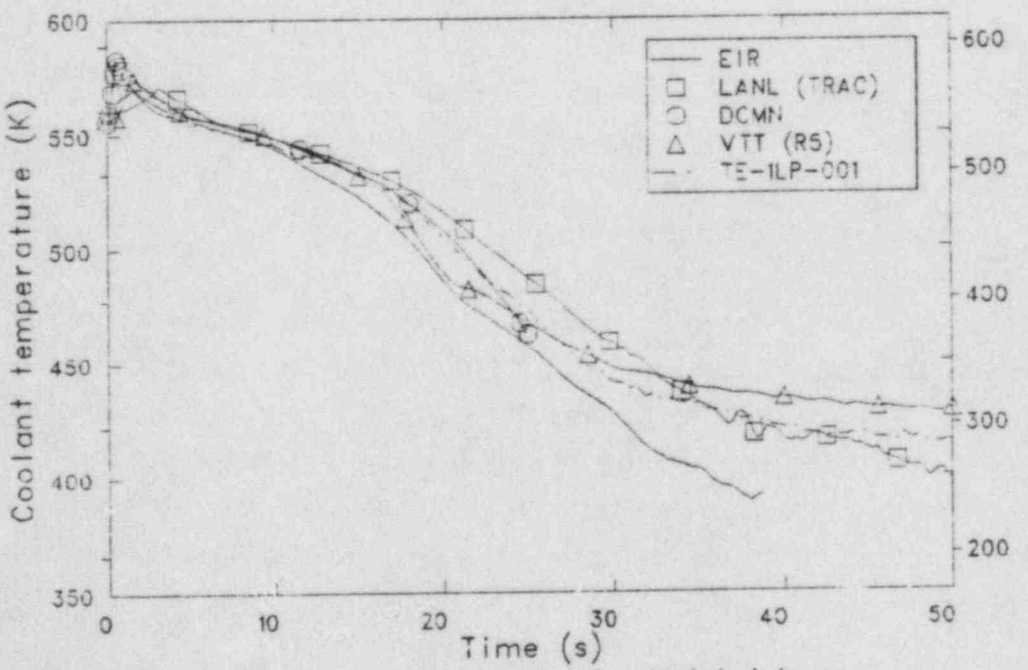

Figure 34. Comparison of measured and calculated lower plenum fluid temperature for the open calculations.

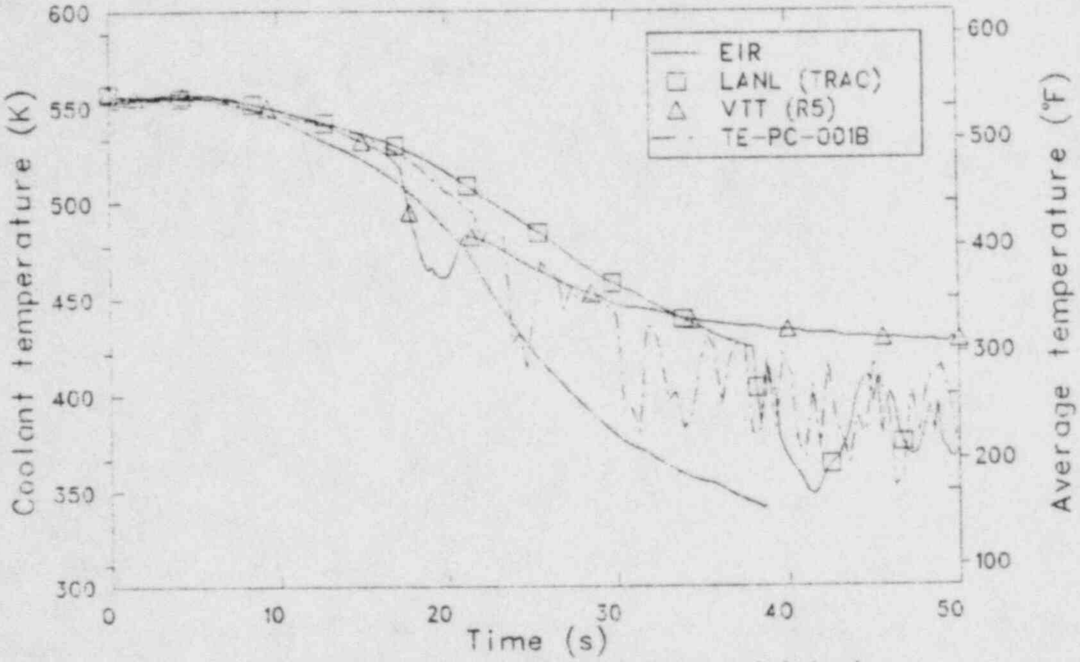

Figure 35. Comparison of measured and calculated intact loop cold leg temperature for the open calculations.

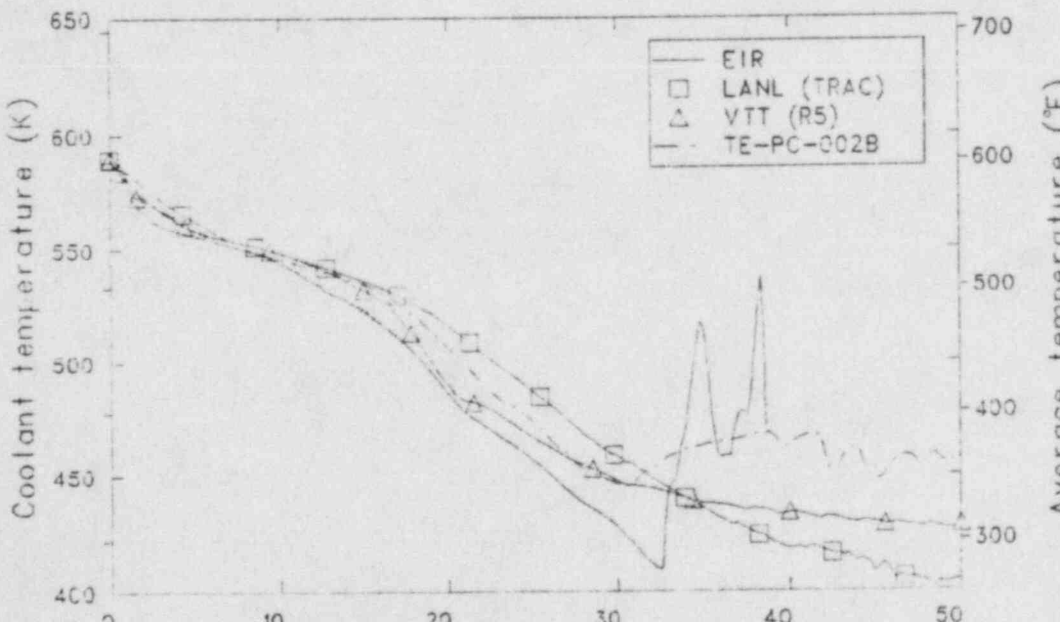

Figure 36. Comparison of measured and calculcted intact loop hot leg temperaure for the open calculations.

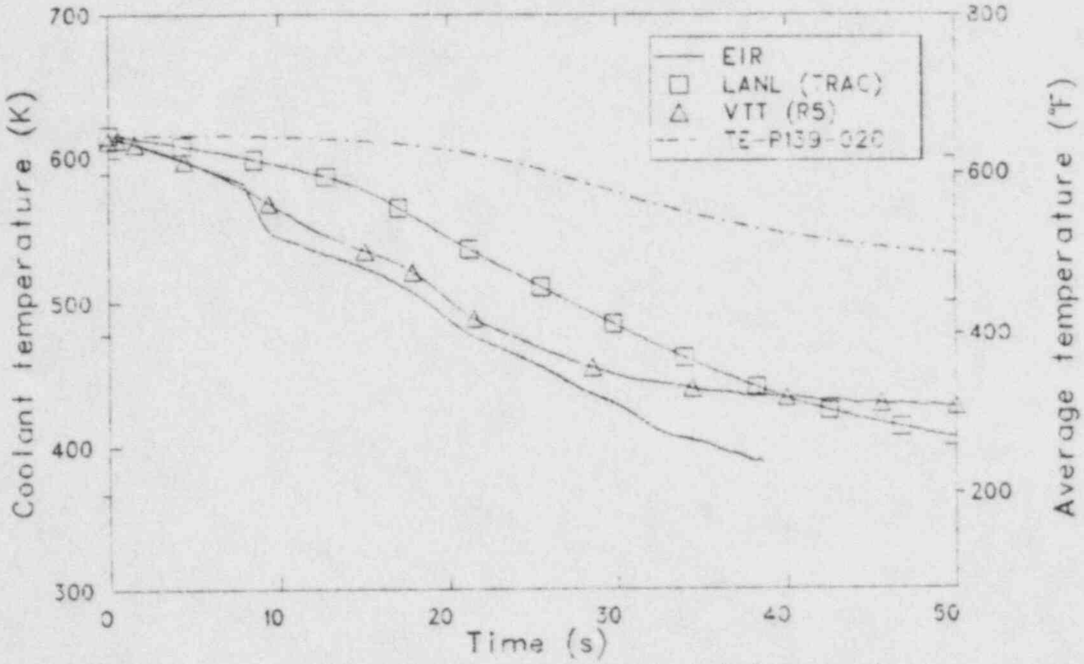

Figure 37. Comparison of measured and calculated pressurizer temperature for the open calculations.

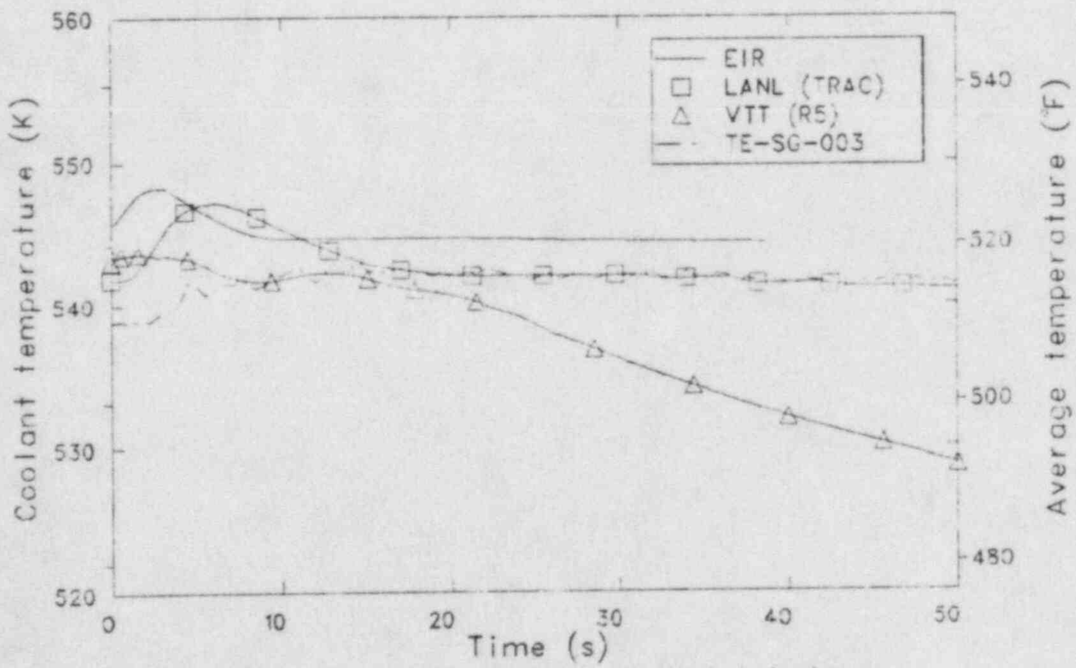

Figure 38. Comparison of measured and calculated steam generator secondary temperature for the open calculations.

the slug flow began varied from 16 s (VTT) to 39 s (LANL). The oscillations calculated by VTT were much less severe than those seen in the experiment and those calculated by other open participants.

Figure 40 compares the calculated average density in the intact loop hot leg with the density seen in the data. All calculations showed similar results with the hot legs simply voiding during the transient. The agreement with data was good for all the calculations.

The comparisons of calculated and measured densities in the broken loop are shown in Figures 41 and 42. All open calculations showed a slower voiding in the cold leg than data for the first 20 s. Both EIR and LANL calculated major slug flow through the cold leg at different times in the transient, but this phenomenon was not observed in the data. In the broken loop hot leg, the calculations showed a faster voiding than was observed in the test for the first 20 s. After this point, all submittals remained voided with the exception of the VTT calculation which experienced slug flow after 44 s.

5.5 Mass Flow

A comparison of calculated core inlet flows is shown in Figure 43. The reverse flow peak, characteristic of a cold leg rupture, was calculated to be much more severe by EIR than either LANL or VTT. However, by 10 s, all calculated flow had essentially stagnated.

One of the most critical comparisons was that of calculated break flow with data and is shown in Figures 44 and 45. These results reflected the various break flow models used by the participants. After 3 s, all of the participants overpredicted cold leg break flow. LANL underpredicted the peak flow in the first 0.5 s, while DCMN and EIR overpredicted the peak by 50 to 70%. VTT nearly matched the initial peak, earlier than data, then underpredicted the flow until 3 s. In the hot leg, VTT overpredicted the flow significantly, as did DCMN. EIR underpredicted the flow, while LANL followed the hot leg flow history reasonably well. However, the bottom

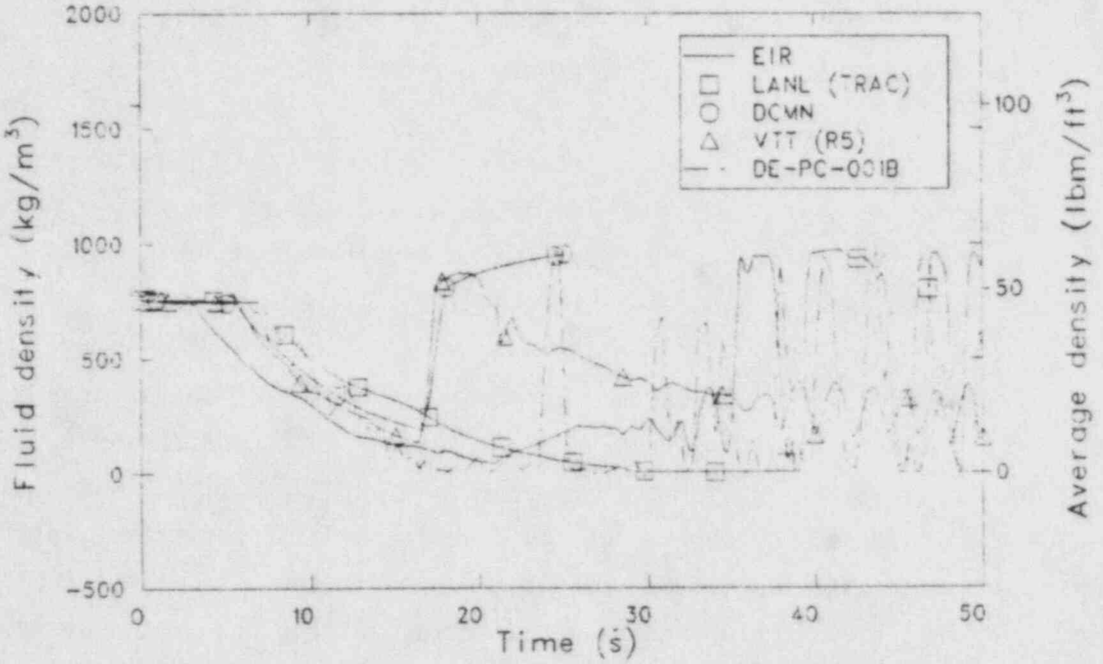

Figure 39. Comparison of measured and calculated intact loop cold leg density for the open calculations.

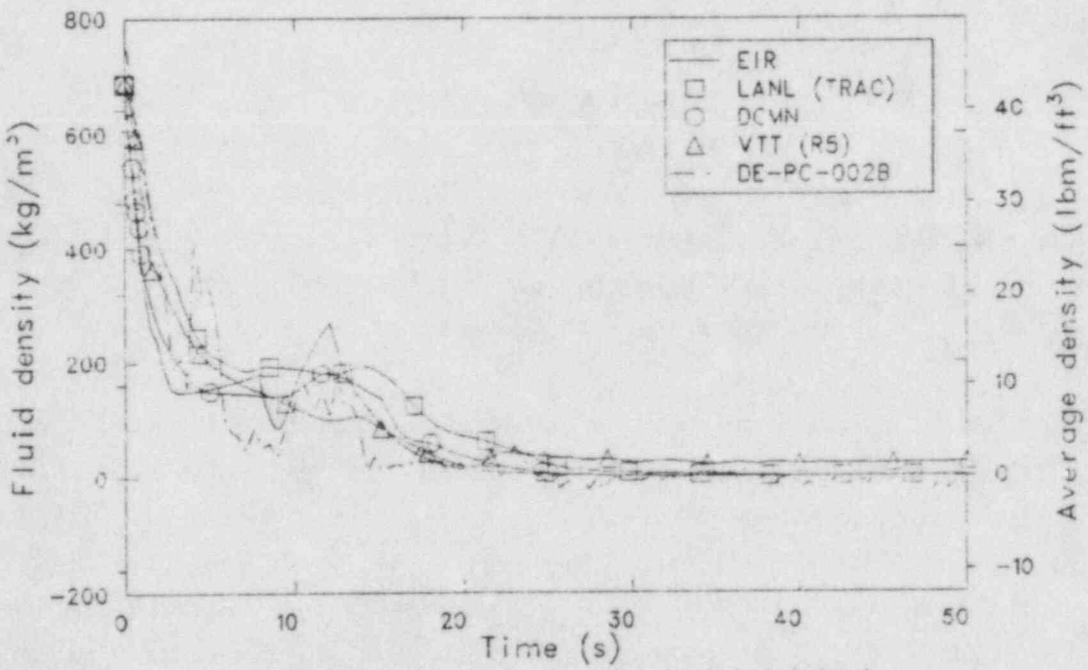

Figure 40. Comparison of measured and calculated intact loop hot leg density for the open calculations.

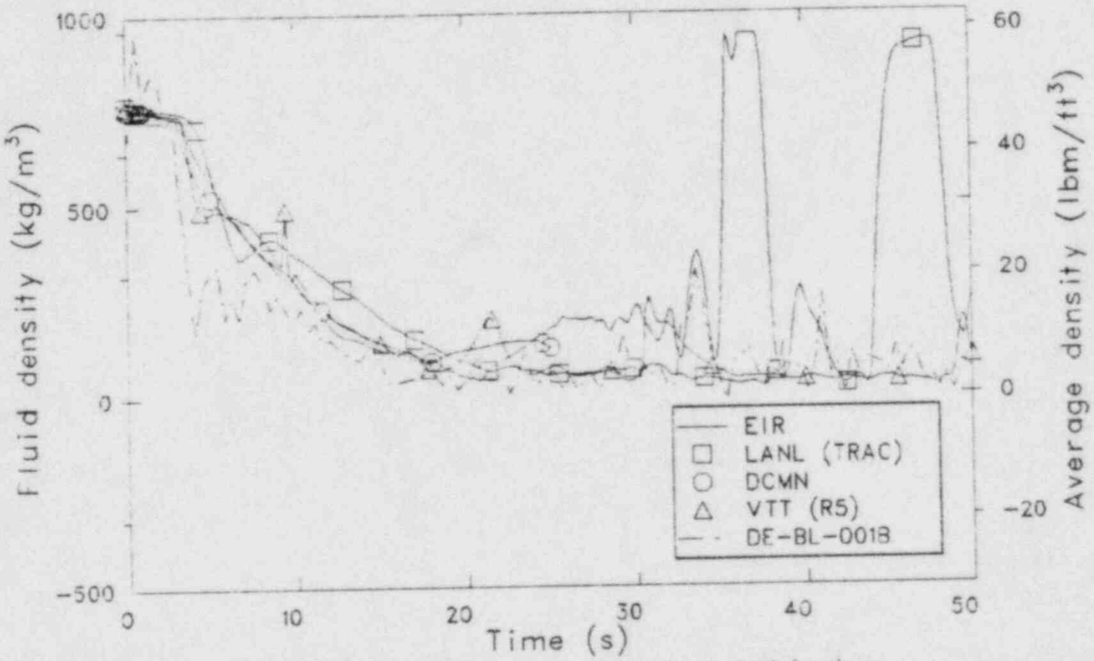

Figure 41. Comparison of measured and calculated broken loop cold leg density for the open calculations.

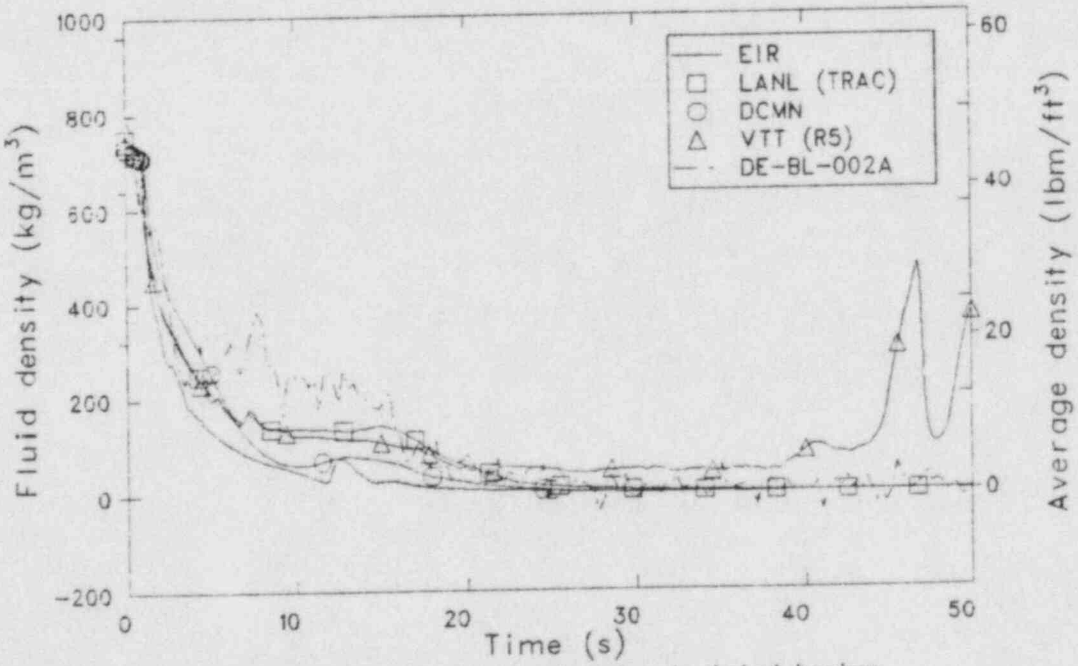

Figure 42. Comparison of measured and calculated broken loop hot leg density for the open calculations.

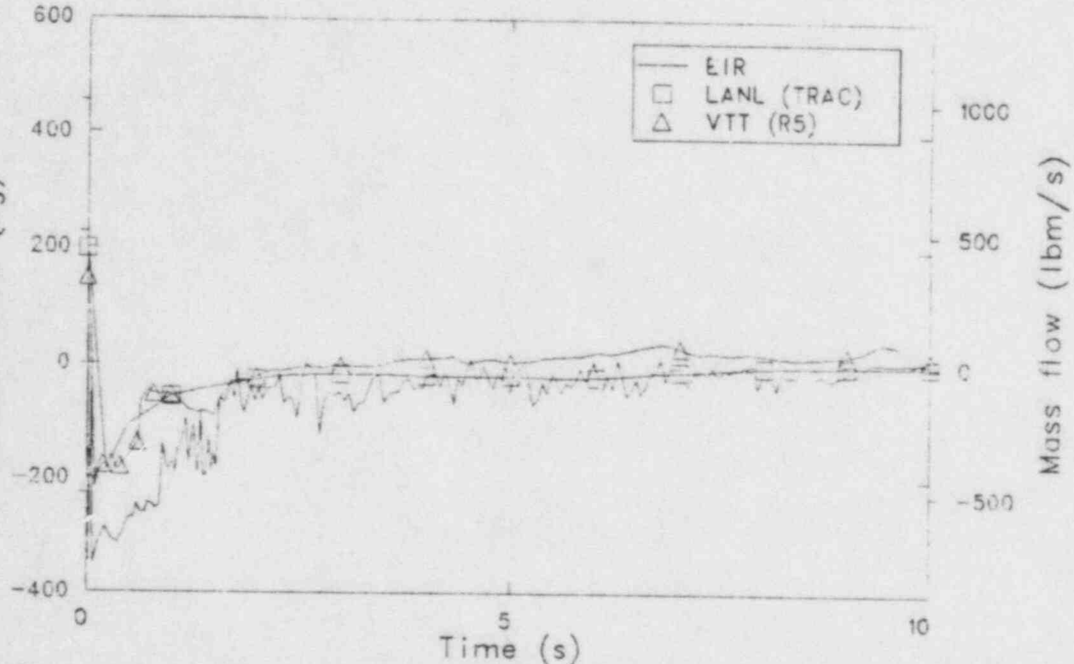

Figure 43. Comparison of calculated core inlet flows for the open calculations.

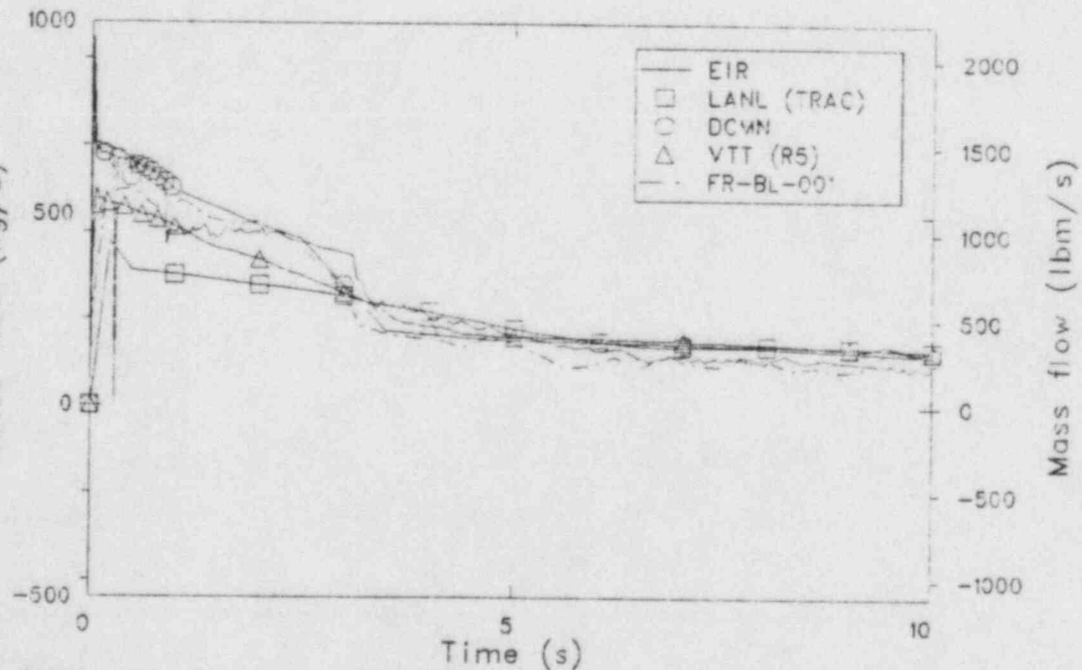

Figure 44. Comparison of measured and calculated broken loop cold leg break mass flow rate for the open calculations.

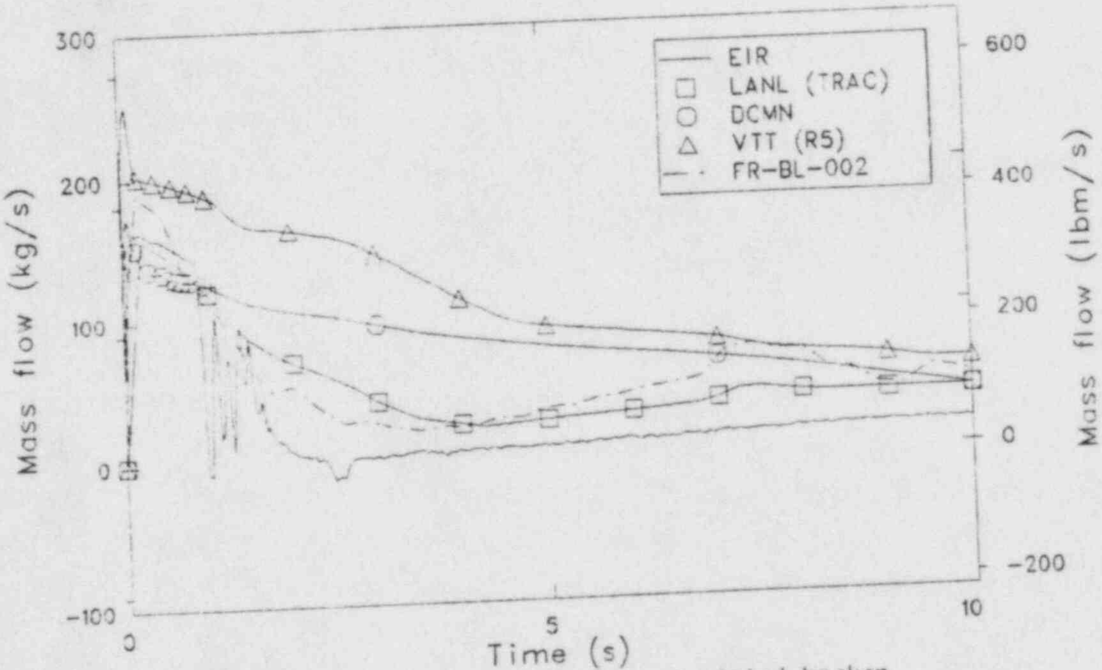

Figure 45. Comparison of measured and calculated broken loop hot leg break mass flow rate for the open calculations.

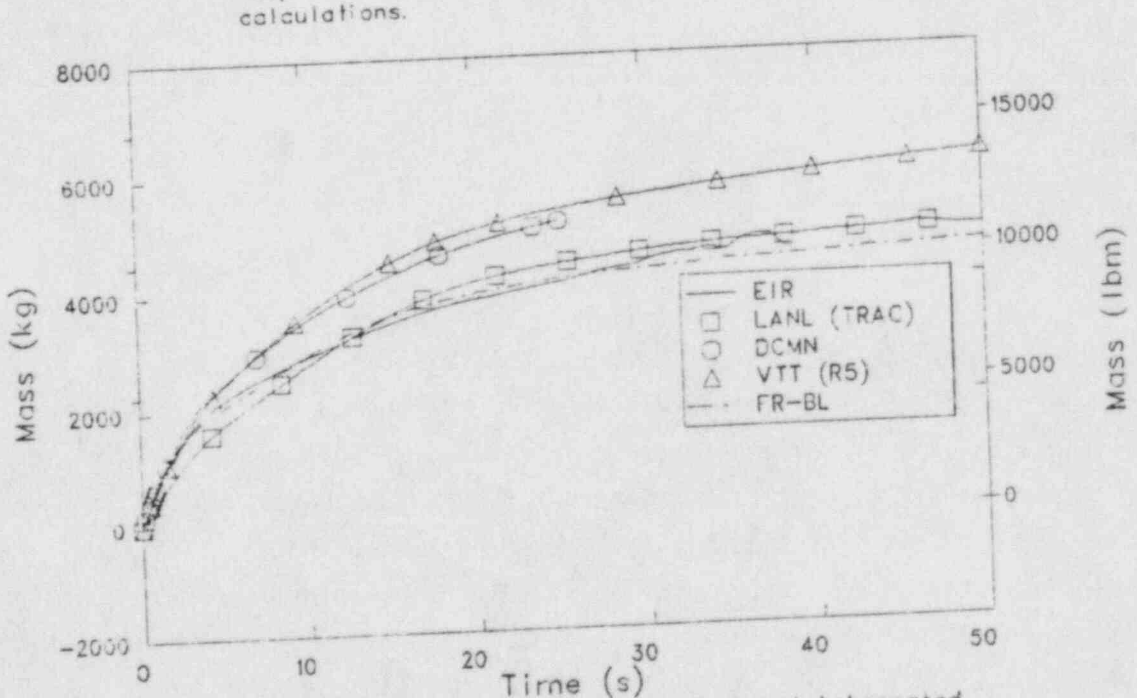

Figure 46. Comparison of measured and calculated integrated break flow for the open calculations.

line, mass lost from the system in Figure 46, showed that EIR came closest to correctly calculating the total mass lost while LANL, DCMN, and VTT overpredicted the event.

A comparison of calculated reactor vessel mass inventories is shown in Figure 47. EIR's initial mass inventory, was significantly lower than LANL or VTT, and all calculations showed differences in final mass inventories. Neither EIR or VTT showed an inventory turnaround or refill while the LANL TRAC calculation began to increase at 20 s.

Emergency core coolant flows are compared to data in Figures 48 and 49. EIR calculated an earlier HPI initiation than the other participants, but the significant difference was LANL's flow rate, approximately two times higher than the data or the other calculations. This high flow was probably a factor in the fast turnaround of LANL's vessel inventory previously mentioned. LPI flow comparisons showed EIR again preceding all calculations, as well as data.

5.6 Pump Speed

Measured and calculated pump speed is presented in Figure 50. Apart from the initial value discrepancy, there were no major problems with any of the submittals.

5.7 Rod Temperatures

Rod cladding temperatures are shown in Figures 51 and 52, at 0.76 m (30 in.) and 0.99 m (39 in.) respectively. As with the blind calculations, the significance of these curves was questionable due to the various modeling approaches to core cladding heat slabs. At the 0.76 m level, VTT's peak temperature at 5.2 s was close to the peak reached in the actual test but the cladding cooled off significantly from that point. Neither EIR or LANL reached the data peak, although the relatively stable high temperature history seen by LANL is more characteristic of data. At the 0.99 m elevation, data showed two major quenches, at 15 s and 46 s. VTT's calculation showed a earlier downturn from 5 to 10 s, then stayed relatively low. LANL calculated a temperature decrease near the first data quench at 14 s and a true quench at 89 s. EIR and DCMN did not display the characteristic quench behavior at all.

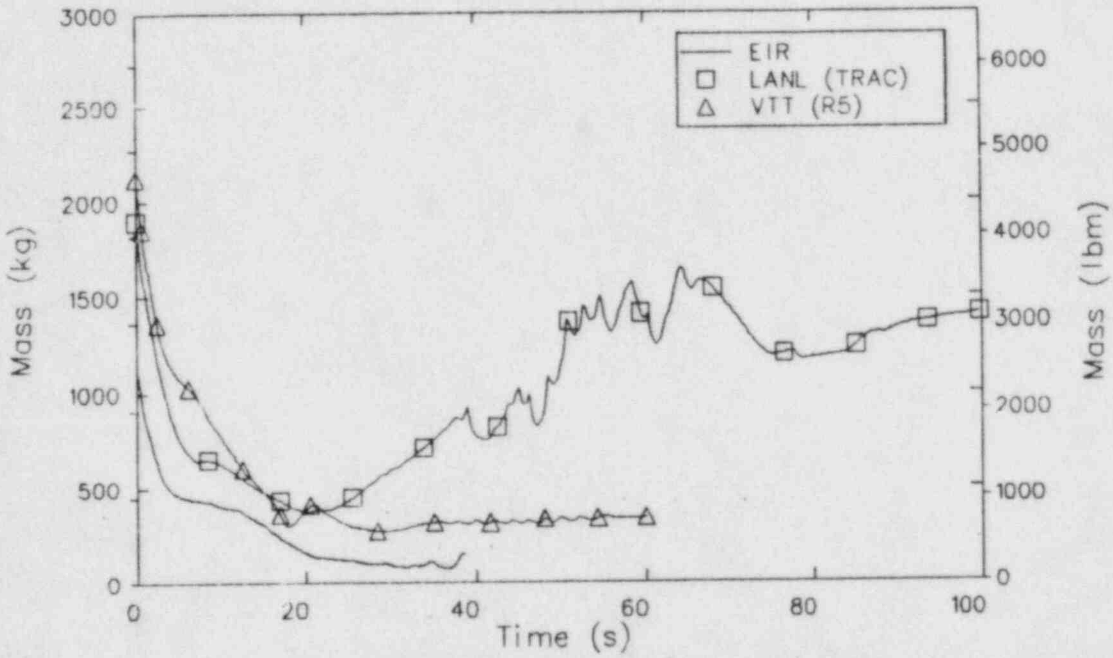

Figure 47. Comparison of calculated reactor vessel mass inventory for the open calculations.

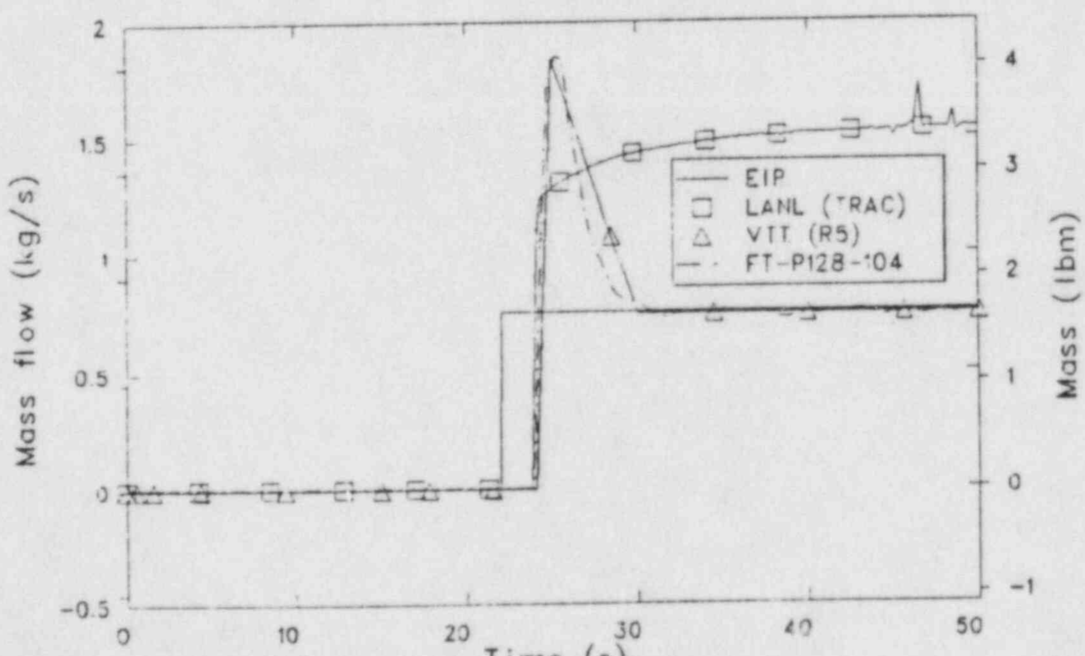

Figure 48. Comparison of measured and calculated HPIS flow for the open calculations.

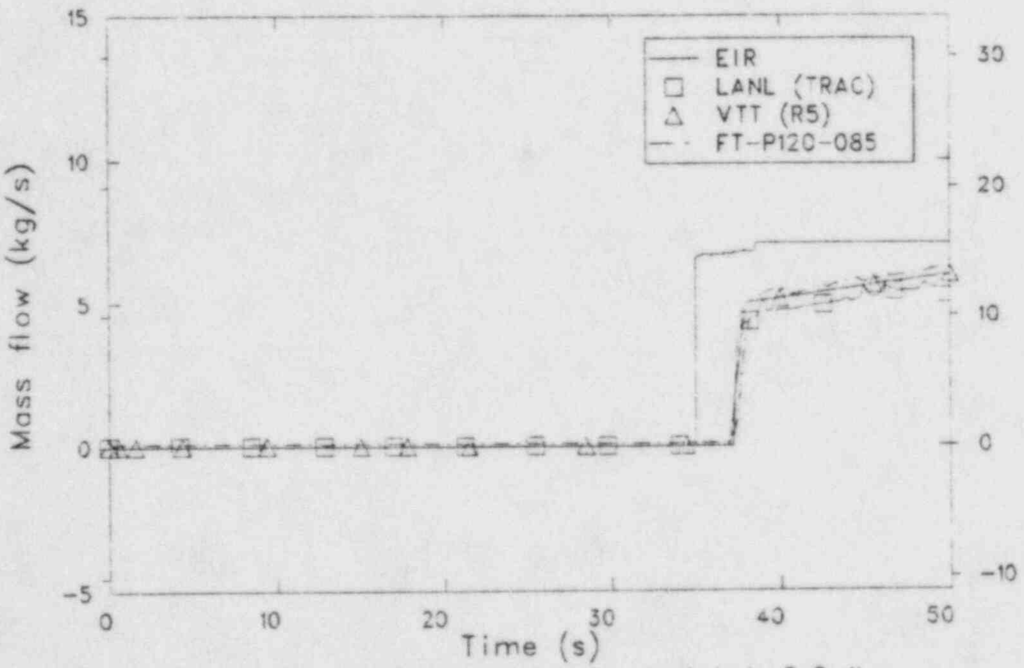

Figure 49. Comparison of measured and calculated LPIS flow for the open calculations.

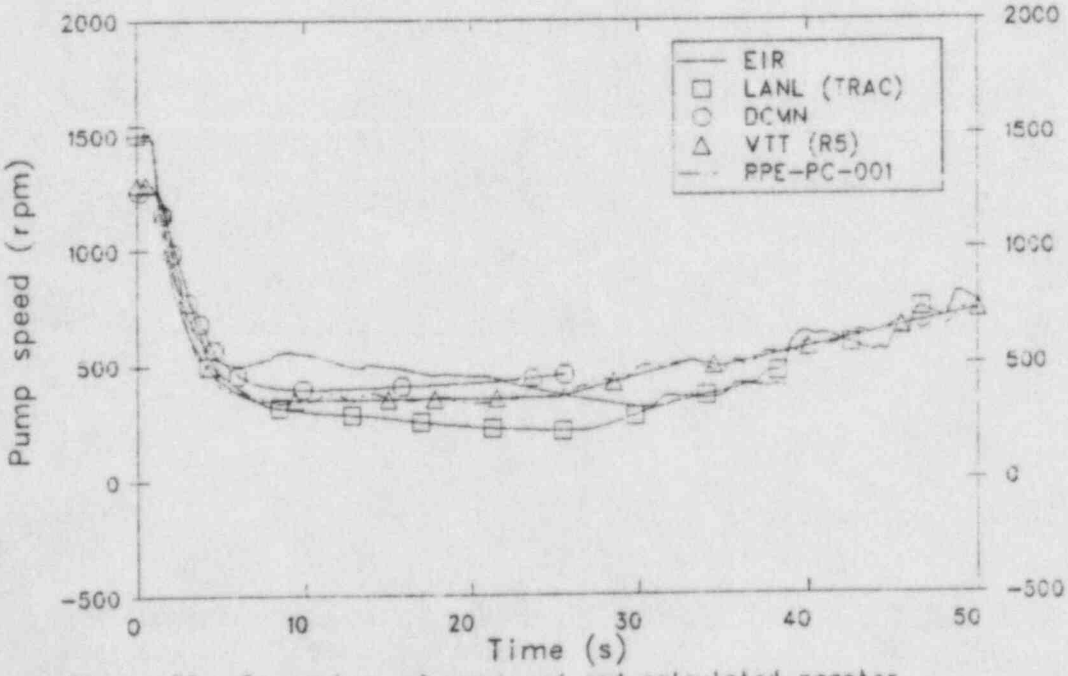

Figure 50. Comparison of measured and calculated reactor coolant pump speed for the open calculations.

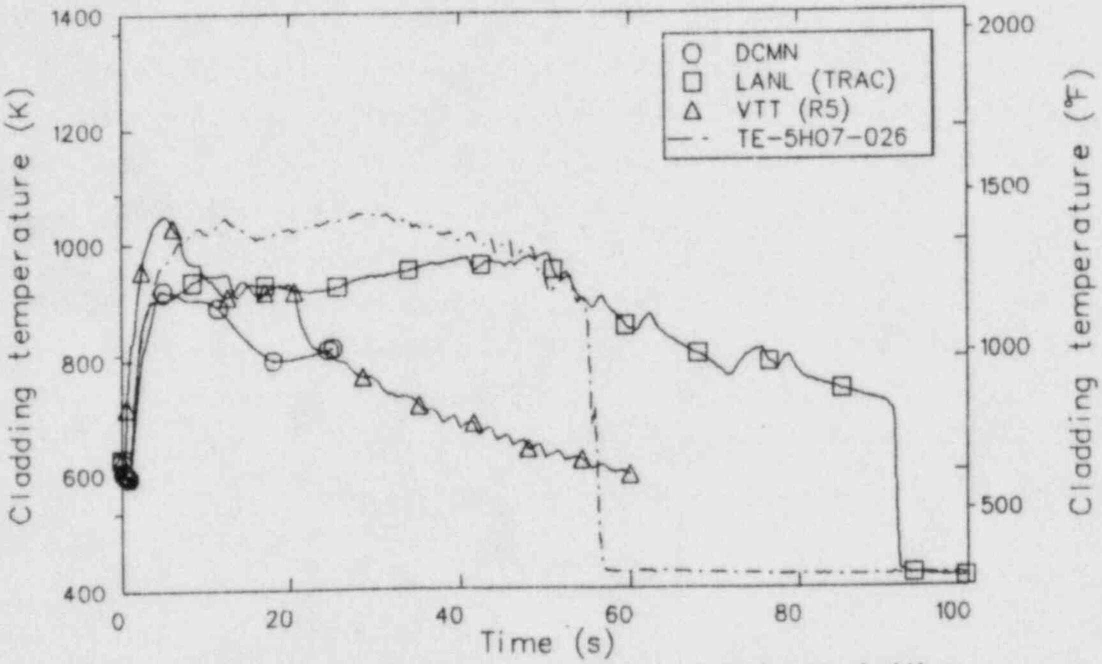

Figure 51. Comparison of measured and calculated rod cladding temperature at the 0.76m elevation for the open calculations.

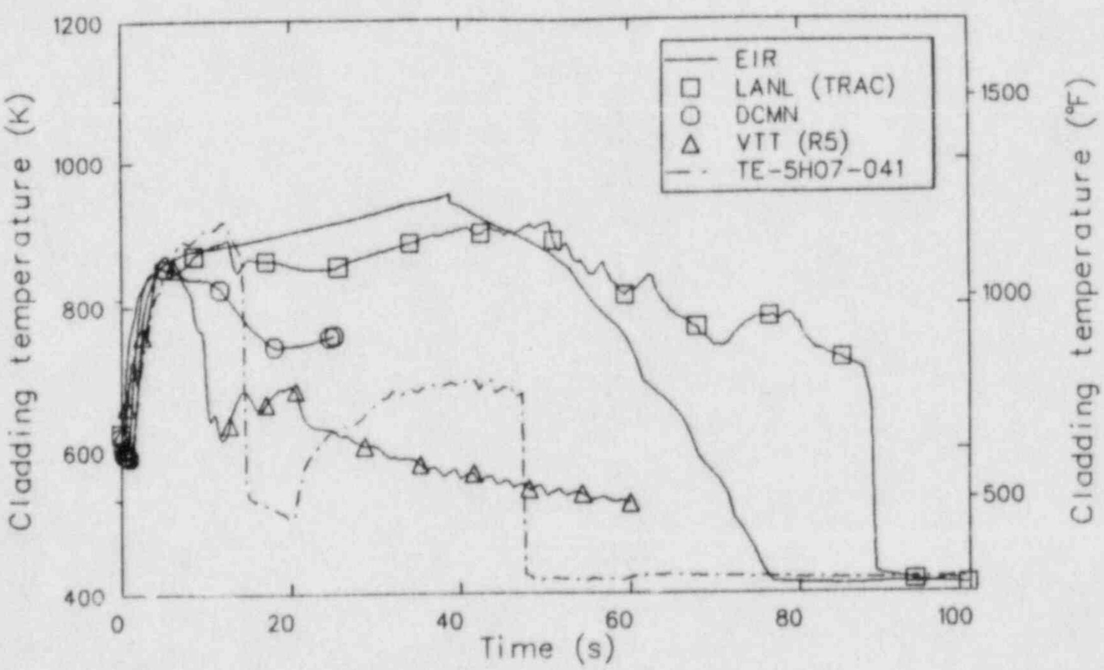

Figure 52. Comparison of measured and calculated rod cladding temperature at the .99m elevation for the open calculations.

5.8 Summary

In summary, as with the blind calculations the open submittals performed well in calculating the hydraulic response of the LOFT system. Pressure-temperature histories were somewhat closer to data than the majority of the blind calculations; subcooling and superheat accounted for the main discrepancies. Slug flow behavior in the intact loop cold leg was handled better in the open calculations than the blind submittals. Slug flow was also calculated to appear in the broken loop although it did not appear in the data. Break flow was overpredicted by everyone except EIR. ECC flow was calculated adequately except by LANL. Rod temperatures was again quite model dependant and, while heatups were calculated adequately quenches were less adequately predicted.

6. CONCLUSIONS AND RECOMMENDATIONS

Comparison of the calculated results with L2-5 data[3] and discussions with the participants[4] have led to the following conclusions.

Hydraulic parameters, such as depressurization rate and fluid temperatures were calculated well by most participants. Some difficulties were experienced when voiding and superheating occurred. (Sections 4.2, 4.3, 5.2, 5.3)

Densities in the hot legs of the facility were calculated correctly, but the densities in the cold leg, which experienced cold ECC flow, were less well predicted. (Sections 4.4, 5.4)

Break flow was overpredicted by nearly all participants with particular problems encountered in flow from the broken loop hot leg. (Sections 4.5, 5.5)

Comparisons of clad temperatures with data were affected by nodalization, heat transfer models, hydrodynamics, and heat slab models. In general, participants calculated the heatup of clad surfaces adequately and predicted the clad quenches less well (Sections 4.7, 5.7).

7. REFERENCES

1. P. D. Bayless and J. M. Divine, Experiment Data Report for LOFT Large Break Loss-of-Coolant Experiment L2-5, NUREG/CR-2826, EGG-2210, August 1982.

2. D. L. Reeder, LOFT System and Test Description (5.5 ft Nuclear Core 1 LOCEs), NUREG/CR-0247, TREE-1208, July 1978.

3. J. D. Burtt and S. A. Crowton, International Standard Problem 13 (LOFT Experiment L2-5) Preliminary Comparison Report, EGG-NTAP-6276, April 1983.

4. Summary Record of the Workshop on International Standard Problem 13, held in Idaho Falls, Idaho on July 18, 19, 1983, SEN/SIN(83)51.

APPENDIX A

ISP-13 SUBMITTAL FROM GESELLSCHAFT FUR REAKTORSICHERHEIT MBH FORSCHUNGSGELAND USING DRUFAN 02 (GRS)

Appendix for the German participation (Gesellschaft für Reaktorsicherheit) in the blind international Standard Problem ISP-13

Listing of the appendix:

1. Description of the nodalisation diagram (Attachment A1)
2. Identification of the computer code (Attachment A2)
3. Description of the critical flow model (Attachment A3)
4. Listing of options (Attachment A4)
5. Discussion of the results of the blind and posttest calculation of L2-5 (Attachment A5)

1. Description of the Nodalisation Diagram

Figure A1 shows the nodalisation diagram, which has been used for the pretest calculation of the LOFT experiment L2-5. The primary and secondary side is described by "lumped parameter" control volumes. All structures are represented.

The active core is simulated by two fluid channels (Fig. A2,A3). 239 fuel rods with the power factor of 1.4, 240 fuel rods with the power factor 1.2 and one average fuel rod are in the hot fluid channel (control volume 77, 78, 79). These 480 fuel rods represent the centre of the active core (fuel bundle 5 and the neighboured fuel rods). 244 average fuel rods and 576 fuel rods with a power factor of approx. 0.75 are in the outer cold channel (control volume 27, 28, 29).These 820 fuel rods represent the outer parts of the active core (fuel bundle 1 - 4 and fuel bundle 6 - 9).

The downcomer is devided into the downcomer stalk I and the downcomer stalk II.

Pressurizer and accumulator are modelled.

HPIS and LPIS are given as input functions.

On the following tables the nodalisation diagram is described:

Description of the control volumes	(table A1)
Description of fills and leaks	(table A2)
Description of valves	(table A3)
Description of pumps	(table A4)
Description of heat slabs	(table A5)

Table A1: Description of the control volumes

index of control volume	description of control volume
1	Intact loop hot leg
2	Intact loop hot leg
3	Steam generator inlet plenum
4	Steam generator primary side (U-tubes)
5	Steam generator primary side (U-tubes)
6	Steam generator primary side (U-tubes)
7	Steam generator primary side (U-tubes)
8	Steam generator primary side (U-tubes)
9	Steam generator primary side (U-tubes)
10	Steam generator outlet plenum
11	Steam generator outlet pipe
12	Steam generator outlet pipe
13	Pump 1 suction pipe
14	Pump 1 suction pipe
15	Pump 2 suction pipe
16	Pump 2 suction pipe
17	Pump 1 outlet pipe
18	Pump 2 outlet pipe
19	Intact loop cold leg
20	Intact loop cold leg
21	Downcomer (stalk 2)
22	Downcomer (stalk 2)
23	Downcomer (stalk 2)
24	Downcomer (stalk 2)
25	Lower plenum, lower volume
26	Lower plenum, upper volume
27	Active Core (cold channel)
28	Active Core (cold channel)
29	Active Core (cold channel)
30	Core-Bypass

Table A1 (continued)

31	Upper core region
32	Upper flow skirt region
33	Dead end of fuel modules
34	Upper plenum
35	Pressurizer Vessel
36	Accumulator A
37	Broken loop hot leg
38	Broken loop hot leg
39	Broken loop steam generator simulator inlet plenum
40	Broken loop steam generator simulator
41	Broken loop steam generator simulator
46	Broken loop steam generator simulator
47	Broken loop steam generator simulator
48	Broken loop steam generator simulator outlet plenum
49	Broken loop pump simulator
50	Broken loop pump simulator
42	Broken loop cold leg
43	Broken loop cold leg
44	Broken loop cold leg
45	Pressurizer surge line
51	Top of riser, separator inlet
52	Downcomer (steam generator)
53	Downcomer (steam generator)
54	Downcomer (steam generator)
55	Condensor
56	Downcomer (steam generator)
57	Steam dome
58	Steam generator outlet pipe
59	Boiler section of steam generator
60	Boiler section of steam generator
61	Boiler section of steam generator
62	Boiler section of steam generator
63	Boiler section of steam generator
64	Lower part of riser
65	Downcomer (steam generator)

Table A1 (continued)

66	Boiler section of steam generator
67	Pipe downstream of steam control valve
68	Feed water pipe
69	Blowdown orifice hot leg
70	Blowdown orifice cold leg
71	RABS of broken cold leg
72	RABS of broken hot leg
73	Downcomer (stalk 1)
74	Downcomer (stalk 1)
75	Downcomer (stalk 1)
76	Downcomer (stalk 1)
77	Active core (hot channel)
78	Active core (hot channel)
79	Active core (hot channel)

Table A2: Description of Fills and Leaks

Junction	Fills and leaks
50	HPIS
51	LPIS
67	Spray of pressurizer
68	Auxiliary feed water

Table A3: Description of valves

Junction	valve
64	Feed water control valve
77	Steam control valve
60, 78	Auxilliary valve
80	Break (hot leg)
81	Break (cold leg)

Table A4: Description of pumps

Junction	Pump
15,18	Primary coolant pumps
63	Feed water pump

Table A5: Description of heat slabs

index of heat slabs	Description of heat slabs
1-6	heat transfer from boiler section to downcomer (steam generator)
7	heat transfer from riser to downcomer (steam generator)
8-19	heat transfer from steam generator primary side to secondary side
20-29	structure of broken loop hot leg
30-32	strcuture of broken loop cold leg
33	structure of RABS (cold leg)
34	strucutre of RABS (hot leg)
35-43	active core (average rod, cold channel)
44-49	structure of the steam generator wall
50	tube sheet
51-56	structure of the vessel (downcomer wall-stalk 2)
57-63	internal structure of the core
64	structure of the upper plenum
65-66	structure of the intact loop hot leg
67	structure of the inlet plenum of the steam generator
68	structure of the outlet plenum of the steam generator
69-74	structure of the pump suction pipes
75-76	structure of the intact loop cold leg
77-78	structure of the pressurizer
79-87	active core (hot rod, power factor 1.4, hot channel)
88-96	active core (cold rod, power factor 0.75, cold channel)
97-100	structure of the vessel (downcomer wall - stalk 1)
101-109	active core (hot rod, power factor 1.2, hot channel)
110-118	active core (average rod, hot channel)

All heat slabs of the core are shown in Fig. A2. The heat slabs 35 - 43 and 88 - 96 are connected to the control volumes 27, 28, 29, and the heat slabs 79 - 87 and 101 - 118 are connected to the control volumes 77, 78, 79.

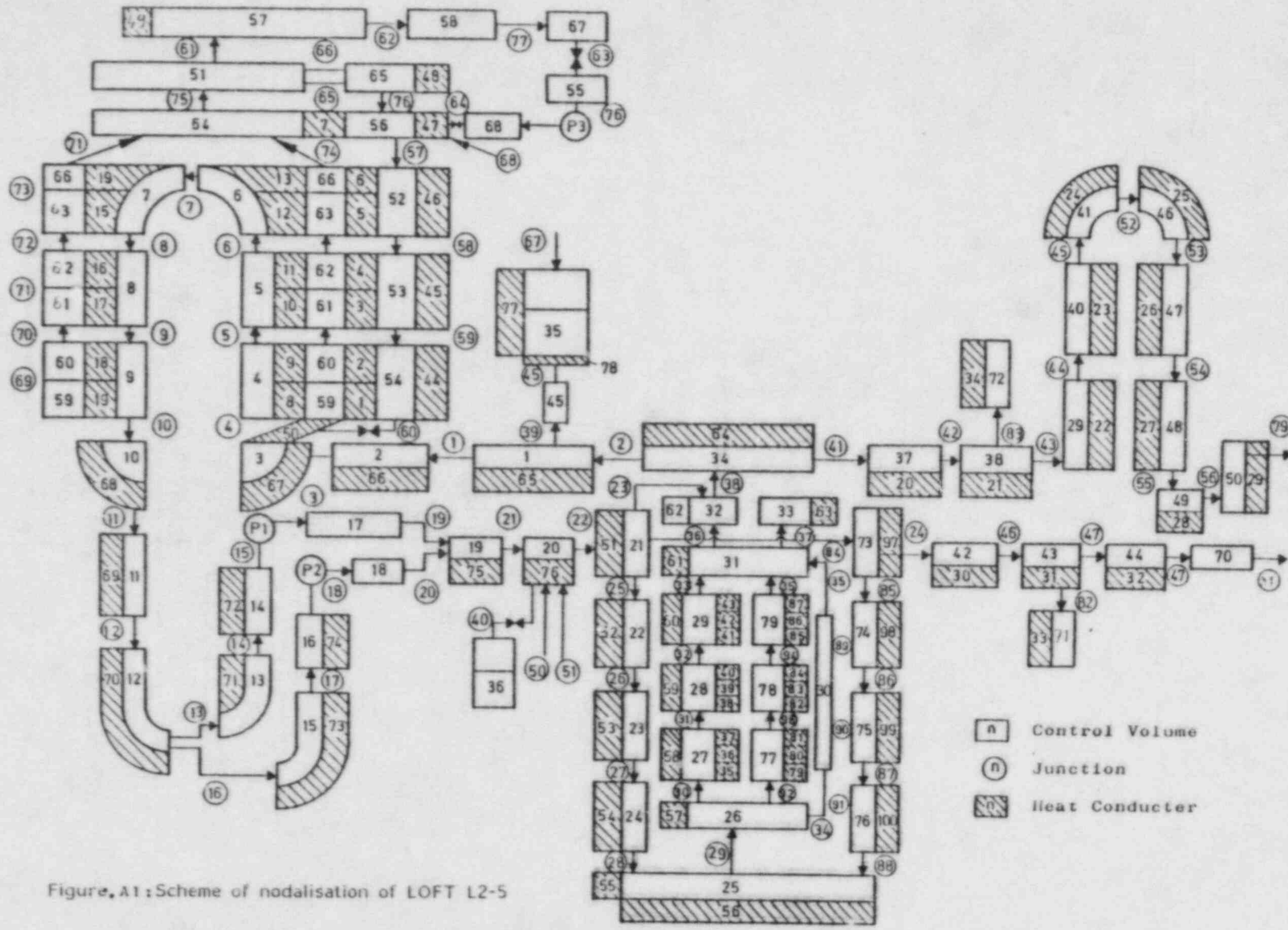

Figure. A1: Scheme of nodalisation of LOFT L2-5

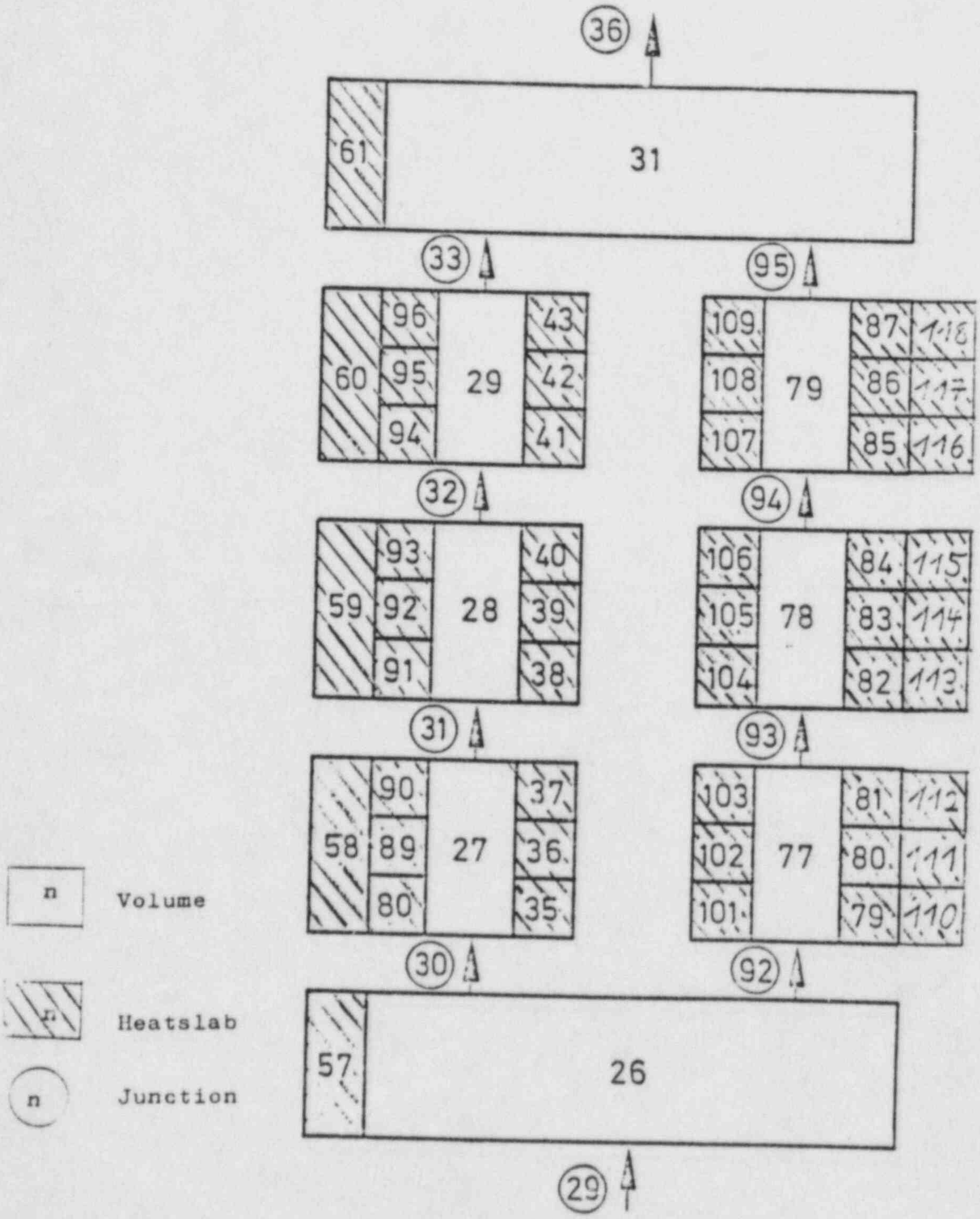

Fig. A2: Nodalisation scheme for the core

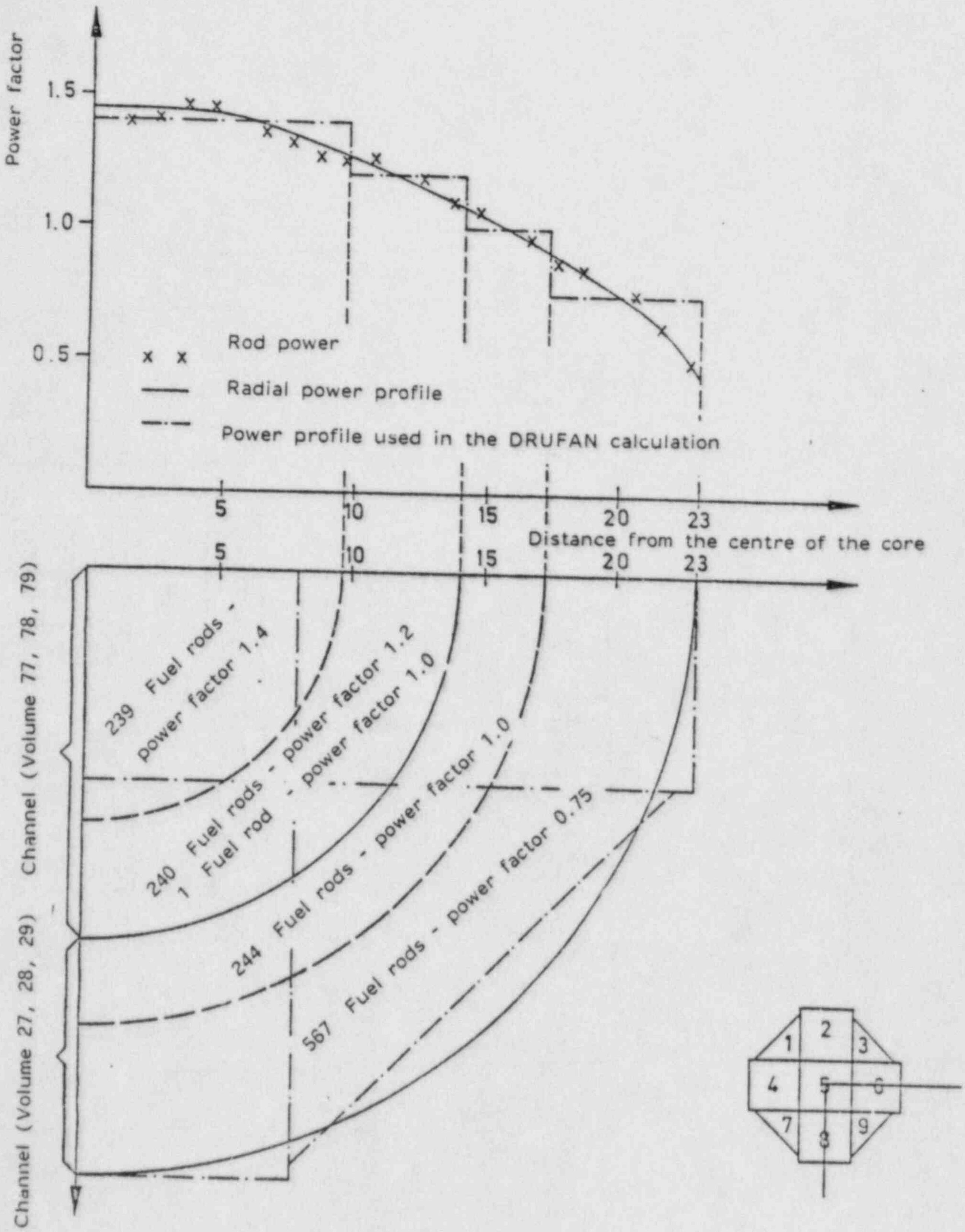

Fig. A3: Radial power profile in the LOFT core and distribution of the flow channels and fuel rods in the DRUFAN calculation

2. Short Description of Code Drufan Ø2

The code DRUFAN has been developed for the simulation of the blowdown and the initial refill phase of LWR-reactors. The code is to be used for the analysis of large, medium sized and small breaks /1,2,3/.

The numerical method applied in DRUFAN is the "lumped parameter approach". The physical system is described by "lumped parameter" control volumes which are connected by flow paths. The ordinary differential equation system of the thermo- and fluiddynamic model is based on the conservation laws for vapour mass, liquid mass, overall energy and overall momentum. The liquid and vapour phases are treated as a homogeneous mixture, or in case of mixture level-tracking as a nonhomogeneous mixture /3/.

The entire range from subcooled liquid to superheated vapour including nonequilibrium effects is simulated by assuming either the liquid or vapour phase to be saturated.

The velocity difference of the liquid and vapour phase may be determined by a drift flux model /3/.

The table for the determination of critical discharge rate at the break is calculated by a one-dimensional nonequilibrium model which is based on the same four conservation equations used for the "lumped parameter" control volumes. In this model the geometry of the discharge flow path is considered /2,4/.

For the simulation of structures, electrical heaters and fuel rods a heat conductor model and a point neutron kinetics model is available. The heat transfer coefficients coupling the structure and thermal hydraulic model are determined by a comprehensive heat transfer package. The heat transfer package contains also a set of critical heat flux correlations. A valve, a pump, an accumulator, a steam generator and a pressurizer model are available for the simulation of components.

The differential equations are integrated by an explicit-implicit integration method with automatic control of time step, order of consistency and local discretization error.

References:

/1/ M.J. Burwell, D. Enix, G. Lerchl, F. Steinhoff
DRUFAN-01/MOD2, Volume I,
Program Description - System Code
GRS-A-646, November 1981

/2/ K. Wolfert
Die Berücksichtigung thermodynamischer Nichtgleichgewichtszustände
bei der Simulation von Druckabsenkungsvorgängen
Dissertation, TU-München, 5.4.1979

/3/ F. Steinhoff
DRUFAN-02
Interim Program Description
Part 1
GRS-A-685, März 1982

/4/ M.J. Burwell, D. Enix
DRUFAN-01/MOD2, Volume II
Program Description - Supporting Code
GRS-A-654, Dezember 1981

3. Description of the critical Flow model

To determine critical discharge rates a 1-D FD model describing the one- and two-phase flow is used to simulate the fluid flow in the flow path close to the discharge orifice where local pressure drop is strongest. The critical mass flow rate is limited to sonic flow at the discharge orifice.

The influence of the hydraulic parameters (length, break-area, friction loss coefficient) on the critical discharge rates is taken into account in this model.

The fluid flow is treated as quasi-stationary due to the relatively slow variation of the discharge rate when the flow is critical.

This assumption permits the calculation of a table of critical discharge rate values for a set of representative upstream fluid conditions in a separate computer run with the code DRUCDR. The 1-D FD model is programmed in this code. As this table is input data for DRUFAN and can be used for many instationary simulations with the same discharge geometry this is a time-saving method.

From the three-dimensional equation system the one-dimensional equation system can be derived on which the discharge model is based.

$$\frac{\partial}{\partial t}\left[\rho_L\cdot(1-\alpha)\cdot F\right] + \frac{\partial}{\partial s}\left[\rho_L\cdot(1-\alpha)\cdot w\cdot F\right] = -\psi\cdot F \qquad \text{(A1)}$$

$$\frac{\partial}{\partial t}\left[\rho_V\cdot\alpha\cdot F\right] + \frac{\partial}{\partial s}\left[\rho_V\cdot\alpha\cdot w\cdot F\right] = \psi\cdot F \qquad \text{(A2)}$$

$$\frac{\partial}{\partial t}\left[\left(\rho\cdot h+\frac{\rho}{2}w^2-p\right)\cdot F\right]+p\,\frac{\partial F}{\partial t} + \frac{\partial}{\partial s}\left[\left(\rho\cdot h\cdot w+\frac{\rho}{2}\cdot w^3\right)\cdot F\right] = q^{*}\cdot F-g\cdot\rho\cdot w\cdot F\,\frac{\partial z}{\partial s} \qquad \text{(A3)}$$

$$\frac{\partial}{\partial t}\left[\rho\cdot w\cdot F\right] + \frac{\partial}{\partial s}\left[\left(p+\rho\cdot w^2\right)\cdot F\right] - p\cdot\,\cdot\frac{\partial F}{\partial s} = -R^{*}\cdot F-g\cdot\rho\cdot F\cdot\frac{\partial z}{\partial s} \qquad \text{(A4)}$$

with

$$\rho \quad = \rho_L \cdot (1-\alpha) + \rho_V \cdot \alpha \tag{A5}$$

$$\rho \cdot h = \rho_L \cdot h_L \cdot (1-\alpha) + \rho_V \cdot h_V \cdot \alpha \tag{A6}$$

This equation system can be brought into form:

$$B \cdot \frac{\partial \bar{u}}{\partial t} + C \cdot \frac{\partial \bar{u}}{\partial s} = \bar{r} \tag{A7}$$

In this equation $\bar{u} = (p, h_L, w, \alpha)^T$ is the solution vector and B and C are matrix valued functions of $\bar{u}$ and $\bar{r}$ is a vector valued fuction of $\bar{u}$. Eigenvalues σ of equation are determined by

$$\det(C-\sigma \cdot B) = 0 \tag{A8}$$

The flow is critical if $\sigma_j = 0$ and $\sigma_i > 0$ for all $i \neq j$.

Specifically

$$\sigma_j = w - \left(\frac{\rho_L}{\rho \cdot \gamma_1}\right)^{1/2} \tag{A9}$$

with

$$\gamma_1 = (1-\alpha) \cdot \frac{\partial \rho_L}{\partial p} - \frac{1}{\rho_L} \left(\rho_V \cdot \alpha \cdot \frac{\partial h_V}{\partial p} - 1\right) \cdot \frac{\partial \rho_L}{\partial h} + \alpha \cdot \frac{\rho_L}{\rho_V} \cdot \frac{\partial \rho_V}{\partial p} \tag{A10}$$

In the one-dimensional calculations the time derivatives in equation (A7) are neglected. Thus, equation (A7) is transformed into

$$\frac{\partial \bar{u}}{\partial s} = C^{-1} \bar{r} \tag{A11}$$

where the boundary values

$$w = \left(\frac{\rho_L}{\rho \cdot \gamma_1}\right)^{1/2}, \quad \sigma_i > 0 \text{ for all } i \neq j$$

are prescribed at the flow path exit. The resulting velocity can be interpreted as Ma = 1.

Equation can be written in the form:

$$\frac{dp}{ds} = -\gamma_2 - \rho \cdot w \cdot \gamma_7 \tag{A12}$$

$$\frac{dh_L}{ds} = \frac{\gamma_8}{w} \tag{A13}$$

$$\frac{dw}{ds} = \gamma_7 \tag{A14}$$

$$\frac{d\alpha}{ds} = \frac{\gamma_9}{w} \quad \text{where} \tag{A15}$$

$$\gamma_2 = g \cdot \rho \cdot \frac{\partial z}{\partial s} + R^* \tag{A16}$$

$$\gamma_3 = \psi \cdot \left[\frac{\rho_L}{\rho_V} + \frac{1}{\rho_L} \cdot (h_V - h_L) \cdot \frac{\partial \rho_L}{\partial h} - 1\right] - \frac{(q^* + \gamma_2 \cdot w)}{\rho_L} \cdot \frac{\partial \rho_L}{\partial h} - \rho_L \cdot w \cdot \frac{1}{F} \frac{\partial F}{\partial s} \tag{A17}$$

$$\gamma_4 = 1 - \rho_V \cdot \alpha \cdot \frac{\partial h_V}{\partial p} \tag{A18}$$

$$\gamma_5 = \frac{1}{\rho_L \cdot (1-\alpha)} \cdot \left[q^* + \gamma_2 \cdot w - \psi \cdot (h_V - h_L) + \frac{\gamma_3 \cdot \gamma_4}{\gamma_1}\right] \tag{A19}$$

$$\gamma_6 = \frac{1}{\rho_D} \cdot \left(\psi - \alpha \cdot \frac{\gamma_3}{\gamma_1} \cdot \frac{\partial \rho_V}{\partial p} - \rho_V \cdot \alpha \cdot w \cdot \frac{1}{F} \cdot \frac{\partial F}{\partial s}\right) \tag{A20}$$

$$\gamma_7 = \frac{\gamma_3 + \gamma_1 \cdot \gamma_2 \cdot w}{\rho_L - \gamma_1 \cdot \rho \cdot w^2} \tag{A21}$$

$$\gamma_8 = \gamma_5 - \frac{\gamma_4 \cdot \gamma_7}{(1-\alpha) \cdot \gamma_1} \tag{A22}$$

$$\gamma_9 = \gamma_6 - \left(1 - \frac{\rho_L}{\gamma_V \cdot \rho} \frac{\partial \rho_V}{\partial p}\right) \cdot \alpha \cdot \gamma_7 \tag{A23}$$

The quasi stationary equation system given above is 'liquid dominant' and is used in the void range from 0 to 0.98. In the void range $\alpha > 0.98$ the 'vapour dominant' equation system is taken which is derived in a similar way.

For a given discharge geometry (Fig. A4) characterized by length L_1, flow cross sectional area F_1, friction loss coefficient ζ and for representative states of p, h_L and α at the inlet of the 1-D FD model, the inlet velocity w is determined by a shooting technique in such a way that

$$w = \left(\frac{\rho_L}{\rho \cdot \gamma_1}\right)^{1/2}$$

is reached at the exit. This means that the sonic velocity exists at the break plane. The system of the equations along the flow path is integrated by the explicit part of the method described in ref. /13, 14/. This method includes convergence control and an automatically controlled step size.

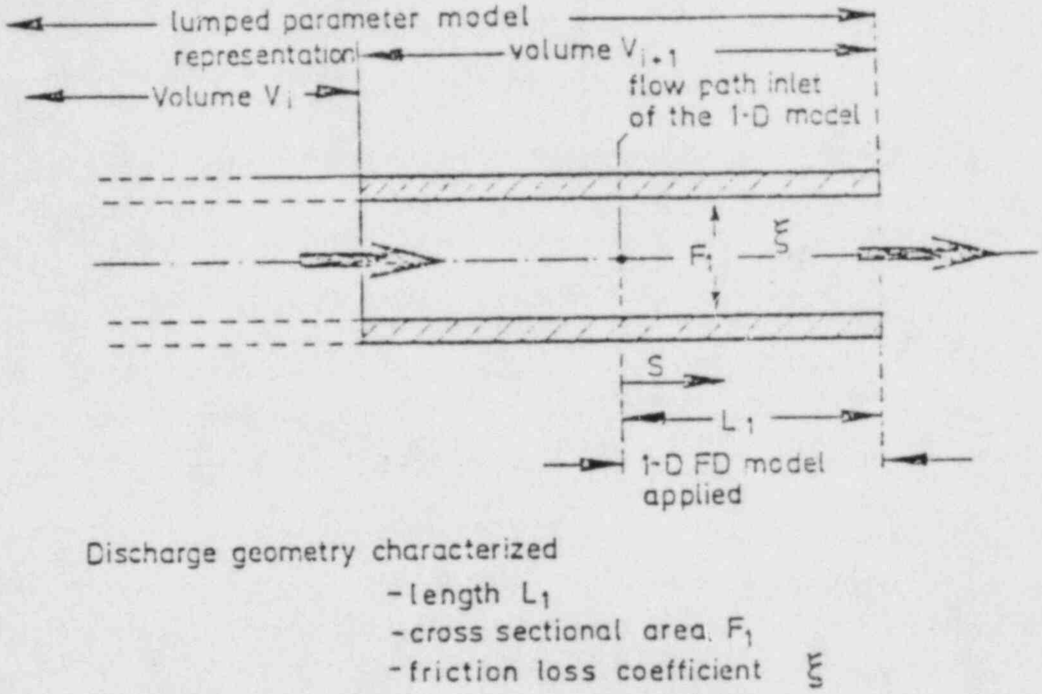

Fig. A4: Application of the 1-D finite difference model

The reduction of the cross section area (C.S.A.) in the break flow path (valve, orifice, nozzle) can be taken into account by calculation with the 1-D FD model.

4. Listing of options

1. Fluid Dynamics

1.1 Drift flux model

The drift flux model (mod. RELAP correlation) is used in all vertical junctions without the downcomer and steam dome of the steam generator.

1.2 Mixture level model

The mixture level model is used in the downcomer and steam dome of the steam generator, in the pressurizer and the accumulator. For the bubble rise the "Wilson" equation is used.

1.3 Collapsed level model

The collapsed level model is used in both downcomer of the reactor vessel, in the core, in the pressurizer, in the accumulator and in the downcomer of the steam generator.

1.4 Critical discharge model

The critical mass flow is calculated by the 1-D FD discharge model.

1.5 HPIS and LPIS

The HPIS and LPIS are time dependet input functions.

2. Active Core

2.1 Heat generation

A point neutron kinetic model is used for the heat generation in the core. The external reactivity and the post decay power is a time dependent input function .

2.2 Critical Heat Flux

The smallest critical heat flux calculated by all following equations will be used:

Westinghouse W3

Babcock-Wilcox BU.W-2

General-Electric

Macbeth

Hench-Levy

Barnett

Hughes

Israel-Casterline-Matzner

Szmolin

3. Heat Transfer

Following heat transfer correlations are used

Dittus-Boelter I

Dittus-Boelter II

Chen

Mod. Dougall-Rhosenow

4. Loss of heat through structures

The loss of the heat through all structures on the primary side amount to 300 kW and on the secondary side to 100 kW under steady state conditions. The surrounding temperature is 35 (Grd C).

5. Heat generation in pumps

The heat flux from the primary pumps to the fluid is added to the control volumes 17 and 18 by a time dependent input function.

6. Stationary calculation

A stationary calculation is made for 5 seconds to have stationary conditions in all control volumes. After 5 seconds the break is initiated. At this moment the steam control valve and the feed water regulation valve begin to close.

5. Discussion of the results of the blind and posttest calculations of L2-5

GRS used the DRUFAN-02 computer code to perform the blind and the posttest calculation at L2-5. In the blind calculation DRUFAN-02 had difficulties in the calculation of the fluid temperature (Fig. 9) and the fluid density (Fig.13) at the ECC injection point in the cold leg of the intact loop. The reason for this difference between the measurement and the calculation was the reduction of the condensation at the condensation point to assure that water packing in the cold leg at the intact loop would never occur. The posttest calculation was performed with the normal condensation model. The results of the posttest calculation for the fluidtemperature TF, the vapour temperature TV (Fig. A5) and density RHOI (Fig. A6) show good agreement with the measurement.

The pressure history of the pressurizer (Fig. A7) was improved in the posttest calculation. The flow resistance was increased in consideration of the flashing of the fluid in the pressurizer surgeline.

The comparison of the measured and calculated rod cladding temperatures (Fig. 25,26) presents only an uncomplete view of the events in the core. The figures A8, A9 show in addition results in the centre of the core and figure A10 shows results in the external region of the core.

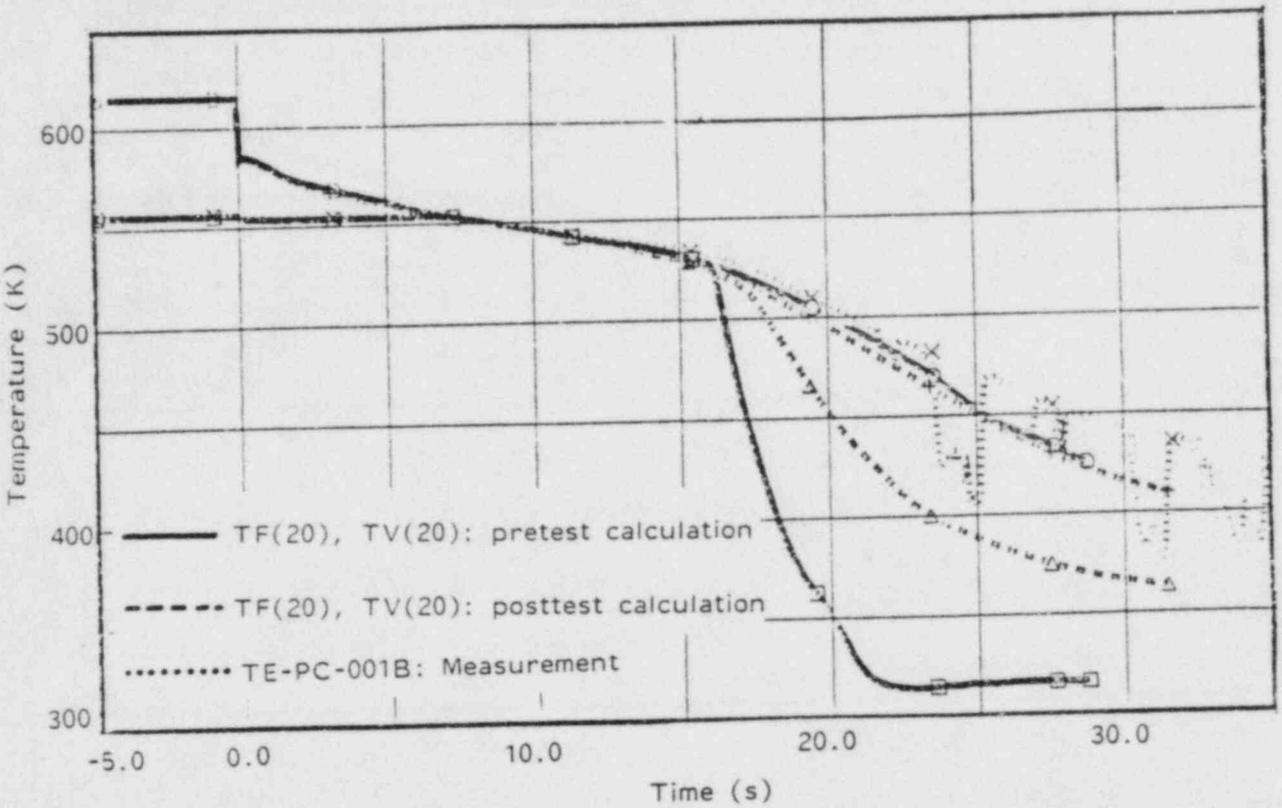

Fig. A5 : Fluid and vapour temperature in the intact loop cold leg

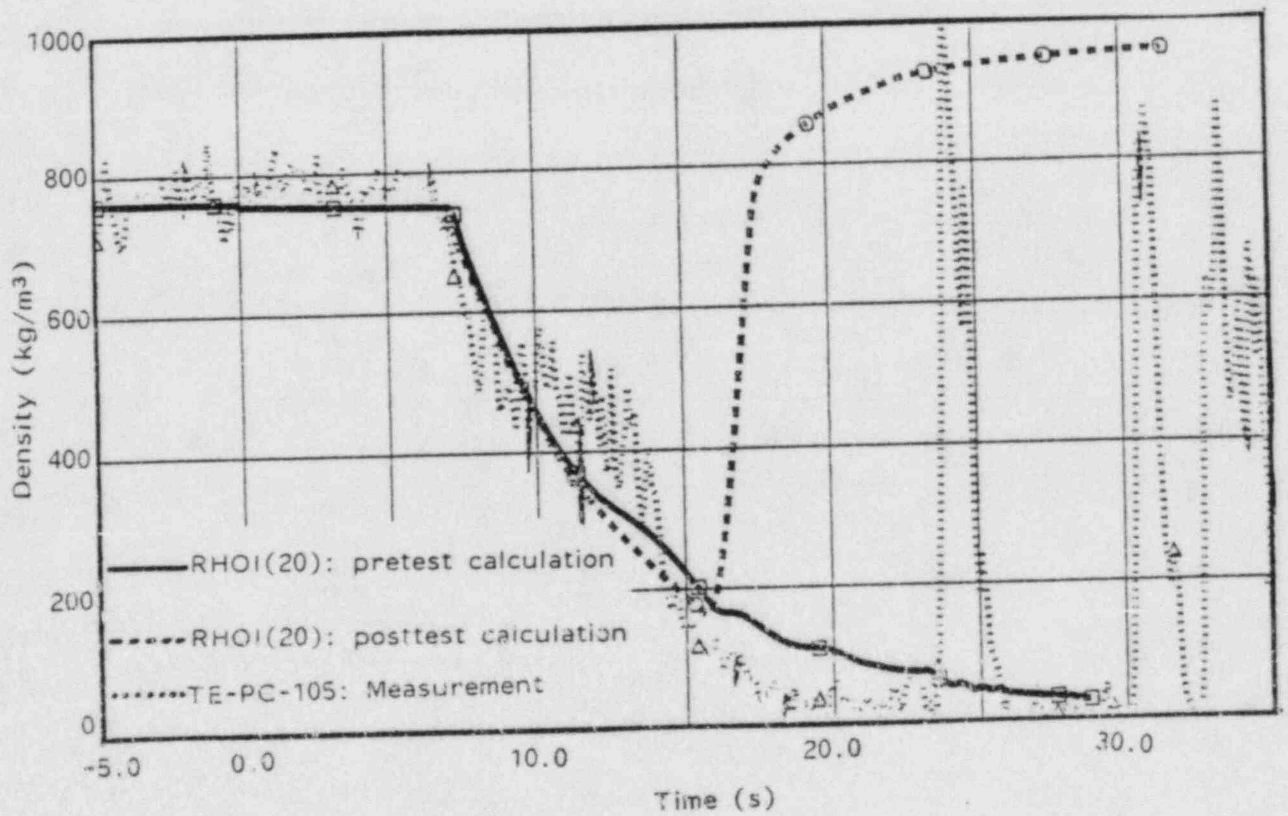

Fig. A6 : Density in the intact loop cold leg

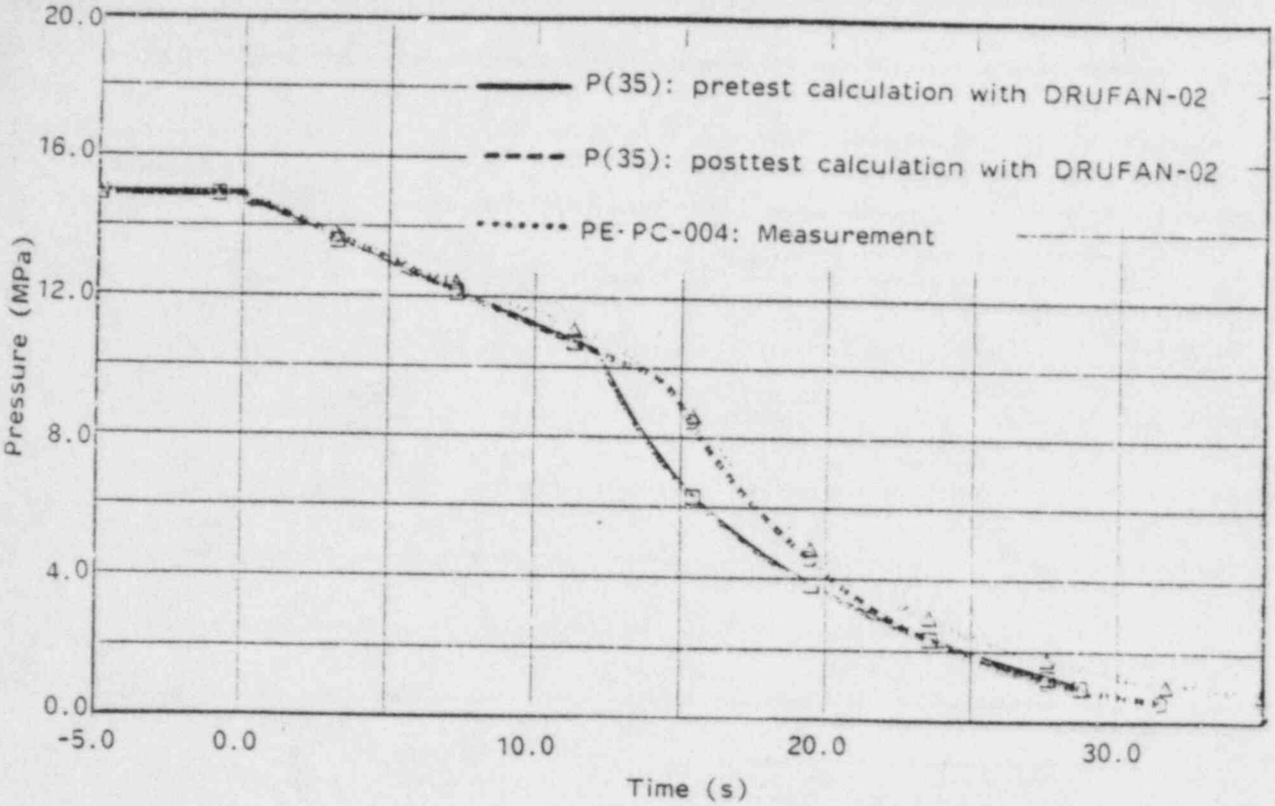

Fig. A7 : Pressure in the pressurizer

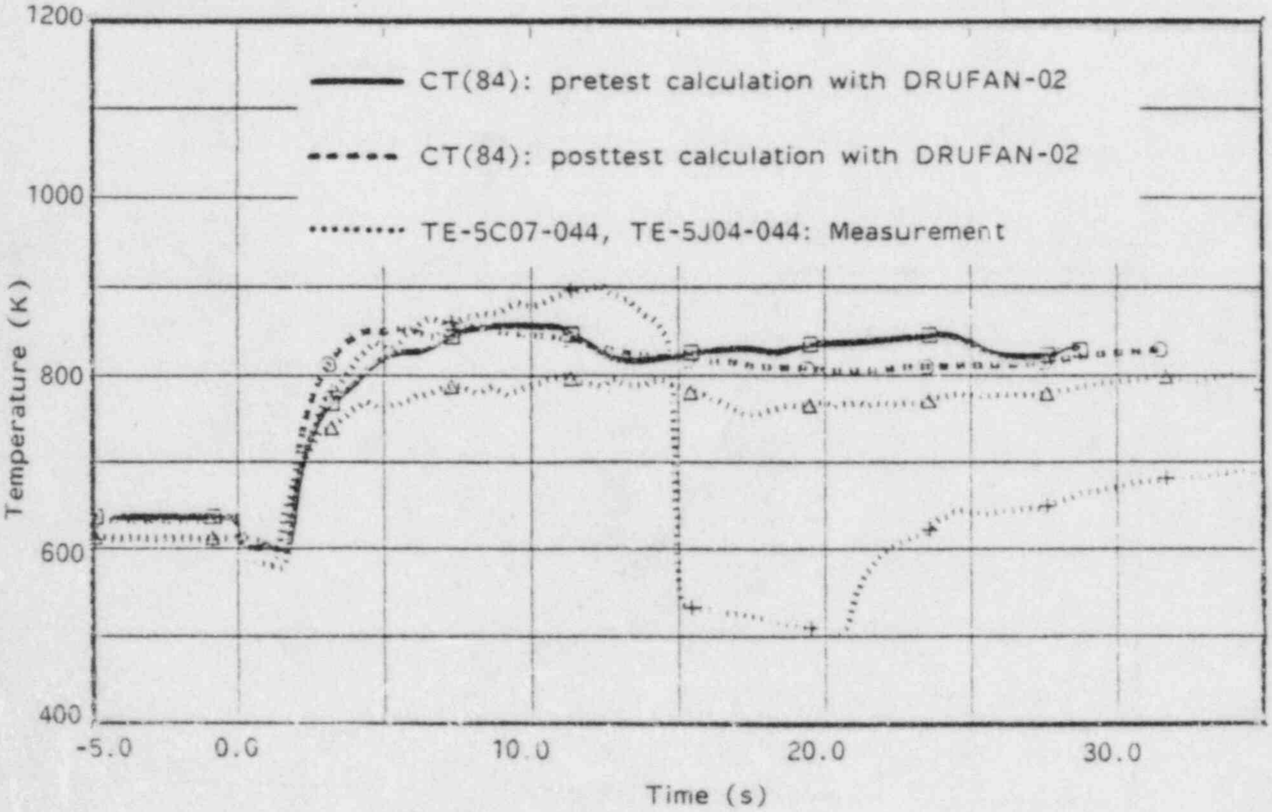

Fig. A8 : Cladding Temperature (Power Factor = 1.4: ELV = 40)

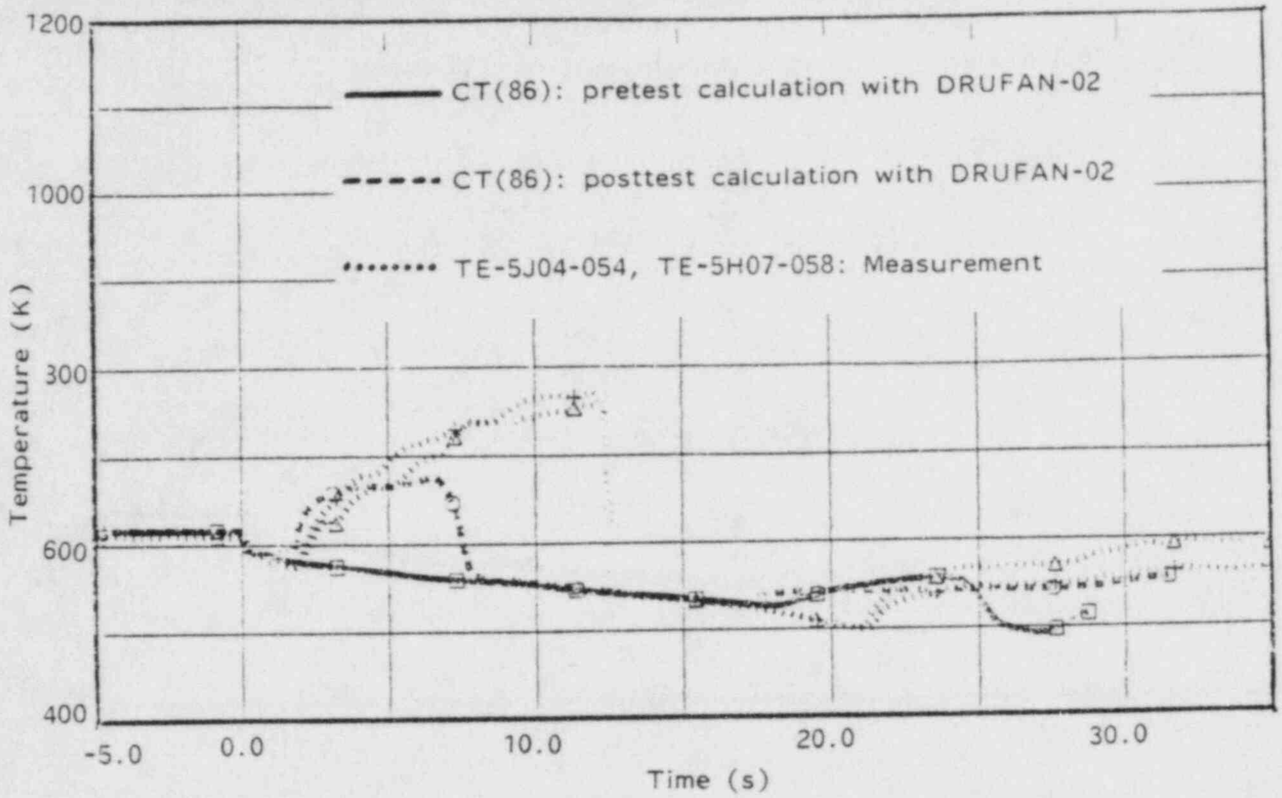

Fig. A9 : Cladding Temperature (Power Factor = 1.4: ELV = 54)

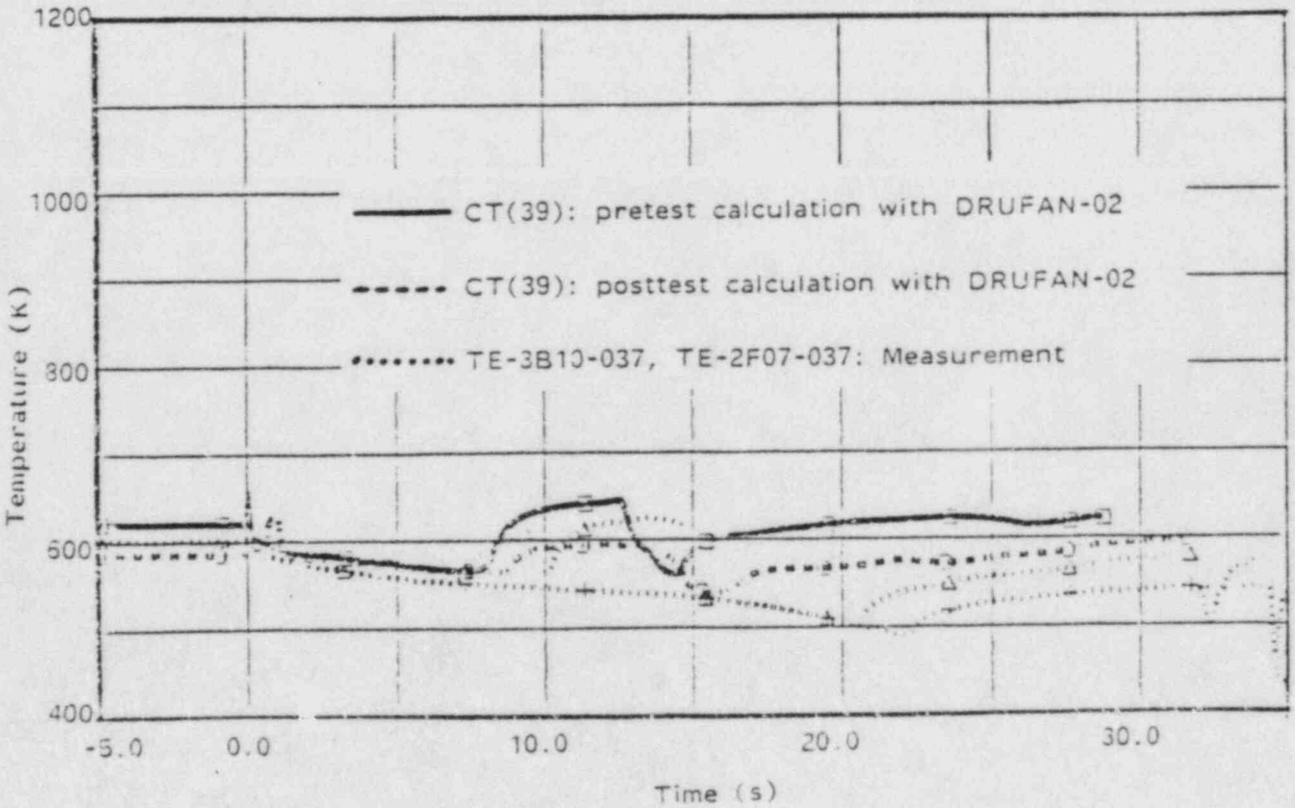

Fig. A10 :Cladding Temperature (Power Factor = 1.0: ELV = 33)

APPENDIX B

ISP-13 SUBMITTAL FROM JAPAN ATOMIC ENERGY INSTITUTE USING RELAP4/MOD6 (JAR)

Appendix B Pre-Test Prediction of LOFT L2-5 with RELAP4/MOD6/U4/J3 (Japanene Contribution ISP 13 (JAR))

1. Nodalization

A schematic nodalization diagram of the LOFT system is shown in Figure 1. The model consists of 41 control volumes, 48 junctions and 25 heat slabs including 12 core fuel slabs. The brief description of each control volume is given in Table 1.

2. Modelling

Models used in this blind calculation are as followed:

a) Henry-Fauske/HEM critical flow model with a discharge coefficient of o.85 for both subcooled and saturated region, and transition quality of 0.002 is used.

b) Two-phase pump head difference cirve was obtained by the analysis of L3-6 experiment.

c) MOD6 blowdown heat transfer model is used. Condie-bengston III film boiling correlation and MOdified Zuber CHF correlation are selected.

d) Macdonald-Broughton gap conductance model is used.

f) Accumulator gas expansion model is used.

3. Discussions of the results

Overall features of the experiment had been well predicted in our blind calculation. The major discrepancies between the prediction and the experimental results are followings;

a) The prediction had not showed rewetting of fuel cladding at 0.99m at about 15 s.

b) The fluid temperature in the lower plenum is superheated in the prediction due to complete voiding. It results from less ECC water flowing into the lower plenum in the prediction due to defect in modelling ECC injection line.

4. Concluding Remarks

Overall features are well predicted with RELAP4/MOD6/U4/J3 especially during blowdown in spite of some difficulties.

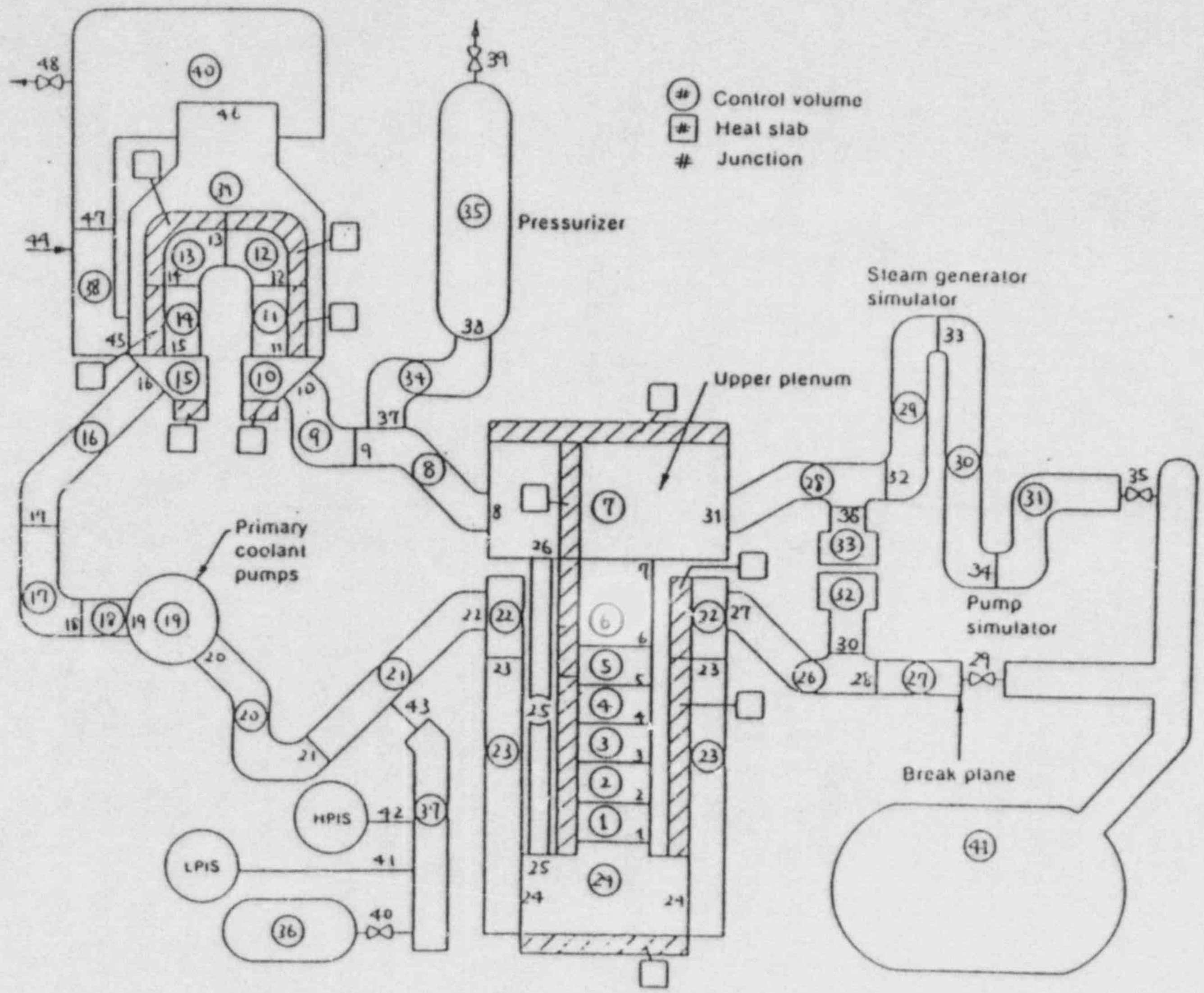

Figure 1 LOFT RELAP4 model schematic diagram.

Table 1 Description of Control Volumes in LOFT System Model

Volume No.	Description
1 through 5	Nuclear core
6 and 7	Upper plenum
8 and 9	Intact loop hot leg
10 and 15	Steam generator inlet plenum and outlet plenum
11 and 14	Straight sections of steam generator tubes
12 and 13	Curved sections of steam generator tubes
16	Steam generator outlet piping
17	14-in. piping leading to the tee precedeing the coolant pumps
18	Piping from tee to primary coolant pumps
19	Primary coolant pumps
20 and 21	Intact loop cold leg
22	Upper annular region of the vessel inlet region
23	Downcomer region of the reactor vessel
24	Lower plenum
25	Core bypass region
26 and 27	Broken loop cold leg
28 through 31	Broken loop hot leg
32 and 33	Reflood assist bypass piping
34	Pressurizer surge line
35	Pressurizer
36	ECC accumulator
37	ECC injection line
38	Steam generator secondary downcomer
39	Steam generator secondary shroud region
40	Steam generator secondary steam dome
41	Supression Tank

APPENDIX C

ISP-13 SUBMITTAL FROM JAPAN ATOMIC ENERGY INSTITUTE
USING THYDE-P1 (JAT)

Appendix C Pre-Test Prediction of LOFT L2-5 with THYDE-P1 (Japanese Contribution to ISP 13 (JAT))

1. Nodalization

The nodalization applied in the present calculation is shown in Fig. 1. The summary of the present THYDE-P1 calculation is shown in Table 1. The characteristic features of the present nodalization are summarized as follows.

(1) The active core was nodalized in 6 nodes(Nodes 18 to 23). Only an average rod in the average channel is taken into consideration.

(2) The downcomer is simulated by one node(Node 14).

(3) The Leakage path from the downcomer-top to the upperplenum is simulated by Node 27.

(4) Both structural heat and ambient heat loss are neglected(no heat slab except the core and SG).

2. Modelling

2.1 Break Flow model

The modified Zaloudek equation and the Moody correlation are implemented in THYDE-P1. The discharge coefficient for the Zaloudek equation is determined in the code so as to smoothly connect the flows at quality zero. The discharge coefficient for the Moody correlation was given by an input to be 0.6.

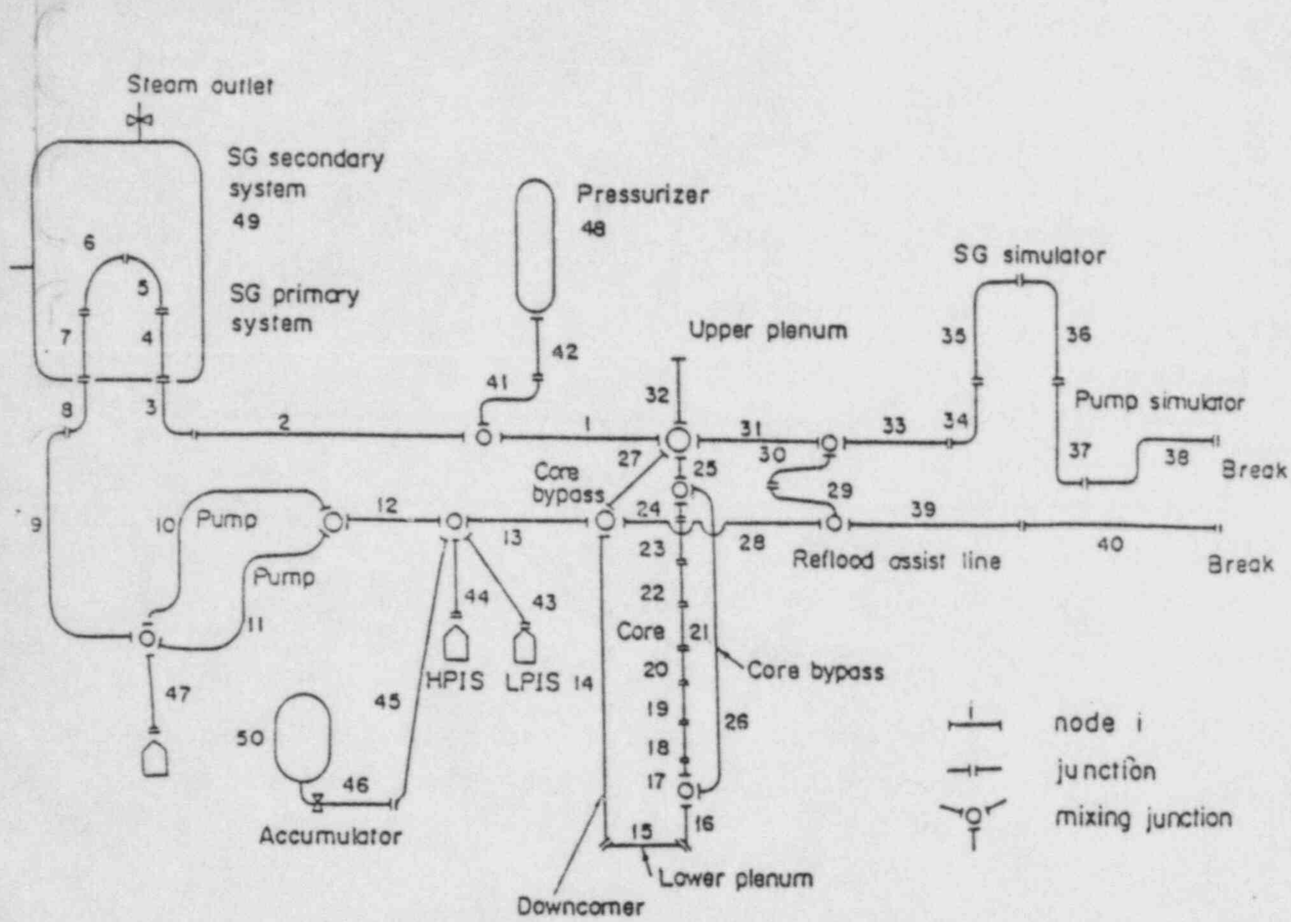

Fig. 1 Nodalization for Pre-Test Prediction of LOFT L2-5 with THYDE-P1

Table 1 Summary of THYDE-P1 Calculation

Volumes	Junctions	Heat slabs
50	43	11 (SG and core)

Transient Time (s)	CPU Time (hr)	CPU Time Ratio (-)	Computer Used
70.	2.24	115.	FACOM M-200

Table 2-1 Pre-CHF heat transfer correlations

Mode	State	Condition	$IHTROP_1$	Correlation
10	Subcool	$T_w < T_{sat}$	-	Dittus-Boelter
21	Subcool	$T_w > T_{sat}$	1	Interpolation between Mode 10 and Mode 31
22	Subcool	$T_w > T_{sat}$	2	Interpolation between Mode 10 and Mode 32
31	Saturate	$T_w > T_{sat}$	1	Jens and Lottes
32	Saturate	$T_w > T_{sat}$	2	Thom
60	Saturate	$T_w > T_{sat}$		Condensation

Table 2-2 Post-CHF heat transfer correlations

(a) Saturated state

Mode	Flow Condition	Condition	Pressure	$IHTROP_2$	Correlation
41	$G > G_{min}$	$x > x_{c1}$	P > 30psia	-	Groenevelt
42	$G > G_{min}$	$x > x_{c1}$	P < 30psia	-	Dougal-Rohsenov
43	$G > G_{min}$	$x < x_{c1}$		-	Interpolation between CHF(x=0.) and Mode 41($x=xc_1$)
44	$G < G_{min}$	$x > x_{c2}$		1	Berenson
				2	Modified Bromley
				3	Bromley-Pomerantz
45	$G < G_{min}$	$x < x_{c2}$		-	Interpolation between CHF(x=0.) and Mode 44($x=xc_2$)

(b) Superheated state

Mode	Flow condition	Correlation
51	3000 > Re	Forced convection
52	3000 < Re < 5000	Interpolation between Mode 51 and Mode 53
53	Re > 5000	McEligot

x_{c1} : Threshold quality (=0.5)
x_{c2} : Threshold quality (=0.1)
G_{min} : Threshold mass flux (=271.2 kg/m^2s)
$IHTROP_1$: Option selection flag given by input
$IHTROP_2$: Option selection flag given by input

2.2 CHF and Heat Transfer Model

The Biasi correlation and the modified Zuber correlation were selected to be used for the CHF correlation set by inputs. The heat transfer correlations implemented in the present version are listed in Tables 2-1 and 2-2.

2.3 Relaxation Model

A relaxation model is implemented in THYDE-P1 to take thermal non-equilibrium effects into consideration. The time constant for the delay of the temporal density change is given by an input for each node in the present version. In the present calculation, the relaxation model was not applied before ACC injection initiation but was applied after that to avoid unrealistically large pressure decrease due to cold water injection. The time constants were determined from the experiences of the past LOFT analyses and several sensitivity calculations.

2.4 Pump Model

The pump model in THYDE-P is almost identical to that in RELAP4 or RELAP5. The input data such as the single-phase and two-phase pump characteristic curves are refferred to the LOFT base input for RELAP-5. The recommented value for the pump inertia during Experiment L2-5 was applied to simulate the atypically fast pump coastdown.

3 Results and Discussion

Figure 3-1 shows the predicted pressure transient along with the experimental data. The overestimation of the pressure before ACC injection initiation might be brought about by the underestimation of the cold leg break flow just after the break as shown in Fig. 3-2. The underestimation of the flow itself may be one of the possible reasons since the mass and energy release are underestimated. In addition to this, the underestimated cold leg break flow might cause the overestimation of the core flow resulting in high heat transfer rate at the core. This may be also the reason for the overestimated pressure. The model to determine the discharge coefficient for the Zaloudek equation stated in Sec. 2 should be improved.

Figure 3-3 shows the comparison of the hot leg break flows. The sudden decrease of the flow observed just after the break could not be predicted by THYDE-P1. The input data for the initial temperature distribution along the broken loop hot leg should be improved.

The three-dimensional views of the calculated cladding surface temperature is shown in Fig. 3-4. Eight curves of the calculated cladding temperatures at the core nodes are shown in one viewgragh in Fig. 3-5. Both figures clearly show that the core-wide early rewet was neither predicted to occur nor observed. In Fig. 3-5, the quenched regions are descriminated by the dotted lines. Both bottom-up quench and the top-down quench were predicted to occur as observed.

Figure 3-6 shows the comparison of the cladding surface temperatures at the hottest spot. The vertical locations of the node and the thermocouple are shown in the right side of the figure by the dashed line and the cross, respectively. The maximum linear heat generation rate in the experiment is is 40 kW/m. In the present calculation, however, it is 25 kW/m since only an average rod is taken into account. Therefore, a quantitative comparison may have less meaning. Qualitatively, the trends are similar to each other in the sense that the early rewet did not occur in both prediction and experiment and the calculated final quenching time is in good agreement with the experimental data.

The calculated cladding surface temperature at the lowest node is shown in Fig. 3-7 along with several experimental curves observed at the peripheral bundle, "Bundle 2". The vertical location of the experimental curve with triangle-mark is corresponding to the calculation. As shown in the experimental data, the early rewet is observed and the trends seem to be similar to those observed in L2-2 and L2-3. In the calculation, such a behavior is predicted to occure at the lowest core node, where the heat generation rate is low.

Figures 3-8 and 3-9 show the comparison of hydraulic behavior at the intact loop cold leg. What is called chagging phenomena induced by ECC injection were observed as shown in these figures. In the calculation, however, it is out of the scope to trace the oscillatory behavior. At present, it may be rather important to simulate overall behavior without numerical difficulties. From this point of view, the relaxation model worked

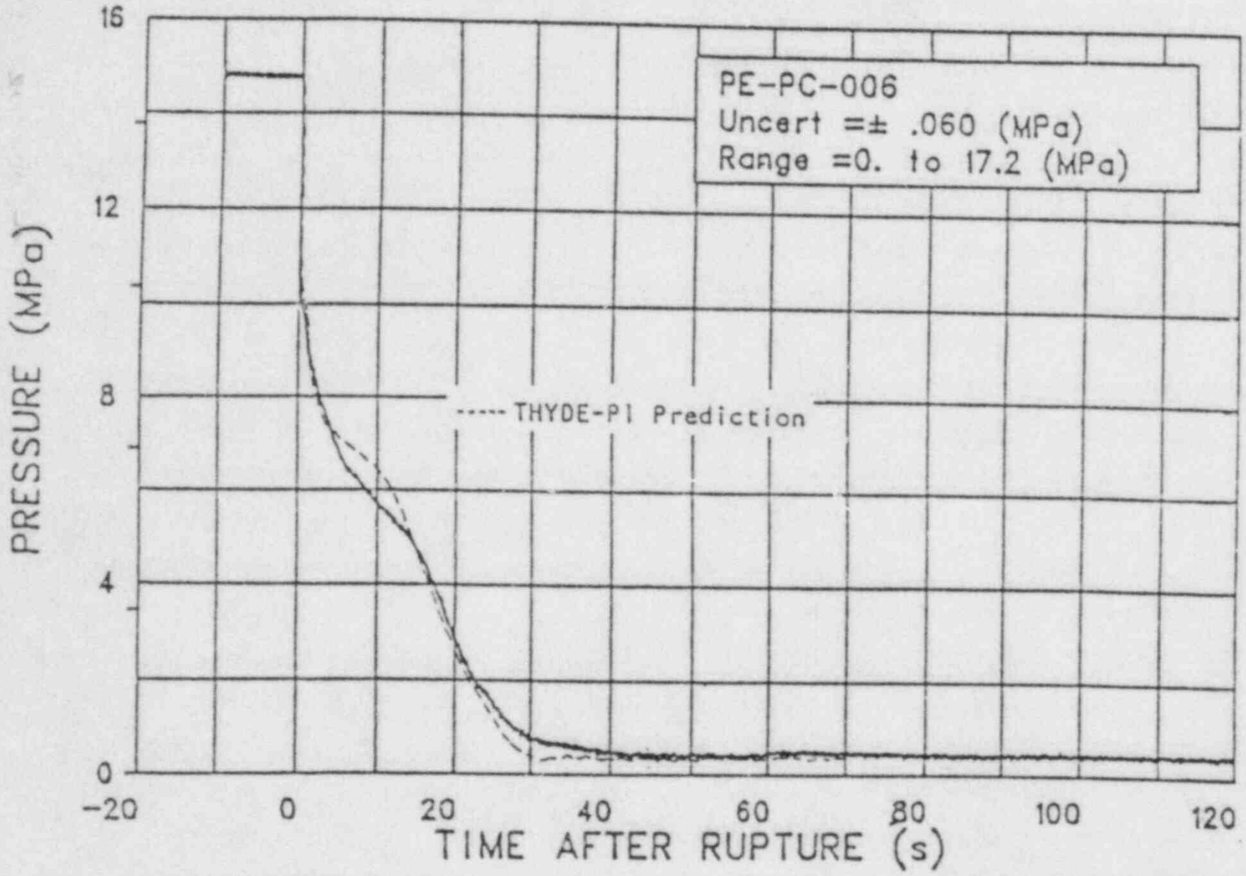

Fig. 3-1 Reference pressure in intact loop between steam generator outlet and primary coolant pump inlet

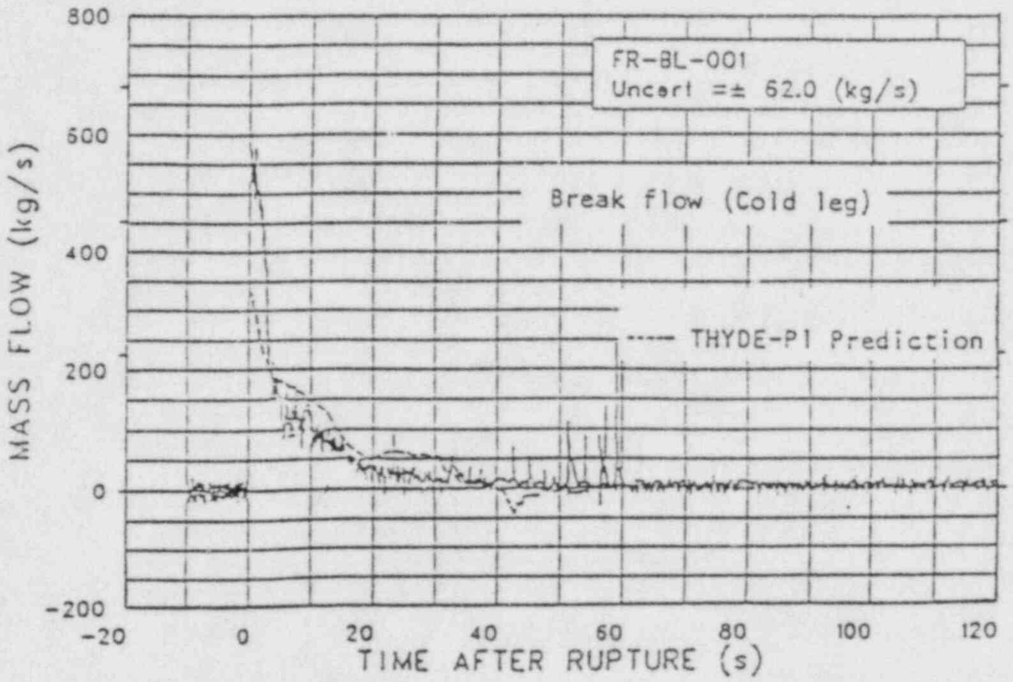

Fig. 3-2 Mass flow rate through break orifice in broken loop cold leg

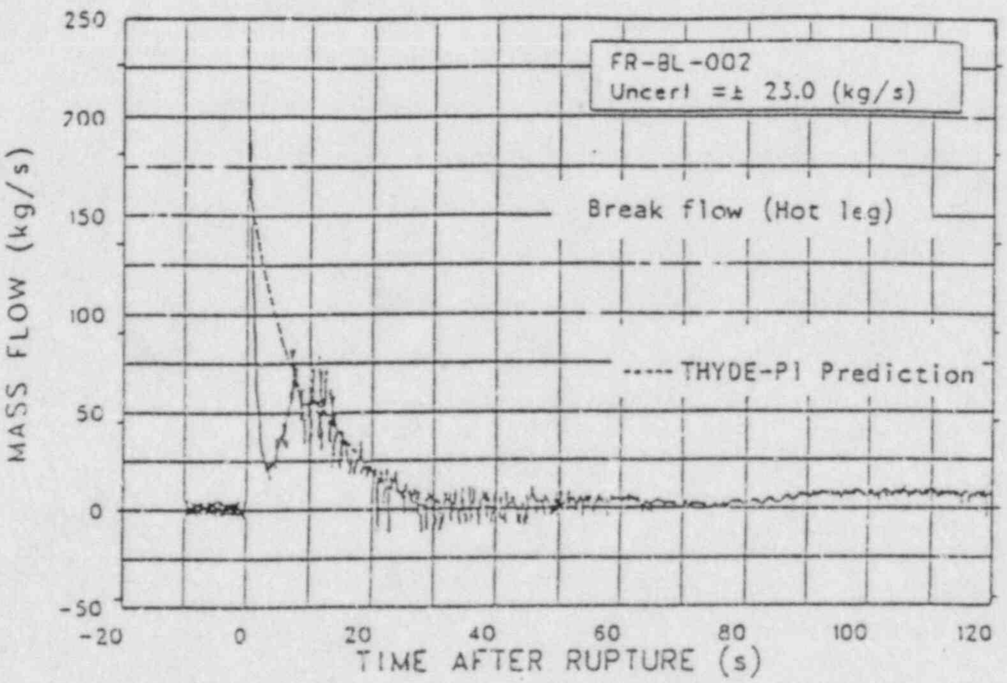

Fig. 3-3 Mass flow rate through break orifice in broken loop hot leg

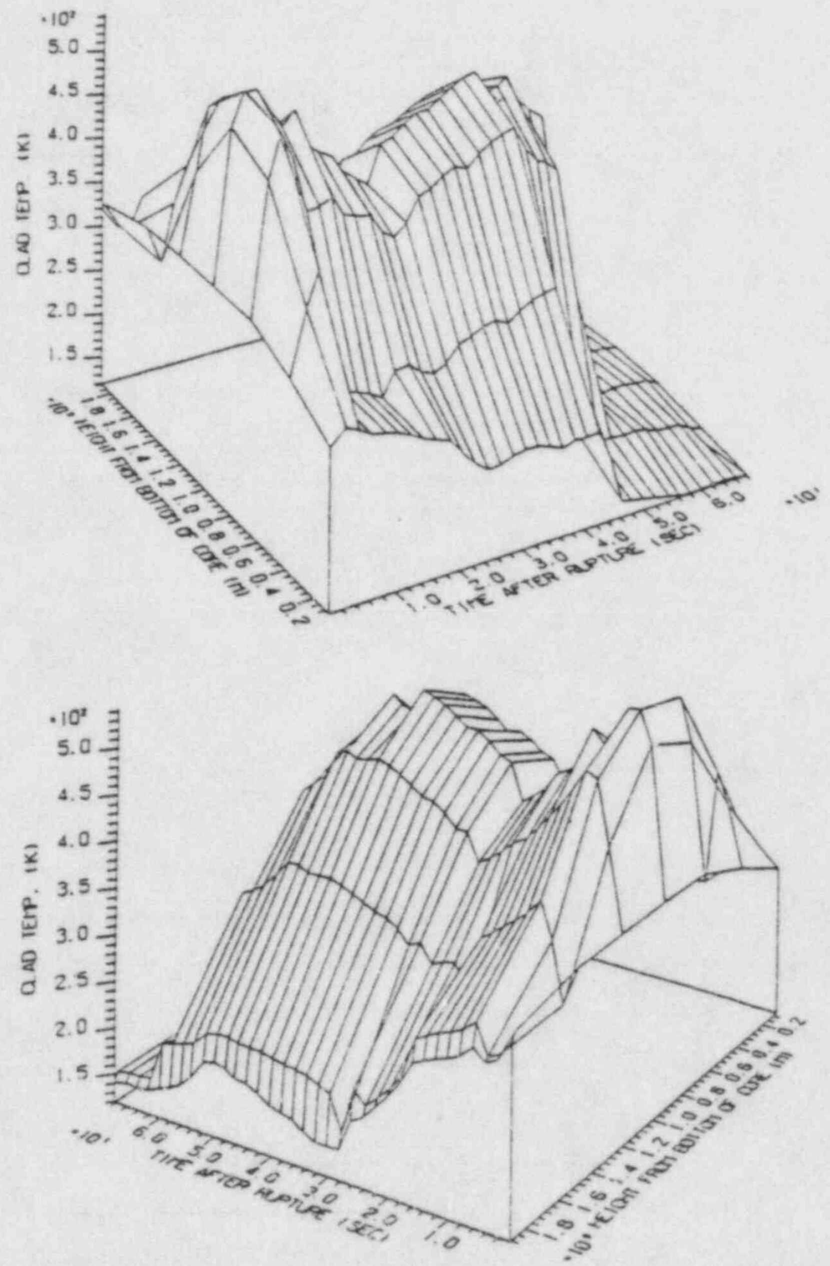

Fig. 3-4

Three-dimensional view of cladding surface temperature

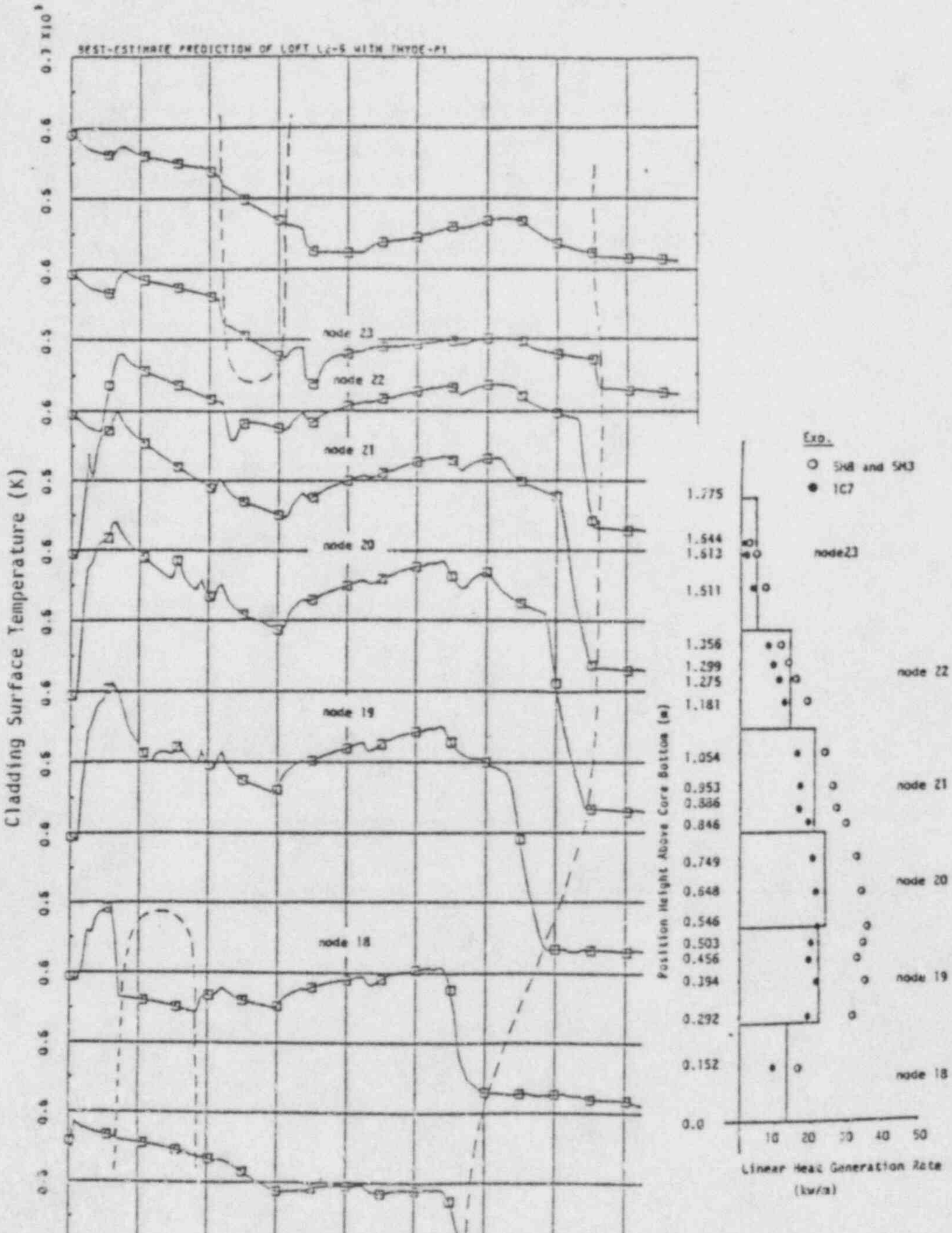

Fig. 3-5 Vertical Distribution of Cladding Surface Temperature

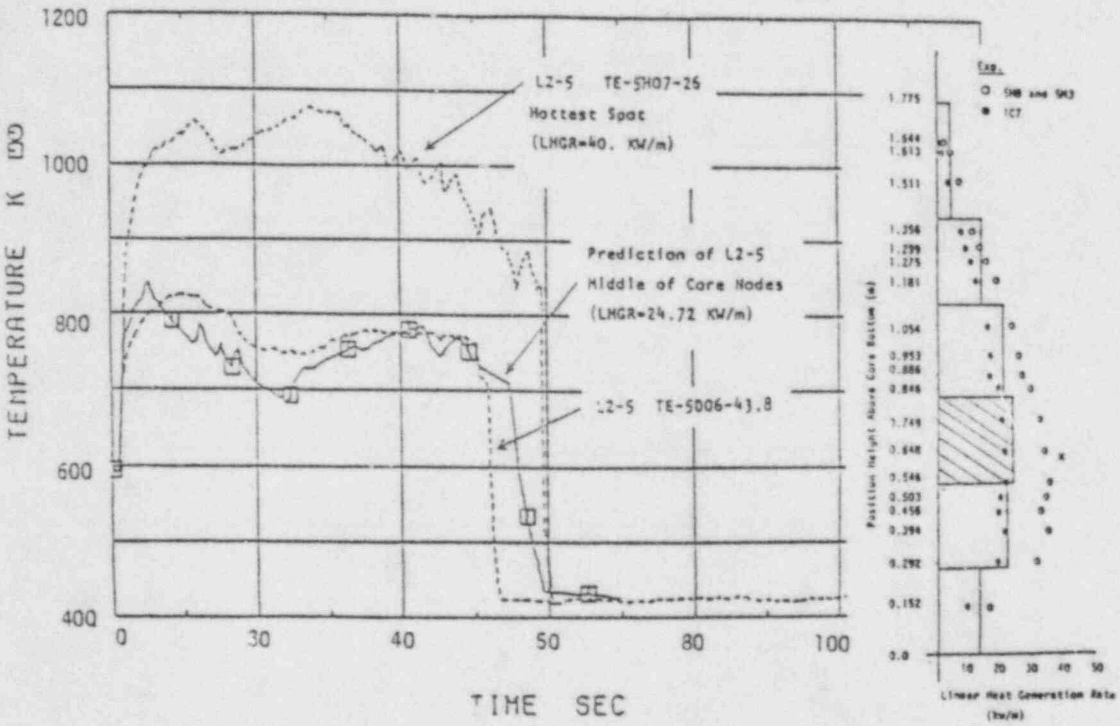

Fig. 3-6 Cladding surface temperature at hottest spot

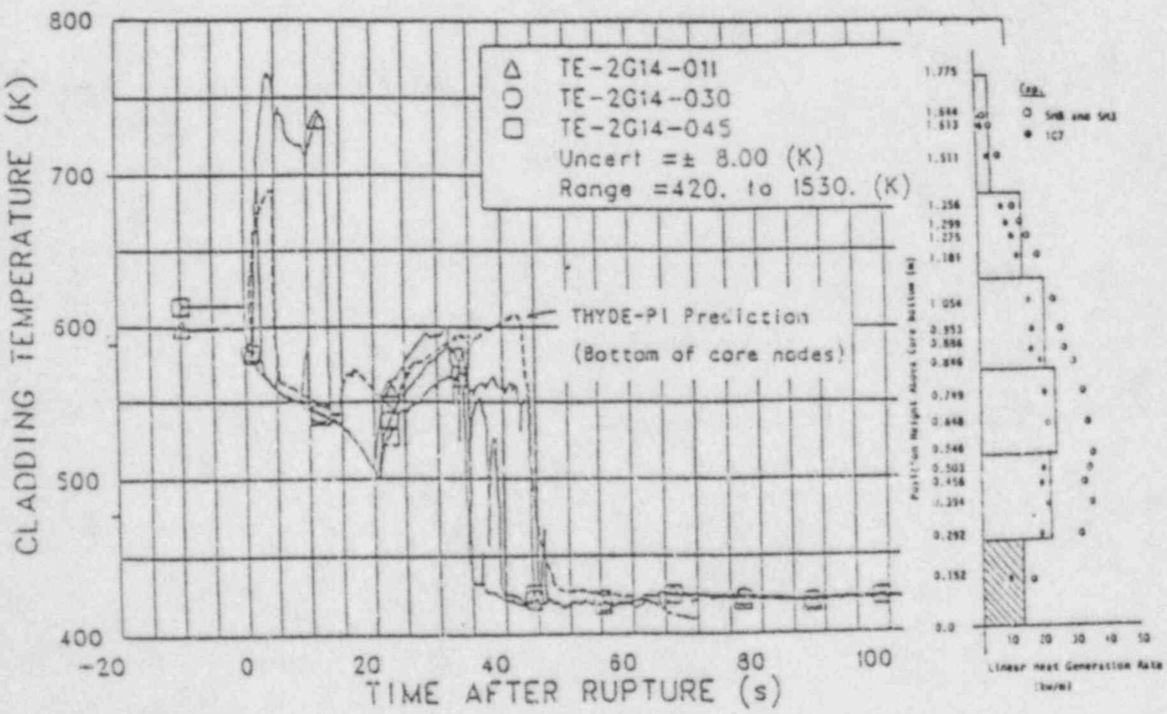

Fig. 3-7 Calculated cladding surface temperatuer at lowest node and experimental data at periferal bundle

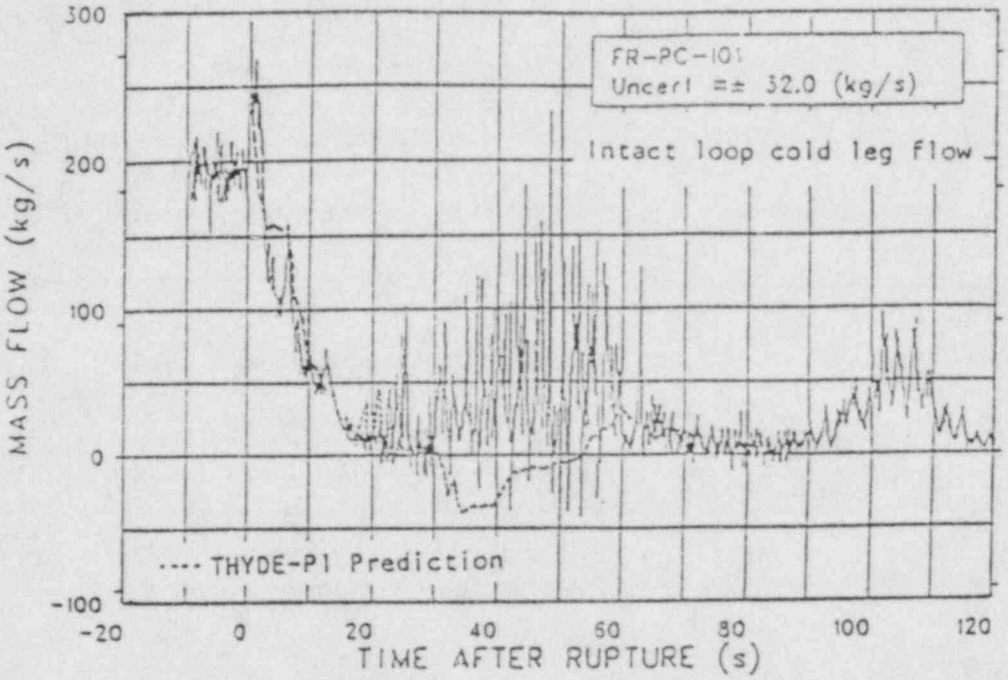

Fig. 3-8 Mass flow rate through intact loop cold leg

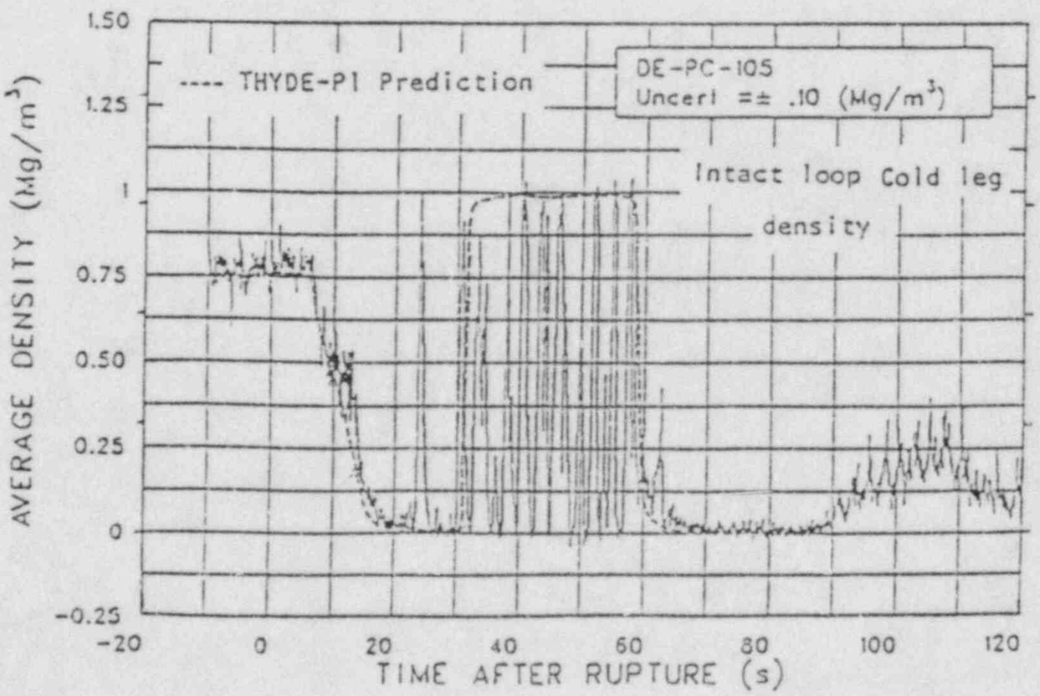

Fig. 3-9 Average fluid density in intact loop cold leg

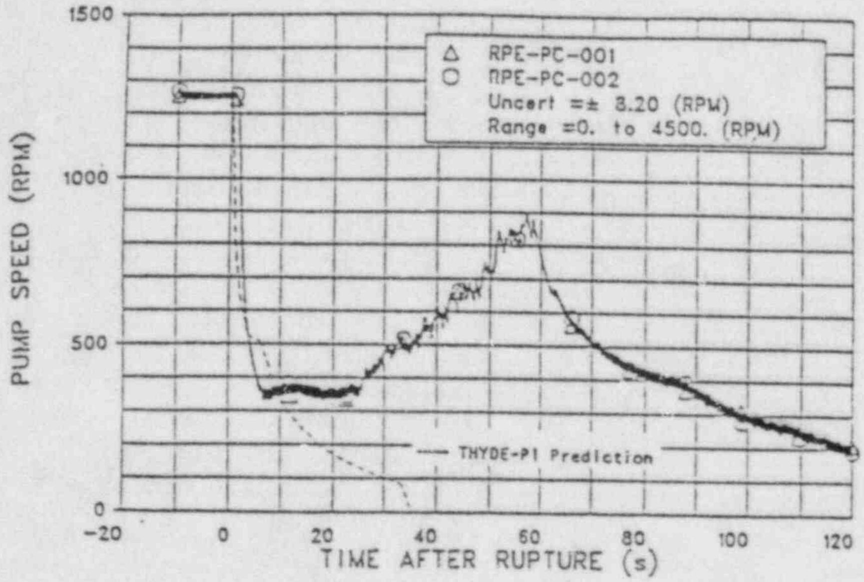

Fig. 3-10 Pump speed for primary coolant pump

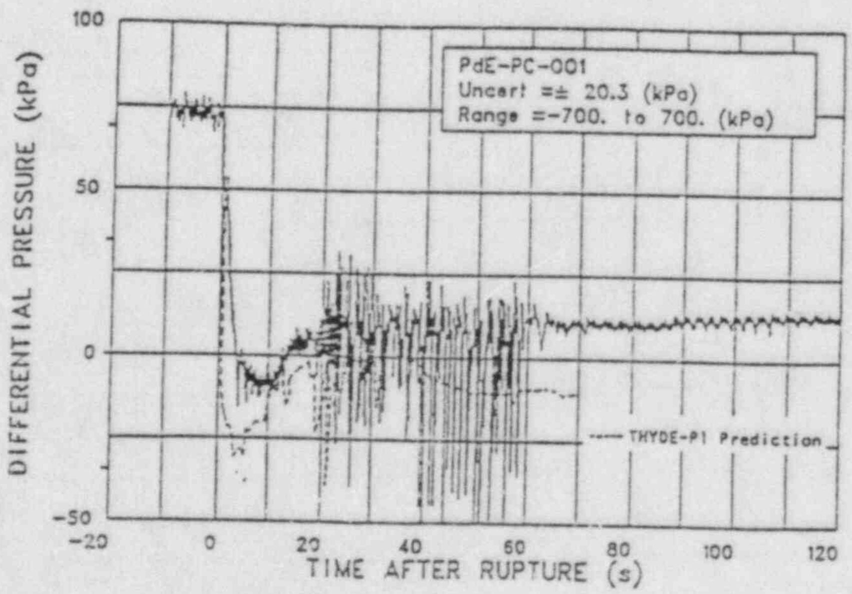

Fig. 3-11 Differential pressure in intact loop across primary coolant pumps 1 and 2

well to avoid so called water-packing or unrealistically large pressure drop and oscillatory behavior was eliminated.

Figures 3-10 and 3-11 show the pump behavior, which is one of the focused parameter in Experiment L2-5. The calculated pump rotational speed is shown in Fig 3-10 along with the experimental data. A relatively good agreement was obtained before ACC injection initiation. The pump behaviour during this period is thought to be important in conjunction with the early rewet. The calculated pump speed showed negative value after about 40 sec due to negative flow induced by condensation effects, but this descrepancy did not have large effects to the overall core behavior. Figure 3-11 shows the comparison of the differential pressure through the pump. Although the pump degradation just after the break is predicted faster than in the experiment, the overall trend is in agreement with the experiment.

4 Concluding Remarks

(1) The behaviors of the parameters of interest are appropriately predicted by the THYDE-P1 blind calculation, especially;

- the pressure transient and the final quenching time are in good agreement with the experimental data, and
- the core-wide early rewet was neither calculated to occur nor observed and the top-down quench is calculated to occure as observed.

(2) As to the following parameters, the agreement is poor;

- the break flows at both cold leg and hot leg just after the break, and
- the pump behavior after ACC injection initiation.

(3) The present THYDE-P1 relaxation model worked well to avoid unrealistically large pressure decrease and/or water packing phenomena due to condensation effects.

APPENDIX D

ISP-13 SUBMITTAL FROM CENTRAL ELECTRICITY RESEARCH LABORATORIES USING RELAP4/MOD6 (CERL)

APPENDIX D

ISP-13 SUBMITTAL FROM CENTRAL ELECTRICITY RESEARCH LABORATORIES USING RELAP4/MOD6 (CERL)

No appendix documentation was received.

APPENDIX E

ISP-13 SUBMITTAL FROM STUDSVIK ENERGITEKNIK AB USING RELAP5/MOD1 (STUD)

APPENDIX E

ISP-13 SUBMITTAL FROM STUDSVIK ENERGITEKNIK AB USING RELAP5/MOD1 (STUD)

No appendix documentation was received.

APPENDIX F

ISP-13 SUBMITTAL FROM EIDGENOSSISCHES INSTITUTE FUR REAKTORFORSCHUNG USING RELAP4/MOD6 (EIR)

APPENDIX

ISP-13 Submission EIR / Switzerland

This appendix presents the information as decided by the ISP-13 workshop group.

The nodalization diagrams prepared for:

i - the blowdown model for the blind calculations,

ii - the blowdown model for the open calculations,

iii - the reflood model for the open calculations,

are presented respectively in figures 1 to 3.

Various RELAP4/MOD6 models used in the two blowdown calculations are shown in Table - 1. This table lists the models used in the blind blowdown calculations and then indicates the additional models used in the open calculations. The reflood models used during the high and the avarage channel reflood calculations (the second phase of the open calculations) are presented on Table - 2. Both blowdown models essentially use the same nodalization and the RELAP4/MOD6 models, however the differences lie in the following area:

- Representation of the core. The blind calculations utilize only one core volume where four heat slabs supply the total power based on a core average heat generation. In the open calculation, the central fuel bundle and the surrounding bundles are separately modelled with each six axially stacked heat slabs in two vertically stacked volumes. One stack of volumes containing the heat slabs representing the central fuel assembly is called as the hot channel, and the other is as the average channel. The flow areas of the channels represent the free flow areas in the central bundle and the rest of the flow area. In the early phase of the open calculations, six horizontally located junctions were used to connect the volumes in the average and the hot channels. These horizontal junctions were eliminated due to numerical problems.
- Representation of the downcomer. One singel downcomer volume representation was used in the blind blowdown model. Two split downcomer model was utili-

zed in the early phase of the open blowdown calculations. However, due also to numerical problems, the single downcomer model was re-employed.

- Representation of the pressurizer. A combined volume of the pressurizer and its surge line was used in both calculations. The resultant volume was modelled with the homogeneous conditions in the blind calculations. This conditions did not display a proper drainage in the pressurizer. The water level remained constant at its initial value during the course of the calculation. This was prevented by applying the Wilson Bubble Rize model in this combined volume and the vertical slip model at the junction connecting the simulated pressurizer volume to the intact loop hot leg for the open calculations.

Discussion of the Results

Pressures, temperatures, densities and mass flows in or through several components calculated in the open or in the blind calculations during the blowdown phase are almost identical except, naturally in the core volumes. The figures presented in the comparison report display adequately all the predicted system response. Therefore, the rest of the text will be devoted only to the analysis of deviations or failures seen in the calculations.

The main cause of the deviation seen in the pressures (fig. 2 to 5 or 28 to 31 of the comparison report) of various components such as the hot leg or the upper plenum is due to the early predicted drainage of the pressurizer (fig. 1 or 27 of the comparison report). This 3-5 seconds early drainage shifted the predicted pressure response by about the same time. The early drainage may be attributable to the loss coefficient (which may be low) used at the connecting junction. The second deviation in the calculated system pressure starts after the calculated system pressure becomes equal to that of the suppression tank pressure. Since the code is an homogeneous-equilibrium code, the predicted system pressure is furhter reduced due to the increased amount of the cold ECCS water in the system, after this time. The open blowdown calculations were terminated at the time when the core reflood started. At this time, since the calculated pressures in the hot or the average channel are slightly lower than the pressure supression tank pressure, the backup pressure used for the reflood calculations is also slightly lower than what it should be.

The other considerable variation from the data is that the density fluctuations seen in the intact loop cold leg are not predicted. The code predicts a full downcomer which causes the code not to predict the indicated density oscillations. A split downcomer model may resolve this problem. But as it was indicated before, this modelling technique was abondened during the early phase of the open calculations. The most considerable deviations are seen in the predicted slab temperatures. Since the predicted slab temperatures during the blind calculations are not relevant with the data, the results of post test calculations will be discussed here. Five more figures are attached to this appendix in order to present the deviations seen in the calculated surface temperatures at three different axial elevations. The predicted qualities in the volumes (where the surface temperatures are presented) and the outlet flows from the hot and the average channels are also presented in order to show where the code fails. The core faces two extreme cooling phases resulting in quenching, one during early stages in the blowdown, and a second one during the reflooding. The one during the early blowdown occurs due to the inflowing surge of the water from the upper plenum. The data shows a quench behaviour at the higher axial positions. This quench behaviour is missed by the code (figures 4, 5 and 6). However the code calculates a certain quality drop around the first 10 seconds in the transient when the top down quenching was detected (figures 4, 5 and 6). This decrease in the quality can be attributable to the incoming flow from the upper plenum (figures 7 and 8). Although the question of this much of small flow causes that much decrease in the quality can not be easily answered, but it can be excepted that it is the main cause of the drop in the quality. Therefore one can conclude that the code hydrodynamically indicated the tred, but failed to follow thermally. The experimental surface temperature at the peak power elevation which do not show this top down rewet, is properly predicted until the ECCS cooling starts (fig. 5). After this time the code misses also this cooling, and results in relatively higher temperature. The predicted reflooding start time is proper. However two more deviations are seen in the reflood phase. The first is the quench times predicted during the reflooding are relatively late. The second is that the particular slope seen in the experimental temperature development curve at quenching was not displayed. This is due to the calculation of the displayed coarse heat slab temperature by averaging of the individual moving mesh temperatures within the coarse heat slab.

Discussion of the code shortcomings and how they were resolved

The RELAP4/MOD6 code is a homogeneous equilibrium and one dimensional code. The bubble rise and the vertical slip models are built in to simulate the non-homogeneous and the vapor superheat model to simulate the non-equilibrium nature existing in the real phenomena. The split downcomer model, two separate core channels with interconnections at various axial elevations are the attempts to include the three dimensional characteristics seen in the LOFT experiment to a certain extend. The inclusions of the above indicated code models are believed to solve certain problems. But the attempts made were unsuccessful. The main problems during the blind and the open calculations were coming from the heat transfer package. Whatever the attempts were by playing the input values, the code always terminated the calculations a few seconds after the simulated pump completed its coastdown. The problems during the blind calculations were solved by adapting all the modifications made for HTS2 of MOD6 in order to obtain HTS2 of the RELAP4/MOD7. This version also created some more problems during the open calculations. The main problem was that the code did not continue the heat up after a certain heat up lasting for sometime at the beginning of the calculations, but it kept the surface temperatures almost constant afterwards. This was tried to be eliminated by lowering the value of the mass flux which causes the code to switch from high flow to low flow film boiling regime. However, this change caused the code to enter the low film boiling heat transfer regime a bit earlier, but did not solve the problem. The new HTS2 logic built in the RELAP4/MOD7 code (called as HSU low flow logic) was also built in the program with certain modifications made for low flow to natural convection heat transfer. The results presented for the open calculations used the new option. However, from the comparison of the surface temperatures predict at the higher elevations showed that further work is necessary in this area.

Input Data

The input listings of the RELAP4/MOD6 blowdown and the two reflood calculations for the open submission are attached at the end of this appendix. The input listing used for the blind calculations, since it is not too different than the open one, is not included in order not to increase the volume of the comparison report.

Table 1 RELAP4/MOD6 Blowdown Models

No. of volumes	: 31 (37)
No. of junctions	: 36 (43)
No. of core heat slabs	: 4 (12)
No. of total heat slabs	: 12 (20)
Code	RELAP4/MOD6
Heat transfer package	: HTS2
Critical flow models	: HF-HEM
at the critical junctions	: 18,22,24,25,26,27,28,29
Multipliers for HF-HEM	: 0.8 0.848
Boundary of transition quality	: 0.0
Slip model-vertical (at junctions)	: 1,2,3,4,5,6,7,10,12,15,31, 32,(27,38,39,40,41,42,43)
Single mixture level calculation (volumes)	: 1,2,(33,32),3,4
Accumulator polytropic expansion model (k=1.401)	: Vol. 19
Solution technique	: Fully implicit
Phase separation model	
Bubble rise model with	
V_{BUB} = -1.0 ALPH = 0.0 (Wilson bubble rise)	: 1,2,3,4,5,6,7,24,28,29, (32,33,34,35,36,37)
V_{BUB} = -2.0 ALPH = 0.8 (complete separation)	: 19,30

The numbers in parentheses indicate the figures used for the open calculations.

Table 2 RELAP4/MOD6 Reflooding Model

- No. of volumes	: 3
- No. of junctions	: 5
- No. of heat slabs	: 6
- Heat transfer package	: HTS4
- Solution technique	: Implicit.
Reflood Heat Transfer Options	
- Exponential decay coefficient for HSU correlation	: 0.0076
- Energy partitioning coefficient	: 2.0
- Multiplier for the Bromley heat transfer coefficient	: 1.0
- Indicator for use of Bromley and HSU correlations	: HSU + Bromley
- Indicator for independent variable in the dispersed flow weighting function	: quality
- Exponent of superheated vapor partion of the weighting function	: 1.0
- Critical quality	: 0.85
Entrainment Correlation	
- Steen Wallis correlation with maximum entrainment fraction of	: 0.7
- Core model numerical coupling	: Implicit.

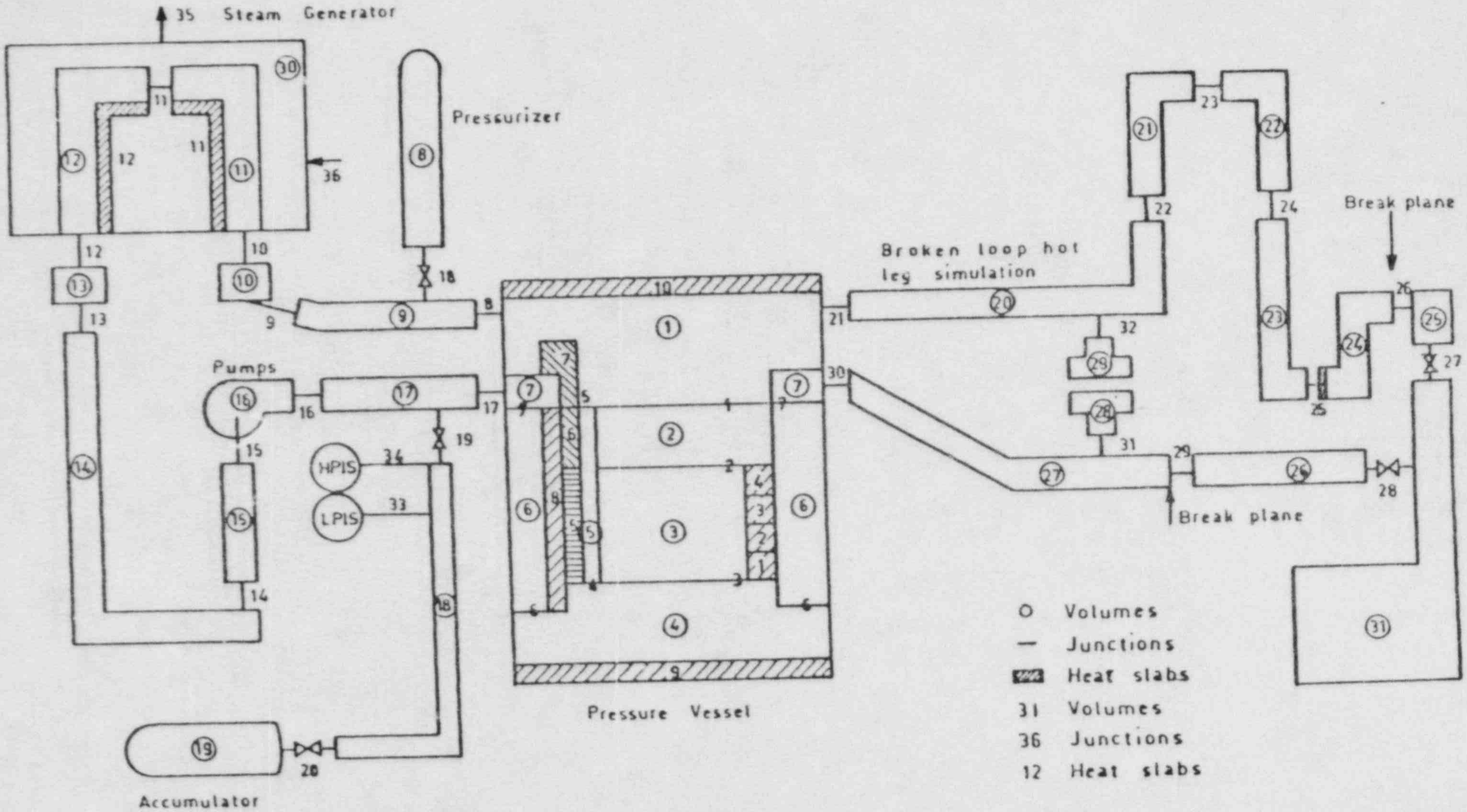

Figure 1 LOFT L2-5 RELAP 4 model schematic diagram (blind calculation)

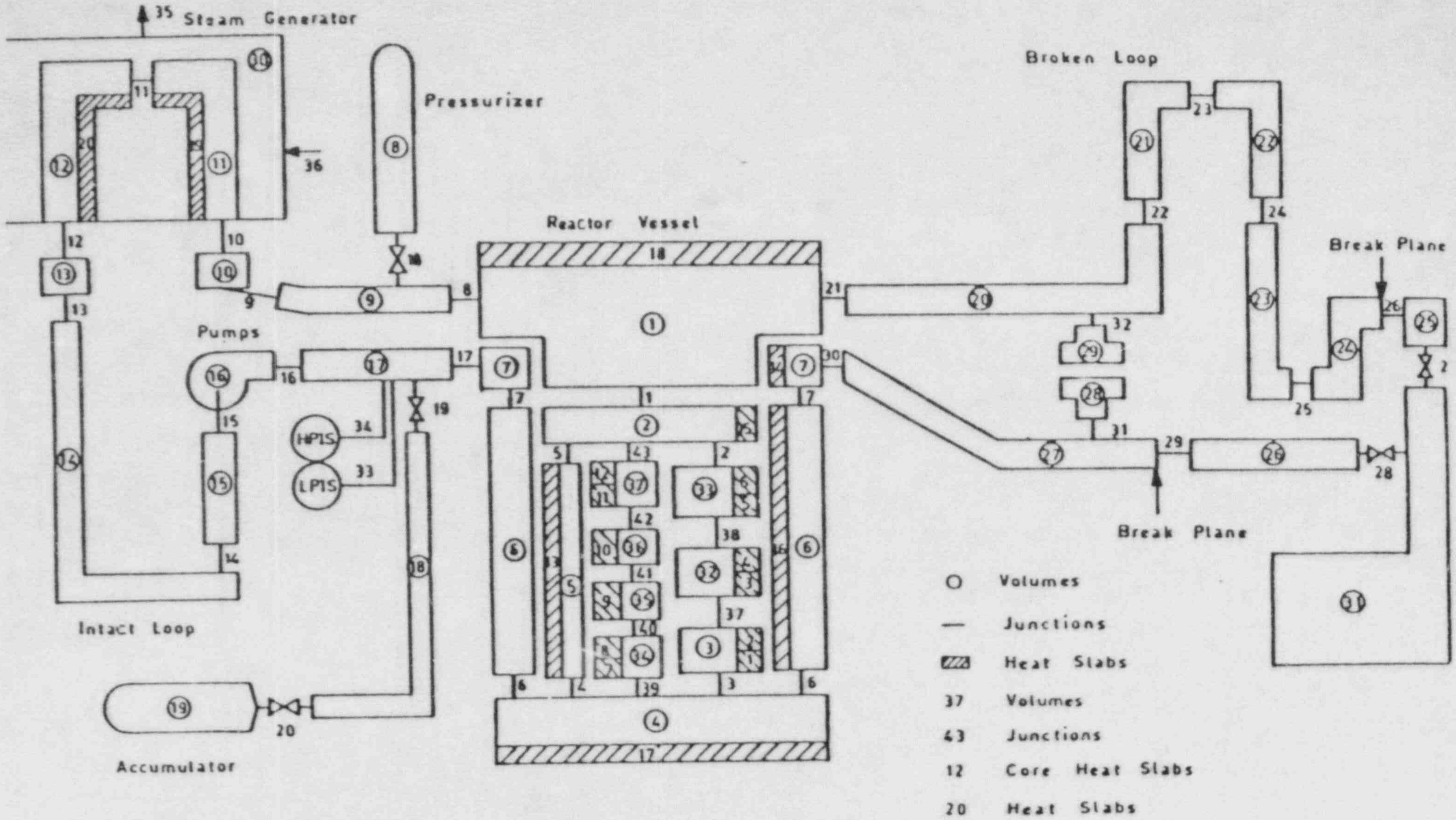

Figure 2 LOFT L2.5 RELAP 4 blowdown model schematic diagram (open calculation)

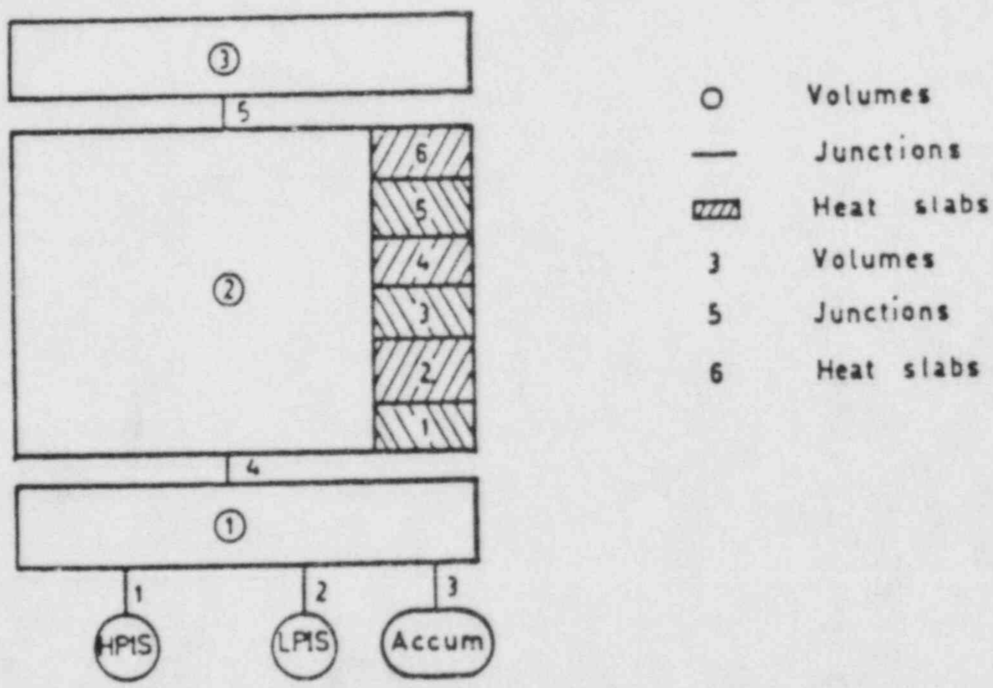

Figure 3 LOFT L2/5 RELAP 4 reflooding model schematic diagram

FIG. 4 CALCULATED QUALITY IN THE CORE VOLUME 32

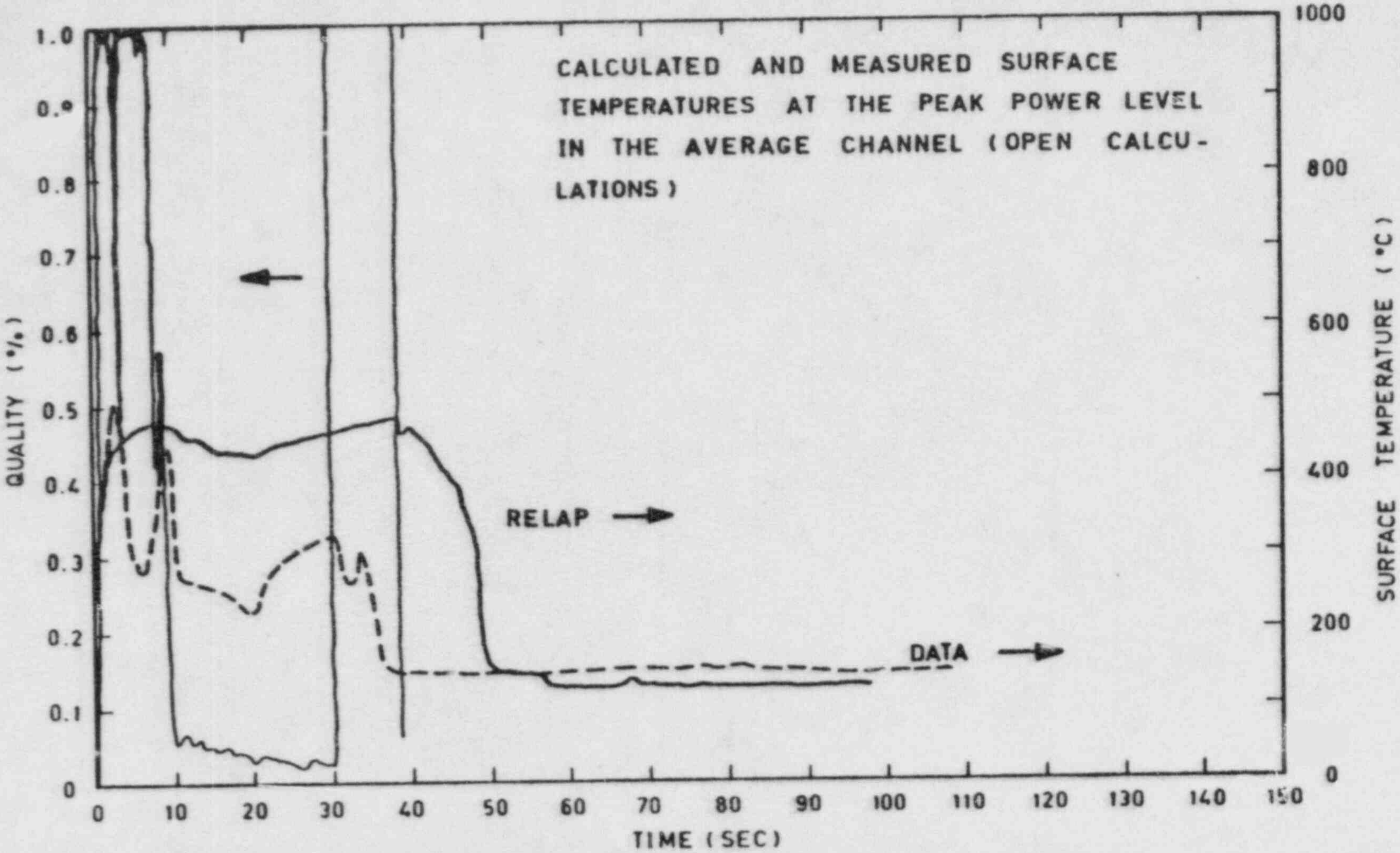

FIG. 5 CALCULATED QUALITY IN THE CORE VOLUME 34

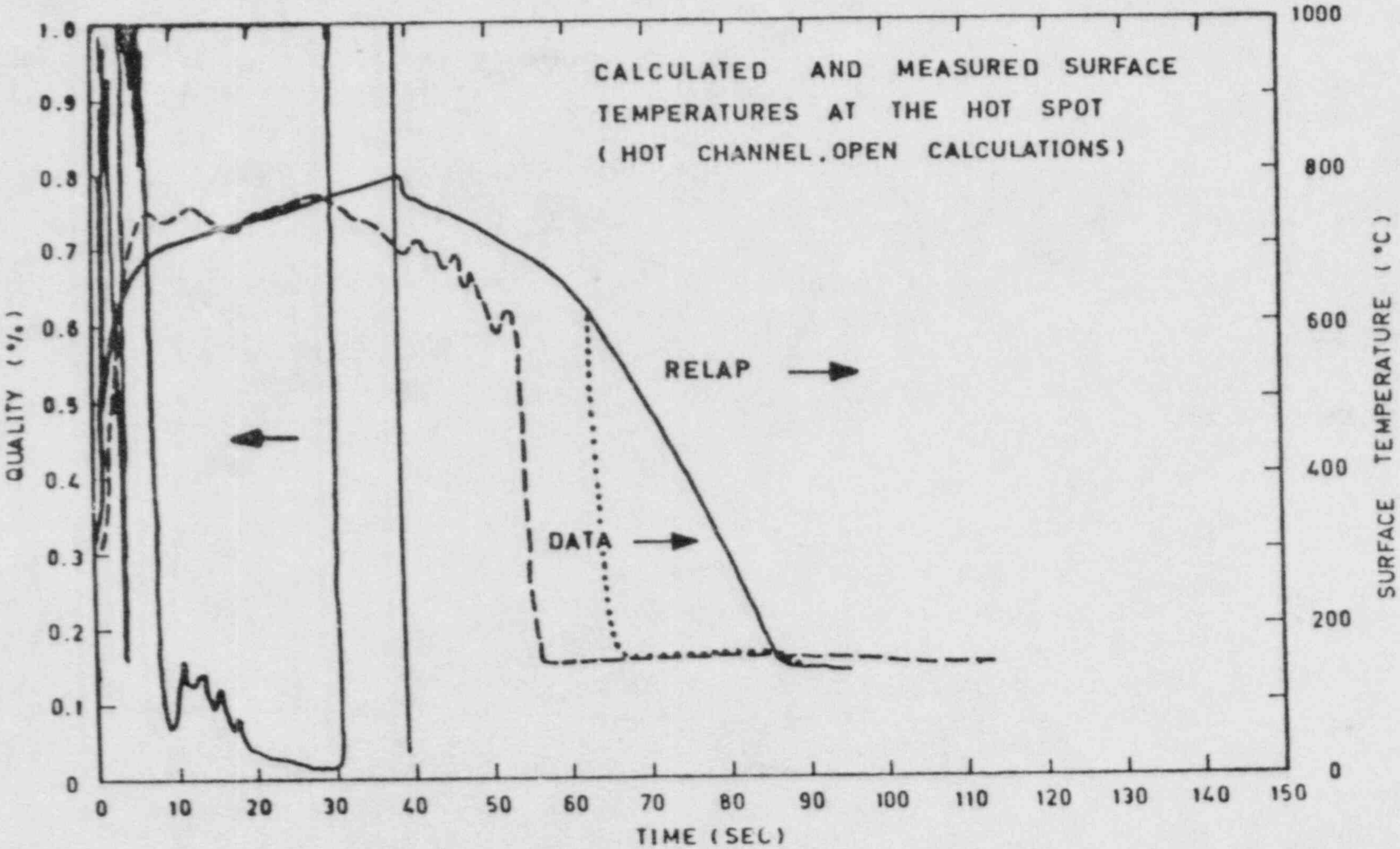

FIG. 6 CALCULATED QUALITY IN THE CORE VOLUME 37

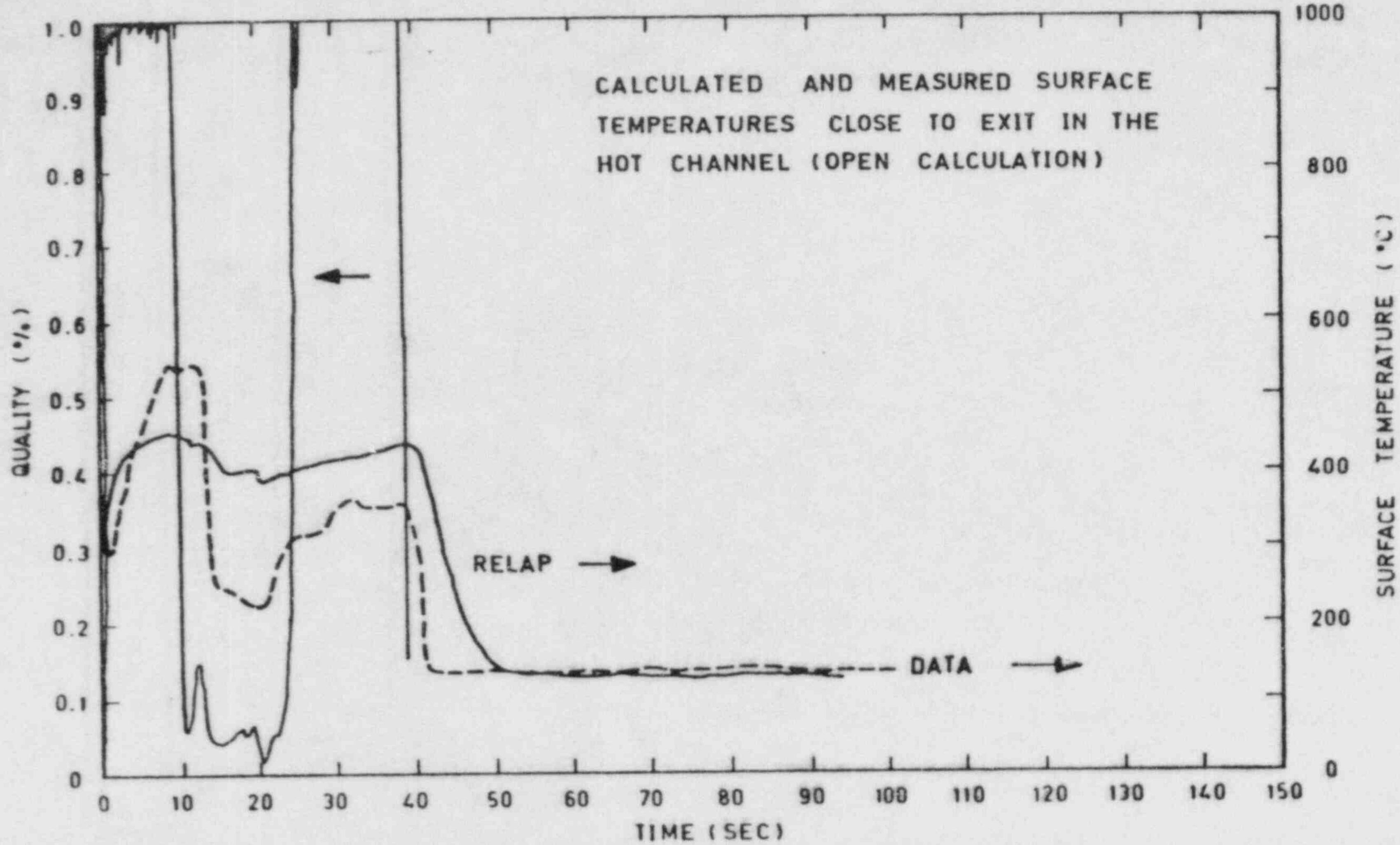

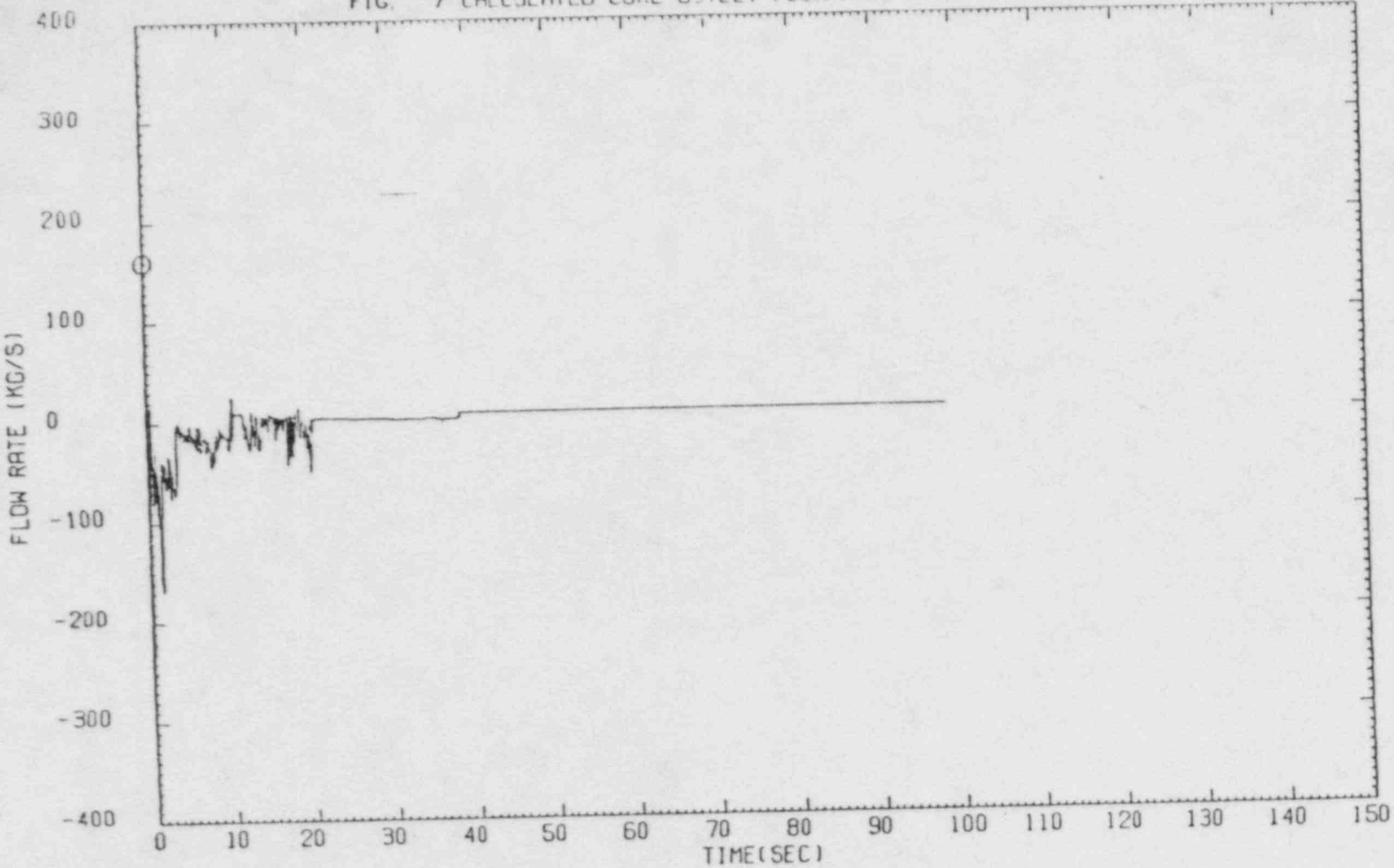

FIG. 7 CALCULATED CORE OUTLET FLOW RATE (AV. CHAN.)

FIG. 8 CALCULATED CORE OUTLET FLOW RATE (HOT CHAN.)

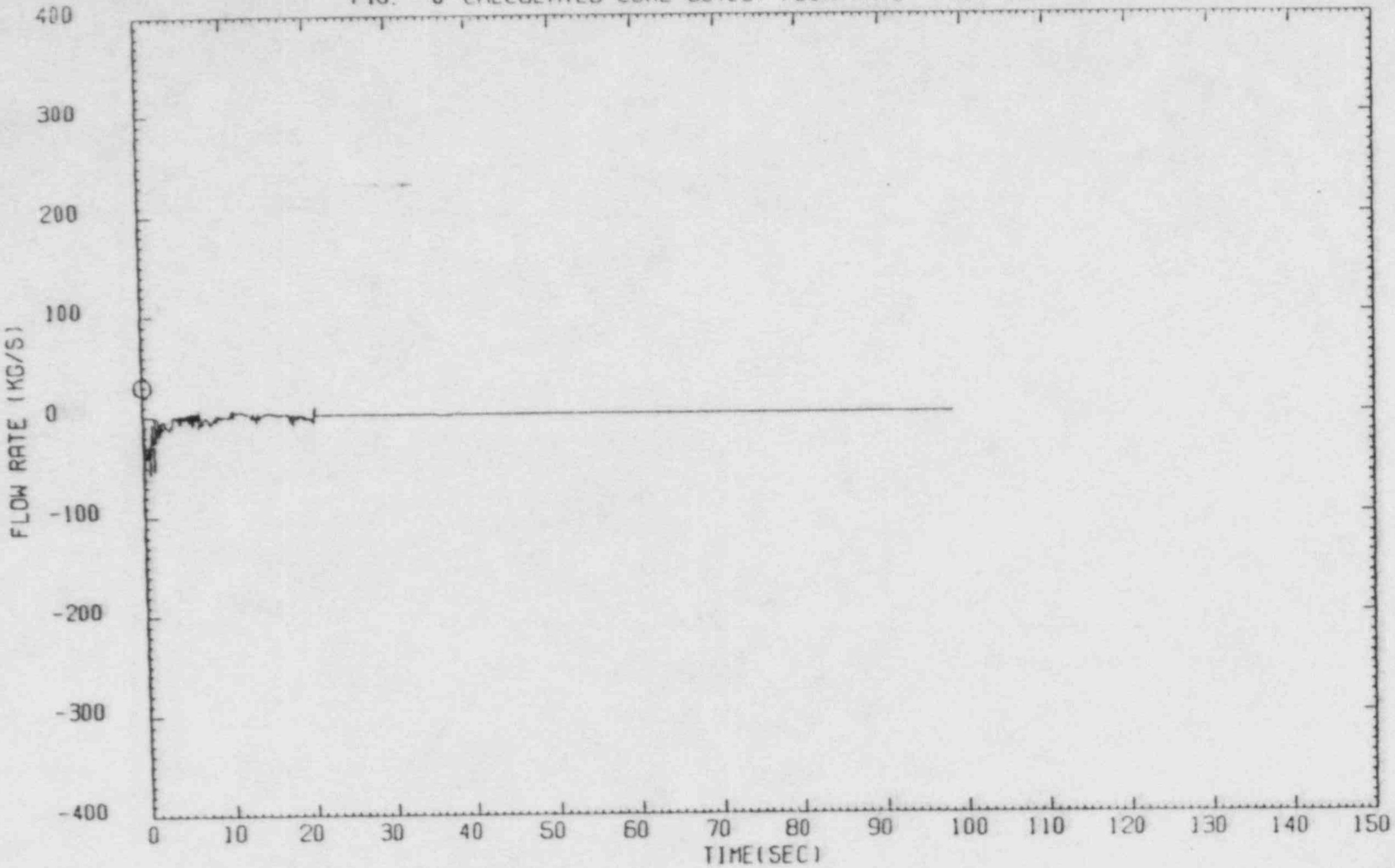

```
150.
= ISP-13,LOFT-L2-5, 200 % LARGE BREAK TEST- OPEN CALCULATIONS (EIR-SWITZERLAND)
*
*  PROBLEM DIMENSIONS DATA
*
*       L N N N N N N N N N N N N N N N N I I
*       D E T T V B T J P C L F S G M C H S U
*       M D C R O U D U M K K L L L A J T P \
*       P I   P L B V N P V   L B P T R X R I
*                       C                 O T
*                                         S S
010001 -2 9 10 11 57 3 1 43 1 4 2 3 20 7 4 12 0 0 2
*
*  PROBLEM CONSTANTS DATA
*
*       POWER  OMEGA  PQUITL  PQUITH  TQUITL  TQUITH
*
010002   37.5    1.0  0.0886  3526.0   32.1   3540.31
*
*
*           MINOR EDIT VARIABLES
*
020000  ML 35  JW 29  ML 2  ML 1  AP 1  ML 37  ML 36  SR 12  SR 6
*
*
*  TIME STEP DATA CARDS
*
*       NMIN  NMAX  NDMP  NCHK  DELTM  DTMIN    TLAST  ENDCPU
*
030010   40    10    6     0    0.01   0.0001    0.1   0.
030020   40    10    6     0    0.01   0.0003    1.76
030030   40    10    6     0    0.01   0.0005    2.0
030040   40    10    6     0    0.01   0.00065   5.0
030050   40    10    6     0    0.1    0.0007    4.
030060   40    10    6     0    0.2    0.00075   9.
030070   40    10    6     0    0.2    0.00085  10.0
030080   40    10    6     0    0.3    0.0009   12.
030090   40    10    6     0    0.4    0.001    15.
030100   40    10    6     0    0.6    0.001   120.
*
*
*  WATER PACKING,CHOKING SMOOTHING,ENTALPY TRANSPORT CARD
*
*       IWPFDT  WPTIME  STCHOK  TIENTH
*
030003    0      0.0     0.0     0.000001
*
*  TRIP CONTROL DATA
*
*       IDTRP  IDSIG   IX1  IX2  SETPT  DELAY
*
040010    1      1      0    0   150.0   0.  * END TIME
040020    2      1      0    0     0.    0.  * BREAK ON
040030    3     -4     17    0   613.37  0.  * ACCUMULATOR VALVE ON
040040    4      1      0    0    0.94   0.  * PUMP OFF
040050    5      1      0    0     0.    0.  * SG FEED WATER TRIP
040060    6      1      0    0 10000.    0.  * PRESURIZER VALVE OFF
040070    7      1      0    0    37.32  0.  * LPIS ON
040080    8      1      0    0     0.    0.  * SG STEAM FLOW TRIP
040090    9      1      0    0    23.9   0.  * HPIS ON
```

040100 10 -5 19 0 3.6348 0. * ACCUMULATOR OFF
040110 11 1 0 0 .24 0. * REACTOR SCRAMMED

*

*

VOLUME DATA CARDS

*	ISUB	IREAD	P	TEMP	HQRX	V	ZVOL	ZM	JTPMU
050011	1	0	2168.19591	604.99	-1.0	18.47346	3.95167	3.95167	0
050021	1	0	2169.71946	608.00	-1.0	13.15693	5.47125	5.47125	0
050031	1	0	2175.0599	552.30	-1.0	2.7313	1.83334	1.83334	0
050041	1	0	2179.0675	540.56	-1.0	24.01397	4.10900	4.10900	0
050051	1	0	2171.04571	540.50	-1.0	1.77260	13.49740	13.49740	0
050061	0	0	2176.54258	540.50	-1.0	19.91747	15.08	15.08	0
050071	0	0	2174.72713	540.50	-1.0	6.07412	2.36833	2.36833	0
050081	1	0	2166.30000	-1.0	0.0	33.2046	5.1097	3.77070	0
050091	0	0	2166.34074	605.00	-1.0	13.56083	0.77336	0.77636	0
050101	1	0	2164.41431	605.00	-1.0	11.84807	2.5	2.5	0
050111	0	0	2162.62000	571.17	-1.0	13.79638	8.75521	8.75521	0
050121	0	0	2162.64814	552.75	-1.0	13.79638	8.75521	8.75521	0
050131	1	0	2164.55134	540.50	-1.0	11.54607	2.5	2.5	0
050141	0	0	2163.37059	540.50	-1.0	6.595	4.60829	4.60829	0
050151	0	0	2162.67507	540.50	-1.0	4.494	2.1745	2.1745	0
050161	0	0	2166.9	540.50	-1.0	6.99230	2.47577	2.47577	0
050171	0	0	2175.7225	540.50	-1.0	12.107	0.82034	0.82034	0
050181	0	0	2174.5025	382.83	-1.0	15.83663	9.1663	9.1663	0
050191	2	0	609.166	91.64	0.0	134.24	9.9437	7.42519	0
050201	0	0	2169.28	540.50	-1.0	6.15666	2.73700	2.73700	0
050211	0	0	2168.69	541.40	-1.0	9.60206	6.757	6.757	0
050221	0	0	2169.08	541.20	-1.0	9.60206	6.757	6.757	0
050231	0	0	2170.85	540.80	-1.0	2.11648	6.71617	6.71617	0
050241	0	0	2170.95	540.50	-1.0	0.57916	4.31775	4.31775	0
050251	0	0	2170.29	540.50	-1.0	3.27720	0.64115	0.64115	0
050261	0	0	2171.52	531.50	-1.0	4.09297	0.80746	0.80746	0
050271	0	0	2171.53	540.50	-1.0	5.45256	0.93233	0.93233	0
050281	0	0	2171.03	540.50	-1.0	7.16653	2.06508	2.06508	0
050291	0	0	2169.00	546.50	-1.0	6.04440	2.69583	2.69583	0
050301	3	0	0.0	522.07	1.912-2	235.0615	27.45	10.20341	0
050311	0	1	14.504	67.64	1.0	3644.4463	16.0937	16.0937	0
050321	1	0	2174.54750	561.665	-1.0	2.7318	1.83334	1.83334	0
050331	1	0	2173.6735	597.985	-1.0	2.7318	1.83334	1.83334	0
050341	1	0	2177.8129	558.295	-1.0	0.4942	1.83334	1.83334	0
050351	1	0	2177.2605	540.61	-1.0	0.2471	.91667	.91667	0
050361	1	0	2176.93714	606.61	-1.0	0.2471	.91667	.91667	0
050371	1	0	2176.44014	622.725	-1.0	0.4942	1.83334	1.83334	0

*

*	FLOWA	DIAM	ELEV	IABLO
050012	2.1875	0.0	-1.285	0
050022	2.5694	0.0	-6.75625	1
050032	1.44011	0.0	-12.25626	32
050042	2.169	0.0	-16.365	3

```
050052  0.12163     0.0   -13.4636      0
050062  1.5279      0.0   -13.9636      0
050072  2.7671      0.0    -1.265       0
050082  5.7154      0.0     0.26117     0
050092  0.68243     0.0    -0.46617     0
050102  1.62535     0.0     0.31219     0
050112  1.62535     0.0     2.81219     0
050122  1.62535     0.0     2.61219     0
050132  7.94161     0.0     0.31219     0
050142  0.75024     0.0    -4.2461      0
050152  0.68243     0.0    -4.2461      0
050162  0.76742     0.0    -2.1216      0
050172  0.88479     0.0    -0.35417     0
050182  6.44704-2   0.0    -9.1663      0
050192 13.49794     0.0    -4.1663      0
050202  0.68243     0.0    -0.46617     0
050212  1.16035     0.0     2.27063     0
050222  2.92671     0.0     2.27063     0
050232  0.56833     0.0    -4.44533     0
050242  9.00366-2   0.0    -4.14846     0
050252  5.59250-1   0.0    -0.40057     0
050262  5.59250-1   0.0    -0.40057     0
050272  0.682430    0.0    -0.46617     0
050282  0.41764     0.0    -0.46617     0
050292  0.41764     0.0    -0.36459     0
050302 17.09955     0.0     1.99        0
050312  9.62111     0.0   -13.5104      0
050322  1.49011     0.0445 -10.42242   33
050332  1.49011     0.0445  -8.58958    2
050342   .26957     0.0434 -12.25626    0
050352   .26957     0.0434 -10.42242    0
050362   .26957     0.0434  -9.50625    0
050372   .26957     0.0434  -8.58458    0

*
*
*
*       ACCUMULATOR POLYTROPIC AIR EXPANSION MODEL
*
*          POLY      WLI
*
060006     1.401     19
*
*       BUBBLE DATA CARDS
*
*         ALPH      VBUB
*
060011     0.0      -1.0   * WILSON BUBBLE RISE MODEL
060021     0.0      -2.0   * COMPLETE PHASE SEPERATION MODEL
060031     0.25      6.6491
*
*       TIME DEPENDENT VOLUME CONDITIONS
*
*
*
*
*            IRIN     TIMTBP     PTABL   TTABL  XTABL      ZTABL
070100       18        2.         13.06  180.64 1.0        16.0937
070101                 7.         22.60  197.64 1.0        16.0937
070102                17.7        34.30  257.64 1.0        16.0937
070103                20.0        36.60  260.64 1.0        16.0937
070104                22.5        36.10  263.64 1.0        16.0937
```

```
070105           25.0       39.50   265.64 1.0      16.0937
070106           30.0       40.80   267.64 1.0      16.0937
070107           32.5       41.20   266.64 1.0      16.0937
070108           35.0       41.50   268.64 1.0      16.0937
070109           37.5       41.61   266.64 1.0      16.0937
070110           40.0       41.61   268.64 1.0      16.0937
070111           45.0       41.50   266.64 1.0      16.0937
070112           50.0       41.10   267.64 1.0      16.0937
070113           70.0       50.76   267.64 1.0      16.0937
070114          100.0       44.96   267.64 1.0      16.0937
070115          150.0       44.96   267.64 1.0      16.0937
070116          1.E+5       14.504   67.64 1.0      16.0937
*
*
*
*     SLIP VELOCITY CARD
*
*     SLVAMX   SLVELZ   SLVPWR   SLVSL1   SLBOPF   SLVYXX   SLVM1   SLVM2
*
060001    0.       0.       0.       0.       0.       0.      0.      0.
*
*        JUNCTION DATA CARDS
*
*     IW1   IW2 IPUMP IVALVE    WP       ADJUN      ZJUNC


080011  2     1    0    0    417.33    0.98458    -1.285
080021 33     2    0    0    351.62    1.05277    -6.75624
080031  4     3    0    0    351.62    .866150   -12.25626
080041  4     5    0    0     21.96    0.12140   -13.9636
080051  5     1    0    0     21.96    0.10950    -0.46620
080061  6     4    0    0    439.29    1.5279    -13.9636
080071  7     6    0    0    439.29    1.5272     -1.2849
080081  1     9    0    0    439.29    0.68265     0.0
080091  9    10    0    0    439.29    0.55600     0.31219
080101 10    11    0    0    439.29    1.62621     2.81219
080111 11    12    0    0    439.29    1.62621    10.84812
080121 12    13    0    0    439.29    1.62621     2.81219
080131 13    14    0    0    439.29    0.55600     0.31219
080141 14    15    0    0    439.29    0.68243    -4.2751
080151 15    16   -1    0    439.29    0.68243    -2.12160
080161 16    17   +1    0    439.29    0.78742     0.0
080171 17     7    0    0    439.29    0.68265     0.0
080181  8     9    0    1      0.0     0.01556     0.26117
080191 18    17    0    2      0.0     0.06447     0.0
080201 19    16    0    3      0.0     0.02060    -9.1663
080211  1    20    0    0      0.0     0.68270     0.0
080221 20    21    0    0      0.0     0.04064     2.27083
080231 21    22    0    0      0.0     0.20603     5.77174
080241 22    23    0    0      0.0     0.09064     2.27083
080251 23    24    0    0      0.0     0.04004    -3.97917
080261 24    25    0    0      0.0     0.09064     0.0
080271 25    31    0    4      0.0     0.52013     0.0
080281 26    31    0    4      0.0     0.52013     0.0
080291 27    26    0    0      0.0     0.69064     0.0
080301  7    27    0    0      0.0     0.68270     0.0
080311 27    28    0    0      0.0     0.41754     0.46617
080321 20    29    0    0      0.0     0.41754     0.36459
080331  0    17    2    0      0.0     1.0         0.0
080341  0    17    1    0      0.0     1.0         0.0
080351 30     0    2    0     42.9902  .040571    16.0671
```

```
080361  0     30     3     0      42.9402     1.0        12.72417
080371  3     32     0     0     351.82       1.30705   -10.42292
080381 32     33     0     0     351.82       1.30706    -9.50458
080391  4     34     0     0      65.51       0.16497   -12.25676
080401 34     35     0     0      65.51       0.23600   -10.42242
080411 35     36     0     0      65.51       0.23600    -9.50625
080421 36     37     0     0      65.51       0.23600    -8.58958
080431 37      2     0     0      65.51       0.16142    -6.75624
*
*
*
*
*          INERTIA      FJUNCF      FJUNCK
*
080012     2.3116       0.1881      0.3401

080022     2.38163      0.8762      0.8762
080032     0.73535      8.46644    12.35505
080042    55.591        1.46461     1.46461
080052    55.64         2.43767     2.43767
080062     5.4403       0.70       20.1
080072     4.1193       0.6783      0.1362
080082     4.545        0.4473      0.6060
080092     4.4910       1.40        1.59
080102     1.601        0.3147      0.4440
080112     2.567        0.02626     0.02626
080122     1.601        0.4440      0.3147
080132     1.3712       1.091       1.2669
080142     9.5614       0.932       1.0597
080152     6.505        2.7151      0.2441
080162     6.174        2.3711      2.4046
080172     6.5          1.615       0.4527
080182    75.33         1.0         5.620
080192   645.99        12.25       12.25
080202   645.94         1.3069      1.3069
080212     4.615        0.7621      1.20314
080222    19.901        0.43595     0.43596
080232     5.7567       5.61634     5.61634
080242    27.257        0.23025     0.23025
080252   132.751        8.78208     8.78208
080262    40.914        0.94663     1.E+9
080272    25.2560       0.0         1.E+9
080282    25.2560       0.0         1.E+9
080292    15.18         0.415       1.E+9
080302     4.366        0.4762      1.0582
080312    24.223        1.247       0.4576
080322    19.336        1.247       0.4576
080332     0.0          1.0         1.0
080342     0.0          1.0         1.0
080352     0.0          0.0         0.0
080362     0.0          0.0         0.0
080372   0.61515      0.012959    0.012959
080382   0.61515      0.006541    0.006541
080392   7.177        0.69015     0.7549
080402   3.460        0.04481     0.04481
080412   3.460        0.04481     0.04481
080422   3.460        0.04481     0.04481
080432  12.260       12.621977   10.0000
*
*
*       JVERIL JCORE JCALCI MVMIX DIAMJ CONCO ICHOKE IHQCUR SMCU? IFLOOD IADJUN
```

*

080013	0	0	0	0	0.0	1.0	-1	0	-1.0	0	0
080023	0	0	0	3	1.78	1.0	-1	0	-1.0	0	0
080033	0	0	0	3	1.78	1.0	-1	0	-1.0	0	0
080043	0	0	0	3	0.0	1.0	-1	0	-1.0	0	0
080053	0	0	0	3	0.0	1.0	-1	0	-1.0	0	0

080063	0	0	0	0	0.0	1.0	-1	0	1.0	0	0
080073	0	0	0	0	0.0	1.0	-1	0	1.0	0	0
080083	1	0	0	0	0.0	1.0	-1	0	0.0	0	0
080093	0	0	0	0	0.0	1.0	-1	0	0.0	0	0
080103	0	0	0	0	0.0	1.0	-1	0	-1.0	0	0
080113	1	0	0	0	0.0	1.0	-1	0	0.0	0	0
080123	0	0	0	0	0.0	1.0	-1	0	1.0	0	0
080133	0	0	0	0	0.0	1.0	-1	0	0.0	0	0
080143	0	0	0	0	0.0	1.0	-1	0	0.0	0	0
080153	0	0	0	0	0.0	1.0	-1	0	-1.0	0	0
080163	1	0	0	0	0.0	1.0	-1	0	0.0	0	0
080173	1	0	0	0	0.0	1.0	-1	0	0.0	0	0
080183	0	5	0	3	0.0	1.0	-1	0	1.0	0	0
080193	0	0	0	3	0.0	1.0	-1	0	0.0	0	0
080203	0	0	0	0	0.0	1.0	-1	0	0.0	0	0
080213	1	0	0	0	0.0	1.0	-1	0	0.0	0	0
080223	0	5	0	0	0.0	1.0	-1	0	0.0	0	0
080233	1	0	0	0	0.0	1.0	-1	0	0.0	0	0
080243	0	5	0	0	0.0	1.0	-1	0	0.0	0	0
080253	1	5	0	0	0.0	1.0	-1	0	0.0	0	0
080263	1	5	0	0	0.0	1.0	-1	0	0.0	0	0
080273	1	5	0	0	0.0	1.0	-1	0	0.0	0	0
080283	1	5	0	0	0.0	1.0	-1	0	0.0	0	0
080293	1	5	0	0	0.0	1.0	-1	0	0.0	0	0
080303	1	0	0	0	0.0	1.0	-1	0	0.0	0	0
080313	0	0	0	3	0.0	1.0	-1	0	-1.0	0	0
080323	0	0	0	3	0.0	1.0	-1	0	-1.0	0	0
080333	0	0	2	3	0.0	1.0	-1	0	0.0	0	0
080343	0	0	2	3	0.0	1.0	-1	0	0.0	0	0
080353	0	0	2	0	0.0	1.0	-1	0	0.0	0	0
080363	1	0	2	3	0.0	1.0	-1	0	0.0	0	0
080373	0	0	0	0	1.78	1.0	-1	0	-1.0	0	0
080383	0	0	0	0	1.78	1.0	-1	0	-1.0	0	0
080393	0	0	0	3	0.5505	1.0	-1	0	-1.0	0	0
080403	0	0	0	0	0.5505	1.0	-1	0	-1.0	0	0
080413	0	0	0	0	0.5505	1.0	-1	0	-1.0	0	0
080423	0	0	0	0	0.5505	1.0	-1	0	-1.0	0	0
080433	0	0	0	3	0.5505	1.0	-1	0	-1.0	0	0

*
* HENRY-FAUSKE HEM CRITICAL FLOW MODEL DIALS
*
* DLHEM DLHRY DLEHRY DLXIFE
*
082003 0.646 0.8 1.0 0.02
*
* HENRY-FAUSKE HEM LOWER LIMIT TRANSITION QUALITY DIAL CARD
*
* DXTRLL
*
082033 0.0

*
* PUMP DESCRIPTION DATA CARDS (COMBINED PUMP)

```
*
*     IPC ITPUM IXP IPM IMT POMGAR PSRAI PFLOWR PHEADR PTORKR PINRTA VRHOI
*
090011  1   4    0   1   0  3530.  .420    10000. 315.00 734.0  60.0    36.31
*
*      TORKF(3)  TORKMR  TORKF(1)  TORKF(2)  TORKF(4)
*
090012  152.994  0.      0.0327    14.455     0.0
*
*       PUMP  HEAD MULTIPLIER
*
*        NPHM  PHOM1   PHOM2
*
091001    -12    0.0    0.0       0.1     0.0      0.2   0.1      0.3    0.2
091002           0.35   0.3       0.4     0.6      0.5   0.6      0.6    0.6
091003           0.7    0.6       0.8     0.5      0.7   0.3      1.     0.0
*
*       PUMP TORQUE MULTIPLIER
*
*       IPTM   PTKM(1)  PTKM(2)
092001    -12    0.0    0.0       0.1     0.0      0.2   0.1      0.3    0.3
092002           0.35   0.5       0.4     0.75     0.5   0.75     0.6    0.75
092003           0.7    0.75      0.8     0.75     0.7   0.5      1.     0.0
*
*       PUMP STOP DATA
*
*        CAVCON  FPUMP  SPUMP
*
095011     0.0       0.   0.0
*
*
*       PUMP CURVE INPUT INDICATOR
*
*       NC1  NC2  NC3  NC4
*
100000 16    0    0    16
*
*    PUMP HEAD AND TORQUE
*
*       IT  IC   N  PHEAD1 PHEAD2
*       IT  IC   PTORK1 PTORK2
101011   1   1   6  0.        1.4036   0.19061   1.3636   0.38953   1.3186    *PUMP-HO
101012                .54346  1.2326   0.7402    1.1336   1.        1.0000    *PUMP-HO
101021   1   2   6  0.        -0.57    0.2       -0.5     0.4       -0.25     *PUMP-HO
101022                .57554  0.       0.74432   0.2563   0.77343   0.3776    *PUMP-HO
101023                .66313  0.0326   1.        1.0000                       *PUMP-HO
101031   1   3   6  -1.       2.4722   -.60574   2.0474   -0.6067   1.631     *PUMP-HO
101032              -.40683   1.624    -.20017   1.4705   0.        1.4036    *PUMP-HO
101041   1   4   6  -1.       2.4722   -.82247   1.4565   -.63332   1.5897    *PUMP-HO

101042              -.45534   1.3274   -.27107   1.1747   -.17715   1.0605    *PUMP-HO
101043              -.04073   1.0156   0.        .93423                       *PUMP-HO
101051   1   5   7  0.        0.25     0.2       0.28     0.4       0.34      *PUMP-HO
101052              0.4116    0.2766   0.59763   0.4564   0.79347   0.6997    *PUMP-HO
101053              1.        1.0                                             *PUMP-HO
101061   1   6  10  0.        .93426   0.0911    0.9229   0.18551   0.8963    *PUMP-HO
101062              .27176    0.575    0.45567   0.8433   0.57441   0.6355    *PUMP-HO
101063              .740576   .8466    .766619   .6454    .871471   0.8836    *PUMP-HO
101064              1.        1.0                                             *PUMP-HO
101071   1   7   6  -1.       -1.      -.9       -.83     -.6       -.3       *PUMP-HO
101072              -.4       -.65     -.2       0.15     0.        0.25      *PUMP-HO
```

```
101081  1  8  6  -1.      -1.      -.8      -.97     -.6      -.95     *PUMP-HD
101082           -.4      -.88     -.2      -.8      0.       -.67     *PUMP-HD
101091  2  1  6  0.       0.6032   0.1930   0.5325   0.393    0.7369   *PUMP-TQ
101092           .59552   0.8331   0.79782  0.9227   1.       1.0      *PUMP-TQ
101101  2  2  7  0.       -.67     .4       -.25     .5       .15      *PUMP-TQ
101102           .73726   .52659   .76805   .60659   .86723   .74366   *PUMP-TQ
101103           1.       1.0                                          *PUMP-TQ
101111  2  3  6  -1.      1.9843   -.86096  1.394    -.60633  1.0975   *PUMP-TQ
101112           -.40666  .822     -.19928  .6648    0.       .6032    *PUMP-TQ
101121  2  4  8  -1.      1.9843   -.82234  1.8308   -.63371  1.6824   *PUMP-TQ
101122           -.45653  1.557    -.26702  1.4362   -.17011  1.3879   *PUMP-TQ
101123           -.08931  1.3481   0.       1.2336                     *PUMP-TQ
101131  2  5  4  0.       -.45     .4       -.25     .5       0.       *PUMP-TQ
101132           1.        .3569                                       *PUMP-TQ
101141  2  6 10  0.       1.23361  .090643  1.1965   1.88569  1.1096   *PUMP-TQ
101142           .27347   1.0416   .458669  .6956    .57448   .7807    *PUMP-TQ
101143           .73616   .6134    .76652   .5849    .870057  .4877    *PUMP-TQ
101144           1.       .3569                                        *PUMP-TQ
101151  2  7  4  -1.      -1.      -.3      -.9      -.1      -.5      *PUMP-TQ
101152           0.       -.45                                         *PUMP-TQ
101161  2  8  4  -1.      -1.      -.25     -.9      -.08     -.6      *PUMP-TQ
101162           0.       -.67                                         *PUMP-TQ
104011  1  1  7  0.    1.0   .1    1.0   .2    1.0    .5    1.0      *PUMP-HDD
104012           .7    1.0   .9    1.0   1.    1.0                   *PUMP-HDD
104021  1  2  8  0.    1.0   .1    1.0   .2    1.0    .3    1.0      *PUMP-HDD
104022           .4    1.0   .8    1.0   .9    1.0    1.    1.0      *PUMP-HDD
104031  1  3 10  -1.   -1.16 -.9   -1.24 -.8   -1.77  -.7   -2.36    *PUMP-HDD
104032           -.6   -2.74 -.5   -2.91 -.4   -2.67  -.25  -1.69    *PUMP-HDD
104033           -.1   -.5   0.    0.                                *PUMP-HDD
104041  1  4 10  -1.   -1.16 -.9   -.78  -.8   -.5    -.7   -.31     *PUMP-HDD
104042           -.6   -.17  -.5   -.08  -.35  0.     -.2   .05      *PUMP-HDD
104043           -.1   .08   0.    .11                               *PUMP-HDD
104051  1  5  6  0.    0.    .2    -.34  .4    -.65   -.6   -.93     *PUMP-HDD
104052           .8    -1.19 1.    -1.47                             *PUMP-HDD
104061  1  6 10  0.    .11   .1    .13   .25   .15    .4    .13      *PUMP-HDD
104062           .5    .07   .6    -.04  .7    -.23   .8    -.52     *PUMP-HDD
104063           .9    -.91  1.    -1.47                             *PUMP-HDD
104071  1  7  2  -1.   0.    0.    0.                                *PUMP-HDD
104081  1  8  2  -1.   0.    0.    0.                                *PUMP-HDD
104091  2  1  6  0.       1.0      .193     1.0      .393     1.0      *PUMP-TQD

104092           .59552   1.0      .79782   1.0      1.       1.0      *PUMP-TQD
104101  2  2  7  0.       1.0      .4       1.0      .5       1.0      *PUMP-TQD
104102           .737255  1.0      .768049  1.0      .86723   1.0      *PUMP-TQD
104103           1.       1.0                                          *PUMP-TQD
104111  2  3  6  -1.      1.9843   -.86096  1.394    -.60633  1.0975   *PUMP-TQD
104112           -.40660  .822     -.19928  .6648    0.       .6032    *PUMP-TQD
104121  2  4  8  -1.      1.9843   -.82234  1.8308   -.63371  1.6824   *PUMP-TQD
104122           -.45653  1.557    -.267023 1.4362   -.170107 1.3879   *PUMP-TQD
104123           -.08931  1.3481   0.       1.23361                    *PUMP-TQD
104131  2  5  4  0.       -.45     .4       -.25     .5       0.       *PUMP-TQD
104132           1.       .3569                                        *PUMP-TQD
104141  2  6 10  0.       1.23361  .090643  1.1965   .188569  1.1096   *PUMP-TQD
104142           .27347   1.0416   .458669  .6956    .57448   .7807    *PUMP-TQD
104143           .73616   .6134    .76652   .5849    .870057  .4877    *PUMP-TQD
104144           1.       .3569                                        *PUMP-TQD
104151  2  7  4  -1.      -1.      -.3      -.9      -.1      -.5      *PUMP-TQD
104152           0.       -.45                                         *PUMP-TQD
104161  2  8  4  -1.      -1.      -.25     -.9      -.08     -.6      *PUMP-TQD
104162           0.       -.67
*       VALVE DATA
```

```
*
*       ITCV IACV LATCH PCV     CV1  CV2  CV3
*
110010  +6    0    0   0.  0.  0.  0.   * PRESSURIZER VALVE TO BE OFF  JUNC.18
110020  +10   0    0   0.  0.  0.  0.   * ACCUMULATOR VALVE TO BE OFF  JUNC.19
110030  -3    0    0   0.  0.  0.  0.   * ACCUMULATOR VALVE TO BE ON   JUNC.20
110040  -2    1    0   0.  0.  0.  0.   * BREAK VALVES TO BE       ON  JUNC.27-2
*
*       LEAK DATA
*
*        NAREA IILEAK  SINK IAREA1 IAREA2
*
120101   -3     2      13.05  0.   0.   .0175   1.      150.      1.0 *BREAK FLOW
120201   -3     2     300.0   0.   0.5    10.0 0.       150.   0. * SG STEAM FLOW
*
*
*
*       FILL TABLE DATA
*
*        ITFILL  ITYPE  NPTS  ICALC  ISATFL  UNITS  PORT   HORX   AFRAC  TAUMX
*
*
130100     9      2      2     4      0     GAL/MIN   100.   75.     0.     0.
130101    0.0  12.       3000. 12.0                                 *HPIS FLOW
*
130200     7      2     13     4      0     GAL/MIN  100.   75.      0.      0.
130201        0.0  114.9   12.3  111.3   62.3   96.6   112.3   79.8
130202      137.3   64.2  162.3   56.1  172.3   50.2   182.3   42.6
130203      192.3   34.2  202.3   24.3  212.3   11.4   220.0    0.0
130204     3000.0    0.0  * LPIS FLOW
*
*
130300     5      1      3     4      0     GAL/MIN 399.25 407.64   0.     0.
*          FILTBL(1)  FILTBL(2)
130301       0.0          300.2651   5.0        0.0      150.     0.0
                                                       * SG FEED WATER FLOW
*
*
*
*       KINETICS CONSTANT DATA
*
*        MODEL  KMUL BOVL RHOIN DOUF PROMPT LAMDA TAU
*
140000     0      0   0.   0.    0.   0.     0.   0.
*
*       SCRAM TABLE DATA
*
*       NSCR  ITSCRM TSCR(1) TSCR(2)
*
141000 -20    11    0.     1.0        0.1    0.400659 0.2    0.2743     0.3  0.153171
141001              0.4    0.110621   0.6    0.083212 1.0    0.064777   1.5  0.063007
141002              2.0    0.059694   3.0    0.057205 4.0    0.055204   6.0  0.052065
141003              8.0    0.049776 10.0    0.047947 15.0   0.044175  20.0  0.042176
141004             30.0    0.039703 40.0    0.036348 60.0   0.031540 150.0  0.001460
                                                                * FROM LOFT L-2-3
*
*
*       HEAT TRANSFER SURFACE DATA
*
*        NSCR  IMSS  IOTB  IOFB
*
```

```
150000     2     0      0    3
*
*      HEAT SLAB DATA
*
*
*
*      I I   I     I  I   I
*      V V   G  I  X  M   M
*      S S   C  S  L  C   C
*      L R   M  B  D  L   R      AHTL           AHTR        VOLS      HDML
*
150011  0  3  1  0  2   0  30     0.           110.9953    0.9758    0.0
150021  0  3  1  1  2   0  30     0.           110.9953    0.9758    0.0
150031  0 32  1  1  2   0  30     0.           110.9953    0.9758    0.0
150041  0 32  1  1  2   0  30     0.           110.9953    0.9758    0.0
150051  0 33  1  1  2   0  30     0.           110.9953    0.9758    0.0
150061  0 33  1  1  2   0  30     0.           110.9953    0.9758    0.0
150071  0 34  1  0  2   0  30     0.            20.6597    0.1816    0.0
150081  0 34  1  1  2   0  30     0.            20.6597    0.1816    0.0
150091  0 35  1  1  2   0  30     0.            20.6597    0.1816    0.0
150101  0 36  1  1  2   0  30     0.            20.6597    0.1816    0.0
150111  0 37  1  1  2   0  30     0.            20.6597    0.1816    0.0
150121  0 37  1  1  2   0  30     0.            20.6597    0.1816    0.0

150131  5  0  2  0  0  30   0   94.5774         0.0        6.791     0.0
150141  7  0  3  0  0  30   0   41.0816         0.0        7.040     0.0
150151  0  2  7  0  0   0  30    0.           556.27       5.794     0.0
150161  6  0  3  0  0  30   0  232.3146         0.0       40.4340    0.0
150171  0  4  4  0  2   0  30    0.0          103.9305     3.303     0.0
150181  0  1  5  0  2   0  30    0.0          642.3700    10.889     0.0
150191 11 30  6  0  0  30  30 1646.2065      1530.0236     7.541360  0.033482
150201 12 30  6  0  0  30  30 1646.2065      1530.0236     7.541360  0.033482
*
*
*     HDMR      DHEL       DHER      CHNL      CHNR      ZBOT      ZTOP
*
150012 0.0        0.0       0.0       0.0       0.0       0.0    .916670
150022 0.0        0.0       0.0       0.0       0.0    .91667   1.833340
150032 0.0        0.0       0.0       0.0       0.0       0.0    .916670
150042 0.0        0.0       0.0       0.0       0.0    .91667   1.833340
150052 0.0        0.0       0.0       0.0       0.0       0.0    .916670
150062 0.0        0.0       0.0       0.0       0.0    .91667   1.833340
150072 0.0        0.0       0.0       0.0       0.0       0.0    .916670
150082 0.0        0.0       0.0       0.0       0.0    .91667   1.833340
150092 0.0        0.0       0.0       0.0       0.0       0.0       0.0
150102 0.0        0.0       0.0       0.0       0.0       0.0       0.0
150112 0.0        0.0       0.0       0.0       0.0       0.0    .916670
150122 0.0        0.0       0.0       0.0       0.0    .91667   1.833340
150132  0.0       0.0       0.0      0.0        0.0       0.0       0.0
150142 0.0        0.0       0.0       0.0       0.0       0.0       0.0
150152 0.1797     0.0       0.0       0.0       0.0       0.0       0.0
150162 0.0        0.0       0.0      15.08      0.0       0.0       0.0
150172 4.9583     0.0       4.9583    0.0       0.0       0.0       0.0
150182 0.0        0.0       0.0       0.0       0.0       0.0       0.0
150192 0.0149062 0.033482 0.149062  8.75521 16.0937   0.32219   9.29576
150202 0.0149062 0.033482 0.149062  8.75521 16.0937   0.32219   9.29576
*
*      STEAM GENERATOR CONVECTION DATA
*
*       ISHG
*
150194     2
```

```
150204     2
*
*      CORE  SLAB DATA CARDS
*
*       ISLAB       NODI    CLTI     QFRAC    QPMOD  QDMOD
*
160010     1          1  2  3   0.    0.127544 0.0168 0.
160020     2          1  2  3   0.    0.197173 0.0168 0.
160030     3          1  2  3   0.    0.201826 0.0168 0.
160040     4          1  2  3   0.    0.150136 0.0168 0.
160050     5          1  2  3   0.    0.084330 0.0168 0.
160060     6          1  2  3   0.    0.020226 0.0168 0.
160070     7          1  2  3   0.    0.036117 0.0168 0.

160080     8          1  2  3   0.    0.055710 0.0168 0.
160090     9          1  2  3   0.    0.055911 0.0168 0.
160100    10          1  2  3   0.    0.040662 0.0168 0.
160110    11          1  2  3   0.    0.023164 0.0168 0.
160120    12          1  2  3   0.    0.007193 0.0168 0.
*
*      SLAB GEOMETRY DATA CARDS
*
*       IG  IGP  NR  IM  NOX      XO          XR          PF
*
170101  2        4    1    1   0.0          0.008964    0.3333
170102      C         1    1                0.003721    0.3333
170103      0         1    1                0.002655    0.3334
170104      C         2    1                0.002625    0.0
170201  2         1   3    1  1.25          0.0625      0.0
170301  2         1   4    1  1.45813       0.16667     0.0
*170401  2         1   3    1  1.54165       0.205634    0.0
170401  2         1   3    1  3.944081      0.08149     0.0
*170501  2         1   3    1  1.25          0.177676    0.0
170501  2         1   3    1 10.50357       0.01894     0.0
170601  2         1   3    1  0.01675       0.004083    0.0
170701  2         1   3    1  0.0           1.0417E-2    .0
*
*      THERMAL CONDUCTIVITY CARDS
*
*   THERMAL CONDUCTIVITY DATA FOR UO2
*
*       NKP  TEMP(F)   COND.(BTU/HR.FT.F)
180100 -20  212.         4.143  392.        3.521  752.        2.710 1112.         2.200
180101      1472.        1.866 1832.        1.623 2192.        1.447 2372.         1.370
180102      2552.        1.320 2732.        1.272 2912.        1.235 3002.         1.220
180103      3020.        1.274 3092.        1.264 3272.        1.315 3632.         1.400
180104      3992.        1.531 4352.        1.731 4712.        2.034 5072.         2.360
*
*   THERMAL CONDUCTIVITY DATA FOR ZIRCALOY
*       NKP  TEMP(F)   COND.(BTU/HR.FT.F)
180200 -20    86.        7.546  212.        8.192  392.        8.910  572.         9.565
180201        752.      10.240  932.       10.902 1112.       11.603 1292.        12.375
180202       1472.      13.247 1490.       13.347 1562.       13.740 1652.        14.244
180203       1742.      14.831 1767.       15.121 1832.       15.412 2012.        16.766
180204       2192.      18.341 2372.       20.166 2552.       22.274 2732.        24.693
*
*   THERMAL CONDUCTIVITY DATA FOR SS-304
*         NCP   TEMP(F)  COND (BTU/HR.FT.F)
*
180301    -17     32.      8.61       212.0  9.42     302.0    10.169     383.2  10.343
180302           410.     10.632     462.2 10.663    501.8    11.094     590.9  11.363
```

```
180303          645.98 11.614    688.3 11.845  747.1    11.95    791.2  12.249
180304          932.0  12.943   1050.4 13.347 1167.6    13.893  1221.6  14.324
180305         1354.0  14.965
*
*   THERMAL CONDUCTIVITY DATA FOR INCONEL 600
*
*       NKP   TEMP(F)    COND.(BTU/HR.FT.F)
180400 -16    68.      8.372   212.        9.152   392.        10.124
180401        572.    11.100   752.       12.076   932.        13.053
180402       1022.    13.536  1112.       14.024  1292.        15.006
180403       1382.    15.491  1472.       15.976  1652.        16.953
180404       1832.    17.929  2012.       18.906  2192.        19.882
180405       2372.    20.855
*
*
*   VOLUMETRIC HEAT CAPACITY DATA FOR UO2
*
*         NCP    TEMP(F)  CP(BTU/FT3.F)
190100 -20  212.      40.321  392.      43.232  752.      46.249 1112.      47.941
190101      1472.     49.174 1832.      50.248 2192.      51.422 2372.      52.161
190102      2552.     53.082 2732.      54.255 2912.      55.754 3002.      56.700
190103      3020.     56.869 3092.      57.648 3272.      59.994 3632.      66.267
190104      3992.     74.856 4352.      85.839 4712.      99.107 5072.     114.41
*
*   VOLUMETRIC HEAT CAPACITY DATA FOR ZIRCALOY
*
*         NCP    TEMP(F)  CP(BTU/FT3.F)
190200 -20   68.      28.106  212.      28.757  392.      29.570  572.      30.373
190201       752.     31.593  932.      32.    1112.      34.835 1292.      34.635
190202      1472.     34.635 1490.      34.635 1562.      53.322 1652.      79.462
190203      1742.     52.055 1787.      34.429 1832.      34.429 2012.      34.429
190204      2192.     34.429 2372.      34.429 2552.      34.429 2732.      34.429
*
*   VOLUMETRIC HEAT CAPACITY DATA FOR SS-304
*
*
*         NCP    TEMP(F)  CP(BTU/FT3.F)
*
190301   -19   32.     43.61
190302          149.04   44.44   299.64   44.94   400.64   44.94   499.64   45.4[illegible]
190303          600.44   45.93   699.44   46.42   800.24   46.91   899.24   47.[illegible]
190304         1000.04   48.39  1099.04   49.88  1199.84   51.38  1300.64   52.[illegible]
190305         1399.64   53.83  1500.44   54.81  1599.44   55.8   1700.24   56.[illegible]
190306         1799.24   56.79  1900.04   57.28
**   VOLUMETRIC HEAT CAPACITY DATA FOR INCONEL 600
*
*       NCP    TEMP(F)   CP(BTU/FT3.F)
190400 -16  68.       55.168   212.       58.274   392.       61.291
190401      572.      63.708   752.       66.061   932.       68.306
190402     1022.      69.526  1112.       71.035  1292.       75.272
190403     1382.      76.504  1472.       77.145  1652.       79.138
190404     1832.      78.893  2012.       79.647  2192.       80.401
190405     2372.      81.156
*
.   *  END OF  DATA
```

LISTING OF INPUT DATA FOR CASE 1

```
* ISP-13,LOFT-L2-5 209 - LARGE BREAK TEST-HIGH POWER CHAN. REFLOOD CALCULATIONS
*
*  PROBLEM DIMENSIONS DATA
*
*          L N  N  N  N  N  N  N  N  N  N  N  N  N  N  N  N  I  I
*          O E  T  T  V  B  T  J  P  C  L  F  S  G  A  C  N  S  U
*          O D  C  R  O  U  O  U  N  K  K  L  L  O  A  O  T  P  N
*          P L     P  L  B  V  N  P  Y     L  B  N  T  B  C  R  I
*                              C                             O  T
*                                                            G  S
*
010001 -2 8  3  4  3  1  1  3  0  0  0  3   6  1 2   6 0   0  2
*
*  PROBLEM CONSTANTS DATA
*
*          POWER  OMEGA  POUITL  POUITH  TOUITL  TOUITH
*
*010002   37.5   1.0  0.0846   3626.0   32.1    8540.31
*
*   POWER PRODUCED IN HIGH POWER CHANNEL IS 0.218757 OF TOTAL PWER
* GENERATED POWER IN HIGH POWER CHANNEL IS 37.5*0.218757
*
010002   8.203388 1.0  0.0846   3626.0   32.1    8540.31
*
*
*       MINOR EDIT VARIABLES
*
*20000  ML 2  SR 1  SR 2  SR 3  SR 4  SR 5  SR  6   AT 2
*
*
*
*
*  TIME STEP DATA CARDS
*
*       NMIN  JHMAX  NOMP  NCHK  DELTM  DTMIN   TLAST  ENDCPU
*
030010   10    12     6     0    0.01   0.001      .2   0.
030020   10    10     5     0    0.2    0.001    10.
030030   10     2     8     0    0.2    0.001   100.
*
*
*  TRIP CONTROL DATA
*
*       IDTRP  IDSIG   IX1  IX2  SETPT  DELAY
*
040010    1      1      0    0    99.0   0.  * END TIME
040020    2      1      0    0     0.    0.  * SCRAM TRIP
040030    3      1      0    0    0.     0.  * MOVING MESH ACTIVATION
040040    4      1      0    0    .1E-7  0.  * FILL TRIP
*
*
*       VOLUME DATA CARDS
*                                                                        J
*          I                                                             T
*          R                                                             P
*          E                                                             R
*          A                                                             U
*     IBUS D     P            TEMP   HOPT       V         ZVOL       ZM
*
050011  0  0    15.2784      219.74   0.     3.67376   4.10900   4.10900    0
050021  1  0    15.2727      417.74   1.1    1.4426    5.5       5.5        0
050031  0  1    15.2700      257.74   1.     2.21553   5.47125   5.47125    0
*                                   I
*                                   A
*                                   B
*                                   L
*                                   C
*       FLOWA    DIAM    ELEV
*
050012  0.26957   0.09  -16.365        0
050022  0.26957   0.33  -12.25625      0
050032  0.26957   0.09   -6.75625      0
*
*
*
*       BUBBLE DATA CARDS
*
*         ALPH     VBUB
*
060011    0.0      -3.0  *
*
*
*     TIME DEPENDENT VOLUME
*
*        IRIM   TIME    PRESS.       TEMP.      QUAL.  ML.
*
070101    1
*
*
*             JUNCTION DATA CARDS
*
*       IW1    IW2 IPUMP IVALVE    WP        ADJUN         ZJUNC
*
080011  0      1    1      0       0.0       1.0        -16.365
080021  0      1    2      0       0.0       1.0        -16.365
080031  0      1    3      0       0.0       1.0        -16.365
080041  1      2    0      0       0.0       0.26957    -12.25625
080051  2      3    0      0       0.0       0.26957     -6.75625
```

```
*        INERTIA     FJUNCF      FJUNCR
080012    0.0         0.0         0.0
080022    0.0         0.0         0.0
080032    0.0         0.0         0.0
080042    0.0         0.0         0.0
080052    0.0         0.0         0.0
*
*
*
*        JVERTL JCOKE JCALCI MVMIX DIAMJ CONCO ICHOKE IMOCOR SRCOS IFLOOD IADJUM
*
080013    0       -1      3     1    0.0    1.0   0.     0     0.0    0     0
080023    0       -1      3     1    0.0    1.0   0      0     0.0    0     0
080033    0       -1      3     1    0.0    1.0   0      0     0.0    0     0
080043    0       -1      3     1    0.0    1.0   0      0     0.0    0     0
080053    0       -1      3     1    0.0    1.0   0      0    -1.0    0     0
*
*
*        FILL TABLE DATA
*
*         FILL FLOW RATE TO HIGH POWER CHANNEL IS APPRAXIMATED WITH THE
*         FLOW AREA OF HIGH POWER CHANNEL TO TOTAL CORE FLOW AREA
*
*         ITFILL  ITYPE  NPTS  ICALC  ISATFL  UNITS  PORT   HORA   AFRAC  TAURA
*
*
130100      4      2      2      4      0     GAL/MIN   100.   75.     0.     0.
*130101    0.0  12.       3000. 12.0                                  *HPIS FLOW

130101    0.0  1.838312       3000. 1.838312           *          HPIS FLOW
*
130200      4      2     13      4      0     GAL/MIN  100.   75.     0.      0.
*130201         0.0  114.9   12.3  111.3    62.3    96.6   112.3   79.8
*130202       137.3   50.2  162.3   56.1   172.3    50.2   182.3   42.6
*130203       192.3   34.7  202.3   24.3   212.3    11.4   220.0    0.0
*130204      3000.0    0.0  * LPIS FLOW
*
130201          0.0   17.60  12.10 17.05    62.3    14.87  112.3   12.22
130202        137.3   10.60 162.3    8.59  172.3     7.60  182.3    6.53
130203        192.3    5.24 202.3    3.72  212.3     1.75  220.0    0.0
130204       3000.0    0.0  * LPIS FLOW
*
*
130300      4      1      4      4      3     GAL/MIN  100.0  75.     0.      0.
*130301         0.0  125.93  1.1   125.83   1.101   0.0    150.    0.0
130301          0.0  19.2762 1.1   19.2762  1.101   0.0    150.    0.0
*                                            * ACCUMULATOR FLOW
*
*
*        KINETICS CONSTMIT DATA
*
*         MODEL  KMUL BUVL RHOIN UOUF PROMPT LAMDA TAU
*
140000    0      0    3.   3.    0.   0.      0.   0.
*
*
*        SCRAM TABLE DATA
*
*        NSCR  ITSCRM TSCR(1) TSCR(2)
*
*
*         DECAY CURVE REFERENCED TO 38.6033 (START OF REFLOODING )
*
141001 -4  2 0.  0.036820  10.  0.034282  21.1787 0.031546 111.3967  0.001460
                                                              * FROM LOFT L-2-3
*
*
*
*        HEAT TRANSFER SURFACE DATA
*
*         NSUR  IMSS  IOTO  IJFB
*
150000     4     0     0     0
*        REFLOOD HEAT TRANSFER OPTION CARD
*
*        TK-8  TK-9  TK-10  IFLAG-10  IFLAG-11  TK-11  TK-12  IFLAG-12  TK-6  TK-7
*
150002  .0076  2.   1.      0         1        1.0    1.0     0        .85   1.
*
*
*        HEAT SLAB DATA
*
*
*         I I   I     I  I   I
*         V V   G  I  K  T   A
*         S S   T  F  L  C   C
*         L R   M  S  D  L   Z    AMIL          AMIA       VOLS        HOML
*
150011   0 2   1  1  2  0  10    0.           20.6377    0.1818      0.0
150021   0 2   1  1  2  0  10    0.           20.6377    0.1818      0.0
150031   0 2   1  1  2  0  10    0.           20.6377    0.1818      0.0
150041   0 2   1  1  2  0  10    0.           20.6377    0.1818      0.0
150051   0 2   1  1  2  0  10    0.           20.6377    0.1818      0.0
150061   0 2   1  1  2  0  10    0.           20.6377    0.1818      0.0
*
```

```
*
*        NUMA      DHIL      DHLA      CHHL      CHHA       ZBOT      ZTOP
*
150012 0.0       0.0       0.0       0.0       0.0  0.        .916670
150022 0.0       0.0       0.0       0.0       0.0  0.91667  1.833340
150032 0.0       0.0       0.0       0.0       0.0  1.833340 2.750010
150042 0.0       0.0       0.0       0.0       0.0  2.750010 3.666680
150052 0.0       0.0       0.0       0.0       0.0  3.666680 4.583350
150102 0.0       0.0       0.0       0.0       0.0  4.583350 5.500000
*
*        CORE  SLAB DATA CARDS
*
*         ISLAB      MODT    GLTI    QFRAG   QFMOD  Q  QD
*
160010     1        1  2  3   0.   0.165101 0.0188 0.
160020     2        1  2  3   0.   0.254666 0.0188 0.
160030     3        1  2  3   0.   0.255565 0.0188 0.
160040     4        1  2  3   0.   0.185877 0.0188 0.
160050     5        1  2  3   0.   0.105489 0.0188 0.
160060     6        1  2  3   0.   0.032442 0.0188 0.
*
*
*       SLAB GEOMETRY DATA
*
*        IG  IGP  MR  IM  NOX      XO        XR        PF
*
170101  2         4   1    1   0.0        0.008984   0.3333
170102      0         1    1              0.003721   0.3333
170103      0         1    1              0.002855   0.3334
170104      0         1    1              0.002025   0.0
*
*        HEAT SLAB NODE TEMPERATURE RESET CARD
*
*
175010  1099.731 1096.054  1092.425  1090.048 1087.671
175020  1474.884 1469.732  1459.614  1454.024 1448.235
175030  1507.874 1498.040  1489.892  1484.393 1478.894
175040  1268.512 1264.192  1260.126  1257.203 1254.441
175050   822.045  821.118   820.094   819.455  818.816
175060   450.446  452.479   452.566   453.880  454.793
*
*        MOVING MESH REFINEMENTS DATA CARD
*
*         LSLAB  MTRIP  NTCHF  DZF  DZR  SMINF  SMINLQ  SMINUP
*
179010  1      3       -1   0.01  0.2   0.6    .6      3.6
*
*        MOVING MESH REFINMENT DATA CARD
*
*          MSMAX
*
179099      100
*
*
*
*          THERMAL CONDUCTIVITY CARDS
*
*     THERMAL CONDUCTIVITY DATA FOR UO2
*
*          NKP   TEMP(F)    COND.(BTU/HR.FT.F)
180100 -20   212.      4.143  392.       3.521  752.       2.710 1112.      2.206
180101       1472.     1.866 1632.       1.673 2192.       1.447 2372.      1.378
180102       2552.     1.370 2732.       1.272 2912.       1.235 3002.      1.220
180103       3020.     1.274 3092.       1.264 3272.       1.315 3632.      1.400
180104       3992.     1.531 4352.       1.731 4712.       2.039 5072.      2.380
*
*     THERMAL CONDUCTIVITY DATA FOR ZIRCALOY
*         NKP   TEMP(F)    COND.(BTU/HR.FT.F)
180200 -20    68.      7.548  212.       8.192  392.       8.916  572.      9.588
180201        752.    10.240  932.      10.902 1112.      11.603 1292.     12.373
180202       1472.    13.247 1490.      13.347 1562.      13.748 1652.     14.249
180203       1742.    14.831 1787.      15.121 1832.      15.412 2012.     16.746
180204       2192.    18.341 2372.      20.166 2552.      22.274 2732.     24.693
*
*
*.  VOLUMETRIC HEAT CAPACITY DATA FOR UO2
*
*          NCP   TEMP(F)  CP(BTU/FT3.F)
190100 -20  212.      40.321  392.      43.232  752.      46.249 1112.     47.941
190101      1472.     49.174 1832.      50.248 2192.      51.422 2372.     52.161
190102      2552.     53.082 2732.      54.253 2912.      55.754 3002.     56.700
190103      3020.     56.889 3092.      57.646 3272.      59.994 3632.     66.267
190104      3992.     74.854 4352.      85.839 4712.      99.107 5072.    114.41
*
*   VOLUMETRIC HEAT CAPACITY DATA FOR ZIRCALOY
*
*          NCP   TEMP(F)  CP(BTU/FT3.F)
190200 -20   68.      28.106  212.      28.737  392.      29.570  572.     30.373
190201       752.     31.593  932.      32.    1112.      34.835 1292.     34.835
190202      1472.     34.835 1490.      34.835 1562.      58.322 1652.     39.942
190203      1742.     52.655 1787.      34.429 1832.      34.429 2012.     34.429
190204      2192.     34.429 2372.      34.429 2552.      34.429 2732.     34.429
*
*
```

```
*
*    ENTRAINMENT CORRELATION CARD
*
*         IENT
*
400011    24
*
*         ENTRAINMENT CARRELATION DATA
*
*        EN2   HC1    HC2
*
400013  0.7   1.E6   3.E-6
*
*         CONE SUPERHEAT MODEL
*
*          V1    V2    V3
*
400017    2
*
*         CURE MODEL NUMERICAL COUPLING CARD
*
*        ISUPEX
*
400016    1   * IMPLICIT COUPLING
*
*
.   *  END OF  DATA
```

LISTING OF INPUT DATA FOR CASE 1

```
* ISP-13,LOFT-L2-5 200 - LARGE BREAK TEST-AV. POWER CHAN. REFLOOD CALCULATIONS
*
*  PROBLEM DIMENSIONS DATA
*
*        L N  N  N  N  N  N  N  N  N  N  N  N  N  N  N  N  I  T
*        O E  T  T  V  B  T  J  P  C  L  F  S  G  A  C  M  S  U
*        M D  C  R  O  U  D  U  A  X  K  L  L  O  A  O  T  P  M
*        P I     P  L  B  V  N  P  Y     L  B  A  I  X  X  R  I
*                           C                             O  T
*                                                         G  S
010001 -2 8  3  4  3  1  1  5  8  0  0  3     8  1  2   8 0  0  2
*
*  PROBLEM CONSTANTS DATA
*
*        POWER  OMEGA  POUITL  POUITH  TOUITL  TOUITH
*
*010002   37.5   1.0  0.0886   3626.0   32.1    8540.31
*
*   POWER PRODUCED IN AV. POWER CHANNEL IS 0.781243 OF TOTAL PWER
*   GENERATED POWER IN AV. POWER CHANNEL IS 37.5*0.781243
*
010002  29.296613 1.0  0.0886  3626.0   32.1    8540.31
*
*
*       MINOR EDIT VARIABLES
*
020000  ML 2  SR 1  SR 2  SR 3  SR 4  SR 5  SR  6   AT'E
*
*
*
*
*  TIME STEP DATA CARDS
*
*        NMIN  NMAX  NOMP  NCHK  DELTN  DTMIN   TLAST  ENDCPU
*
030010   10    12    6     0    0.01   0.001      .2   0.
030020   10    10    6     0    0.2    0.001    10.
030030   10    2     8     0    0.2    0.001    100.
*
*  TRIP CONTROL DATA
*
*        IDTRP  IDSIG  IX1  IX2  SETPT  DELAY
*
040010    1      1      0    0    99.0   0.  * END TIME
040020    2      1      0    0     0.    0.  * SCRAM TRIP
040030    3      1      0    0    0.     0.  * MOVING MESH ACTIVATION
040040    4      1      0    0     .1E-7 0.  * FILL TRIP
*
*
*        VOLUME DATA CARDS
*
*           I                                                      J
*           R                                                      T
*           G                                                      P
*           A                                                      R
*      IBUB O      P          TEMP   HORX        V          ZVOL        ZR       U
*
050011  0  0    31.7424      253.578  0.    20.11520   4.10900    4.10900    0
050021  1  0    31.742294    292.04   1.1    8.1954    5.5        5.5        0
050031  0  1    31.7400      253.576  1.    11.14130   5.47125    5.47125    0
*
*                                 I
*                                 A
*                                 B
*                                 L
*         FLOWA   DIAM    ELEV     O
*
050012  1.49011   0.00  -16.365       0
050022  1.49011   0.00  -12.25625     0
050032  1.49011   0.00   -6.75625     0
*
*
*
*       BUBBLE DATA CARDS
*
*         ALPH     VBUB
*
060011     0.0     -3.0  *
*
*
*     TIME DEPENDENT VOLUME
*
*         TRIN   TIME    PRESS.      TEMP.     QUAL.  ML.
*
070101     1
*
*
*            JUNCTION DATA CARDS
*
*        IW1   IW2 IPUMP IVALVE    VP       ADJUN       ZJUNC
*
080011  0     1    1     0      0.0      1.0        -16.365
080021  0     1    2     0      0.0      1.0        -16.365
```

```
080031  0    1    3    0      0.0      1.0       -16.363
080041  1    2    0    0      0.0      1.49011   -12.25623
080051  2    3    0    0      0.0      1.49011    -6.75623
*
*          .INERTIA    FJUNCF      FJUNCR
080012     0.0         0.0         0.0
080022     0.0         0.0         0.0
080032     0.0         0.0         0.0
080042     0.0         0.0         0.0
080052     0.0         0.0         0.0
*
*
*
*         JVERTL JCOKE JCALCI NVHIX DIAMJ CONCO ICHOKE IHQCOR SRCOS IFLOOD IADJUN
*
080013    0      -1     3    3   0.0   1.0   0     0     0.0    0     0
080023    0      -1     3    3   0.0   1.0   0     0     0.0    0     0
080033    0      -1     3    3   0.0   1.0   0     0     0.0    0     0
080043    0      -1     3    3   0.0   1.0   0     0     0.0    0     0
080053    0      -1     3    3   0.0   1.0   0     0    -1.0    0     0
*
*
*       FILL TABLE DATA
*
*        FILL FLOW RATE TO AV. POWER CHANNEL IS APPRAXIMATED WITH THE
*        FLOW AREA OF AV. POWER CHANNEL TO TOTAL CORE FLOW AREA
*
*        ITFILL  ITYPE  NPTS  ICALC  ISATFL  UNITS  PORT  HCPX  AFRAC  TAUMX
*
*
130000     4     2     2     4     0     GAL/MIN  100.  75.    0.     0.
*130111    0.0   12.      3000.  12.0                        *HPIS FLOW

*                                                  0.           0.
130200     4     2    13     4     0     GAL/MIN  100.  75.    0.
*130201        0.0  114.9   12.3  111.3    62.3   96.6   112.3   79.8
*130202      137.3   69.3  162.3   56.1   172.3   50.2   182.3   42.6
*130203      192.3   34.3  202.3   24.3   212.3   11.4   220.0    0.0
*130204     3000.0    0.0  * LPIS FLOW
*
130201         0.0   97.30 112.30 64.25   62.3   81.80  112.3   67.38
130202       137.3   54.60 162.3  47.51  172.3   42.51  182.3   36.07
130203       192.3   28.96 202.3  20.58  212.3    9.65  220.0    0.0
130204      1000.0    0.0  * LPIS FLOW
*
130300     4     1     4     4     0     GAL/MIN  100.0  75.    0.     0.
*130301        0.0 125.83  1.1  125.83   1.101   0.0   150.    0.0
130301         0.0 106.5538 1.1 106.5538 1.101   0.0   150.    0.0
                                         ACCUMULATOR FLOW
*
*
*
*       KINETICS CONSTANT DATA
*
*        MODEL  KMUL  BOVL  RHOIN  UOUF  PROMPT  LAMDA  TAU
*
140000    0     0   0.   0.    0.   0.     0.   82
*
*
*       SCRAM TABLE DATA
*
*       NSCR  ITSCRM TSCR(1) TSCR(2)
*
*
*        DECAY CURVE REFERENCED TO 38.6033 (START OF REFLOODING )
*
141001 -4  2 0.  0.036928  10.  0.034282  21.3967 0.031546 111.3967  0.001460
                                                             * FROM LOFT L-2-3
*
*
*
*       HEAT TRANSFER SURFACE DATA
*
*        NSUR  INSS  IOTB  IQFB
*
150000   4    0    0    0
*       REFLOO  HEAT TRANSFER OPTION CARD
*
*       TK-8  TK-9  TK-10  IFLAG-10  IFLAG-11  TK-11  TK-12  IFLAG-12  TK-6  TK-7
*
150002  .0076  2.   1.      0          1      .1.0    1.0     0.      .85   1.
*
*
*       HEAT SLAB DATA
*
*
*        I I   I . I I   I
*        V V   Q I X A   M
*        S S   U S L C   C
*        L R   M B O L   R    AHTL         AHTR        VOLS        NORL
*
150011  0  2  1  0  2  0  30    0.          110.9953    0.9758      0.0
150021  0  2  1  1  2  0  30    0.          110.9953    0.9758      0.0
150031  0  2  1  1  2  0  30    0.          110.9953    0.9758      0.0
150041  0  2  1  1  2  0  30    0.          110.9953    0.9758      0.0
150051  0  2  1  1  2  0  30    0.          110.9953    0.9758      0.0
150061  0  2  1  1  2  0  30    0.          110.9953    0.9758      0.0
*
*
```

```
*         HOMR      DHEL       DHER       CHNL       CHNR       ZBOT       ZTOP
*
150012 0.0      0.0        0.0        0.0        0.0  0.         .916670
150022 0.0      0.0        0.0        0.0        0.0  0.91667   1.833340
150032 0.0      0.0        0.0        0.0        0.0  1.833340  2.750010
150042 0.0      0.0        0.0        0.0        0.0  2.750010  3.666680
150052 0.0      0.0        0.0        0.0        0.0  3.666680  4.583350
150062 0.0      0.0        0.0        0.0        0.0  4.583350  5.500000
*
*         CORE  SLAB DATA CARDS
*
*         ISLAB      NODT   CLTI     QFRAC    QPMOD  QDMOD
*
160010     1        1  2  3   0.    0.163258 0.0188 0.
160020     2        1  2  3   0.    0.252384 0.0188 0.
160030     3        1  2  3   0.    0.256340 0.0188 0.
160040     4        1  2  3   0.    0.192176 0.0188 0.
160050     5        1  2  3   0.    0.107951 0.0188 0.
160060     6        1  2  3   0.    0.025891 0.0188 0.
*
*
*      SLAB GEOMETRY DATA
*
*        IG  IGP  NR  IN  NDX      XO        XR         PF
*
170101  2       4    1   1   0.0          0.004984   0.3333
170102      0        1   1                0.003721   0.3333
170103      0        1   1                0.002855   0.3334
170104      0        2   1                0.002025   0.0
*
*        HEAT SLAB NODE TEMPERATURE RESET CARD
*
*
175010    368.751  368.060   367.390    366.968  369.546
175020   1153.389 1148.569  1143.795   1141.095 1138.395
175030   1067.013 1062.810  1050.731   1056.289 1053.847
175040    911.806  909.354   906.958    905.448  903.938
175050    459.001  458.728   458.424    458.158  457.893
175060    510.433  510.394   510.321    510.273  510.224
*
*        MOVING MESH REFIMEMENTS DATA CARD
*
*         LSLAB  MTRIP  MTEMP  DZF  DZN  SMINF  SMINLO  SMINUP
*
179010    1      3       -1   0.01  0.2   0.6    .6       5.8
*
*        MOVING MESH REFINMENT DATA CARD
*
*          MSMAX
*
179099     100
*
*
*
*         THERMAL CONDUCTIVITY CARDS
*
*      THERMAL CONDUCTIVITY DATA FOR UO2
*
*         NKP  TEMP(F)   CON.(BTU/HR.FT.F)
170100 -20  212.       4.[illegible]3  392.       3.521  752.       2.71C 1112.       2.2[illegible]
170101      1472.      1.956 1832.       1.623 2192.       1.447 2372.       1.378
170102      2552.      1.337 2732.       1.272 2912.       1.235 3092.       1.220
170103      3272.      1.[illegible] 3092.       1.284 3272.       1.315 3632.       1.400
*
*      THERMAL CONDUCTIVITY DATA FOR ZIRCALOY
*         NKP  TEMP(F)   CON.(BTU/HR.FT.F)
180200 -20   68.       7.540  212.       8.192  392.       8.916  572.       9.588
190201       752.      10.249  932.      10.902 1112.      11.603 1292.      12.375
190202      1472.      13.247 1490.      13.347 1562.      13.748 1652.      14.249
180203      1742.      14.931 1787.      15.121 1832.      15.412 2012.      16.766
180204      2192.      18.341 2372.      20.166 2552.      22.274 2732.      24.693
*
*
*      VOLUMETRIC HEAT CAPACITY DATA FOR UO2
*
*          NCP   TEMP(F)  CP(BTU/FT3.F)
190100 -20  212.       40.321  392.       43.232  752.       46.249 1112.       47.941
190101      1472.      49.174 1832.       50.248 2192.       51.422 2372.       52.161
190102      2552.      53.002 2732.       54.239 2912.       55.754 3002.       56.700
190103      3020.      56.899 3092.       57.646 3272.       59.994 3632.       66.267
190104      3992.      74.856 4352.       85.839 4712.       99.107 5072.      114.41
*
*      VOLUMETRIC HEAT CAPACITY DATA FOR ZIRCALOY
*
*          NCP   TEMP(F)  CP(BTU/FT3.F)
190200 -20   68.       28.106  212.       28.737  392.       29.570  572.       30.373
190201       752.      31.593  932.      32.    1112.       34.835 1292.       34.633
190202      1472.      34.839 1490.      34.839 1562.       58.322 1652.       79.462
190203      1742.      32.655 1787.      34.429 1832.       34.429 2012.       34.429
190204      2192.      34.429 2372.      34.429 2552.       34.429 2732.       34.429
*
*
```

```
*
*     ENTRAINMENT CORRELATION CARD
*
*          IENT
*
400011     24
*
*          ENTRAINMENT CARRELATION DATA
*
*        EMI   MG1    MG2
*
400013  0.7   1.E6   1.E-6
*
*          CORE SUPERHEAT MODEL
*
*           V1    V2    V3
*
400017     2
*
*          CORE MODEL NUMERICAL COUPLING CARD
*
*         ISUPEX
*
400018     1   * IMPLICIT COUPLING
*
*
.   *  END OF  DATA
```

APPENDIX G

ISP-13 SUBMITTAL FROM LOS ALAMOS NATIONAL LABORATORY USING TRAC-PD2 (LANL)

APPENDIX G

ISP-13 SUBMITTAL FROM LOS ALAMOS NATIONAL LABORATORY USING TRAC-PD2 (LANL)

No appendix documentation was received.

APPENDIX H

ISP-13 SUBMITTAL FROM ENEL-CRTN USING RELAP4/MOD6 (ENEL)

APPENDIX H: LOFT L2-5 TEST ENEL ANALYSIS

H1. INTRODUCTION

The following appendix documents the blowdown, refill and reflood analysis of LOFT Experiment L2-5, performed at ENEL by the Nuclear Safety Area of Thermal and Nuclear Research Center as prediction for International Standard Problem 13, using RELAP 4/MOD 6 Update 4 Computer Code/1/.

The appendix presents some information about the nodalization, initial conditions, analytical models and code options used for the calculation.

A sequence of events from the code prediction is included, and the results of the blowdown, refill and reflood calculation are discussed.

H2. INPUT MODELS

The ENEL prediction of ISP13 was performed using two models: a model with a detailed nodalization for the blowdown portion of the transient and a model with a coarser nodalization for the refill/refloc portion of the transient. This section discusses the model nodalizations and the major modeling options chosen to perform each calculation.

For the first part of transients (blowdown) the LOFT/2/ test facility was modelled by 39 volumes, 47 junctions and 26 heat slabs as shown in Fig. 1 and described in Table 1 and 2.

The blowdown analysis involved the use of numerous analytical modeling features contained in the RELAP 4/MOD 6 computer code.

Comments on the major modeling options used (both analytical and systemic) are listed below.

a) Compressible flow with momentum flux was used at all junctions, except incompressible flow with no momentum flux was used at:

JCN 31	(pressurizer outlet)
JCN 32	(accumulator outlet)
JCN 45	(steam generator secondary feedwater inlet)
JCNS 43,44	(LPIS, HPIS)

JCNS 12,20 (upper plenum to hot intact/broken loop)
JCN 19 (Annulus to cold leg broken loop)

b) Vertical slip was used in the following junctions:
JCNS 8, 9 (downcomer inlet/outlet)
JCNS 10,11 (core bypass inlet/outlet)
JCNS 13,15 (steam generator inlet/outlet)
JCNS 21,22,23 (simulated s.g. junctions)
JCN 24 (simulated pumps suction)
JCN 31 (pressurizer outlet)
JCN 35 (lower plenum)

c) Wilson bubble rise model was used only in the pressurizer (VOL 31). Complete separation was used in the following volumes:
VOL 27 (suppression tank)
VOL 32 (accumulator A)
The bubble rise model with a constant bubble velocity (α = .8 v = 3 ft/s) was used in the steam generator secondary (VOL 30).

d) Heat slab were included in the upper plenum.

e) A single channel downcomer was employed.

f) The pressurized surge line volume was lumped into the pressurizer volume.

g) The Henry Fauske/HEM critical flow model was used with a transition quality of 0.02 and disharge coefficients of 0.865 and 0.7 for subcooled and saturated flow, respectively.

h) RELAP 4/MOD 5 heat transfer correlations with their logic (HTRC subroutine) was used.
For all slabs Dougall Rosenow and B&W Barnett, modified Barnett as film boiling and transition boiling respectively was used.

i) The accumulator polytropic air expansion model with a coefficient of 1.3 was employed.

l) The natural convection heat tran sfer model across steam generator slabs was used.

m) LOFT pumps caratteristics with single/two pkase head-torque difference models (set 3 and 4) was used /2/.

As principal feature a double channel for the core re gion was used without comunications between average and hot regions.

The reflood model used for the ISP13 prediction is shown in Fig. 2 and described in Table 3. The model consists of 8 volumes, 12 junctions, and 16 heat slabs. The reflood analysis involved the use of several analytical modeling features contained in the RELAP 4/MOD 6 computer code. Comments on the major modeling options used are listed below.

a. Incompressible flow with no momentum flux was used at all junctions.

b. Wilson bubble rise model was used in the lower plenum, upper plenum and downcomer. Complete phase separation was modeled in the accumulator A and suppression tank.

c. The Steen-Wallis implicit entrainment model was used in the core with the following imput parameters.
HC1 (Core Shaping Factor): 1×10^6
HC2 (Entrainment Onset Factor): 3×10^{-6}
EN2 (Maximum Entrainment Fraction): .75

d. The core superheat model was used in both core channels. The HTS4 refood heat transfer surface was used with the following heat transfer options:
Exponent in Hsu correlation: 0.0115.
Energy partitioning coefficient internally calculated.
Multiplier on Bromley-Pomeranz correlation: 1.0.
Maximum of Bromley-Pomeranz and Hsu correlations used for transition from transition boiling to film boiling.
Independent variable used in the dispersed flow weighting function was quality.
The exponents in the liquid and vapor weighting factors are 0.333 and 1.0, respectively.
Dryout void fraction and quality are 1.0.
Quality times mass flux was used to calculate Reynolds number for superheated vapor.

e. Numerical model coupling for alla case volumes was explicit scheme.

f. The moving mesh option was not used due too large cpu time employed.

The refill/reflood calculation was initiated starting from the end of blowdown and the correspondent values of parameters at that time were used in the new modellization.

The core was modelled using two hydraulic volumes and two stack of heat slabs simulating hot and average power rods.

The intere intact loop was lumped in one single volume and the broken leg were modelled as equivalente junctions.

H3. COMPUTER CODE DESCRIPTION

The ENEL ISP13 analysis was performed using the standard IBM version of the RELAP 4/MOD 6 update 4 code stored on ENEL computer system, IBM 3032.

The calculation was performed using code best estimate options.

The running time was about 280 minutes for the calculation of the complete transient, 80 minutes for the blowdown phase and 200 for the refill and reflood phases.

H4. CONCLUSIONS

The results/4/ of blowdown analysis of ISP13 indicates that use of 0.865 and 0.7 break flow multiplier respectively in the bubcooled and saturated region with the HF-HEM critical model provides a good prediction of system pressure and break mass flow rates response during the transient.

The sequence of events from the computer code prediction is described in Table 4.

The use of the accumulator politropic air expansion model with a constant at 1.3 provides a good prediction of the LOFT accumulator pressure response.

The cladding temperature response does not strictly agree experiment, in particulary the early rewet of core due to upper plenum fallback phenomena, that was not predicted in the model.

The results of the ISP8 reflood calculation indicate that use of current recommended reflood options in RELAP/4/ /MOD 6 in conjunction with a parallel core channel model do not adequately predict the experiment. In fact the results of calculation show a later core rewet that in experimental transient.

H5. REFERENCES

/1/ RELAP 4/MOD 6
"A Computer Program for Transient Thermal-Hydraulic Analysis of Nuclear Reactors and Related Systems"
User's Manual, CDAP TR 003, January 1978.

/2/ DOUGLAS L. REEDER
"LOFT System and Test description"
NUREG/CR-0247 TREE-1108, Julay 1978.

/3/ P.D. BAYLESS, J.M. DIVINE
"Experimental Data Report for LOFT Large Break Loss-of-Coolant Experiment L2-5"
NUREG/CR 2826 EGG-2210, August 1982.

/4/ L. BELLA F. DONATINI
"ISP13 LOFT L2-5 Test ENEL Analysis Report"
N6-82-09 December 1982.

VOLUME No.	DESCRIPTION
7	Upper plenum
8	Annulus
12	Intact loop hot leg
13	Steam generator primary and inlet plenum
14	Steam generator primary and outlet plenum
15	Pump suction
16,17	Pumps
18,19	Intac: loop cold leg - downstream of pump
9	Dowcomer
39,10	Lower plenum
1,2,3,4,5,6	Average core channel
33,34,35,36,37,38 .	Hot core channel
11	Core by pass
29,28	Broken loop cold leg
20	Broken loop hot leg - vessel to simulated steam generator
21,22	Simulated steam generator
23	Broken loop hot leg - simulated steam generator to simulated pump
24	Simulated pump
25,26	Broken loop hot leg - simulated pump to break nozzle
32	Accumulator
30	Steam generator secondary
27	Pressure suppression tank
31	Pressurizer

Table 1: Volume description for the blowdown calculation

HEAT SLAB No.	DESCRIPTION
1,2,3,4,5,6	Average power rods
7,8,9, 10,11,12	Hot power rods
24	Lower plenum structures
15	Downcomers vessel wall
14	Core barrel
18,19	Steam generator tubes
26	Upper plenum structures
23	Vessel upper head
39	Vessel bottom
25	Vessel filler
13	Annulus structures

Table 2: Heat slab description for the blowdown calculation

VOLUME No.	DESCRIPTION
4.	Upper plenum
6.	Intact loop/Steam generator primary
1.	Downcomer - inlet annulus
2.	Lower plenum
8.	Average core channel
3.	Hot core channel
5.	Pressure suppression tank
7.	Accumulator A

HEAT SLAB No.	DESCRIPTION
1,2,3,4,5,6.	Average power rods
7,8,9,10,11,12	Hot power rods
13	Barrel
14	Vessel, cylindrical region
15	Vessel bottom
16	Lower plenum internals

Table 3: Volume and heat slab description for the refill/reflood calculation

EVENT	Time After Experiment Initiation (s)
Experiment L2-5 initiated	0.
Reactor scrammed	0.1
Primary coolant pumps tripped	0.9
Subcooled break flow ended (cold leg)	3.3
Pressurizer emptied	5.
Accumulator A injection initiated	19.3
HPIS injection initiated	23.9
Maximum cladding temperature reached	50.
LPIS injection initiated	37.3
Accumulator emptied	68.
Core cladding quenched (Average channel)	70.
Core cladding quenched (Hot channel)	110.

Table 4: Calculated sequence of events for ISP13

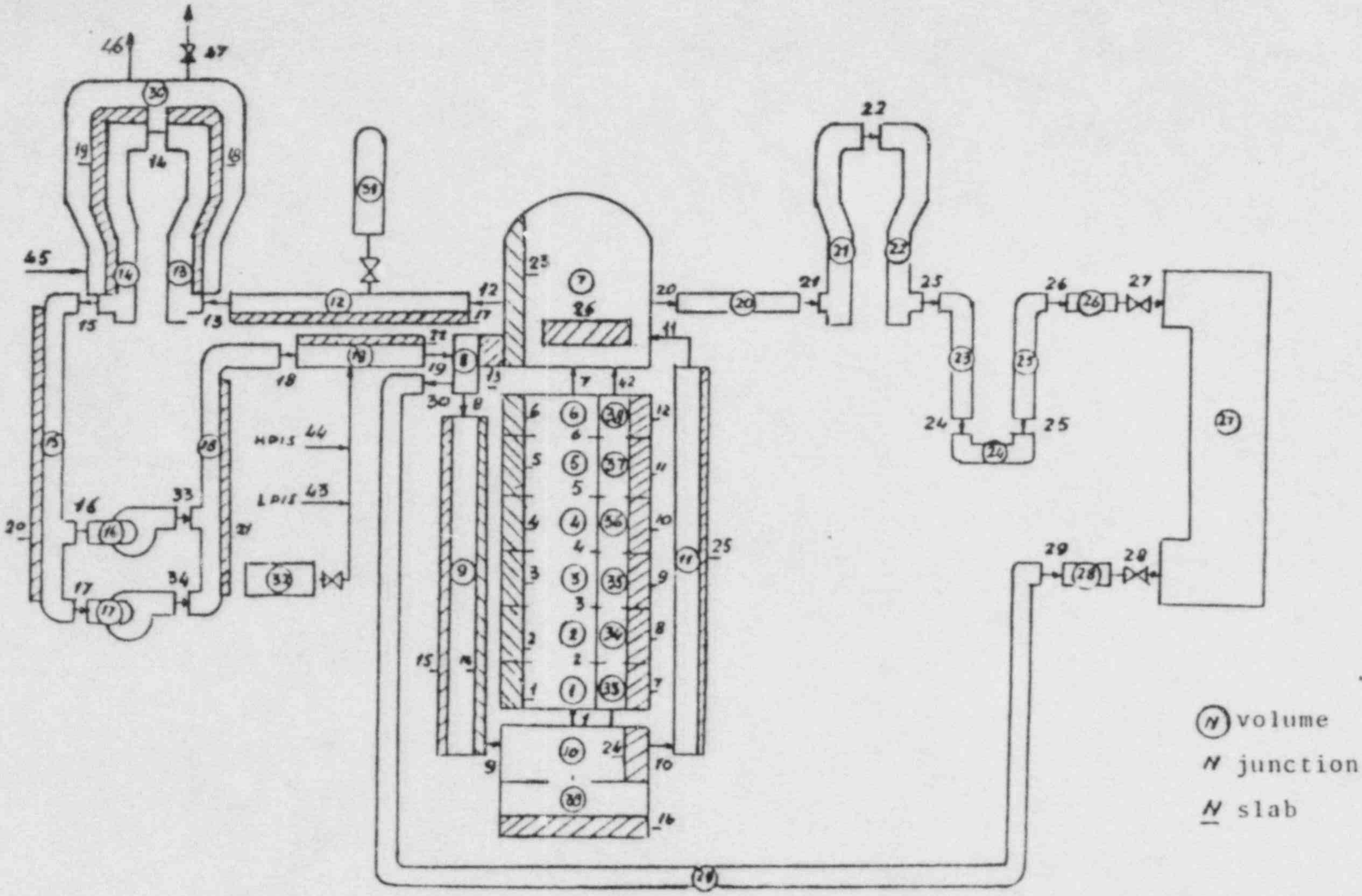

Fig. 1: L2-5 test blowdown nodalization

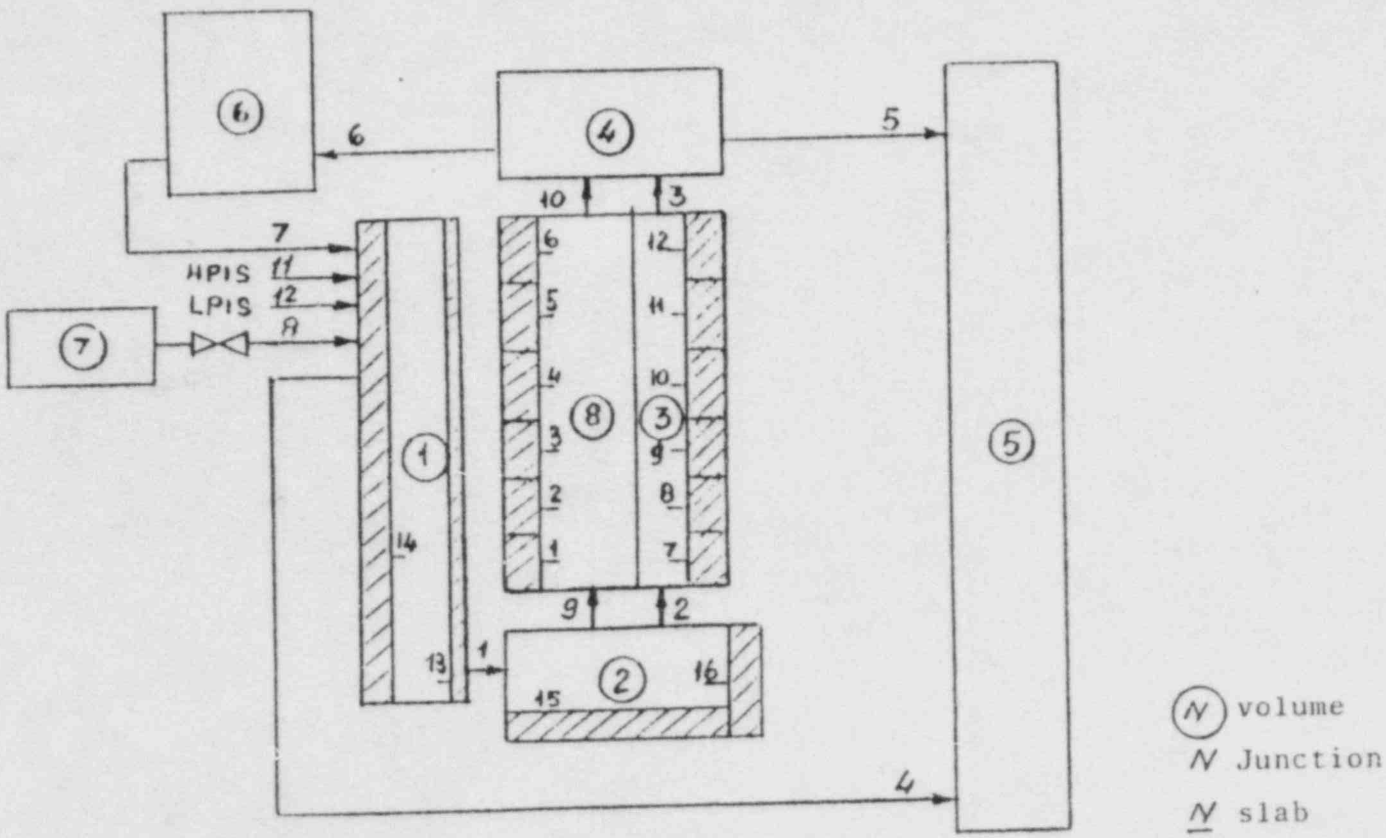

Fig. 2 : Refill/reflood L2-5 test nodalization

APPENDIX I

ISP-13 SUBMITTAL FROM DIPARTIMENTO DI CONSTRUZIONI MICCANICHE E NUCLEARI USING RELAP4/MOD6 (DCMN)

UNIVERSITA' DEGLI STUDI DI PISA

DIPARTIMENTO DI COSTRUZIONI
MECCANICHE E NUCLEARI

APPENDIX I: DCMN RELAP4 MOD 6 CALCULATION

S. Boncompagni
G.M. Galassi
M. Mazzini
F. Oriolo

*Work performed whitin the frame work of
ENEA LWR research program.*

APPENDIX I: DCMN RELAP4 Mod 6 CALCULATION

I.1 - INTRODUCTION

The "Dipartimento di Costruzioni Meccaniche e Nucleari" (DCMN) of the University of Pisa performed the study of LOFT experiment L2-5 /1/, chosen as the International Standard Problem n. 13 (ISP13), by CSNI, by RELAP4 Mod 6 Code, running on the IBM 370/168 computer of CNUCE-PISA.

The study has been carried out in the framework of the ENEA safety research program.

I.2 - SIMULATION MODELS

For ISP13 analysis, two simulation models have been used: a detailed nodalization for the blowdown and refill portion of the experiment; a coarse nodalization for the reflood phase.

Two cases have been modelled for both portions of the experiment, with 1 and 2 core channels, respectively.

I.2.1 - Blowdown and refill phase

I.2.1.1 - Plant nodalization

The nodalization shown in Fig. I.1 has been used for the calculation of the reference case (see Table I.1); it consists of 38 control volumes, 43 junctions and 33 heat slabs.

The LOFT vessel is modelled by 12 control volumes: 5 in the core, 2 in both the lower and the upper plena, the others

TABLE I.1 - Comparison among the main runs of the ISP13 analysis

JOB IDENTIFICATION	NUMBER OF VOLUMES	NUMBER OF SLABS	NUMBER OF JUNCTIONS	CPU TIME/REAL TIME/N.OF VOLUMES	MAIN STUDY OBJECT	ANALYZED TIME INTERVALL
1 Channel	38	33	43	1.29	Reference case	20 s before the break 36 s after the break
2 Channels	41	33	51	1.33	Hot channel effect	20 s before the break 38 s after the break

A) Blowdown and refill analysis

JOB IDENTIFICATION	NUMBER OF VOLUMES	NUMBER OF SLABS	NUMBER OF JUNCTIONS	CPU TIME/REAL TIME/N. OF VOLUMES	MAIN STUDY OBJECT	ANALYZED TIME INTERVALL
1 Channel	7	12	10	15.13	Reference case	73 s after refill
2 Channels	8	22	13	32.78	Hot channel effect	65 s after refill

B) Reflood analysis

simulating the core-bypass, the downcomer distributor anulus and the downcomer anulus, respectively.

The structures of the reactor vessel and the filler are collapsed in one slab; while another slab simulates the barrel; 3 slabs are put in both the lower and the upper plena and one slab describes the heat exchanges between the upper plenum and the distributor anulus.

The pressurized surge line is lumped together the pressurize control volume.

The steam generator has been detailed in 5 control volumes (included the two plena), with 5 heat slabs; the secondary side of the steam generator is a time-dependent volume, which exchanges heat with the primary side by natural convection through 3 slabs.

Two control volumes, each with a heat slab, connect the pressure vessel to the steam generator and the steam generator to the pumps, which are modelled by a homogeneous control volume.

The cold leg intact loop consists of 2 control volumes, with 1 heat slab: the accumulator is represented by 1 volume, without the surge-line and heat slabs.

The HPIS and LPIS are simulated by 2 fill junctions, turned on by a time-elapsed trip.

The broken loop hot leg is detailed by 8 volumes, without heat slabs (preliminary runs showed no influence of the broken loop structures on the flow from the related break-plane).

Finally, two control volumes, each with one heat slab, represent the broken loop cold leg, while the suppression tank is modelled by a time-dependent volume.

Core thermal power production is simulated by 12 slabs, divided into 2 stacks: 5 to simulate the average fuel assembly and 7 the hot one. To assign the power to the core slabs, the criterium been used of weighting the axial linear power distribution on the number of pins of the fuel assembly (256 for the hot channel, 1096 for the average one).

For the 2 core channels model, the nodalization shown in Fig. I.2 has been used.

Now the core is simulated by 2 channels, each with four control volumes and six heat slabs: the "hot" channel silulates the central fuel assembly, the "average" one the remaining fuel rods. A junction connects each control volume in one channel to the corresponding volume in the other channel. The same criterion used in the 1 channel nodalization has been employed to assign the power to the core slabs.

The other nodalization options are unchanged with respect to the 1 channel nodalization.

I.2.1.2 - Physical models

a) Critical flow models

The critical flow models finally used are those of Henry Fauske and Homogeneous Equilibrium (HF/HEM) with dials 0.84 for the saturated flow and 1. for the subcooled phase; the boundary quality of the transition region has been chosen equal to 0.003.
These values are the result of a number of sensitivity runs carried out to detect their influence on mass flow at the break planes[2].
The inertial model is used in the pressurizer-hot leg junction.

b) Momentum equations

The complete momentum equation (MVMIX=0), with momentum flux, is applied to all junctions with clearly defined flow direction in the connected volumes.
All T junctions and the junctions at the lower plenum outlet and at the upper plenum inlet are calculated with the simpler incompressible momentum equation form (MVMIX=3); according to this criterium the MVMIX=3 option is used in junctions 6, 8, 20, 21, 22, 26, 29 of Fig. I.1 and in junctions 2, 4, 16, 17, 18, 22, 25 of Fig. I.2.

c) Bubble rise and slip models

The homogeneous model is applied to the primary circuit. The vertical slip model has been used in all reactor vessel junctions and at the inlet and outlet of the steam generator simulator in the broken loop and of the steam gene rator in the intact loop.

Bubble rise models are applied in the other control volumes; with values of the rise velocity (V_B) and of the density gradient (α) listed in Table I.2.

TABLE I.2 - Bubble sise parameters in the blowdown and refill analysis

DESCRIPTION	α	V_B (ft/sec)
Pressurizer	0.8	Calculated by Wilson model
Accumulator	0.0	Complete separation (10^6)
Suppression tank	0.0	" " "
SG secondary side	1.0	3.0

d) <u>Accumulator gas expansion model</u>

The behaviour of the gas present in the upper part of the accumulator is simulated by a polytropic expansion wiht $n = 1.40$.

e) <u>Heat transfer correlations</u>

The RELAP 4 Mod 6 blowdown correlations (subroutine HTS2) are used in the calculations of the blowdown and refill phases, with the following option:

-implicit wall temperature solution;

-DNB correlation: W3, Hsu-Becker and modified Zuber;

-transition boiling correlation: modified Tong-Young;

-film boiling correlation; Condie-Bengston III.

The natural convection option is adopted for the heat transfer on the secondary side of the S.G. heat slabs.

f) Pumps

As indicated above, the two LOFT pumps are simulated by one volume; the standard homologous LOFT pump curves are used.

g) Other code options

The two-phase friction multiplier with Fanning friction losses and smooth pipe walls are implied to calculate distributed frictional losses.
Water packing, choking and enthalpy transport models are used to activate the calculation procedure for incompressible flow.
Mixture level smoophing is also used to activate another calculation procedure, to avoid loss of CPU time when a control volume is empty.

I.2.2 - Reflood phase

I.2.2.1 - Plant Nodalizations

The reflood phase starts at the end of the refill phase, i.e. when the lower phenum is full of water. For the reinitialization of the calculations, the assumption that all junction flows are zero is made; of course, this is not the real situation but it makes the new initialization much easier, with no trouble arising from the residual terms in the momentum balance equation. Besides, it would be difficult to specify the junction flows on the basis of the experimental data report, due to the use of a plant simplified nodalization and to the low value of flow rates at the reflood starting time.

The other initial conditions for volumes and slabs are taken from the previous calculation for the blowdown and refill phases.

A first study was performed with the nodalization used in the ISP8[3,4] and ISP11[5]; with poor results, due to the injection of subcooled water into a volume containing steam.

Other runs were performed using a control volume to simulate the LOFT pumps and with the downcomer and lower plenum volumes separated or combined: both runs stopped, due to the very high depressurization rate in the pump volume.

Finally, the nodalization shown in Fig. I.3 has been chosen: the only difference with the first one is that all ECCS inject into the lower plenum (which is filled with liquid water), instead of into the downcomer.

As is shown in Fig. I.3, this nodalization includes 7 control volumes, 10 junctions and 12 heat slabs.

One control volume simulates the core, with 10 core heat slabs, equally spaced; they represent combined high and low powered rods, in such a way that the total core power is preserved.

The upper plenum comprises the broken loop hot leg and another control volume describes the whole intact loop; the downcomer and the lower plenum are separated into two volumes.

The vessel structures alone are simulated by two slabs, one placed in the lower plenum and the other in the upper plenum.

The accumulator is simulated by a control volume and the suppression tank by a time-dependent volume.

Two fill junctions represent the high and the low pressu re injection systems.

The heat transfer between the primary and the secondary loop is not taken into consideration.

Also the reflood phase has been studied by a two channel nodalization of the core (Fig. I.4): now, each of the two core volume is equipped with a heat slabs stacks, each subdivided into 10 heat slabs.

I.2.2.2 - Physical models

a) Critical flow models

The same models and parameters as for the blowdown and refill phases have been used.

b) Momentum equation

The incompressible single stream flow without momentum flux (MVMIX=3) has been used in all the junctions.

c) Bubble rise and slip models

Complete separation between steam and liquid water is assumed in the intact loop volume, in the accumulator and in the suppression tank volumes.
In the volume simulating the upper and lower plenum and the downcomer, the Wilson model is applied, with a bubble density gradient = 0.8.
The special reflood option to activate Mod 6 implicit entrainment calculation is used in the core.
The slip correlation is applied in the junction at the core exit.

d) Accumulator gas expansion model

The same model has been assumed as used in the blowdown analysis.

e) Heat transfer correlations

The RELAP4 Mod 6 reflood heat transfer correlations have been used in the analysis (subroutine HTS4) with an implicit wall temperature solution.

The important input parameters for reflood correlations are as follows: .

- the coefficient of the exponential decay for Hsu correlation (=0.0115);
- the energy partitioning coefficient for the core superheat model, calculated in subroutine HTS4;
- the indicator for the use of Bromley and Hsu correlations;
- the choice of the independent variable in the dispersed flow weighting function (= void fraction);
- the exponent of the superheated vapor portion of the weighting function (=1);
- the calculation of Reynold's number for the Dittus-Boelter superheat vapor equation, considering quality times total mass flux in the core;
- the dry-out void fraction (=1);
- the dry-out void quality (=1).

Sensitivity tests have been performed for the following parameters(*):

(*) - For each parameter, in addition to the value suggested in the user manual, a second limit value has been used, with the aim to understood the relative influence.

- multiplier for the Bromley-Pomeranz heat transfer coefficient (1 or 10);
- exponent of the independent variable in the liquid portion of the weighting function (0.33 or 60);
- maximum entrainment fraction (0.75 or 1) and entrainment fraction exponential factor parameter HC2 (10^6 or $3 \cdot 10^{-6}$);
- use of Wallis flooding correlation.

I.3 - ANALYSIS OF THE RESULTS

In the following section some measured experimental data are compared with the calculation results.

The comparison of the time sequence of the events is reported in Table I.3.

TABLE I.3 - Sequence(°) of events for ISP13

EVENT	Experiment	DCMN Calculation 1 Channel	2 Channels
Experiment L2-5 initiated	0.0	0	0
Subcooled blowdown ended	0.043±0.01	-	-
Reactor scrammed	0.24 ±0.01	0.24··	0.24··
Cladding temperatures initially deviated from saturation	0.91 ±0.2	0.9±0.2	0.9±0.2
Primary coolant pumps tripped	0.94 ±0.01	0.94··	0.94··
Subcooled break flow ended (cold leg)	3.4 ±0.5	3.	2.5
Partial rewet initiated	12.1 ±1.0	10.···	14.···
Pressurizer emptied	15.4 ±1.0	(14.5,15)	(14.5,15)
Accumulator A injection initiated	16.8 ±0.1	16.9	17.9
Partial rewet ended	22.7 ±1.0	23.···	22.5···
HPIS injection initiated	23.90 ±0.02	23.9··	23.9··
Maximum cladding temperature reached	28.47 ±0.02	44.···	44.···
LPIS injection initiated	37.32 ±0.02	37.32··	37.32··
Accumulator emptied	49.6 ±0.1	50.··	50.··
Core cladding quenched	65 ±2	62.···	85.···

(°) Time (s) after Experiment Initiation
(··) used as input data (···) at hot spot

I.3.1 - Blowdown and refill phases

The most interesting phenomenon during a large break LOCA is the behaviour of the nuclear fuel rods. Figs 5÷10 show the comparison between cladding temperatures calculated by the 1 and 2 channels nodalizations and measured in the high-powered fuel rods at different axial levels.

With regard to the blowdown and refill phases, the high powered fuel assembly thermal response can be best characterized by examining separately the lower half (0÷0.84 m, Figs 5÷8) and the upper half (0.84÷1.68 m, Figs 9 and 10) of the rods.

Cladding temperatures in the first region depart from saturation within the first 2 s after the beginning of the experiment; then they quickly rise in response to degraded cooling and reach a plateau within 10 s, where remain up to 30 s. The maximum measured cladding temperature of 1077 °K occurs at about 28 s. At approximately 30 s a gradual cooling begins, as the ECCS water fills the lower plenum.

A very different thermal response has been measured in the second region, as shown in Fig. 9: the cladding behaviour is similar to that in the first region for nearly 15 s. At this point a top down quench occurs, lasting about 5 s; it is followed by a second cladding temperature excursion with a generally lower peak value.

The 2 channels calculation foresees an earlier onset of CHF in the hot channel, due to the overestimation of the coolant enthalpy in the whole core; the values of the cladding temperature maxima are generally well calculated[(*)].

(*) The uncertainties associated with the heat transfer correlations (Mod 5 of Mod 6 package) are analysed in /2/.

In the 1 channel calculation, on the contrary, the CHF onset is in good agreement with the experiment, but the peak cladding temperature is underestimated: as a consequence of the averaging on the whole core cross-section, the cool t enthalpy is now too low.

All the calculated cladding temperatures show a partial rewet (a sudden and rapid decrease, without reaching in the hot channel the saturation temperature), due to an increase of the reverse coolant mass flow in the period of 6.÷12. s, after the emptying of the intact loop hot leg; in the test, this phenomenon occurs only in the upper part of the core. The discrepancy is probably caused by incorrect assumptions for the input pressure loss coefficients in the intact loop /1/.

The pressure trends are shown in Fig. I.11 for the pressurizer and in Fig. I.12 for the intact loop hot leg; the agreement between the calculations and the data is excellent during most of the transient (the calculated pressures are within 0.3 MPa of the measured values).

During the first phase of the blowdown the calculated system pressure decays rapidly than the measured one, reaching saturation conditions earlier than in the test. Such a tendency might be a consequence of the overestimation of the mass flowrate through the break orifice in the broken loop hot leg (Fig. I.13).

On the contrary the mass flowrate through the break orifice in the broken loop cold leg has been calculated well (Fig. I.14). (*)

The distribution of coolant inventory in the intact and in the broken loops is documented in /1/.

(*) The results of a sensitivity study performed to improve the evaluation of the mass flowrate through the break orifice, are reported in /2/.

I.3.2 - Reflood phase

The reflood calculation starts as mentioned above, when the lower plenum liquid level rises to the core bottom (end of refill phase). In the experiment, this happens about 8 seconds earlier than in the calculation (in the reference case), due to the lower residual mass in the loop during the blowdown phase. At this point the pressure and temperature conditions of the various volumes of the LOFT plant remain almost constant.

This allows of studying the reflood phase by gathering most of volumes of the previous nodalization, provided the vessel is represented relatively in detail; this simplification has no noticeable influence on the most important physical phenomena in the reflood transient.

However, during this phase non-homogeneous and non-equilibrium phenomena occur, while the RELAP4 code is based on a zero-dimensional, homogeneous, equilibrium treatment of the two-phase thermalhydraulics; this means that local quantities cannot be provided with accuracy.

In particular, the lack of a non-equilibrium volume model causes a too high depressurization in the plant at the beginning of the ECCS injection compared with the experimental data: the istantaneous mixing of injected subcooled water and saturated fluid present in the volume, assumed by the code, does not happen, due to stratification phenomena. A fluid injection at high temperature (the adjustment used to solve the problem during the blowdown-refill phase) is not possible during the reflood phase, because it would prevent the rewetting or delay it for too long time. Therefore, it is necessary to make the ECCS injection into a volume filled with liquid-steam mixture: so the lower plenum has been chosen.

The combining of the broken loop hot leg volume with upper plenum volume improves the results: the steam generated in the core has a greater expansion space and this allows easier rewetting.

The core thermal response is, of course, the most important variable also in the reflood phase and special models can be used to improve the results of the calculations:
- HTS4 heat transfer coefficients set;
- moving mesh;
- local mass flux;
- core superheat.

Figures I.5 ÷ I.10 show the calculated and the measured trends of the cladding temperature in the central fuel assembly for the reflood phase too.

As far as the 2 channel nodalization is concerned, all calculated cladding temperatures present an initial quenching, followed by a new temperature climb and a plateau which lasts until the final quench. The RELAP4 assumption of saturation conditions leads to a quickly decrease in the heat transfer rate and to a delay in the final quenching. The 1 channel calculation is less sensitive to this phenomenon, perhaps because the volume of the single channel is greater as compared to each of the two channels in the previous nodalization.

The experimental data show a falling back and a bottom quench front. Due to the fact that the RELAP4 Mod.6 version running at DCMN is unable to simulate the former phenomenon, the calculations present only a bottom quench front(*); then

(*) The results of a sensitivity analysis of the core rewetting phase are reported in /2/.

the rewetting time of the upper half of the high powered fuel rods is greatly overestimated.

On the other hand the behaviour of the average fuel rod in this core region matches the experimental data fairly closely, even in the 2 channels nodalization.

The quench times, calculated on the basis of the 1 channel nodalization in the lower half region of the core, are generally in closer agreement with the experimental data than those obtained through the 2 channels nodalization.

I.4 - CONCLUSIONS

The analysis presented in the previous chapter shows the capability of RELAP4 code to predict the blowdown, refill and reflood phases of large LOCAs; a suitable nodalization allows one to save CPU time without loss in the reliability of the results.

The calculations of blowdown and refill phases show, in particular, the importance of a good simulation of the following aspects (for a LARGE LOCA analysis):

- stationary conditions;
- break mass flow-rate;
- heat transfer in core region.

The hot rod peak cladding temperature is well calculated in the blowdown-refill phase, but the overall trend is not well reproduced, probably due to excessive top-down quench as far as the experiment is concerned.

The reflood results are more interesting. They confirm the conclusions of the ISP8 /3,4/ and ISP11 /5/:

- provided the pressure drops at vessel inlet and outlet are well simulated, some volumes of the blowdown nodalization can be collapsed in a single volume, without influencing the core thermal and hydraulic response;

- the effect of the intact loop pumps need not be taken into account due to head losses.

The changes in the input heat transfer coefficients of the Bromley-Pomeranz correlation /2/ improve the results of the reflood phase calculation; in this way, pratically, the inadequacy of the code in studying non-equilibrium conditions (subcooled liquid - superheated steam) in the core region can be overcame.

It can be stated, however, that the gathering of some volumes and the "reinitialization" for the reflood calculation involves assumptions in the input therlakhydraulic conditions (quality, pressure losses, etc.), which require experience and a good sensitivity of the code user.

REFERENCES

/1/ P.D. BAYLESS, J.M. DIVINE
"Experimental Data Report for LOFT Large Break Loss-of--Coolant Experiment L2-5"
NUREG/CR-2826, EGG-2210 (August 1982).

/2/ S. BONCOMPAGNI, G.M. GALASSI, M. MAZZINI, F. ORIOLO
"Post-Test Analysis of LOFT Nuclear Experiment L2-5, Using RELAP 4 Mod 6 Computer Code"
Presented at OECD-CSNI Workshop on International Standard Problem n. 13 - Idaho Falls (USA), July 18-19, 1983.
RL 042(83).

/3/ L. BELLA, F. DONATINI, F. ORIOLO, B. PATTI
"Analisi del transitorio termoidraulico nella prova S-06-3 del programma SEMISCALE, con l'impiego del codice RELAP 4 Mod. 6"
XXXVI Congr. Naz. dell'Associazione Termotecnica Italiana - ATI - Viareggio 4-9 Ottobre 1981.

/4/ F. DONATINI, G. GALASSI, M. MAZZINI, F. ORIOLO
"The Analysis of Refill and Reflood Phases in SEMISCALE Test S-06-3 Using RELAP 4 Mod 6 Computer Code"
XXXVIII Congresso Naz. dell'Associazione Termotecnica Italiana - ATI - Padova, 27 Settembre-1 Ottobre 1982.

/5/ G.M. GALASSI, M. MAZZINI, F. ORIOLO, B. PATTI
"The analysis of L3-6/L8-1 LOFT experiment (OECD-CSNI) International Standard Problem n. 11 by RELAP 4 Mod 6 Computer Code"
9th Meeting of CSNI Working Group on ECC and Fuel Behaviour in Water Reactor - TOKAI MURA 24th-28th May,1982.
SINDOC (82)150.

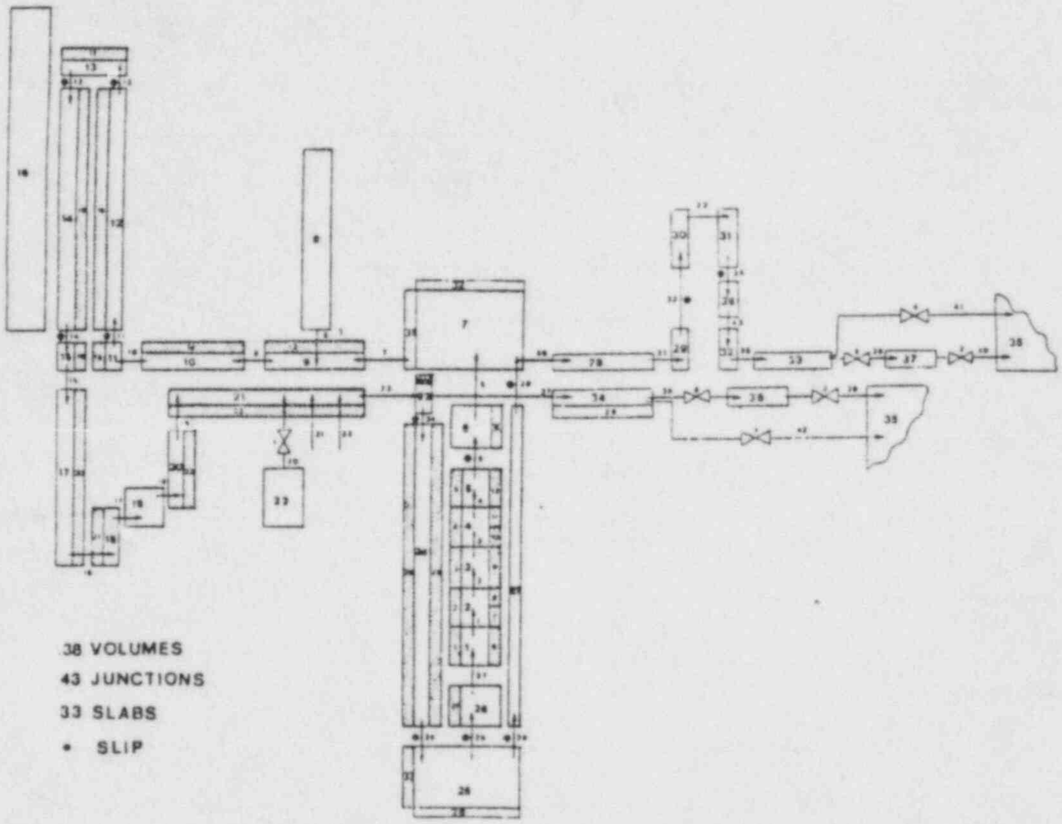

Fig. I.1. - LOFT plant 1 Channel nodalization for the blowdown and refill phases.

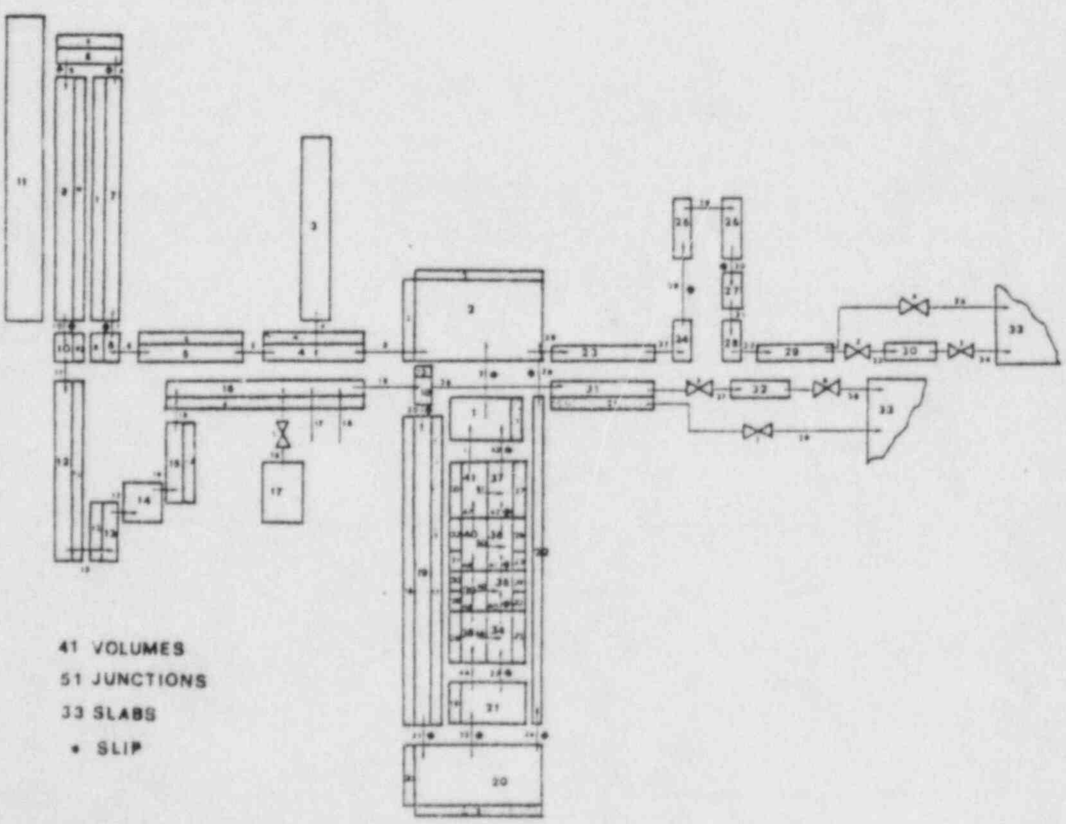

Fig. I.-2 - LOFT plant 2 Channels nodalization for the blowdown and refill phases.

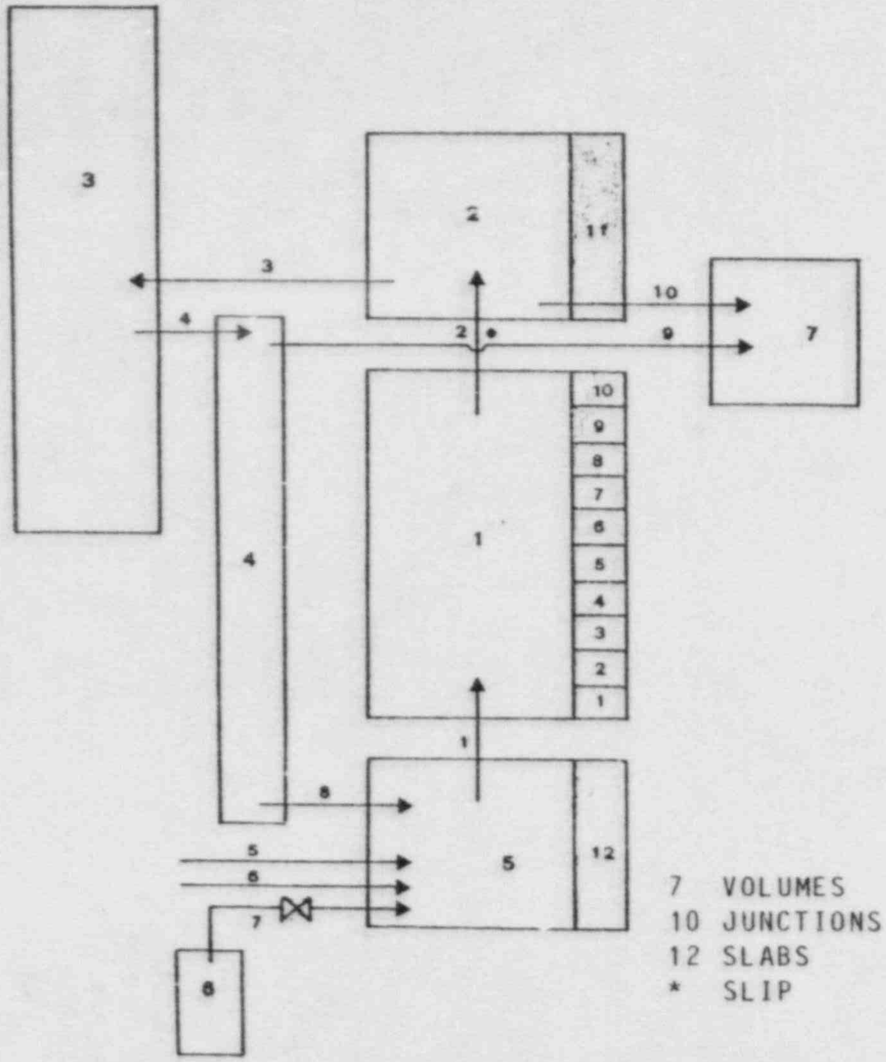

Fig. I.3 - LOFT plant 1 Channel nodalization for the reflood phase.

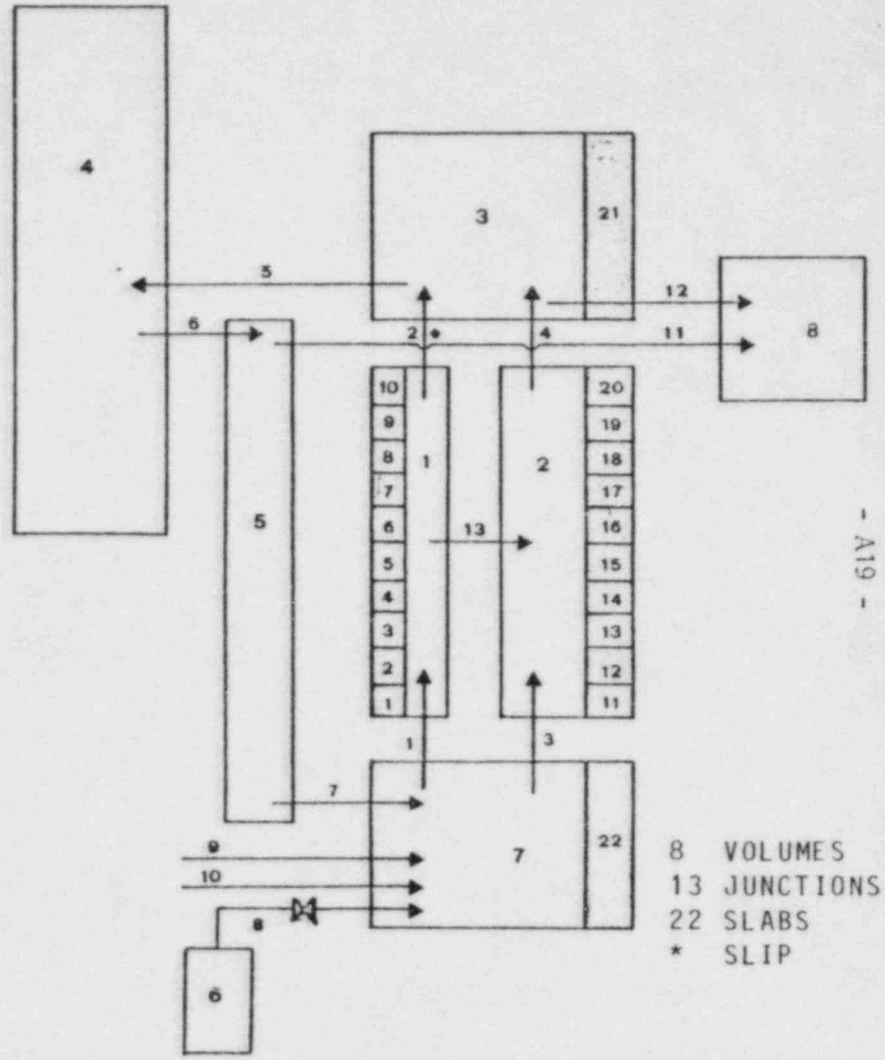

Fig. I.4 - LOFT plant 2 Channels nodalization for the reflood phase.

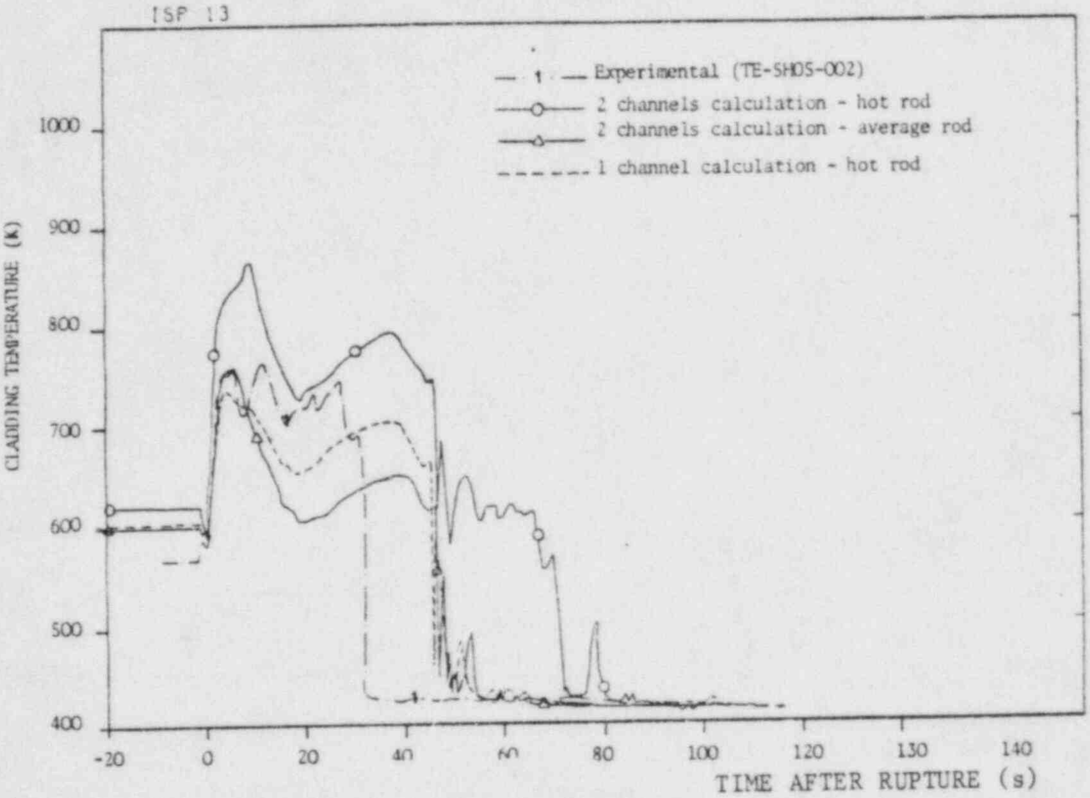

Fig. I.5 - Cladding temperature behaviour at level 0,08 m.

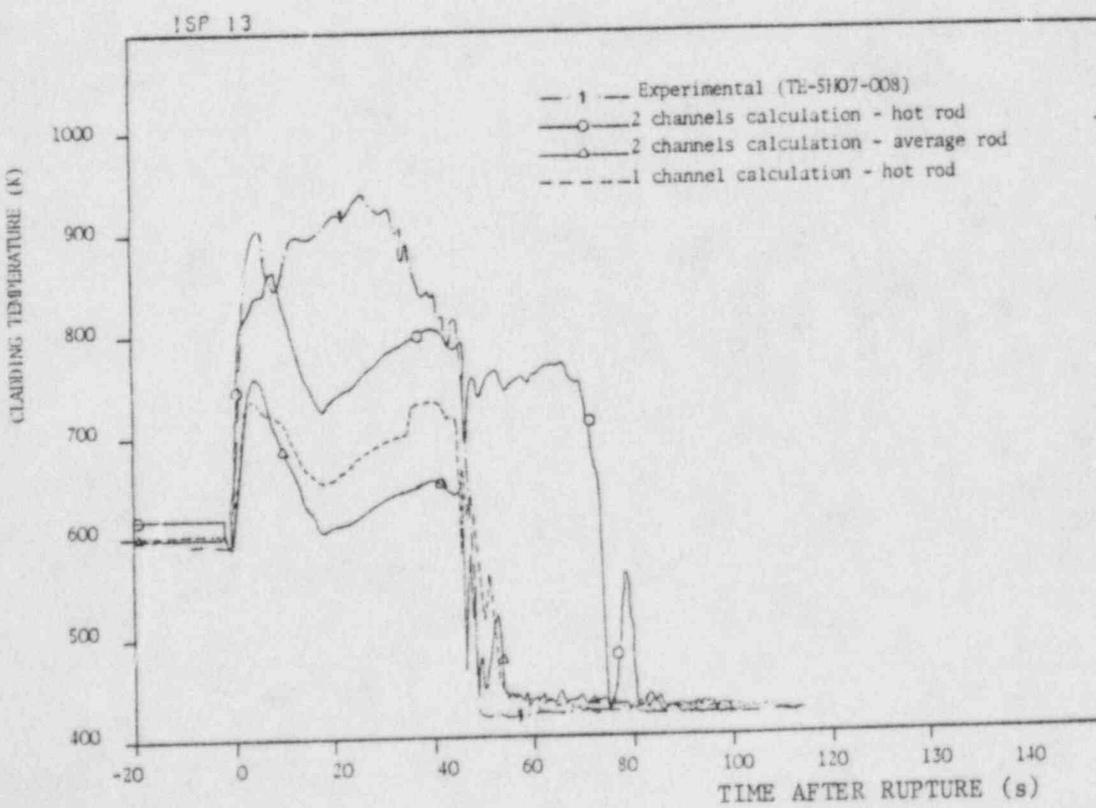

Fig. I.6 - Cladding temperature behaviour at level 0,25 m.

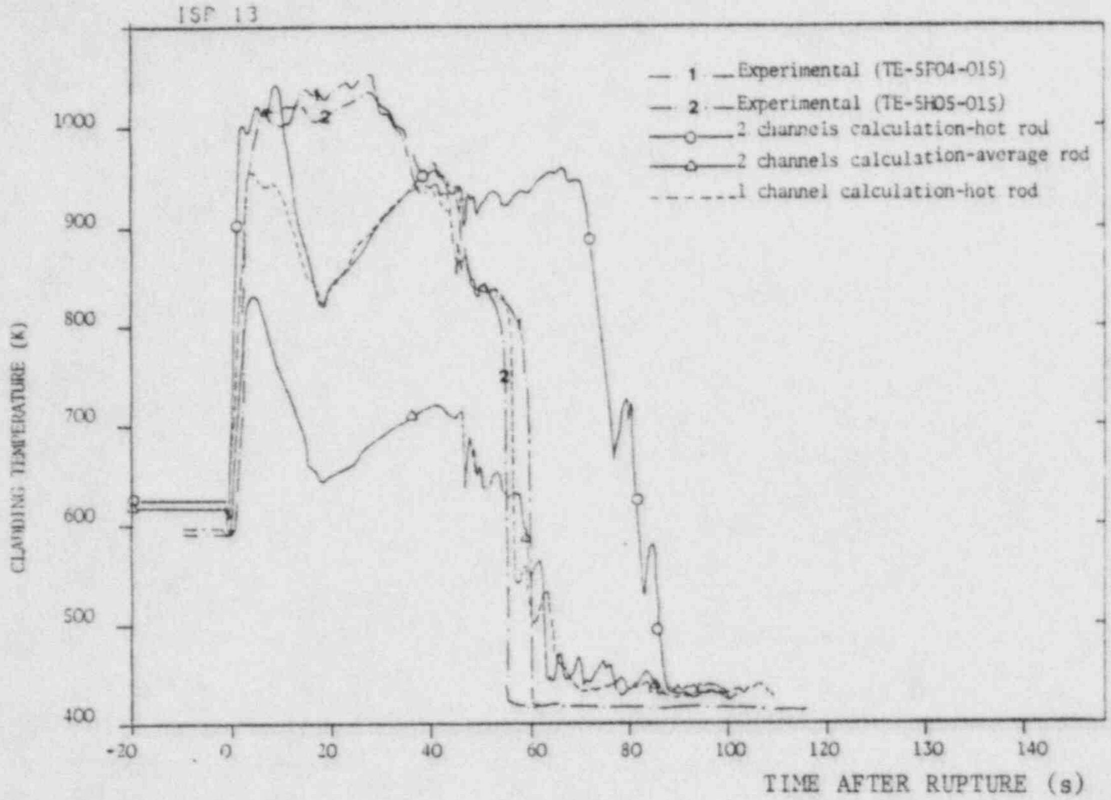

Fig. I.7 - Cladding temperature behaviour at level 0,59 m.

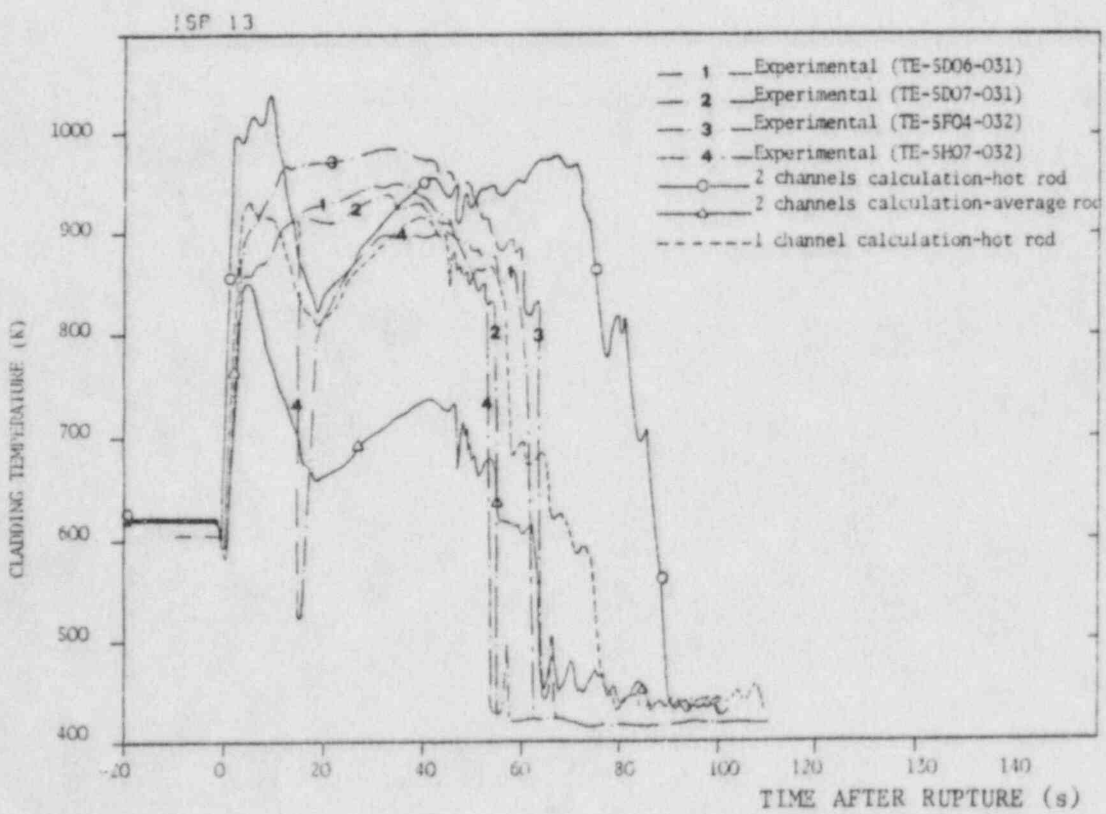

Fig. I.8 - Cladding temperature behaviour at level 0,75 m.

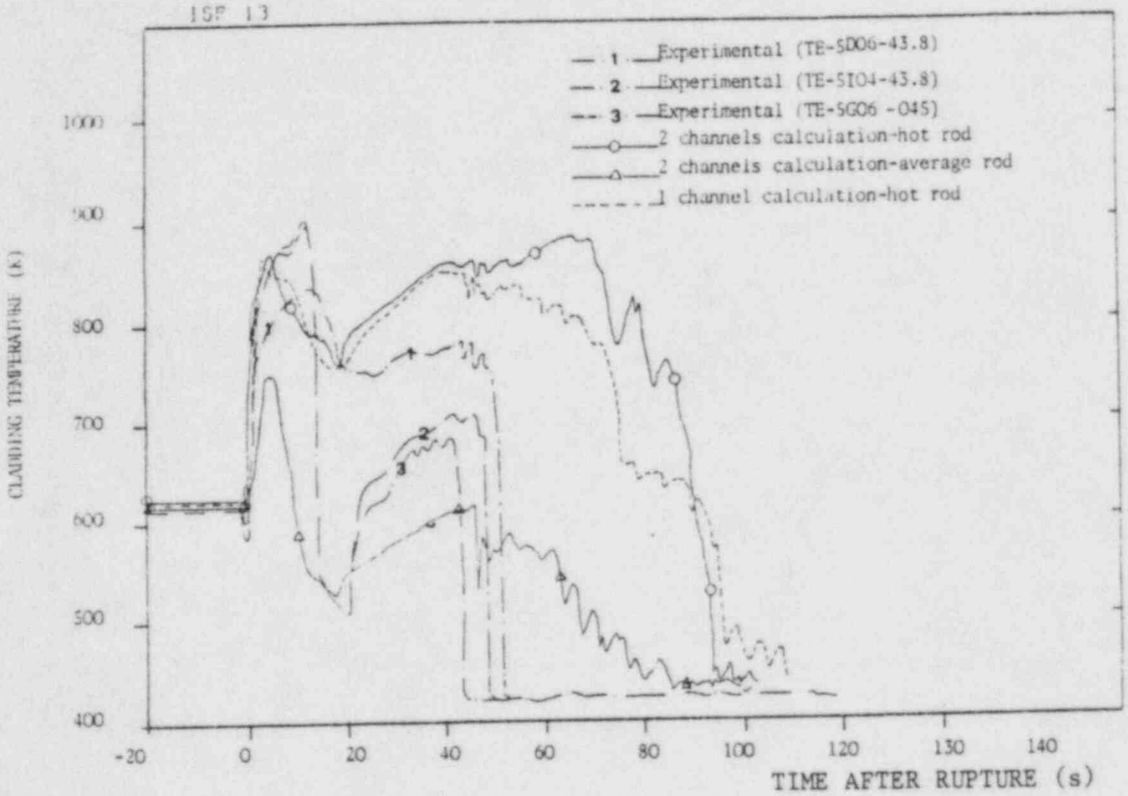

Fig. I.9 - Cladding temperature behaviour at level 1,09 m.

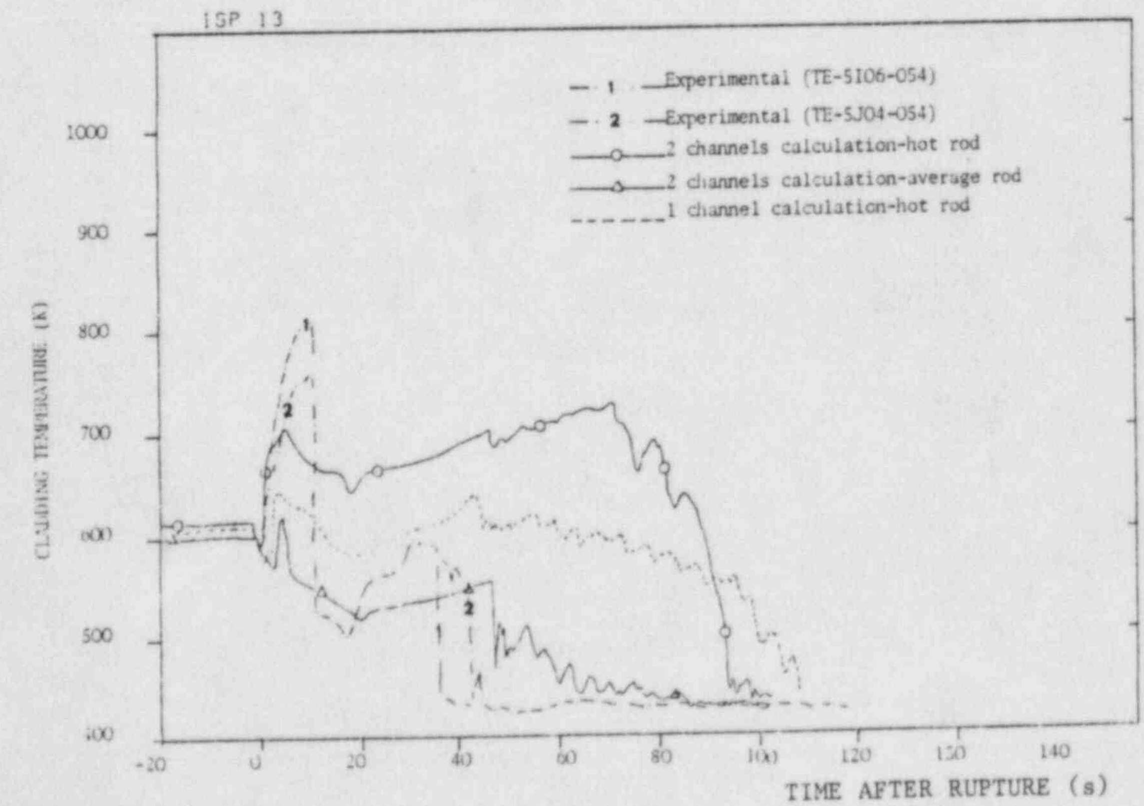

Fig. I.10 - Cladding temperature behaviour at level, 1,42 m.

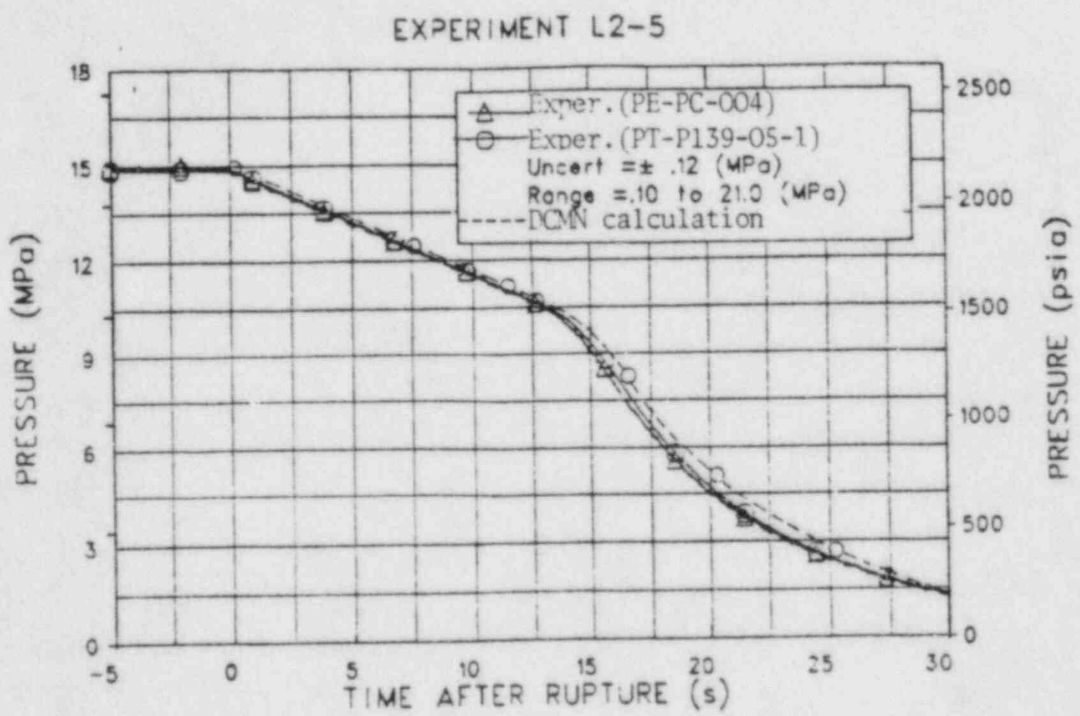

a) 1 CHANNEL NODALIZATION

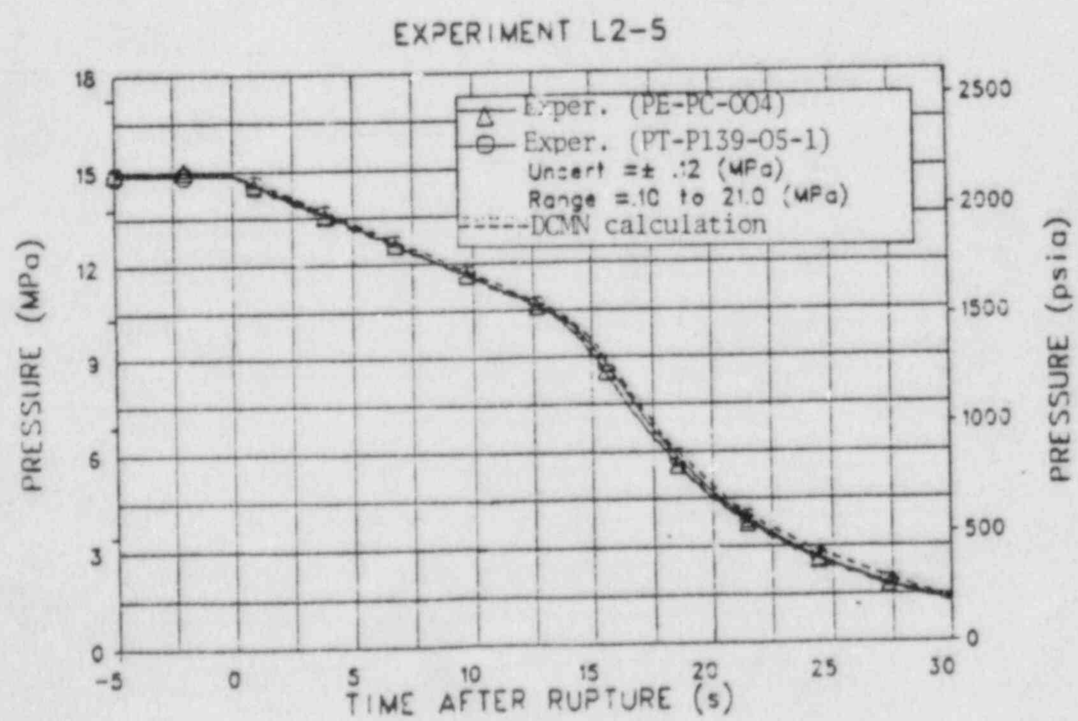

b) 2 CHANNELS NODALIZATION

Fig. I.11 - Pressure in the pressurizer

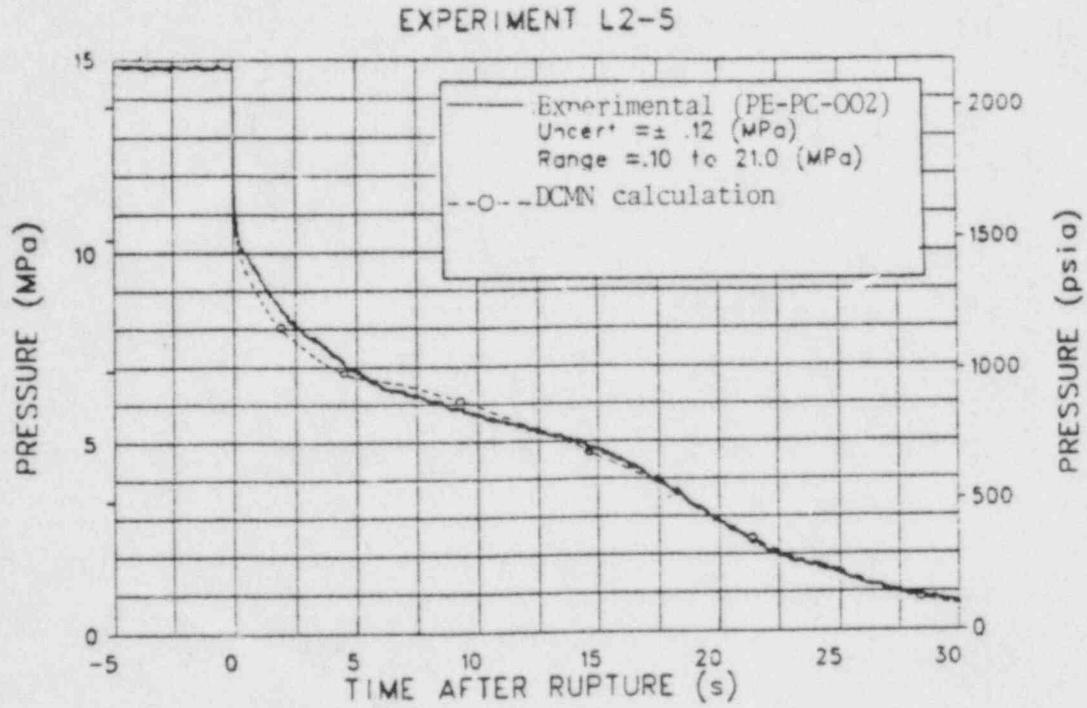

a) 1 CHANNEL NODALIZATION

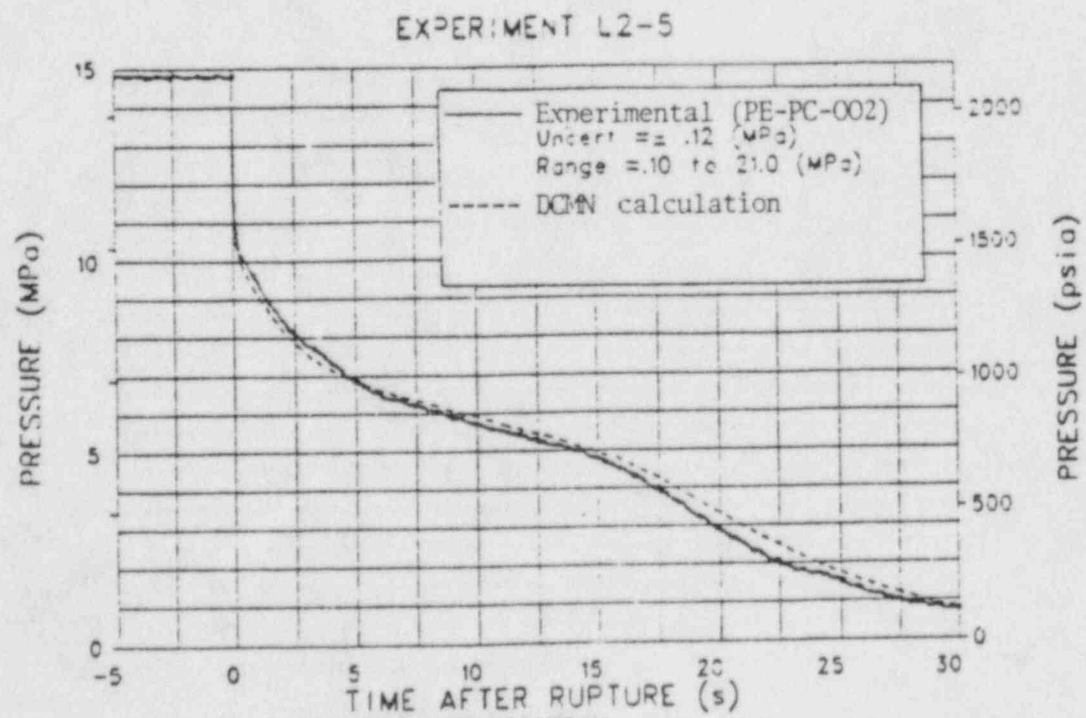

b) 2 CHANNELS NODALIZATION

Fig. I.12 - Pressure in intact loop hot leg

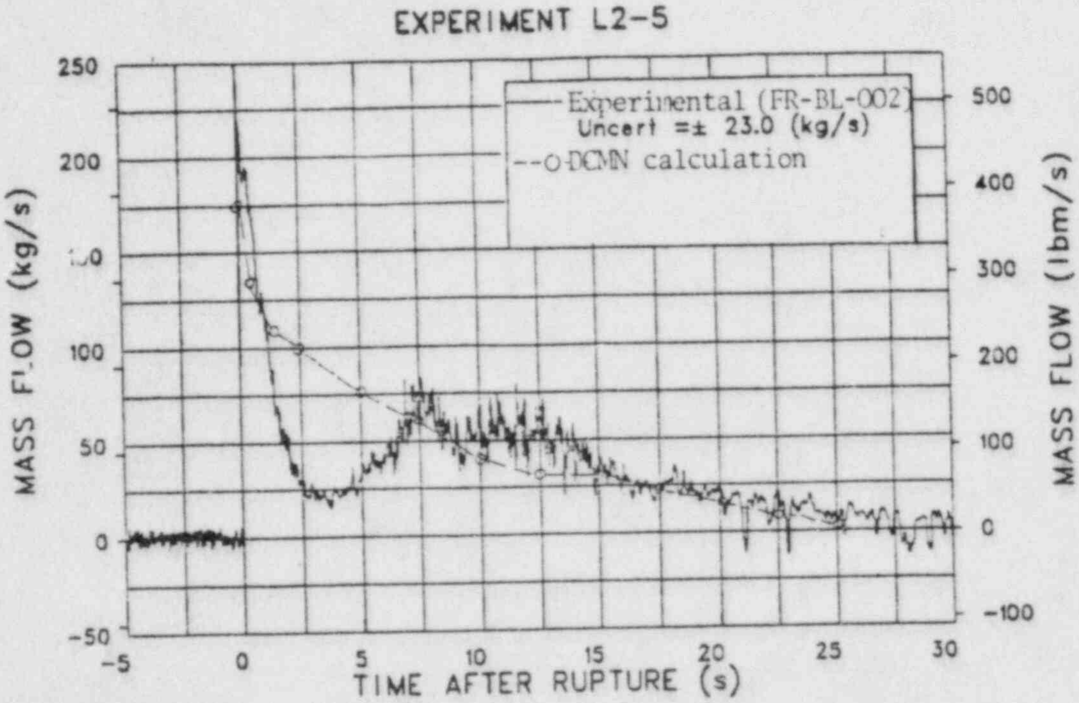

a) 1 CHANNEL NODALIZATION

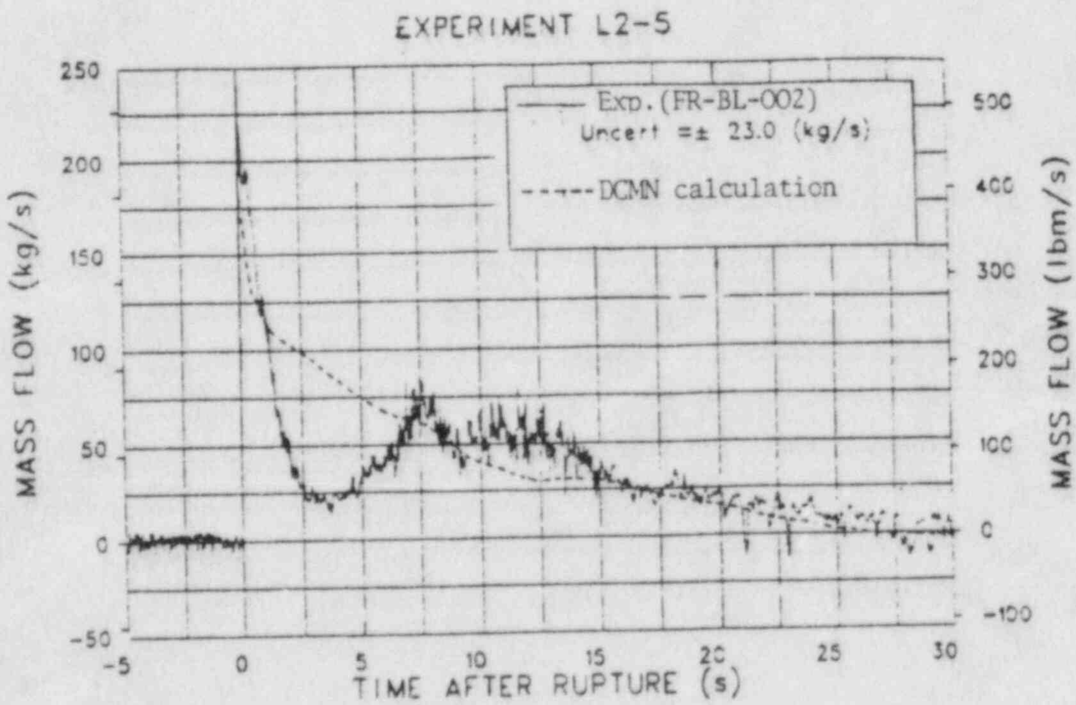

b) 2 CHANNELS NODALIZATION

Fig. I.13 - Mass flow-rate through break orifice in broken loop hot leg

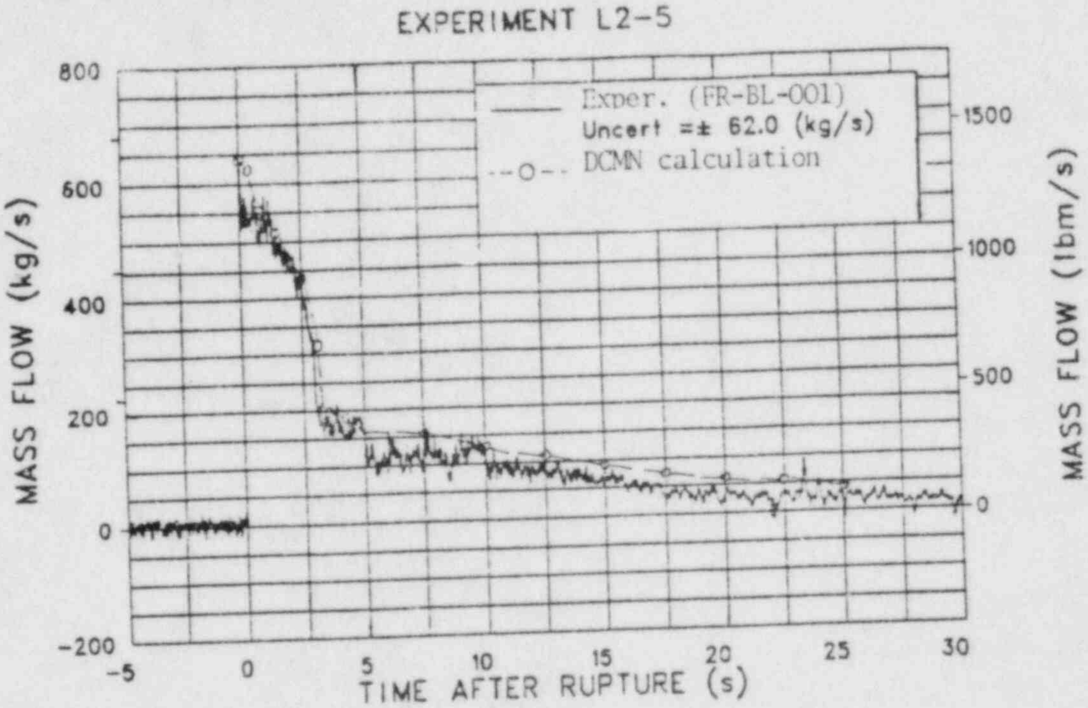

a) 1 CHANNEL NODALIZATION

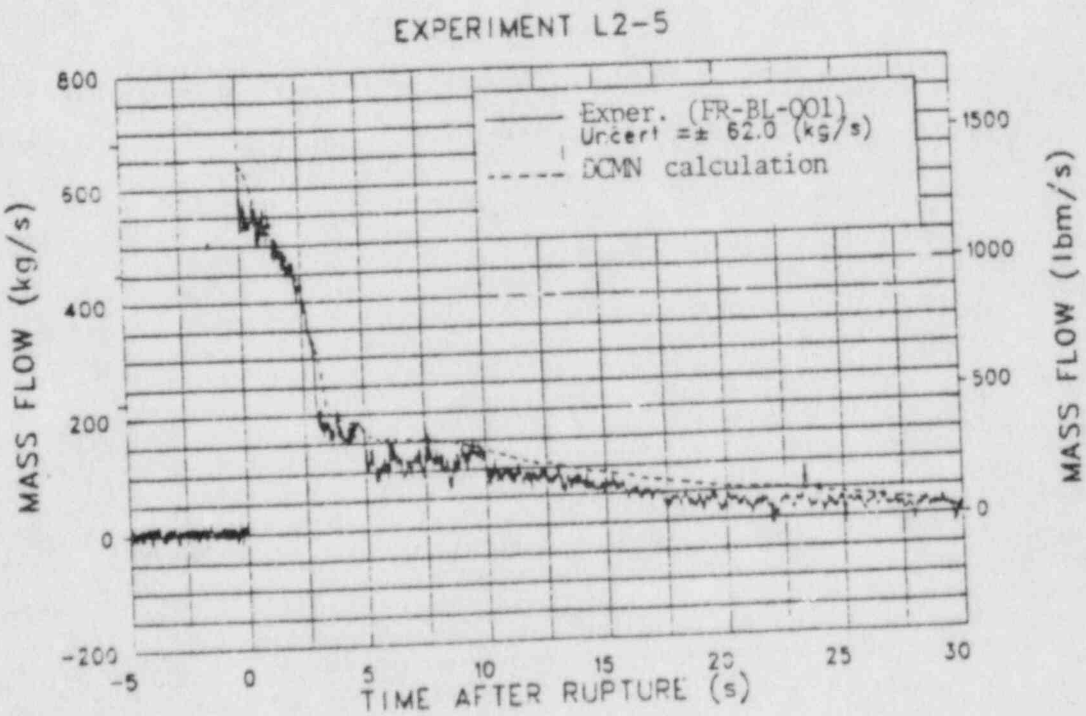

b) 2 CHANNELS NODALIZATION

Fig. I.14 - Mass flow-rate through break orifice in broken loop cold leg

APPENDIX J

ISP-13 SUBMITTAL FROM TECHNICAL RESEARCH CENTRE OF FINLAND USING RELAP5/MOD1 (VTT)

TECHNICAL RESEARCH CENTRE OF FINLAND
Nuclear Engineering Laboratory
P.O.Box 169, SF-00181 Helsinki 18
FINLAND

1984-01-03

FINNISH CONTRIBUTION TO THE NEA/CSNI INTERNATIONAL STANDARD PROBLEM 13 LOFT LARGE BREAK EXPERIMENT L2-5

APPENDIX J OF THE ISP13 FINAL COMPARISON REPORT

H. Holmström
V. Yrjölä

NEA/CSNI ISP 13 (LOFT TEST L2-5) - FINNISH CALCULATIONS

1. INTRODUCTION

The calculations have been carried out using the RELAP5/MOD1/Cycle 19 computer program. A FIDRAG smoothing update (by Chow) has been added. This modification smooths the calculation of the interfacial drag when the flow patterns change.

The computer code characteristics are summarized in Table J-1.

The nodalization of the whole system consisted of 83 volumes, 101 junctions and 78 heat structures.

The average CPU/real time ratio for the calculation of the LOFT experiment L2-5 to 60 seconds was 107 with VTT's non-LCM CDC Cyber 173 computer.

2. MODELLING THE FACILITY

The nodalization used for the calculation was based on an earlier nodalization for ISP11 (LOFT L3-6). However, a number of important changes were made. A new steam generator model was applied. The models for the reactor vessel and the broken loop were made more detailed. The inlet annulus and downcomer were split into two parallel flow paths with branch components and cross flow junctions. The core was modeled using two parallel six-volume channels (average- and hot channel) with branches and cross flow junctions. The hot channels represented the center fuel assembly.

The final nodalization diagram is shown in Figure J-1. Descriptions of the components and heat slabs are given in Tables J-2 and J-3.

In addition to those discussed above the following features of the nodalization may be worth listing:

1) Both of the primary coolant pumps are represented by one pump in the model.

2) The 0.25 in filler gap (second downcomer) in the reactor is modeled.

3) The walls of the steam generator, pressurizer, main primary piping and reactor vessel are modeled by heat slabs with ambient heat losses.

4) Tees are normally modeled by one dimensional branching (exceptions: ECC injection, reactor vessel inlet)

5) No leaks in the reflood assist bypass valve or the main steam control valve are modeled. Leak from the inlet annulus of the reactor vessel to upper plenum is modeled.

The core bypass flow rates were set as follows:

1) Lower plenum to upper plenum 4.5 % of the total primary loop flow.

2) Inlet annulus to upper plenum 3.4 % of the total primary loop flow.

At the break junctions the two velocity option and a discharge coefficient of 0.84 for both the subcooled and saturated critical flow regimes was used.

The pump speed was given in a table as a function of time (measured data).

The following heat transfer coefficients between the walls and the environment (T = 311 K) were applied:

1) pressurizer: 0.0 (insulated)
2) steam generator wall: 13.0 W/m^2K
3) other: 12.0 W/mK

3. INITIALIZATION AND CALCULATIONS

A rather satisfactory steady state compared to the measured initial conditions was achieved. An exception was the secondary side pressure, which was clearly lower than measured. Some of the main initial conditions for the transient calculation were as follows.

1) Pressurizer pressure = 14.9 MPa
2) Secondary side pressure = 5.5 MPa
3) Core power = 36 MW
4) Total primary loop flow = 195.15 kg/s
5) Pump speed = 134.7 rad/s
6) Pressure difference across pump = 72 kPa
7) - " - reactor vessel = 27 kPa
8) - " - steam generator = 36 kPa
9) Secondary side steam flow rate = 19.0 kg/s

The calculated sequence of events was the following:

1) L2-5 initiation at 0.0 s
2) Fist voiding in the core occured at 0.06 s
3) Reactor scram at 0.1 s
4) Cladding temperature rise began at about 0.5 s
5) Primary coolant pump trip at 0.94 s
6) Subcooled cold leg break flow ended at about 4 s
7) Pressurizer emptied at about 15 s
8) Accumulator injection initiated at 16.3 s
9) HPIS injection initiated at 24.0 s

10) Maximum cladding temperature reached at 5.2 s

11) LPIS injection initiated at 37.2 s

12) Accumulator did not empty before 60 s

13) Core cladding did not quench before 60 s

Compared to the data, e.g. the following may be observed. The pressurizer was calculated to empty clearly too fast (Figure 27). The system pressure prediction in Figures 28 trough 31 (except in the secondary side, Figure 32), however, was quite good, although the hot leg break flow rate in Figure 45 was severily overpredicted for the first 7 seconds. Accumulator flow was underpredicted due to the too high pressure loss of the accumulator line. The density calculations in Figures 40 and 41 were rather satisfactory, although some problems exist, particularly concerning the intact loop cold leg in Figure 39 (accumulator flow!) and the broken loop hot leg in Figure 42 (density increase between 5 and 16 seconds, which no code could predict). The slug flow behaviour in the intact loop cold leg was impossible to simulate with the coarse nodalization used in the calculation. The fluid temperature increase in the upper plenum and hot leg in Figures 33 and 36 at about 30 seconds was not predicted. The calculated peak cladding temperature in Figure 51 was close to the measured value, but after reaching the peak the cooling was overpredicted, probably due to excessive entrainment of water in the steam.

The RELAP5/MOD1 code ran well, but all the results of the calculation were not satisfactory. One of the main problems is the need for a large number of nodes in order to model phase separation accurately enough (liquid level). Another major source of problems is the heat transfer package of the computer code.

One additional calculation was done with minor changes in the discharge coefficient, the pressure loss coefficients of the accumulator line and the core cross flow and heat losses to the environment. However, the results did not change much.

A sensitivity study of the fluid density and the flow rate in the broken loop hot leg was also performed by varying the initial temperature distribution along the loop. The RELAP5/MOD1 code had a strong tendency to smooth the fluid conditions between hydrodynamic volumes. So the initial temperature distribution disappeared soon and it was impossible to achieve the same kind of shape for the break flow rate curve as was measured.

Table J-1: Computer Code Characteristics

Name and version of the computer code	RELAP5/MOD1/CYCLE19
Changes in the computer code not included in the basic code description	FIDRAG smoothing update (by Chow) for the calculation of the interfacial drag
Classification of the hydrodynamic model	A two-fluid, five equation model for two-phase flow
Critical flow model	RELAP5 standard model (A choking model by Ransom and Trapp)
Interphase drag model	RELAP5 standard model with FIDRAG smoothing update by Chow
Wall friction model	RELAP5 standard model (HTFS modification of the Baroczy two-phase friction multiplier modification of correlation)
Flashing/Condensation model	RELAP5/MOD1 standard model-no superheat is required for flashing (Vaporization model, condensation model and nucleation criterion)
Heat transfer models	RELAP5 standard model: (from RELAP4/MOD6 package) Forced convection heat transfer: Dittus-Boelter Saturated Nucleate Boiling: Chen Subcooled Nucleate Boiling: Modified Chen High flow transition boiling: Modified Condie-Bengston High flow film boiling Condie-Benston Low Flow Post-CHF Transition and Film boiling Condensation
CHF-correlation	RELAP5 standard correlations: High Flow Subcooled CHF Correlation: Tong High Flow Saturated CHF Correlation: Hsu and Beckner Low flow CHF Correlation: Modified Zuber

Table J-2. Description of the components

Components	Description
100,106,108	Intact hot leg
110	Steam generator (without plenums)
111,112,114	Intact cold leg before pump
115	Pump
120,124,125	Intact cold leg after pump
200,204	Vessel inlet annulus
280,284	Vessel inlet annulus (broken loop side)
205,206,207	Intact loop side downcomer
285,286,287	Broken loop side downcomer
251,252	Filler gap (0.25 inches)
210	Lower plenum
215	Lower core support structure
221...226	Average core
291...296	Hot channel of core
228	Core bypass channel
230	Upper core support structure
235	Upper flow skirt region
245	Upper plenum
300,310	Broken loop hot leg from vessel to SG simulator
315	Steam generator-pump-simulator
370,380,375	Reflood assist bypass system
335,345,350	Broken loop cold leg
800,805	Suppression tank
330	Hot leg break junction
365	Cold leg break junction
415,420	Pressurizer
405	Pressurizer surge line valve
400	Pressurizer surge line
500,505,510,515,520,530	Secondary side
540	Steam control valve
550	Air-cooled condenser
536	Feed water tank
524	Feed water line
620	Accumulator vessel
600,630	Accumulator surge line
615,616	Borated water storage tanks for HPIS and LPIS
650	HPIS line
651	LPIS line

Table J-3. Description of the heat slabs

Heat slabs	Volumes	Description
100	100,E	Intact hot leg wall
112	112,E	Intact cold leg wall (before pump)
122	120,E	Intact cold leg wall (after pump)
305	315,E	Steam generator simulator wall
335	335,E	Broken loop cold leg wall
110	110,515	Steam generator tubes
500,510	500,505,510,515	Steam generator shroud
525	500,505,510,520,E	Steam generator wall
200,280	200,280,E	Top filler block in vessel
204,284	204,284,251	Middle filler blocks
205,285	205,206,207,210, 251,252,285,286, 287,282,E	Lower filler blocks
251,261	251,252,E	Vessel wall
210	210,E	Vessel bottom
216	215	Lower core support structure
201	200,204,205,206, 207	Core support barrel (intact loop side)
281	280,284,285,286, 287	Core support barrel (broken loop side)
215	215,221...226, 230,235	Flow skirt
221	221...226	Average core fuel rods
291	291...296	Core hot channel fuel rods
246	235	Fuel modules
230	230	Upper core support structure
240	245	Upper plenum internals
243	245	Upper plenum top plate
245	245	Upper plenum core support barrel
415	415,420	Pressurizer wall

Note! E = Environment

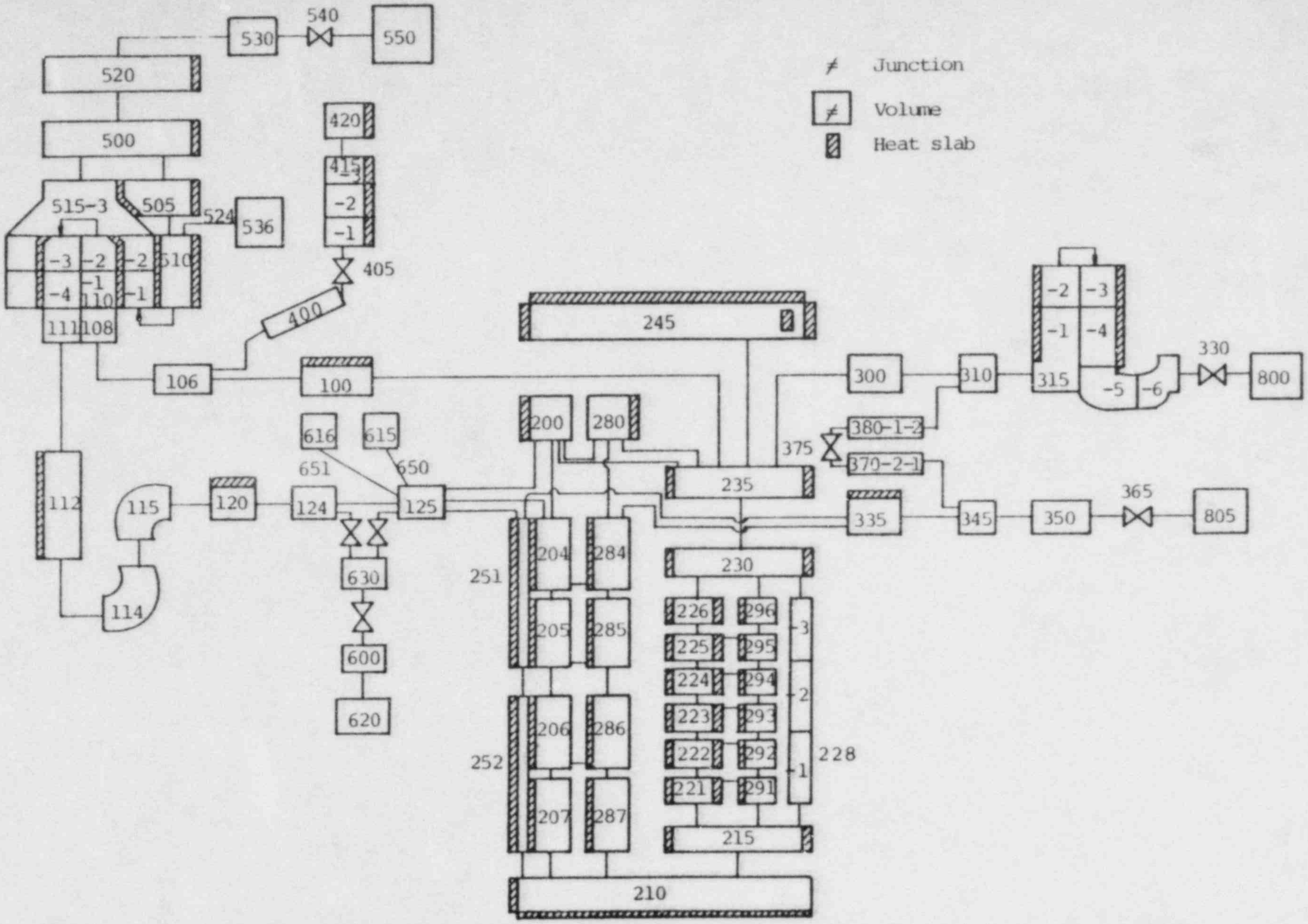

Figure J-1. RELAP5/MOD1/CY19-LOFT nodalization for the Finnish ISP13 calculations

APPENDIX K

ISP-13 SUBMITTAL FROM ATOMIC ENERGY ESTABLISHMENT, WINFRITH USING TRAC-PD2

APPENDIX K

ISP-13 SUBMITTAL FROM ATOMIC ENERGY ESTABLISHMENT, WINFRITH USING TRAC-PD2

The submittal from AEEW was not included in the data comparison section because it was not received in time. The submittal was reported to the participants at the July 1983 workshop and is included here for information purposes.

APPENDIX K

AEEW CALCULATIONS OF L2-5 USING TRAC-PD2

I BRITTAIN

1. INTRODUCTION

The LANL calculations for L2-5 submitted for the ISP13 comparison exercise were carried out using a version of TRAC-PD2 different from the released version. The calculations have been repeated at Winfrith using the LANL data deck and the standard released version of TRAC-PD2. This note compares the two sets of calculations.

The standard version of TRAC-PD2 will be referred to as MOD1, and the LANL version as MOD1*.

2. NODALISATION

The nodalisation used is shown in Figures 1-4. It will be seen that the reactor vessel is modelled in 3D using a total of 192 fluid cells. A complete listing of the input data is also given.

3. DIFFERENCES IN TRAC CODE AND MODEL

The significant changes in MOD1* were as follows:

(a) The condensation model was changed in such a way that condensation rates were significantly lower.

(b) The accumulator phase separation model was altered to improve mass conservation.

(c) Control system logic was incorporated to allow greater flexibility in valve operation.

The Winfrith version also included a (different) modification in the accumulator model. In the event the required mass discharge was obtained by manual intervention on restart. The steam generator secondary side valves were also controlled "manually" in the Winfrith runs. This gave a different secondary side transient to that obtained by LANL, but it is believed that this has a negligible effect on the primary side transient.

The only input data difference appears to be that the RABV flow was reduced to 1½% in the LANL model, whereas the earlier Winfrith deck modelled the total core by-pass of ~6% through the RABV.

4. RESULTS OF CALCULATIONS

Figures 5 and 6 show the intact loop cold leg densities. It can be seen that the MOD1 oscillations start at about 30 seconds, whereas in MOD1* they are delayed to ~38 seconds. The experimental data support the MOD1 results, thus suggesting that the condensation model in MOD1 is better than that in MOD1*.

Figure 7 shows the vessel liquid mass. The difference between MOD1 and MOD1* is clearly visible during accumulator injection, with the increased condensation of MOD1 giving increased oscillations and a slower average refill. However these differences are essentially lost at later stages. From 50 to 60 seconds it can be seen that the two calculations are giving oscillations of the same frequency, but different amplitudes.

Figure 8 shows the core liquid fraction predicted by MOD1, while Figure 9 shows the response of an in-core SPND. It is seen that the SPND results give qualitative support for the TRAC calculations.

Figure 10 shows the downcomer liquid fractions, showing minor differences, but overall agreement.

Figures 11 and 12 show the peak clad temperatures on two of the rods. It is seen that the two code versions are in general agreement. The major difference seen during blowdown, where MOD1* predicts a period of cooling not seen in MOD1, is believed to be due to the difference in the RABV flows. The lower flow used in MOD1* gives clad temperature behaviour closer to that seen experimentally.

5. COMPARISON WITH EXPERIMENT

This Appendix concentrates on the differences between the standard version of TRAC-PD2/MOD1 and the version used at LANL. For a more detailed discussion of the comparison with experiment the reader is referred to the LANL contribution. In general, the conclusions of the Winfrith study are in agreement with those of LANL.

6. PROBLEMS IN RUNNING THE CODE

No significant problems were encountered in performing the calculation.

AEE
WINFRITH
JUNE 1984

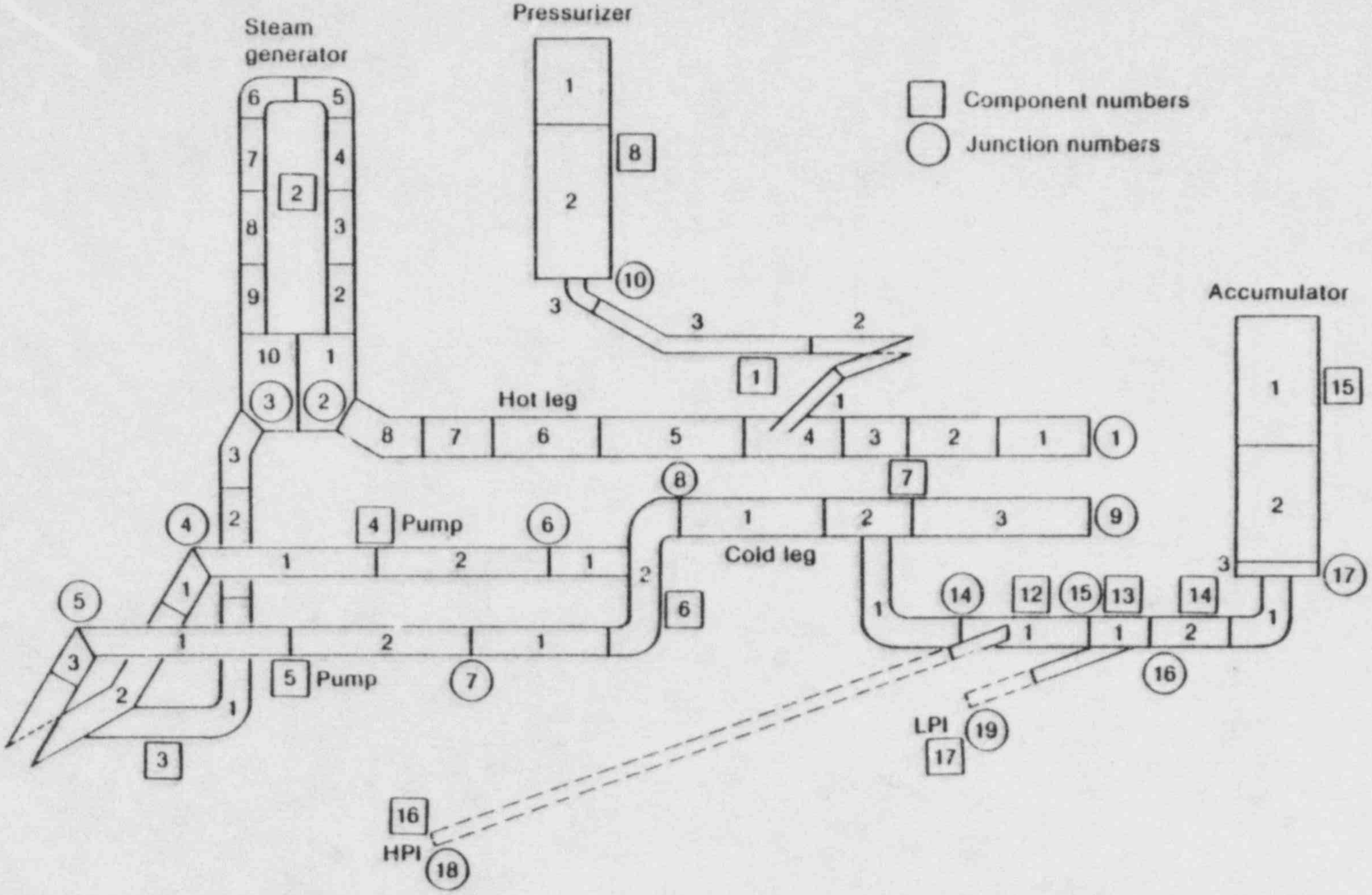

Figure 1. Intact Loop Nodalization

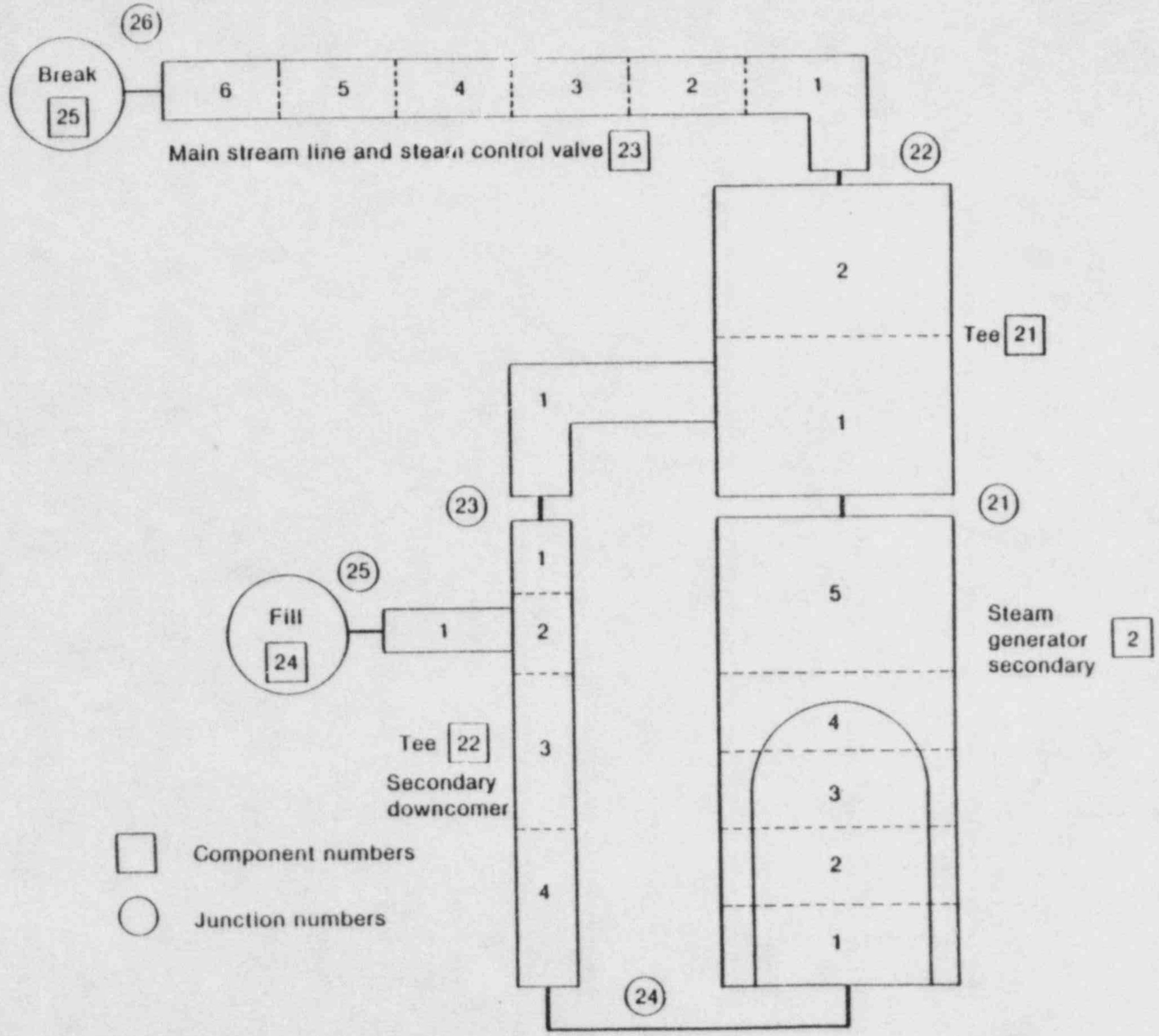

Figure 2. Steam Generator Secondary Nodalization

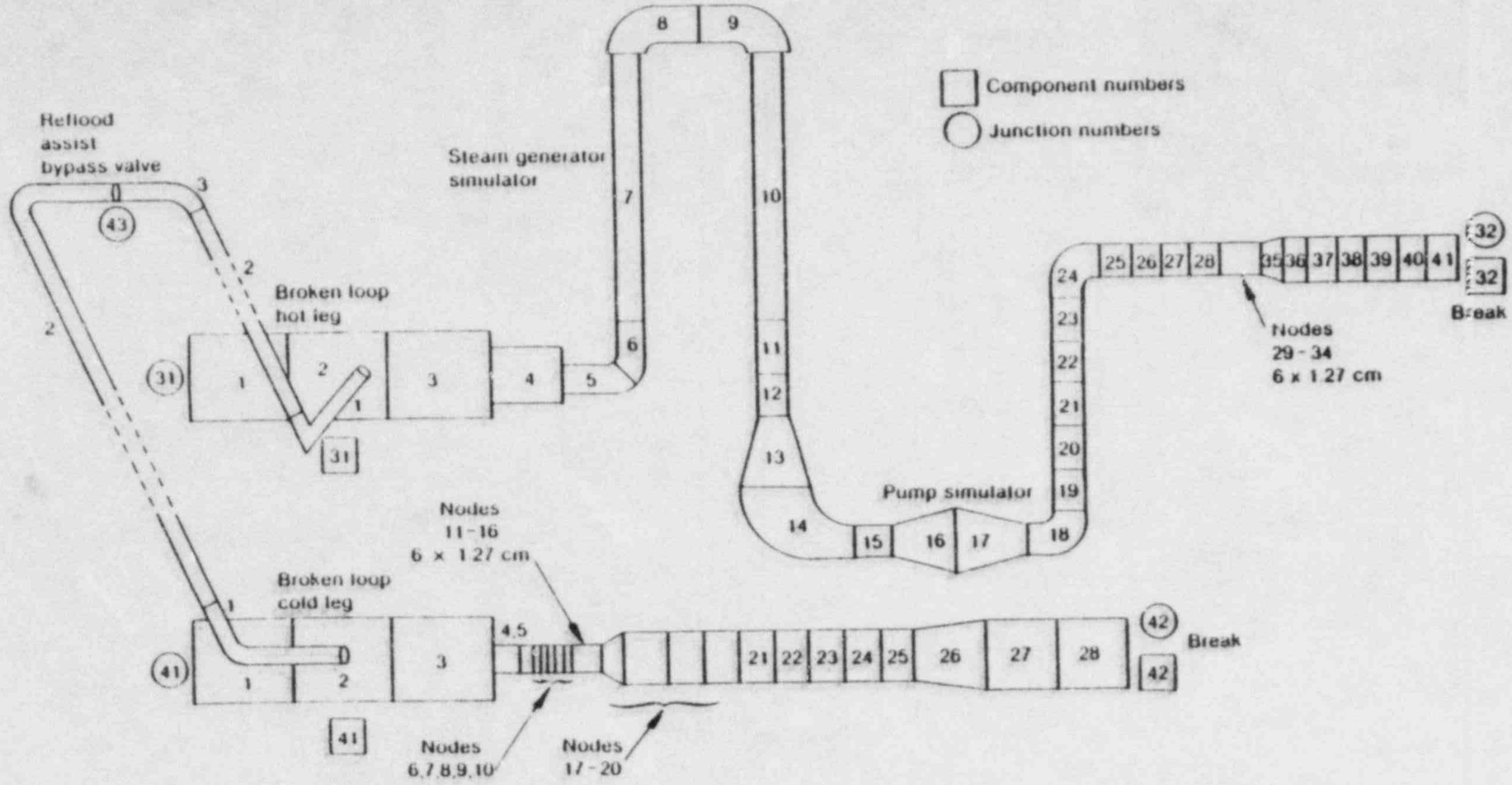

Figure 3. Broken Loop Nodalization

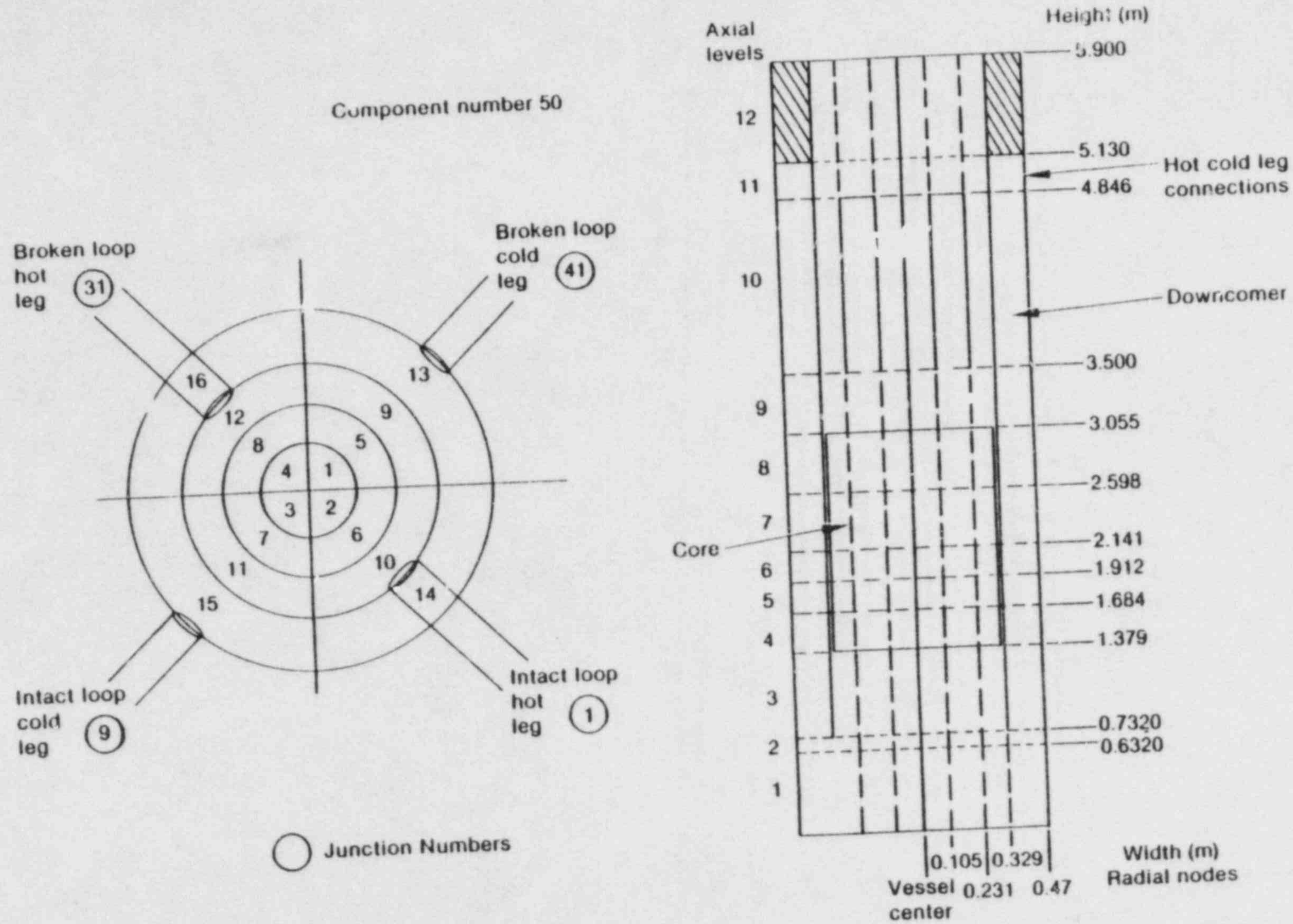

Figure 4. Reactor Vessel Nodalization

L2-5 UN TRAL PD2/MOD1

THE FOLLOWING ARE PLOTTED AGAINST REACTOR TIME

MIXTURE DENSITY

KEY			
SYMBOL	LOCATION	MNEMONIC	DATA FILE
—	7/ 0/ 1	DNMP	1
MIXTURE DENSITY		,KG/M**3	

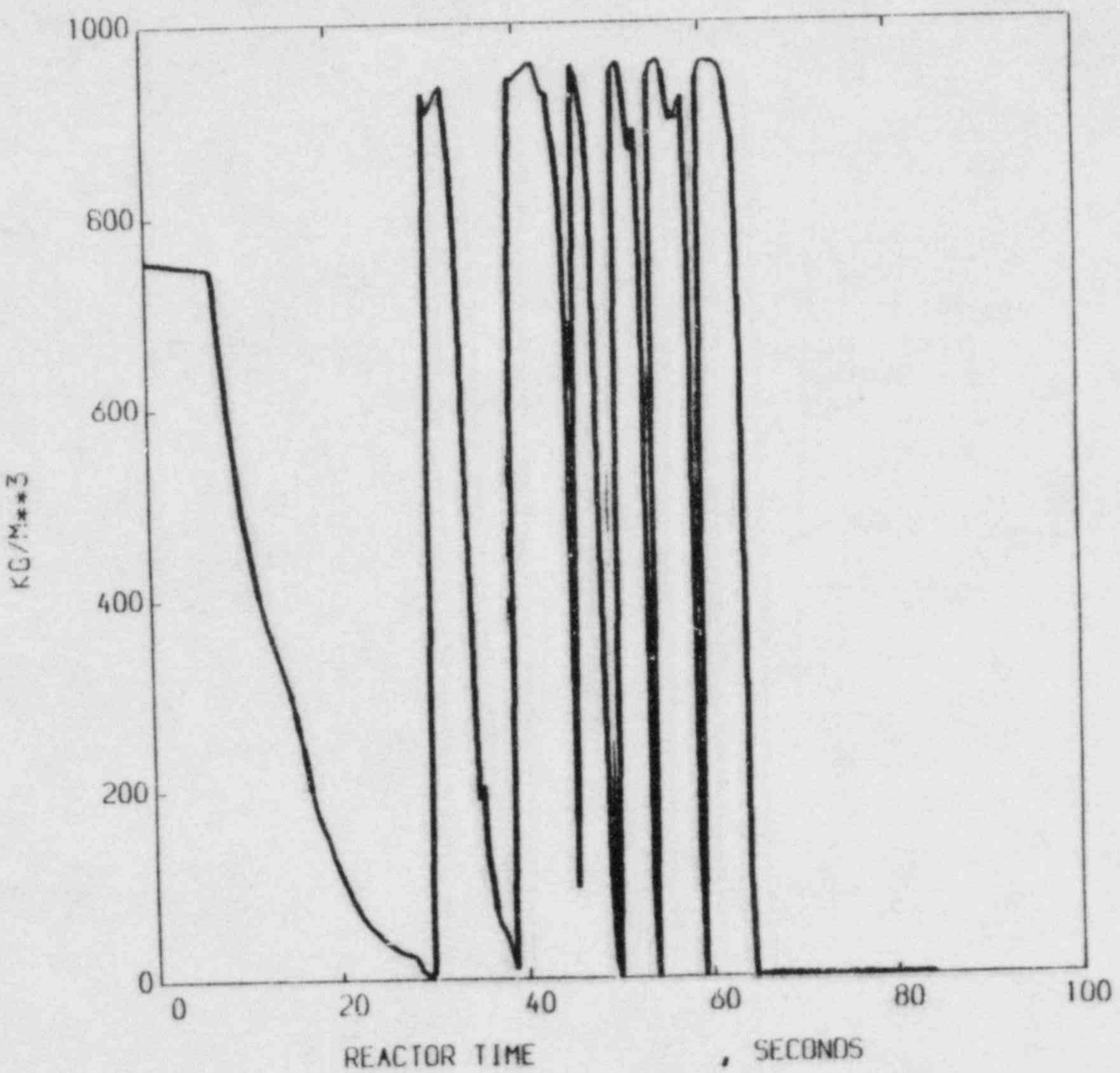

FIG 5

FIGURE 6

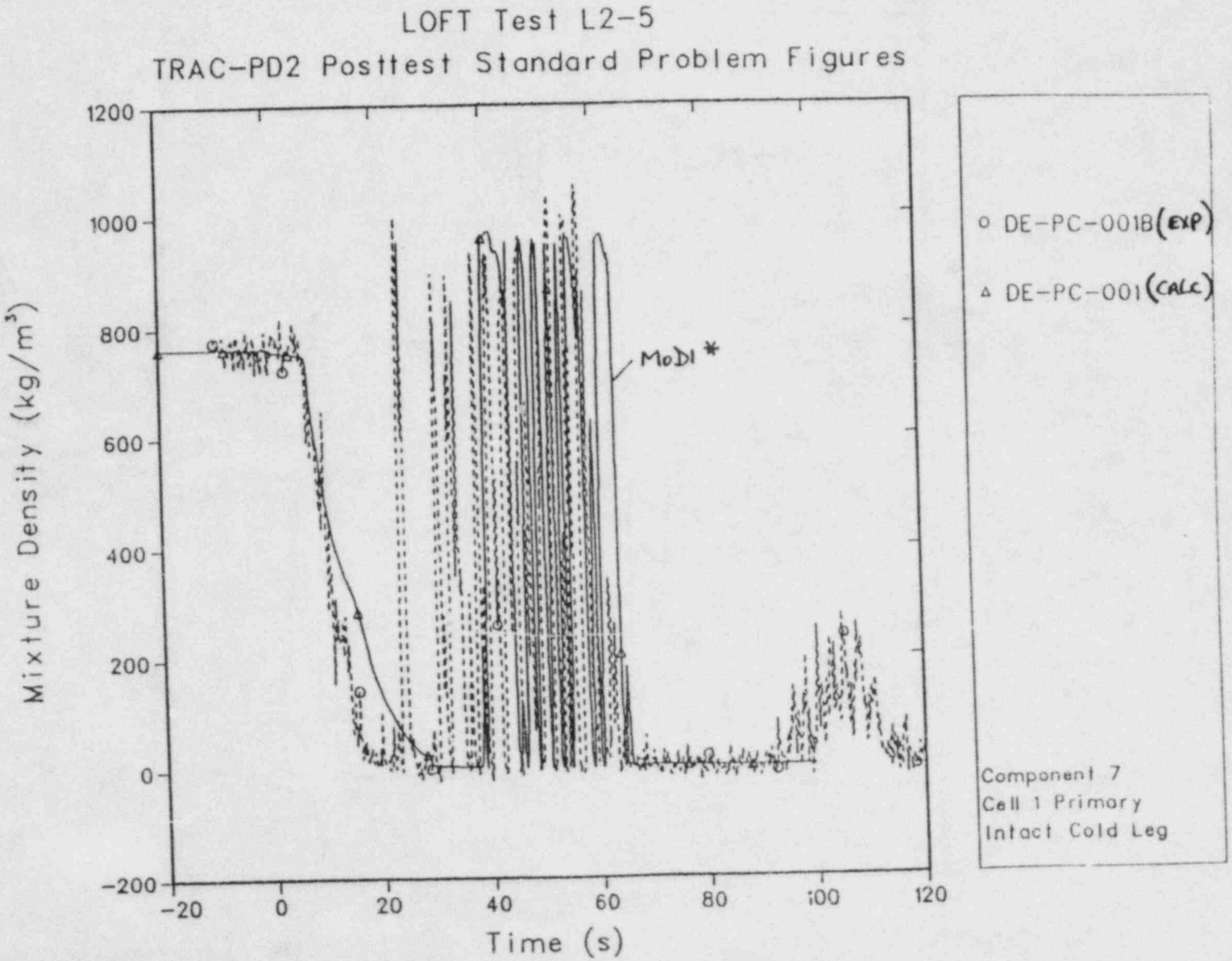

LOFT Test L2-5
TRAC-PD2 Posttest Standard Problem Figures
Mixture Density (kg/m³)
Time (s)
1200
1000
800
600
400
200
0
-200
-20
0
20
40
60
80
100
120
MoDI *
○ DE-PC-001B(EXP)
△ DE-PC-001(CALC)
Component 7
Cell 1 Primary
Intact Cold Leg

L2-5 VESSEL LIQUID MASS

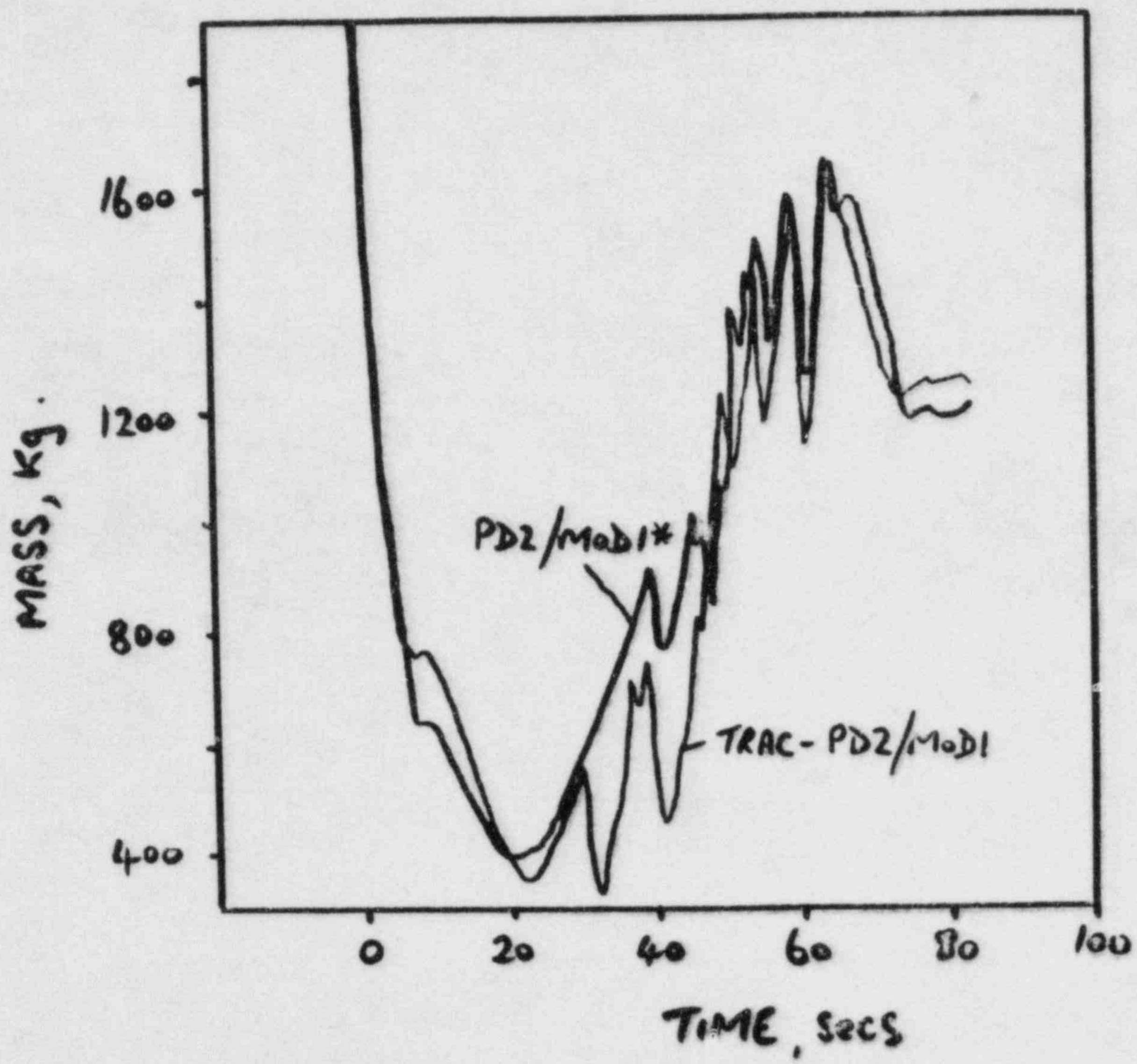

FIG 7

L2-5 ON TRAC PD2/MOD1

THE FOLLOWING ARE PLOTTED AGAINST REACTOR TIME

CORE LIQ VOL FRAC

KEY			
SYMBOL	LOCATION	MNEM UNIC	DATA FILE
——	50/ 0/ 1	LFCO	1
CORE LIQ VOL FRAC			

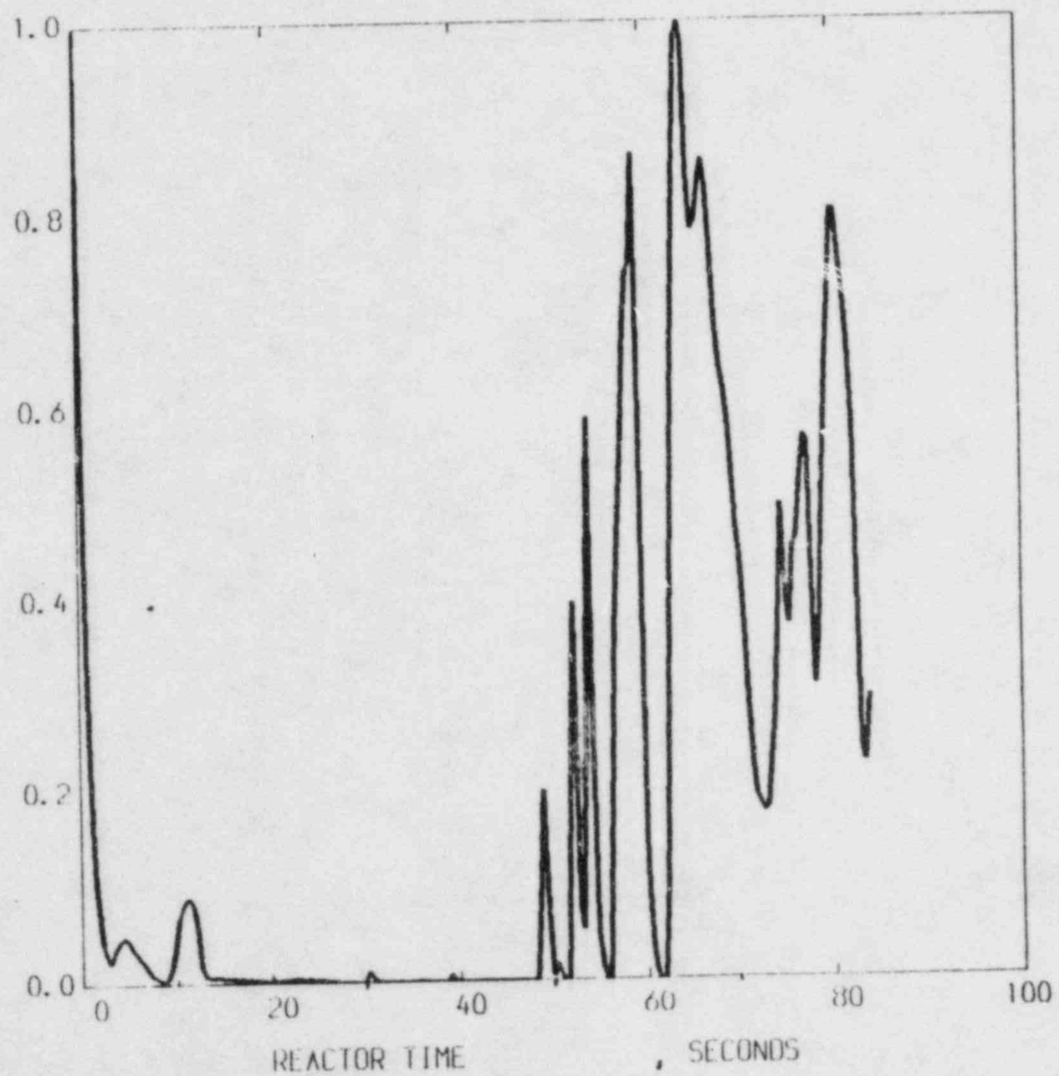

FIG 8

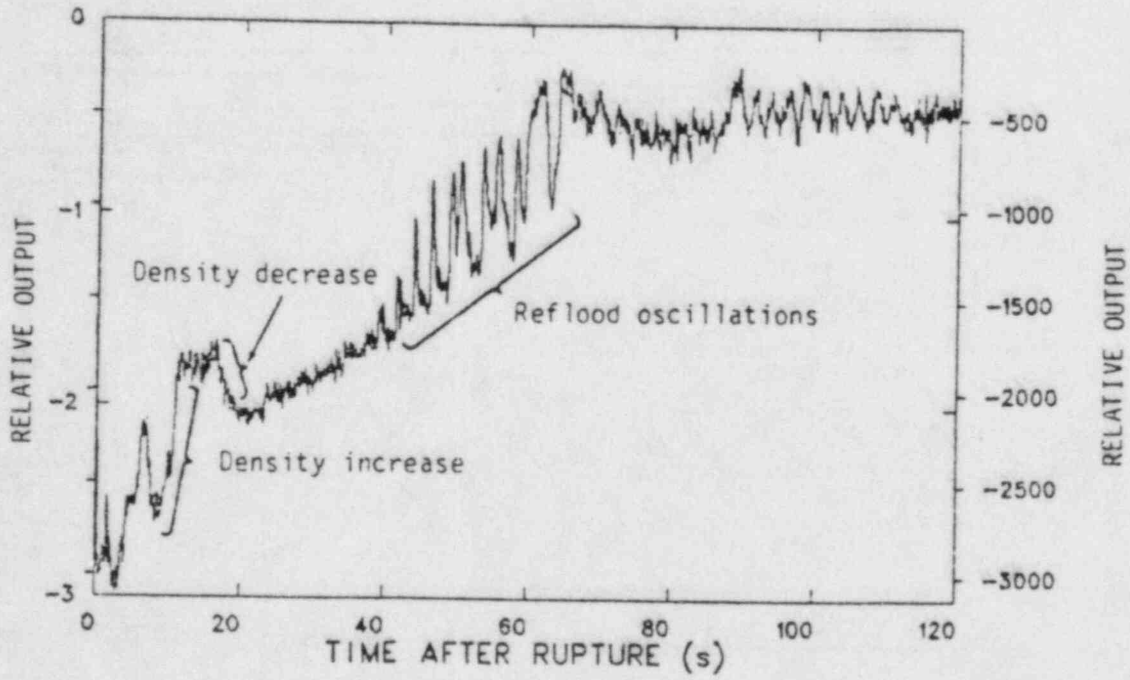

FIGURE 9

RESPONSE OF SPND IN A PERIPHERAL FUEL ASSEMBLY FOR EXPERIMENT L2-5

COMPARISON OF TRAC RESULTS: THICK CURVE AEEW , DASH CURVE LANL

THE FOLLOWING ARE PLOTTED AGAINST REACTOR TIME

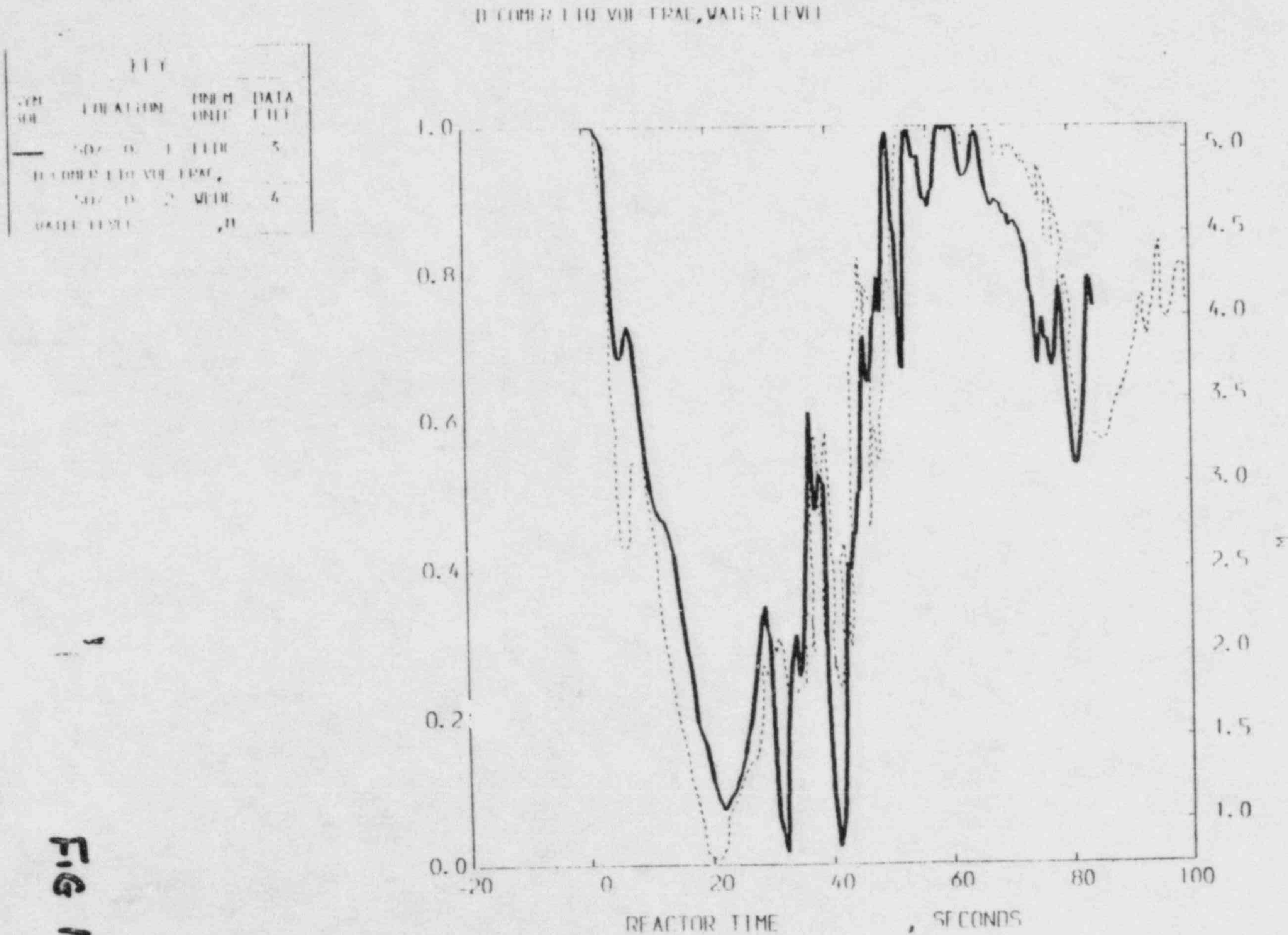

FIG 10

COMPARISON OF TRAC RESULTS: THICK CURVE=AEEW , DASH CURVE=LANL

THE FOLLOWING ARE PLOTTED AGAINST REACTOR TIME

CLADDING TEMP - FINE, CLADDING TEMPERATURE

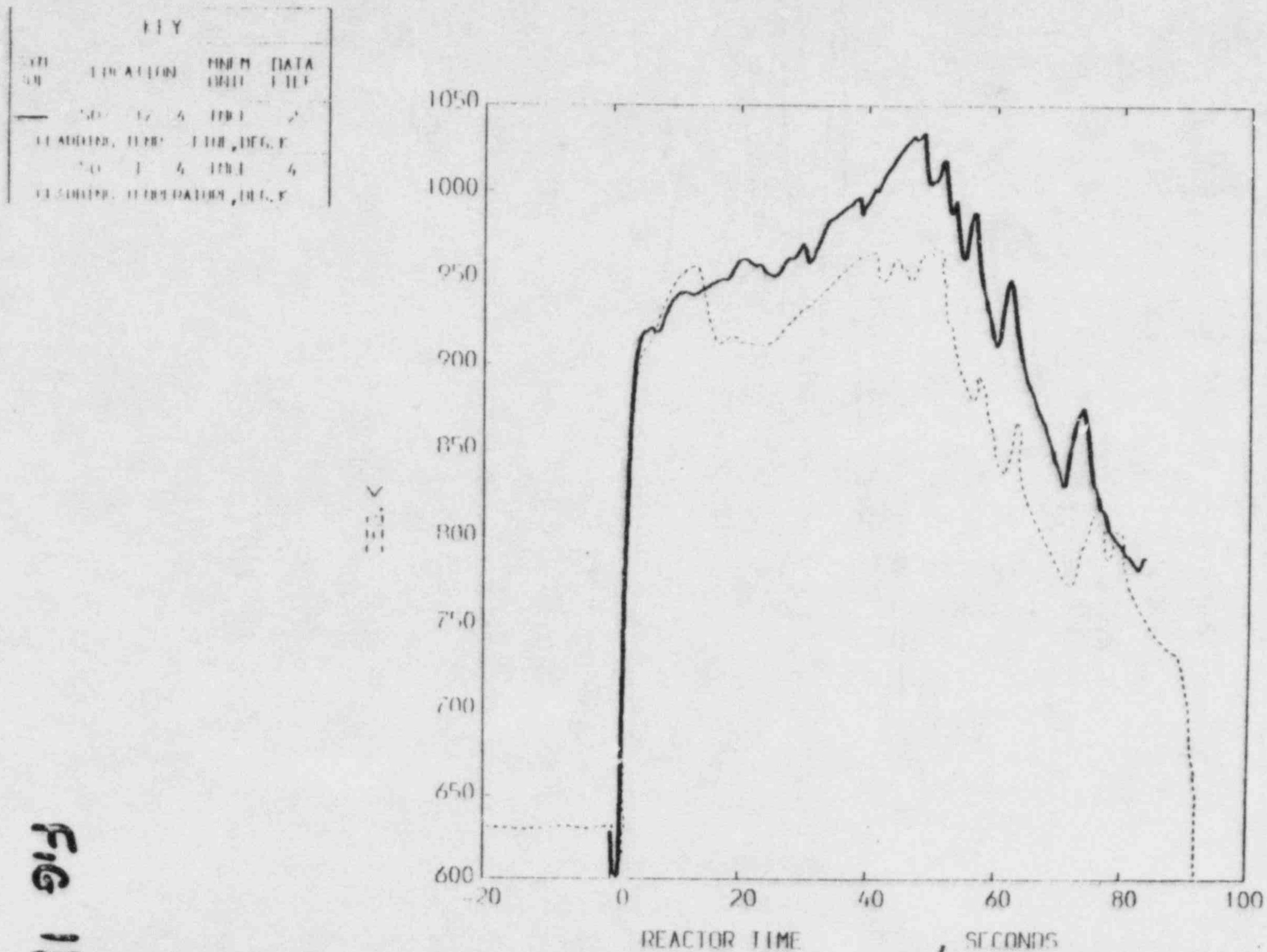

FIG 11

COMPARISON OF TRAC RESULTS: THICK CURVE-ALEW , DASH CURVE=LANL

THE FOLLOWING ARE PLOTTED AGAINST REACTOR TIME

CLADDING TEMP -FINE,CLADDING TEMPERATURE

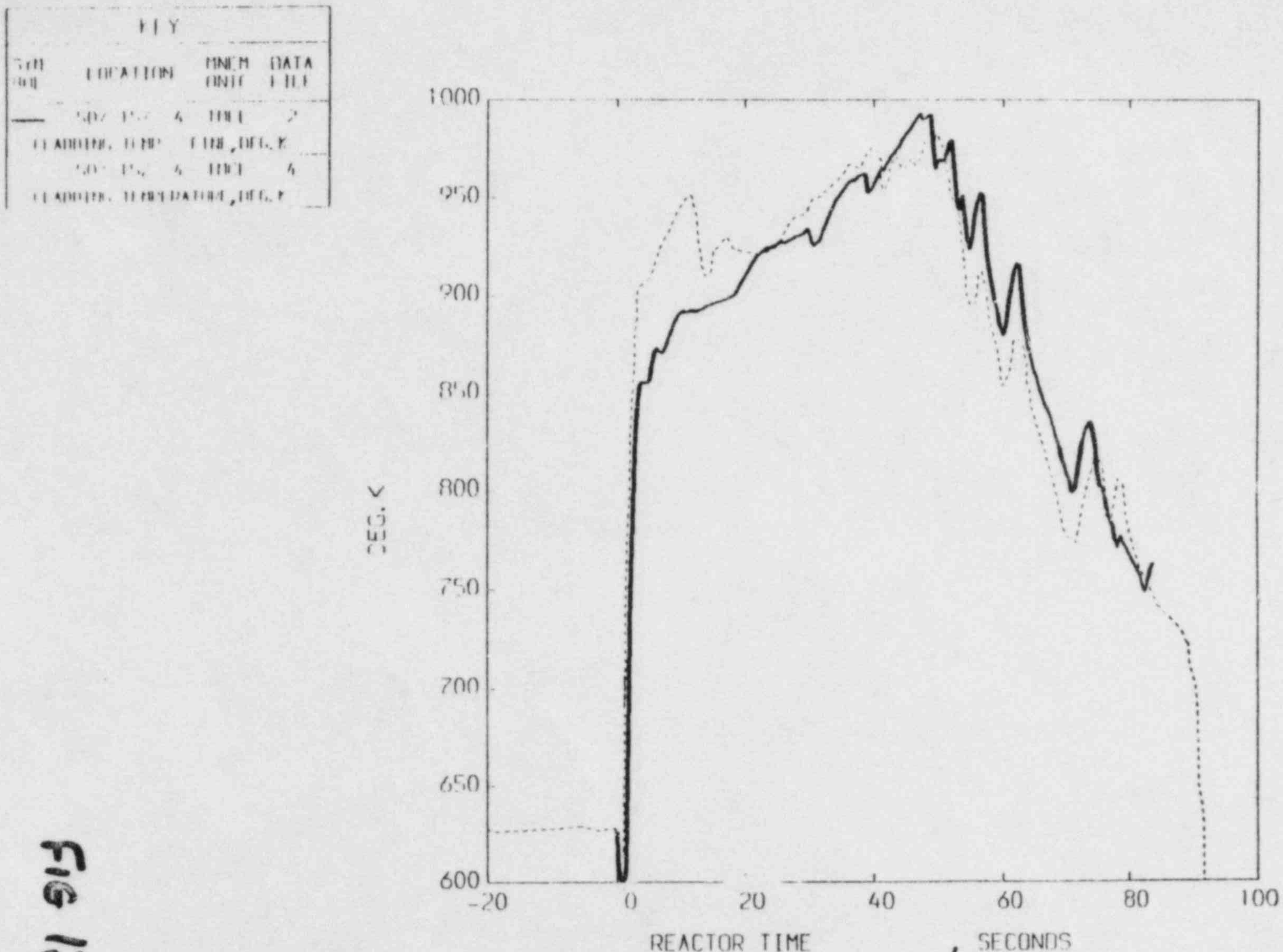

FIG 12

APPENDIX L

ISP-13 SUBMITTAL FROM COMMISARIAT A L'ENERGIE ATOMIQUE
USING RELAP4/MOD6 (CEA)

APPENDIX L

ISP-13 SUBMITTAL FROM COMMISARIAT A L'ENERGIE ATOMIQUE USING RELAP4/MOD6 (CEA)

No appendix documentation was received.

NRC FORM 335 (2-84) NRCM 1102, 3201, 3202

U.S. NUCLEAR REGULATORY COMMISSION

BIBLIOGRAPHIC DATA SHEET

SEE INSTRUCTIONS ON THE REVERSE

1. REPORT NUMBER (Assigned by TIDC, add Vol. No., if any): NUREG/CR-4115 EGG-2369

2. TITLE AND SUBTITLE: International Standard Problem 13 (LOFT Experiment L2-5) Final Comparison Report

3. LEAVE BLANK

4. DATE REPORT COMPLETED: MONTH December YEAR 1984

5. AUTHOR(S): John D. Burtt

6. DATE REPORT ISSUED: MONTH December YEAR 1984

7. PERFORMING ORGANIZATION NAME AND MAILING ADDRESS (Include Zip Code): EG&G Idaho, Inc. P.O. Box 1625 Idaho Falls, Idaho 83415

8. PROJECT/TASK/WORK UNIT NUMBER

9. FIN OR GRANT NUMBER: A6047

10. SPONSORING ORGANIZATION NAME AND MAILING ADDRESS (Include Zip Code): United States Nuclear Regulatory Commission Office of Nuclear Regulatory Research Washington, DC 20555

11a. TYPE OF REPORT: Technical

b. PERIOD COVERED (Inclusive dates)

12. SUPPLEMENTARY NOTES

13. ABSTRACT (200 words or less)

LOFT Experiment L2-5 was designated International Standard Problem 13 by the Organization for Economic Cooperation and Development. Comparisons between measurements from Experiment L2-5 were made with calculations from 11 international participants using five different computer codes. LOFT Experiment L2-5 simulated a double ended guillotine cold leg rupture of a primary coolant loop of a large pressurized water reactor, coupled with a loss of offsite power.

14. DOCUMENT ANALYSIS - a. KEYWORDS/DESCRIPTORS

b. IDENTIFIERS/OPEN ENDED TERMS

15. AVAILABILITY STATEMENT: Unlimited

16. SECURITY CLASSIFICATION (This page): Unclassified (This report): Unclassified

17. NUMBER OF PAGES

18. PRICE

120555078877 1 IANIR4
US NRC
ADM-DIV OF TIDC
POLICY & PUB MGT BR-PDR NUREG
W-501
WASHINGTON DC 20555

EG&G Idaho, Inc.
P.O. Box 1625
Idaho Falls, Idaho 83415